

**TWO-STEP SYNTHESIS OF NANO HETEROMETALLIC  
CATALYSTS FOR WATER TREATMENT AND  
BIOGASOLINE PRODUCTION**

**MUSHTAQ AHMAD**

**FACULTY OF ENGINEERING  
UNIVERSITY OF MALAYA  
KUALA LUMPUR**

**2016**

**TWO-STEP SYNTHESIS OF NANO  
HETEROMETALLIC CATALYSTS FOR WATER  
TREATMENT AND BIOGASOLINE PRODUCTION**

**MUSHTAQ AHMAD**

**THESIS SUBMITTED IN FULFILMENT OF THE  
REQUIREMENTS FOR THE DEGREE OF DOCTOR OF  
PHILOSOPHY**

**FACULTY OF ENGINEERING  
UNIVERSITY OF MALAYA  
KUALA LUMPUR**

**2016**

**UNIVERSITY OF MALAYA**

**ORIGINAL LITERARY WORK DECLARATION**

Name of Candidate: Mushtaq Ahmad

Registration/Matric No: KHA120123

Name of Degree: Doctor of Philosophy

Title of Project Paper/Research Report/Dissertation/Thesis (“Two-Step Synthesis of Nano Heterometallic Catalysts for Water Treatment and Biogasoline Production”):

Field of Study: Modelling and Simulation (Chemical Process)

I do solemnly and sincerely declare that:

- (1) I am the sole author/writer of this Work;
- (2) This Work is original;
- (3) Any use of any work in which copyright exists was done by way of fair dealing and for permitted purposes and any excerpt or extract from, or reference to or reproduction of any copyright work has been disclosed expressly and sufficiently and the title of the Work and its authorship have been acknowledged in this Work;
- (4) I do not have any actual knowledge nor do I ought reasonably to know that the making of this work constitutes an infringement of any copyright work;
- (5) I hereby assign all and every rights in the copyright to this Work to the University of Malaya (“UM”), who henceforth shall be owner of the copyright in this Work and that any reproduction or use in any form or by any means whatsoever is prohibited without the written consent of UM having been first had and obtained;
- (6) I am fully aware that if in the course of making this Work I have infringed any copyright whether intentionally or otherwise, I may be subject to legal action or any other action as may be determined by UM.

Candidate’s Signature

Date:

Subscribed and solemnly declared before,

Witness’s Signature

Date:

Name:

Designation:

## ABSTRACT

Heterometallic catalysts are important in large-scale industrial production of green fuels, chemicals and industrial effluent treatment. The efficiency of a heterometallic catalyst is dependent on the molecular homogeneity, surface-morphological properties and metal compositions. These features are being enhanced with recent developments in nanotechnology. Currently, several chemical methods are available and more methods are being developed or modified to synthesize nano heterometallic catalysts. However, obtaining the required features remains a challenging task as the physical and chemical properties of nanoparticles differ significantly when used in bulk. To overcome this challenge, several researchers have developed nano-size heterometallic catalysts via Metal Organic Frameworks (MOFs) methods. In these methods, metals are attached to a suitable organic framework (ligand). However, these methods are not suitable for the synthesis of a wide range of heterometallic catalysts as each of these methods only produces a specific type of catalyst, which limits their use for industrial applications. Therefore, there is a need to develop a suitable method that can formulate a wide range of nano-size heterometallic catalysts for industrial processes. In this work, a two-step chemical process was developed and used to synthesize nano-size heterometallic catalysts. In the first step, precipitation method was effectively employed to produce monometallic and polymetallic complexes. 2,2'-bipyridine was used as the ligand to interlink metal atoms (Ni, Zn, Fe, Cu and Al). In the second stage, heterometallic complexes were thermally decomposed to produce nano oxide clusters. The crystalline products were characterized for particle size, structure, morphology, surface area and thermogravimetric property. The two-step process was found to greatly improve the size, morphology and yields of the crystalline materials. The yield of Ni, Zn and Al clusters were 81%, 80% and 78% respectively, while the yield of Ni-Zn, Zn-Al and Ni-

Zn-Al complexes were 85%, 78.5% and 77% respectively. The two-step process was further utilized to produce supported type catalyst where Fe-ZSM-5, Fe-Zn-ZSM-5, and Fe-Zn-Cu-ZSM-5 heterogeneous catalysts were produced. Subsequently, the catalysts were used to treat wastewater containing organic recalcitrant contaminants (through Fenton oxidation process) and to produce biogasoline from palm oil. In the Fenton oxidation process, about 99% of color removal and 77% of total organic content (TOC) reduction were obtained. These values were significantly higher than the reported values in literature. When the same catalyst was used in the production of bio gasoline, the yield was about 56%, which was almost more than 8% compared to the literature values. The leaching analysis of the catalyst for the Fenton oxidation process revealed that only less than 2ppm of the metals were leached after a single use, which was in the permissible range as a heterometallic catalyst. Therefore, the present study proved that the newly developed two-step process was efficient and economical to produce heterometallic catalysts, which have a great potential for wastewater treatments and green energy applications due to higher degree of uniformity. In addition, availability of ligand (2,2'-bipyridine), solvents (ethanol, 2-propanol and DMF) and their relevant information in the literature makes this 2-step process an attractive process for the production of a variety of heterometallic catalysts.

## ABSTRAK

Mangkin heterometalik adalah penting di dalam industri pembuatan berskala besar bagi bahan api hijau, bahan kimia dan rawatan efluen perindustrian. Kecekapan mangkin heterometalik adalah bergantung kepada kehomogenan molekul, sifat-sifat morfologi permukaan dan komposisi logam. Ciri-ciri ini sedang dipertingkatkan dengan perkembangan terkini dalam teknologi nano. Kini, terdapat beberapa kaedah kimia yang telah sedia ada dan lebih banyak kaedah sedang dibangunkan atau diubahsuai untuk mensintesis mangkin nano heterometalik. Walaubagaimanapun, mendapatkan ciri-ciri yang dikehendaki masih kekal menjadi cabaran disebabkan oleh sifat-sifat fizikal dan kimia bagi zarah nano adalah berbeza dengan ketara apabila digunakan secara pukal. Bagi mengatasi masalah ini, beberapa penyelidik telah membangunkan mangkin heterometalik bersaiz nano melalui kaedah Rangka kerja logam organik. Dalam kaedah ini, logam dilekatkan pada rangka kerja organik yang sesuai (ligan). Namun, kaedah ini tidak sesuai bagi mensintesis pelbagai jenis mangkin heterometalik kerana setiap kaedah ini hanya menghasilkan jenis mangkin tertentu, yang menghadkan penggunaannya untuk aplikasi industri. Oleh itu, terdapat keperluan untuk membangunkan satu kaedah yang sesuai yang boleh menghasilkan pelbagai julat mangkin heterometalik bersaiz nano bagi proses perindustrian. Dalam kajian ini, proses kimia dua-langkah telah dibangunkan dan digunakan untuk mensintesis mangkin heterometalik bersaiz nano. Dalam langkah pertama, kaedah pemendakan telah digunakan dengan berkesan untuk menghasilkan jaringan monometalik dan polymetalik. 2,2'-bipyridine telah digunakan sebagai ligan untuk menyambungkan atom logam (Ni, Zn, Fe, Cu dan Al). Pada peringkat kedua, jaringan heterometalik telah diuraikan secara terma untuk menghasilkan kelompok nano oksida. Produk-produk berhablur telah dicirikan bagi saiz zarah, struktur, morfologi, luas permukaan dan sifat termogravimetri. Proses dua-langkah didapati amat meningkatkan saiz, morfologi dan hasil bahan habluran. Hasil

kelompok Ni, Zn dan Al adalah masing-masing sebanyak 81%, 80% dan 78%, manakala hasil kelompok Ni-Zn, Zn-Al dan jaringan Ni-Zn-Al adalah masing-masing sebanyak 85%, 78.5% dan 77%. Proses dua- langkah terus digunakan untuk menghasilkan pelbagai jenis mangkin di mana mangkin heterogen Fe-ZSM-5, Fe-Zn-ZSM-5, dan Fe-Zn-Cu-ZSM-5 telah dihasilkan. Seterusnya, mangkin telah digunakan untuk merawat air sisa yang mengandungi bahan cemar organik degil (melalui proses pengoksidaan Fenton) dan untuk menghasilkan biogasolin daripada minyak sawit. Dalam proses pengoksidaan Fenton, kira-kira 99% penyingkiran warna dan 77% pengurangan kandungan organik (TOC) diperolehi. Nilai-nilai ini adalah sangat ketara lebih tinggi daripada nilai yang dilaporkan dalam literatur. Apabila mangkin yang sama digunakan dalam penghasilan biogasolin, hasil adalah kira-kira 56%, yang merupakan hampir lebih daripada 8% berbanding dengan nilai-nilai dalam literatur. Analisis larut lesap bagi mangkin untuk proses pengoksidaan Fenton menunjukkan bahawa hanya kurang daripada 2% daripada logam telah terlarut lesap selepas penggunaan tunggal, yang berada dalam julat yang dibenarkan sebagai mangkin heterometalik. Oleh itu, kajian ini membuktikan bahawa proses dua-langkah yang baru dibangunkan adalah berkesan dan ekonomi untuk menghasilkan mangkin heterometalik, yang berpotensi tinggi untuk rawatan air sisa dan aplikasi tenaga hijau berikutan darjah keseragamannya yang tinggi. Di samping itu, kewujudan maklumat berkaitan ligan (2,2'-bipyridine) dan pelarut (etanol, 2-propanol dan DMF) di dalam literatur menjadikan proses dua-langkah ini satu proses yang menarik untuk penghasilan pelbagai jenis mangkin dan aloi istimewa.

## ACKNOWLEDGEMENTS

I would like to express my sincere gratitude to Prof. Abdul Aziz Bin Abdul Raman for his assistance and would like acknowledge his advice and guidance during this research. As a supervisor, he provided constant academic and moral supports throughout the project. I am also thankful to Assist. Prof. Wan Jeffrey Basirun from department of chemistry, faculty of Science, University of Malaya and Prof. Suresh K. Bhargava from Advanced Materials and Industrial Chemistry Group, School of Applied Sciences, RMIT University, Melbourne (Australia) for their support in this work.

My sincere gratitude goes to the University of Malaya, for granting me the opportunity to pursue my PhD program, allowing access to laboratories, equipments, library resources and all other supports during the period of study.

I am also grateful to the University of Malaya High Impact Research Grant (HIR-MOHE-D000038-16001) from the Ministry of Higher Education Malaysia which financially supported this work.

My heartfelt appreciation goes to my dear parents, brothers, wife and kids; Ayaan Mushtaq and Adeena Emaan for their unconditional emotional and spiritual support during the program.

## TABLE OF CONTENTS

Abstract .....	iii
Abstrak .....	v
Acknowledgements .....	vii
Table of Contents .....	viii
List of Figures .....	xiii
List of Tables.....	xvi
List of Symbols and Abbreviations.....	xviii
<b>CHAPTER 1: INTRODUCTION.....</b>	<b>1</b>
1.1 Background.....	1
1.2 Problem Statement.....	2
1.3 Conceptual Frame Work.....	3
1.4 Research Aim.....	9
1.5 Research Objectives.....	9
1.6 Research Scope.....	10
1.7 Research Novelty.....	11
1.8 Limitations of This Research.....	11
1.9 Outline of the Thesis.....	12
<b>CHAPTER 2: LITERATURE REVIEW.....</b>	<b>17</b>
2.1 Introduction.....	17
2.2 Frame Work for Literature Review .....	18
2.3 Metal Organic Frameworks (MOFs) .....	19
2.3.1 Catalysis by MOFs .....	22

2.4	Synthesis of MOFs .....	31
2.4.1	Synthesis of MOFs with Unsaturated Metal Sites.....	33
2.4.2	Synthesis of MOFs with Metal as Structural Units.....	35
2.4.3	Postsynthesis Modifications of MOFs .....	36
2.4.1	MOFs Derived Heterometallic Catalysts Synthesis .....	40
2.5	Summary of Overall Literature Review .....	43
<b>CHAPTER 3: GENERAL METHODOLOGY .....</b>		<b>44</b>
3.1	Introduction.....	44
3.2	Synthesis of Unsupported Catalysts .....	44
3.3	Synthesis of Supported Catalysts .....	45
3.4	Characterization.....	47
3.5	Application of the Synthesized Catalysts .....	47
3.6	Optimization Techniques.....	48
3.7	Process Safety Measures and Material Safety Data Sheet.....	49
<b>CHAPTER 4: DEVELOPMENT OF A TWO-STEP PROCESS .....</b>		<b>50</b>
4.1	Introduction.....	50
4.2	Background.....	50
4.3	Methodology.....	53
4.3.1	Materials .....	53
4.3.2	Synthesis of Monometallic Complex .....	53
4.3.3	Synthesis of Heterobimetallic Complex.....	53
4.3.4	Deposition of Heterobimetallic Thin Film .....	54
4.3.5	Characterization.....	55
4.4	Process Optimization.....	56
4.5	Results and Discussion .....	59

4.5.1	Confirmation of Crystalline Products.....	59
4.5.2	ANOVA Analysis of Monometallic Complex Precipitation.....	66
4.5.3	ANOVA Analysis of Heterobimetallic Complex Precipitation .....	70
4.6	Summary.....	73

## **CHAPTER 5: SYNTHESIS OF NANO HETEROMETALLIC CATALYSTS 74**

5.1	Introduction.....	74
5.2	Background.....	74
5.3	Experimental Details .....	77
5.3.1	Materials.....	77
5.3.2	Synthesis of Monometallic Complexes.....	78
5.3.3	Synthesis of Bimetallic Complexes.....	78
5.3.4	Synthesis of Trimetallic Complex.....	79
5.3.5	Deposition of Thin Films by AACVD .....	79
5.4	Results and Discussion .....	80
5.5	Summary.....	87

## **CHAPTER 6: SYNTHESIS AND APPLICATION OF A SUPPORTED CATALYST.....88**

6.1	Introduction.....	88
6.2	Background.....	89
6.3	Materials and Methodology .....	92
6.3.1	Reagents .....	92
6.3.2	Catalyst Preparation .....	92
6.3.3	Experimental Design .....	94
6.4	Experimentation.....	98
6.4.1	Analysis .....	98

6.4.2	Taguchi Optimization Steps .....	99
6.4.3	Leaching and Deactivation of Fe-ZSM-5.....	102
6.5	Results and Discussion .....	102
6.5.1	Characterization of Fe-ZSM-5 .....	102
6.5.2	Process Optimization by Coupling the Taguchi Method with PCA .....	104
6.5.3	Analysis of Variance (ANOVA) .....	113
6.5.4	Interaction of Operating Parameters.....	113
6.5.5	Long Term Stability and Reusability of Fe-ZSM-5 .....	118
6.5.6	Efficiency of Synthesized Fe-ZSM-5 for Mixture of Dyes.....	120
6.6	Summary.....	121
<b>CHAPTER 7: PROCESS OPTIMIZATION FOR SUPPORTED CATALYSTS .....</b>		<b>123</b>
7.1	Introduction.....	123
7.2	Background.....	123
7.3	Materials and Methodology .....	126
7.3.1	Catalyst Synthesis.....	126
7.3.2	Process Optimization.....	128
7.3.3	Efficiency Evaluation of the Synthesized Fe-ZSM-5.....	131
7.3.4	Deactivation of Synthesized Fe-ZSM-5 .....	132
7.4	Results and Discussions.....	133
7.4.1	Characterization of Synthesized Fe-ZSM-5 Catalyst.....	133
7.4.2	Process Optimization and ANOVA Analysis .....	137
7.4.3	Effect of Process Variables on Yield .....	139
7.4.4	Efficiency and Stability Evaluation of the Fe-ZSM-5 catalyst .....	143
7.4.5	Catalyst's Evaluation for Mixture of Dyes.....	146
7.4.6	Comparison of the Fe-ZSM-5 with Existing Catalysts .....	148
7.5	Summary.....	153

**CHAPTER 8: NANO OXIDE INTEGRATED CATALYSTS FOR BIOGASOLINE PRODUCTION.....154**

8.1	Introduction.....	154
8.2	Background.....	154
8.3	Materials .....	157
8.3.1	Catalyst Preparation .....	157
8.3.2	Characterization.....	158
8.4	Experimental Design for Palm Oil Cracking Process .....	160
8.4.1	Experimentation .....	161
8.5	Results and Discussions.....	162
8.5.1	Characterization of Synthesized Catalysts .....	162
8.5.2	Palm Oil Catalytic Cracking.....	166
8.5.3	Optimization Study.....	171
8.6	Efficiency of Other Integrated Catalysts .....	173
8.7	Summary.....	174

**CHAPTER 9: CONCLUSIONS AND RECOMMENDATIONS FOR FUTURE WORK.....176**

9.1	Recommendations for Future Work .....	178
9.1.1	Scale up of the Two-Step Process .....	179
9.1.2	Design of an Efficient Solvent Recovery System .....	180
	References .....	182
	Appendix A: Calibration Graphs and Biogasoline Yield Calculations.....	212

## LIST OF FIGURES

Figure 1.1: Conceptual Frame Work for Two-Step Process .....	8
Figure 2.1: Framework for Literature Review .....	19
Figure 2.2: Nitrogen Sorption Isotherms for MOF-2, MOF-5, MOF-177, Measured at 77K.....	21
Figure 2.3: A Monometallic MOF with Only One Type of Metal Center (M) (a) and A Bimetallic MOF with Both Structural (M2) and Catalytic (M1) Sites (b).....	22
Figure 2.4: MOFs with Reactive Functional Groups .....	23
Figure 2.5: Styrene Radical Polymerization Procedure Inside MOFs .....	25
Figure 2.6: Polycarboxylic Aromatic Molecules, Bipyridines, and Polyazaheterocycles as linkers for MOFs Preparation .....	32
Figure 2.7: A Free Coordination Position in the Metal after Removal of H <sub>2</sub> O .....	34
Figure 2.8: Material with two types of exposed Mn sites: (a) five-coordinated sites I (b) two-coordinated sites II.....	34
Figure 2.9: Postsynthesis Modification of a MOF Bearing an Azide Ligand through Copper Catalyzed Click Reaction .....	38
Figure 2.10: The modification of the Amino Groups of IRMOF-3 to Form the Imine Leading to Au(III)-Schiff Base Complex .....	38
Figure 2.11: Isomorphous Substitution in MOFs.....	39
Figure 3.1: Process Flow Diagram for the Synthesis of Unsupported Catalysts .....	45
Figure 3.2: Process Flow Diagram for Supported Catalysts .....	46
Figure 4.1: Aerosol-Assisted Chemical Vapor Deposition (AACVD) Detail Assembly.....	55
Figure 4.2: FTIR of the Monometallic and Bimetallic Complexes .....	59
Figure 4.3: FESEM Images of Al-Complex (a, b) and Zn-Complex (c, d) .....	60
Figure 4.4: Zn-Al Bimetallic Complex (a, b and c) with Enhanced Porosity and Better Crystal Morphology .....	61
Figure 4.5: Zn-Al Thin Film Supported on SS Substrate .....	61

Figure 4.6: Elemental Distribution of C (a), Zn (b), Al (c), N (d) and Cl (e) atoms inside the Zn-Al Bimetallic Complex.....	62
Figure 4.7: TGA/DSC Curves Showing Pyrolysis of Zn-Al Bimetallic Complex at A Heating Rate of 10°C/min.....	64
Figure 4.8: XRD Patterns of Mono-Metallic and Polymetallic Complexes .....	65
Figure 4.9: XRD Patterns of the Thin Film, Deposited on SS Substrate.....	65
Figure 4.10: Perturbation Plot (a), A is Temperature, B is Reaction Time, C is Stirring Speed, and Comparison Plot (b) for Zn-complex .....	69
Figure 4.11: Perturbation Plot (a), A is Temperature, B is Reaction Time, C is Stirring Speed, and Comparison Plot (b) for Al-Complex.....	70
Figure 4.12: Perturbation Plot (a), A is Temperature, B is Reaction Time, C is Stirring Speed, and Comparison Plot (b) for Zn-Al-Complex.....	72
Figure 5.1: IR Spectra of Monometallic and Polymetallic Complexes .....	81
Figure 5.2: Ni (a), Zn (b) and Al (c) Monometallic Complexes.....	82
Figure 5.3: Zn-Ni (a), Zn-Al (b) and Zn- Ni-Al (c) Heterometallic Complexes .....	82
Figure 5.4: FeSEM Images (a & b) and Electron Image (c) of Zn-Al Thin Film Supported On SS Substrate .....	83
Figure 5.5: Zn-Ni-Al Thin Film Supported On FTO Glass Substrate .....	84
Figure 5.6: Zn-Ni-Al Thin Film on SS Substrate.....	84
Figure 5.7: XRD Patterns of Monometallic and Heterometallic Complexes.....	85
Figure 5.8: XRD Patterns of Thin Films.....	86
Figure 5.9: Yield of the Crystalline Materials .....	86
Figure 6.1: Chemical Structure of Acid Blue 113.....	92
Figure 6.2: FeSEM images of (a) the Fe(byp) complex, (b) ZSM-5, and (c) Fe-ZSM-5 ..	103
Figure 6.3: FTIR Data for (a) the ZSM-5, (b) Fe-ZSM-5, and (c) Fe(byp) Complex ..	103
Figure 6.4: Mean TPCI Plots with Respect to Parameter Changes.....	109
Figure 6.5: Interaction of Parameters with Respect to TOC.....	114

Figure 6.6: Interaction of Parameters with Respect to Decolorization .....	116
Figure 6.7: Interaction of Parameters with Respect to Degradation .....	117
Figure 6.8: SEM Images of the (a) Fresh and (b) Spent Fe-ZSM-5 .....	119
Figure 6.9: FTIR Spectra of the (a) Fresh Fe-ZSM-5 and (b) Spent Fe-ZSM-5.....	120
Figure 6.10: Degradation and TOC Removal of Mixture of Dyes Using Fe-ZSM-5 ...	121
Figure 7.1: Elemental Compositions of the Fe-ZSM-5 Prior to Calcination .....	134
Figure 7.2: SEM Images of Fe(byp) Complex (a), ZSM-5 (b), Fe-ZSM-5(c), and HRTEM Images of Fe-ZSM-5(d & e). .....	135
Figure 7.3: XRD Analysis of Fe-ZSM-5, ZSM-5, and Fe(byp)-Complex(c) .....	137
Figure 7.4: Perturbation Plot (A is Temperature, B is Reaction Time, and C is Stirring Speed) and Comparison Plot for Fe-MOFs.....	140
Figure 7.5: Contour Plot and Three Dimensional Plot Showing Combine Effect of Time and Temperature on Fe-MOF's Yield.....	141
Figure 7.6: Contour Plot and Three Dimensional Plot Showing Combine Effect of Time and Stirring Speed on Fe-MOF's Yield .....	142
Figure 7.7: Degradation of Individual Dye (a), in Mixture Form (b), and TOC Reduction for Reactive Black 5, Methyl Orange, Mixture 1, Mixture 2, Mixture 3, and Mixture 4 (c) ....	147
Figure 8.1: XRD Analysis of Synthesized Catalysts .....	164
Figure 8.2: FeSEM (a, b, c, e, & g) and HRTEM (d, f, & h) Images of the Synthesized Catalysts .....	165
Figure 8.3: Effect of Process Parameters on Yield Of Biogasoline, Calculated on the Basis of S/N Ratios .....	168
Figure 8.4: Interaction of Parameters with Respect to Gasoline Yield (%).....	170
Figure 9.1: Process Flow Diagram for the Scale Up of Two-Step Process .....	180
Figure 9.2: Two-Step Process with Proposed Recovery of Solvent .....	181

## LIST OF TABLES

Table 1.1: Thesis Layout Illustrating Objectives Achieved and Activities Carried Out	15
Table 2.1: MOFs with Metal Active Sites (Corma et al., 2010)	27
Table 2.2: MOFs with Reactive Functional Groups (Corma et al., 2010)	30
Table 2.3: MOFs Based Monometallic and Heterometallic Catalysts	42
Table 4.1: Process Parameter for Zn/Al Monometallic Precipitation Process	56
Table 4.2: Experimental Design and Response of Zn-complex Precipitation Process	57
Table 4.3: Experimental Design and Response of Al-complex Precipitation Process	57
Table 4.4: Process Parameter for Zn-Al Heterobimetallic Precipitation Process	58
Table 4.5: Experimental Design and Response of Zn-Al-complex Precipitation Process	58
Table 4.6: EDX Analysis of the Synthesized MOFs	63
Table 4.7: ANOVA Analysis of Zn-Complex Precipitation	67
Table 4.8: ANOVA Analysis of Al-Complex Precipitation	68
Table 4.9: ANOVA analysis of Zn-Al Heterobimetallic Complex Precipitation	71
Table 5.1: EDX Analysis of the Clusters and Thin Films	81
Table 6.1: EDX analysis of ZSM-5 and Fe-ZSM-5	93
Table 6.2: Pore Structure Characteristics of the ZSM-5 and Fe-ZSM-5 Catalyst	94
Table 6.3: Taguchi Design Factors and Their Levels	95
Table 6.4: L27 Orthogonal Design, Experimental Results, and Taguchi Analysis	96
Table 6.5: Theoretical Framework of the Taguchi Method Coupled With Principle Component Analysis (PCA)	101
Table 6.6: The Obtained S/N Ratios, Normalized S/N Ratios, and TPCI Values	106
Table 6.7: Eigenvalues Obtained Through PCA Processing of the Normalized S/N Ratios	108
Table 6.8: List of TPCI responses	110

Table 6.9: Optimized values for heterogeneous Fenton oxidation .....	112
Table 6.10: ANOVA Analysis for Fenton Oxidation Parameters.....	112
Table 7.1: Process Parameters for Fe Monometallic Precipitation Process.....	129
Table 7.2: Experimental Design and Response of Fe-MOF's Precipitation Process....	130
Table 7.3: EDX Analysis of the ZSM-5 Support and Synthesized Fe-ZSM-5.....	133
Table 7.4: ANOVA Analysis of Fe-MOF's Precipitation .....	138
Table 7.5: Efficiency of the Synthesized Catalyst at Optimized Conditions.....	145
Table 7.6: Mixtures of Three Dyes, Their Degradation and TOC Removal.....	148
Table 7.7: Comparative Study of the Synthesized Catalyst with Other Available Catalysts .....	152
Table 8.1: Composition of ZSM-5(30) Support and Synthesized Catalysts (31-33)....	159
Table 8.2: BET analysis of the ZSM-5 support (31) and synthesized catalysts (31-33) ...	159
Table 8.3: Process Factors with Their Three Level Values Used for Taguchi Design .	160
Table 8.4: Experimental Results of Palm Oil Cracking and Taguchi Analysis .....	161
Table 8.5: Response Table for Signal to Noise Ratios.....	172
Table 8.6: ANOVA Analysis for Process Parameters .....	172
Table 8.7: At Optimized Values, Efficiencies of the ZSM-5 and Synthesized Catalysts..	174

## LIST OF SYMBOLS AND ABBREVIATIONS

AACVD	:	Aerosol-assisted chemical vapor deposition
BET	:	Brunauer-Emmett-Teller
CCD	:	Central composite design
DSC	:	Differential scanning calorimetry
EDX	:	Energy-dispersive X-ray spectroscopy
FeSEM	:	Field emission scanning electron microscopy
FTIR	:	Fourier transform infrared spectroscopy
HPLC	:	High performance liquid chromatography
HRTEM	:	High resolution transmission electron microscopy
MOFs	:	Metal organic frameworks
NPs	:	Nano particles
RSM	:	Response surface methodology
SEM	:	Scanning electron microscopy
TGA	:	Thermal gravimetric analysis
XRD	:	X-ray powder diffraction
ZSM-5	:	Zeolite Socony Mobile-5
t	:	Time (s)
Abs <sub>i</sub>	:	UV absorption (AU) measured initially at time; t = 0 s
Abs <sub>t</sub>	:	UV absorption (AU) measured after certain time; t s
C <sub>o</sub>	:	Concentrations (mg/L) measured initially at time; t = 0 s
C <sub>t</sub>	:	Concentrations (mg/L) measured after certain time; t s
TOC	:	Total organic carbon (mg/L)

## CHAPTER 1: INTRODUCTION

### 1.1 Background

Heterogeneous catalysts are used extensively in many chemical, pharmaceutical and refinery processes. Approximately ninety percent of chemical processes utilize heterogeneous catalysts and the value created by utilizing catalysts is approximately three orders of magnitude higher than the amount invested in them (Gomez & Tigli, 2013; Guo et al., 2013).

Among heterogeneous catalysts, pure metallic (e.g., Ni) and metal oxides (e.g., TiO<sub>2</sub>, NiO, ZnO) type catalysts have been remained the center of focus for a variety of industrial applications due to their chemical and thermal stability (Deutschmann et al., 2009; Thomas & Thomas, 2014). Catalytic properties of metallic catalysts are significantly improved by combining different metals. These properties are also strongly affected by the preparation method, production conditions, and quality of source materials. Therefore, it has been proven that combining different metals using suitable production method leads to exciting opportunities for creating catalyst with well-defined morphology and size (Bell, 2003). These properties are the essential considerations for almost all the industrial catalytic processes (Gomez & Tigli, 2013; Guo et al., 2013). Likewise, it is becoming increasingly possible to produce well-defined porous matrices, which can serve as catalyst supports, from a wide variety of inorganic materials. These capabilities are contributing to the production of single-site catalysts, in which all of the active sites closely resemble each other.

Recent developments in nanotechnology have made it possible to synthesized heterometallic catalysts of nano porous structures with improved features like molecular homogeneity, surface-morphological properties and metal compositions. (Gomez &

Tigli, 2013; Guo et al., 2013). Nano-sized porous structures provide high surface area and significantly improve product yields (Bell, 2003). Porosity of the material normally depends on the method by which it is produced (Kumar et al., 2012). Catalysts with highly ordered structures, which are composed of building blocks that contain multiple channels, have higher porosity compared to catalysts with less ordered structures. These unique porous structures of the polymetallic catalysts are important for many industrial applications (Czaja et al., 2009; Jiang & Xu, 2011).

To-date, various methods have been developed and introduced to design microporous and mesoporous materials and their nano particles (Bazer-Bachi et al., 2014; Jiao et al., 2011; Patete et al., 2011b; Yang & Xiaohong, 2014). These synthesis techniques can be categorized as physical or chemical methods (Liu et al., 2014b). Physical methods are effective in producing catalysts and alloys even at room temperature without toxic solvent or reducing agents (Nayak et al., 2010). However, it is not possible to precisely control the mixing of solids particles and their narrow size distribution. Physical methods also require highly sophisticated equipments and complex accessories with high maintenance cost. Due to these problems, chemical methods (e.g., chemical reduction, precipitation, co-precipitation, thermal decomposition, electrochemical method and sol-gel) have attracted the attention of researchers. Desired size, porosity and elemental distribution can be controlled up to certain extent in chemical methods (Hong et al., 2009; Salavati-Niasari et al., 2011) which are the main requirements of the advanced catalysts for their effective use (Sankar et al., 2012).

## **1.2 Problem Statement**

Chemical methods for the production of heterometallic catalysts, require toxic chemicals and long reaction time for their completion (Sankar et al., 2012). In addition, adsorption of surfactants on the active sites of nano particles (NPs) and oxidation of

metallic NPs reduce their available surface areas and effectiveness (Parveen et al., 2012). In addition to these, precise control over chemical composition, morphology and microstructural properties remains a challenging task for the scientists and engineers for the synthesis of cost effective catalytic nano size catalyst at the bench scale and then processing it at a large scale for industrial use. This is because the physical and chemical properties of nanoparticles are relatively changed from those of their bulk ingredients. Therefore, recent researches have focused on improving the porosity, morphology and effective costs of crystalline nano materials that are to be used as catalysts.

In this respect, metal–organic frameworks (MOFs) have shown outstanding potential because of their controllable structure, unique electrochemical properties and large surface areas (Feng et al., 2013). Use of MOFs for clean energy production has been widely considered. Several researchers have prepared heterogeneous catalysts via MOFs. These methods have significantly improved the efficiency, stability and the reusability of catalysts. However, these methods can produce specific catalysts and cannot produce a wide range of heterometallic catalysts. Therefore, there is a high demand for a suitable method that can formulate a wide range of the required heterometallic catalysts for industrial processes. Beside this the process must be environment friendly and cost effective.

### **1.3 Conceptual Frame Work**

MOFs are the highly crystalline and porous materials synthesized through metal–ligand coordinate bridging, which is normally stronger than other weak bonding such as p-p stacking (Corma et al., 2010). Due to high degree of crystallinity, porosity and coordinate bonding, MOFs exhibit dynamic properties (Deng et al., 2012; Furukawa et al., 2013; Geyer et al., 2015). Like zeolites, three-dimensional arrangement of the

structural units forms the system of cavities and channel. Another attractive property of MOFs is that various metal cations (mainly di, tri or tetravalent) can be used in the development of MOFs' frameworks, which is not possible in case of conventional zeolite (Hasan & Jung, 2015). Normally, zeolites contain only a few cations such as Al, Si, and P. Therefore, due to high surface area, diverse properties and porosity, MOFs based materials are surpassing the zeolites (Hasan & Jung, 2015). It is surprising that, the organic part of the MOF can support acid, base, or acid-base pairs that, individually or in combination form, facilitate to perform cascade reactions. Similarly, MOFs offer the synthesis of enantioselective catalysts, a theme that cannot be possible using zeolites (Corma et al., 2010).

Synthesis of MOF-5 in 1999 was the milestone which has opened new avenue for the development of MOFs. This composite contains tetrahedral  $Zn^4O^{6+}$  groups interconnected through terephthalate groups and exhibits even higher specific surface area of  $2900 \text{ m}^2\text{g}^{-1}$ . Another milestone was achieved with the synthesis of MOF-177, which has a surface area of  $4500 \text{ m}^2\text{g}^{-1}$  (Chae et al., 2004; Deng et al., 2012; Yoon et al., 2011). MOF-177 is particularly prominent due to its largest reported surface area (Rowsell & Yaghi, 2004). Further research in this field revealed that choice of the organic ligand, the size of the MOFs' pores can be customized. In addition, due to these tunable pore properties, loading of metals and extremely high surface areas, MOFs are getting prominence in various applications (Deng et al., 2012; Furukawa et al., 2013; Rowsell & Yaghi, 2004; Tang et al., 2015).

MOFs are usually synthesized through the coordination of the metals with ligands. A large number of metals particularly, transition metals are used to synthesize the MOFs. In case of organic ligand, rigid molecules are normally used, since they result into highly crystalline, stable and porous (Corma et al., 2010; Nazir et al., 2011; Yoon et al.,

2011). In addition, 2,2'-bipyridine is found the most widely used ligand, because of its ease of functionalization and robust redox stability.

MOFs are usually synthesized in the liquid phase, either by using a single solvent or a blend of solvents. In most of the cases, MOFs are synthesized through the mixing of two solutions containing the organic ligand and metal component, either at ambient conditions or under solvothermal environment. Sometime addition of an secondary molecules is also required. A variety of the metals atoms with their stable oxidation states have been utilized to synthesize MOFs. These metals from the groups include alkaline, alkaline earth, transition metals and even rare earth group. In case of organic ligand, rigid molecules are normally used, since they result into highly crystalline, stable and porous MOFs (Corma et al., 2010; Nazir et al., 2011; Yoon et al., 2011).

All of the MOFs have three main parts including inorganic part (metals), organic part (ligand) and the channel or pore system. Therefore, three different categories are made to describe the MOFs based catalysts. In the first category of MOFs, catalytic activity is directly linked with the metallic part, either as a single metal center or as metallic clusters, sheets or chain. Here, organic ligand only facilitates for formation of building blocks, channels and cavities, while metal part simultaneously take part in the formation of structural units and also provides the active sites for catalytic activity. In several cases, MOFs contain two different kinds of metals: one of them involves in the formation of porous structures while other is the responsible for the catalytic activity.

In the second kind of MOFs, catalytic activity is related with the functional groups of the ligand part. These organic ligands contain different functional groups, which have ability to catalyze the specific reactions. A limited number of MOFs belonging to this class are available. This is due to the reactive group should be free and available to interact with the catalytic substrates and not be coordinated to the metal ions of the

MOF. Therefore, the synthesis of such type of MOFs is quite difficult as organic reactive groups have the natural tendency to interact with metals.

In the third scheme, both metal part and ligand part do not take part in catalysis. In this category of MOFs, porosity of the materials plays its role by providing physical space or offers its services as a cage where catalytic sites can be encapsulated. Styrene is polymerized inside the MOFs pores through this type of mechanism.

Bearing in mind the ease of the production of MOFs and their less cost, it will be essential to explore if MOFs can perform in asymmetric reactions or at larger scale, effectively substituting the homogeneous catalysts. Researchers are hopeful that, as like zeolites, gradual introduction of MOFs as industrial catalysts will boost further research in this area (Corma et al., 2010; Rowsell & Yaghi, 2004; Sugikawa et al., 2013; Wijngaarden et al., 2008). Details of MOFs as possible replacement of other heterogeneous catalysts have been provided in chapter 2.

However, despite their higher metal content compared to zeolites, the use of MOFs in heterogeneous catalysis is restricted due to their relatively low stability at elevated temperature and in the presence of water vapor or chemical reagents. In addition, the metal ions in MOFs are often blocked by the organic linker molecules and are therefore not accessible for catalytic reactions (Corma et al., 2010; Deutschmann et al., 2009; Thomas & Thomas, 2014).

Several researchers have successfully transformed MOFs into nano sized heterometallic catalysts (Cao et al., 2014; Nazir et al., 2013). These methods have significantly improved the efficiency, stability and the reusability of catalysts (Ahmed et al., 2015; Ahmed et al., 2014). However, these methods cannot produce a wide range of heterometallic catalysts. In addition, among all the promising supports for

heterogeneous process, ZSM-5 has captured the attention of many researches due to its high stability, large surface area, remarkable porosity, and unique surface chemistry (Akolekar & Bhargava, 1998; Gupta et al., 2011; Jauhar et al., 2014; Lucking et al., 1998; Oliveira et al., 2007; Pirkanniemi & Sillanpaa, 2002; Soon & Hameed, 2013). Heterometallic particles supported on ZSM-5 matrix are widely used for environmental and green energy applications (Gonzalez-Olmos et al., 2011; Queiros et al., 2015; Shahbazi et al., 2014). Therefore, in this research focus has given to develop a suitable method that can produce a wide range of the required heterometallic catalysts via MOFs. In the next step, the synthesized nano heterometallic particles will be spread on the ZSM-5 matrix. This would induce the extra properties of zeolites in the synthesized catalysts and also enable the recovery and regeneration of the catalysts from the large scale applications. Figure 1.1 illustrates the detail conceptual model for this research. From the literature it was revealed that approximately 24 – 28% of produced catalysts were sold to the chemical industry and 38 – 42% to petrochemical companies including refineries. 28– 32% of solid catalysts were used in environmental protection, and 3 – 5% in the production of pharmaceuticals (Deutschmann et al., 2009). As a whole energy and environmental applications consumes about 70% of the total produced catalysts. Therefore the both of these sectors will be considered for the evaluation of the synthesized catalyst.

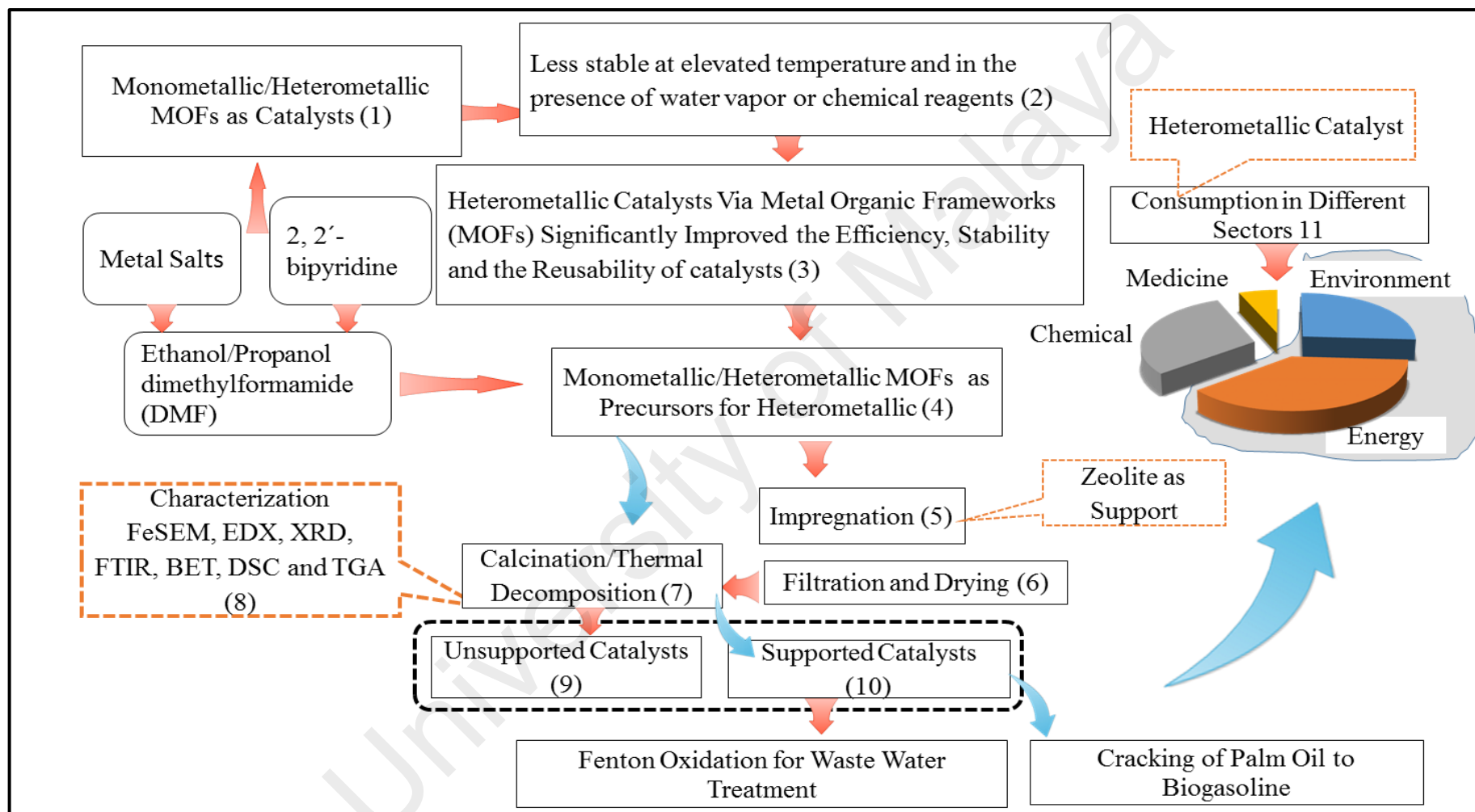


**Figure 1.1:** Conceptual Frame Work for Two-Step Process

#### 1.4 Research Aim

This work aims at the development of a process to synthesize nano heterometallic (unsupported and supported type) catalysts with enhanced features for environmental and green energy applications.

#### 1.5 Research Objectives

Development of a nano heterometallic catalyst needs an efficient process for its synthesis and activity evaluation in suitable applications. Keeping in mind, the aim and scope of this work, following specific objectives have been set:

1. Development and optimization of a two-step process to synthesize a wide range of heterometallic catalysts at low temperature and pressure conditions.
2. Characterization and activity evaluation of the synthesized heterometallic catalysts for wastewater treatment and biogasoline production.

To achieve first objective, following activities will be carried out.

##### *(a) Unsupported type catalysts synthesis*

- i. Synthesis of Zn, Ni, Al, and Cu metal organic frameworks (MOFs)
- ii. Synthesis of Zn-Al, Ni-Al, and Zn-Ni-Al, heterometallic complex and their nano oxides

##### *(b) Supported type catalysts synthesis*

- i. Synthesis of Fe-ZSM-5, Fe-Zn-ZSM-5, Fe-Zn-Cu-ZSM-5 and Fe-Zn-Cu-Ni-ZSM-5

To achieve second objective, following activities will be carried out to.

(c) ***Characterization***

- i. Characterization of ligand, monometallic and heterometallic complexes and resulting nano oxides

(d) ***Activity Evaluation***

- i. Activity evaluation of the synthesized supported type catalysts for the waste water treatments using Fenton oxidation process and also to identify the optimum conditions.
- ii. Activity evaluation of the synthesized supported type catalysts for biogasoline production from palm oil and also to identify the optimum conditions for the cracking.

## **1.6 Research Scope**

From the literature it was revealed that the catalytic properties of solid catalysts are strongly affected by the preparation method, production conditions, and quality of source materials. In addition, heterometallic catalysts synthesized via MOFs are effective and stable for many industrial applications. Therefore, in this research, whole focus would be on development of a chemical method to synthesize a wide range of nano heterometallic catalysts via MOFs. Synthesis of both unsupported and supported type catalysts will be considered to achieve the first objective.

It was also revealed that approximately 65 –70% of produced heterometallic catalysts are sold to petrochemical companies (including refineries) and environmental protection agencies, covering a huge capital of about \$13 X10<sup>9</sup> per year (Deutschmann et al., 2009). Therefore, both of these sectors will be considered to evaluate the efficiencies of the synthesized catalysts. Since catalysts recovery and regeneration are highly required

to optimize the process cost. Supported type catalyst will be suitable for these applications due to added characteristics of ZSM-5 support and ease of recovery and regeneration, while, unsupported type catalysts will be synthesized but not consider for applications in this work.

### **1.7 Research Novelty**

This work will enable the development of a chemical process to synthesize a wide range of heterometallic materials via MOFs for environmental and green energy applications. In addition, findings of this work will add useful information to available literature and possibly fill the gap, required to transform MOFs into heterometallic materials. There are several important areas where this study will make an original contribution to both industry as well as human development. It is anticipated that this study will provide an exciting opportunity to advance the researchers' knowledge about the heterometallic materials via MOFs and will cause to open new research avenues in this field.

### **1.8 Limitations of This Research**

The main limitation of this work is the lab scale development of a chemical process to produce heterometallic catalysts. Development of a new process or a new material at lab scale is the first step to perform prior to scale up applications. However, obtaining the required features remains a challenging task with scaling up, particularly in case of nano materials as the physical and chemical properties of nanoparticles differ significantly when produced in bulk. This is due to the process conditions, such as mixing, temperature, pressure and etc are difficult to maintain at larger scale production as compared to lab scale.

Another potential problem is that the catalysts evaluation will be carried out against model wastewater containing textile dyes and refined palm oil. At industrial level, nature of real effluents may be different. Similarly, the feed stock of palm oil may have different properties. Therefore, there may be chance the developed catalyst will not able to meet efficiency as noticed at lab scale.

In order to delimit the synthesis at larger scale, optimization techniques will be employed to capture a real picture of the synthesis environment along with a reliable model. This model will be further investigated through rigorous experiments, and solid implications will be provided for the scale up of this process. Similarly, in case of catalysts evaluation, particular in wastewater treatment, high concentrations of the recalcitrant content as well as mixture of different dyes will be used to reflect the actual findings.

## **1.9 Outline of the Thesis**

This thesis is written in the article style format using the guidelines of Institute of Post Graduate Studies (IPS), University Malaya. This thesis consists of nine chapters, including five articles dealing with different aspects relevant to the topic of the study. In addition following detail, Table 1.1 illustrates the chapters' descriptions with respect to covered objectives and activities carried out.

### **Chapter 1: Introduction**

This chapter includes a brief introduction to the research and objectives of the study.

### **Chapter 2: Literature Review**

This chapter reviews the history and role of MOFs based catalysis in process industry, their synthesis methods and characterization techniques. Transformations of

MOFs into heterometallic catalysts and unit operations involved are also described in detail.

### **Chapter 3: General Methodology**

This chapter briefly describes the general methodology of a two-step process to synthesize heterometallic catalysts (supported and unsupported). Process Flow diagrams along with required chemical, solvents and materials detail are provided here.

### **Chapter 4: Development of a two-step process**

This chapter includes the development of a two-step process to synthesize and optimize the unsupported type nano size Zn-Al bimetallic catalyst and its characterization.

### **Chapter 5: Synthesis of nano heterometallic catalysts using two-step process**

The developed two-step was successfully employed to synthesize Ni-Zn and Zn-Ni-Al heterometallic nano catalysts. Detail of the heterometallic synthesis and characterization are described in this chapter.

### **Chapter 6: Synthesis and application of a supported catalyst**

The developed two-step was further used to synthesize supported type, Fe-ZSM-5 catalyst. Synthesized catalyst was effectively used to degrade and decolorize the waste water containing organic recalcitrant contaminants through Fenton oxidation process. Detail of the Fenton oxidation process and its optimization has been described in this chapter.

## **Chapter 7: Process optimization for supported type catalysts**

In this chapter, optimization study was made for the production of Fe-ZSM-5 catalyst. Furthermore, the efficiency of the catalyst, produced at optimized environment was also evaluated against mixture of dyes. Both the adsorption and oxidation effects were considered.

## **.Chapter 8: Nano oxide integrated catalysts to produce biogasoline**

The developed two-step was further employed to synthesize ZSM-5 based catalysts loaded with heterometallic nano oxides of Fe, Zn, Cu and Ni and used for the palm oil cracking to produce biogasoline. In addition to palm cracking, effects of the process variables were also optimized to maximize the yield of biogasoline.

## **Chapter 9: Conclusions and Recommendations for Future Work**

In the last chapter, results and findings of the study were summarized. In addition, recommendations for future work were also provided.

**Table 1.1:** Thesis Layout Illustrating Objectives Achieved and Activities Carried Out

Research Aim	Chapter No.	Description	Specific Objectives Achieved	Specific Activities Carried Out	Activity No.
Development of a chemical process to synthesize nano heterometallic catalysts	1	Introduction	Brief background, objectives and scope the research		
	2	Literature Review	Overall literature of MOFs, their application as catalysts, and their role as precursors for heterometallic catalysts' synthesis		
	3	General Methodology	General methodology including materials, main process steps and characterization techniques adopted.		
	4	Article 1	Development and optimization of a two-step process to synthesize unsupported type bimetallic catalyst	Synthesis of Zn, Al, and Zn-Al metal organic frame works (MOFs) Characterization of ligand, monometallic and heterometallic complexes and nano oxides	a (i, ii) c (i)
	5	Article 2	Synthesis of unsupported type heterometallic catalysts	Synthesis of Cu, Ni, Ni-Al, and Zn-Ni-Al MOFs and their nano oxides Characterization of monometallic and heterometallic complexes and nano oxides	a (i, ii) c (i)
	6	Article 3	Synthesis of supported type Fe-ZSM-5 catalyst	Synthesis of supported type Fe-ZSM-5 catalyst Characterization of Fe-ZSM-5 catalyst Activity evaluation of the synthesized supported type catalysts for the waste water treatments using Fenton oxidation process (Oxidation effects are considered only)	b (i) c (i) d (i)

**Table 1.1:** Thesis Layout Illustrating Objectives Achieved and Activities Carried Out (Continued)

Research Aim	Chapter No.	Description	Specific Objectives Achieved	Specific Activities Carried Out	Activity No.
Development of a chemical process to synthesize nano heterometallic catalysts	7	Article 4	Optimization and activity evaluation of supported type Fe-ZSM-5 catalyst	Identified the optimum conditions for the synthesis of supported type Fe-ZSM-5 catalyst Characterization of Fe-ZSM-5 catalyst Activity evaluation of the synthesized catalyst (prepared at optimized conditions) against the three selected dyes; individually and in mixture form, using Fenton oxidation process. Both adsorption and oxidation effects are considered.	b ( i ) c ( i ) d ( i )
	8	Article 5	Synthesis of supported Fe-Zn-ZSM-5, Fe-Zn-Cu-ZSM-5 and Fe-Zn-Cu-Ni-ZSM-5 catalysts for biogasoline production	Synthesis of supported Fe-Zn-ZSM-5, Fe-Zn-Cu-ZSM-5 and Fe-Zn-Cu-Ni-ZSM-5 catalysts Characterization of synthesized catalysts Activity evaluation of the synthesized catalysts for the cracking of palm oil to produce biogasoline	b ( i ) c ( i ) d ( i )
	9	Conclusions and Recommendations for Future work	Overall conclusions of the research carried out and possible future directions.		

## CHAPTER 2: LITERATURE REVIEW

### 2.1 Introduction

Heterometallic catalysts are frequently used in advance oxidation processes for the treatment of waste waters and pollutants and for green energy applications (Abdullah & Wong, 2010; Bolova et al., 2011; Karthikeyan et al., 2012; Kiss et al., 2006; Liotta et al., 2009). The efficiency of a heterometallic catalyst depends on molecular homogeneity, surface-morphological properties and chemical composition (Pirkanniemi & Sillanpaa, 2002). Advances in the synthesis of materials are leading to exciting opportunities for creating catalyst particles that are all of the same size and shape. Likewise, it is becoming increasingly possible to produce well-defined porous matrices, which can serve as catalyst supports, from a wide variety of inorganic materials. These capabilities are contributing to the production of single-site catalysts, in which all of the active sites closely resemble each other (Bell, 2003).

Apart to synthesize heterometallic catalysts and supports separately, development of the multifunctional catalysts is also gaining attention as these type of catalysts can give promising results, particularly in the energy applications though simultaneously enhancing the catalytic cracking and hydrodeoxygenation of the bio feed stock. Multifunctional catalysts are able to give a selective product stream and also to provide shed light on the complex mechanisms of catalytic reforming and cracking, which are still not well defined. In this regard, zeolites doped with heterometallic nano catalysts have captured the researchers' attention (Dickerson & Soria, 2013; Vu et al., 2015b). Numerous efforts were also made to integrate the doped zeolites into the cracking equipment and in situ upgradation of the catalysts (Dickerson & Soria, 2013; Vu et al., 2015b). Several researchers synthesized MOFs based materials and applied for waste

water and green energy applications as multifunctional catalysts. Several mechanisms for the catalytic mode of MOF compounds were developed and evaluated. These mechanisms were based on three different parts including metallic part, ligand part and the pore system. Therefore, three modes of MOFs catalysis have been described. Remarkable efficiencies were noticed in a variety of applications.

In spite of morphological improvements like porosity and surface areas, MOFs based catalysts were found to be less stable at high temperatures, which limits the usage of MOFs as catalysts. Several researchers extended the application of MOFs as the precursor for the nano size heterometallic catalysts. These approaches have significantly improved the efficiency of catalysts (Yang et al., 2011). However, these methods can synthesize specific catalysts and cannot produce a wide range of heterometallic catalysts. Therefore, this work will focus to develop a chemical method that can overcome these issues.

## **2.2 Frame Work for Literature Review**

In this work, literature is reviewed to develop a chemical process for the synthesis of a wide range of heterometallic catalyst materials with enhanced features. Due to scope of study, a brief description of MOFs, their catalytic behaviors, synthesis methods and transformation into heterometallic are required. Therefore, synthesis techniques for MOFs, mode of catalysis and application in chemical processes have been discussed. In addition to challenges faced during synthesis or applications, transformations into heterometallic materials are also described. Figure 2.1 illustrates the selected dimensions for the literature survey to be conducted for this research work.

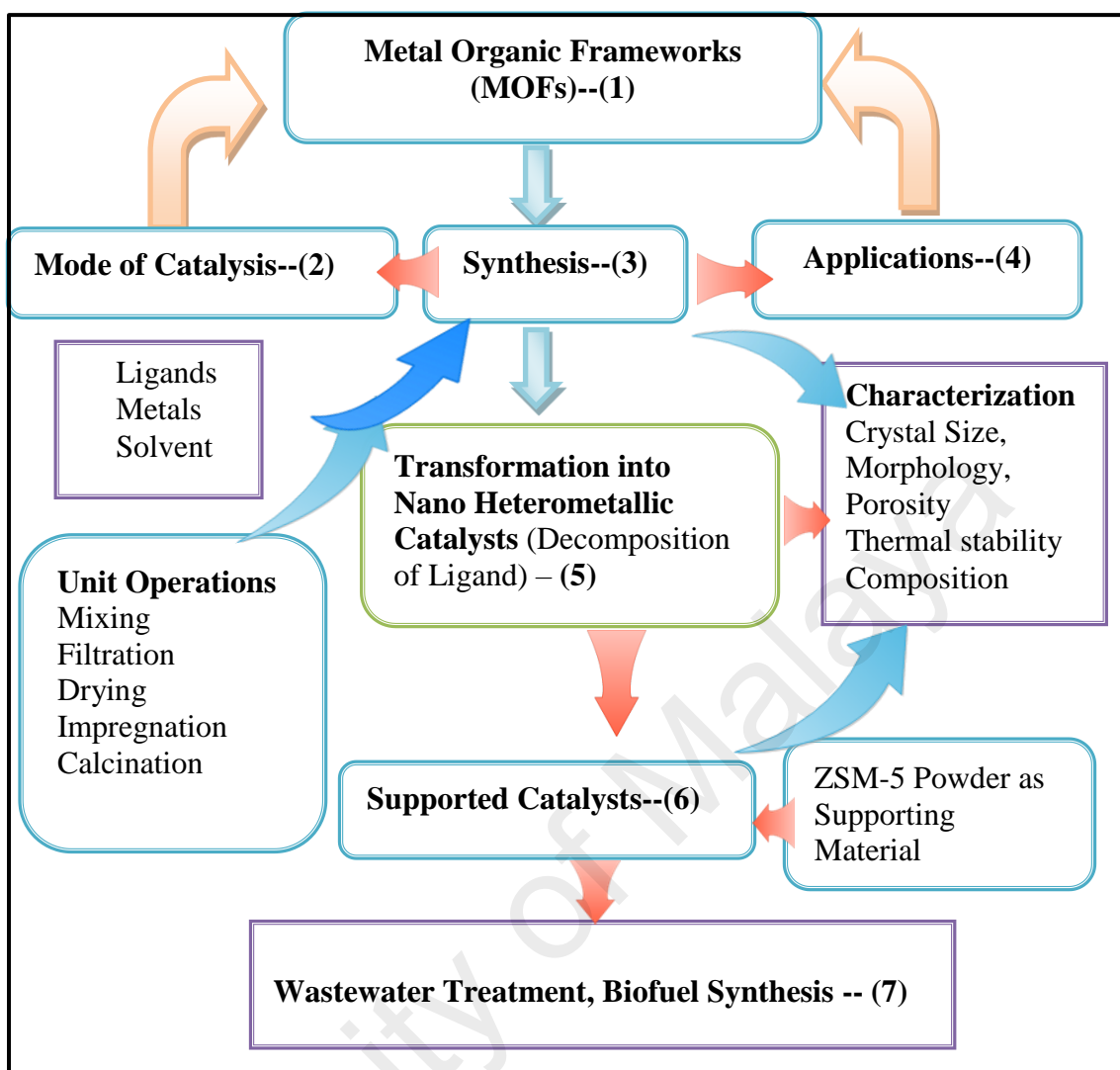


**Figure 2.1:** Framework for Literature Review

### 2.3 Metal Organic Frameworks (MOFs)

MOFs are the highly crystalline and porous materials synthesized through metal-ligand coordinate bridging, which is normally stronger than other weak bonding such as p-p stacking (Corma et al., 2010). Due to high degree of crystallinity, porosity and coordinate bonding, MOFs exhibit dynamic properties (Deng et al., 2012; Furukawa et al., 2013; Geyer et al., 2015). Like zeolites, three-dimensional arrangement of the structural units forms the system of cavities and channel. Another attractive property of MOFs is that various metal cations (mainly di, tri or tetravalent) can be used in the

development of MOFs' frameworks, which is not possible in case of conventional zeolite (Hasan & Jung, 2015). Normally, zeolites contain only a few cations such as Al, Si, and P. Therefore, due to high surface area, diverse properties and porosity, MOFs based materials are surpassing the zeolites.

Synthesis of MOF-5 in 1999 was the milestone which has opened new avenue for the development of MOFs (Chae et al., 2004; Deng et al., 2012; Yoon et al., 2011). This composite contains tetrahedral  $Zn^{4}O^{6+}$  groups interconnected through terephthalate groups and exhibits even higher specific surface area of  $2900\text{ m}^2\text{g}^{-1}$ . Another milestone was achieved with the synthesis of MOF-177, which has a surface area of  $4500\text{ m}^2\text{g}^{-1}$  (Chae et al., 2004; Deng et al., 2012; Yoon et al., 2011). Figure 2.2 illustrates the: Nitrogen sorption isotherms for MOF-2, MOF-5, MOF-177, measured at 77K. These materials show type I behavior, which is mainly expected from compounds having uniform micropores. MOF-177 is particularly prominent due to its largest reported surface area (Rowsell & Yaghi, 2004). Further research in this field revealed that choice of the organic ligand, the size of the MOFs' pores can be customized. In addition, due to these tunable pore properties, loading of metals and extremely high surface areas, MOFs are getting prominence in various applications (Furukawa et al., 2013).

Use of MOFs for clean energy production has been widely considered (Rowsell & Yaghi, 2004). Particular emphasis is given to selection and utilization of MOFs as potential platforms for storage and/or; production of hydrogen, separation of  $\text{CH}_4/\text{CO}_2$  mixtures, solar cells, fuel cells, and other green energy applications (Ho et al., 2014; Prajapati et al., 2009).

Similarly, encouraging results have been reported particularly with stable Pd-MOFs for Suzuki C–C reactions, alcohol oxidation, and olefin hydrogenation (Xamena et al.,

2007). It can be anticipated that the MOFs will capture the attention of more researchers for their used as catalytic studies in other fields. Different modes of MOFs' catalytic are discussed in the subsequent sections. Recently, MOFs have been employed as promising composites for liquid phase adsorption of a variety of hazardous and recalcitrant compounds, including nitrogen and sulfur containing compounds from both non aqueous and aqueous media. Several reviews were made to investigate the adsorption mechanisms of MOFs, used to remove the hazardous materials from aqueous medium (Hasan & Jung, 2015).

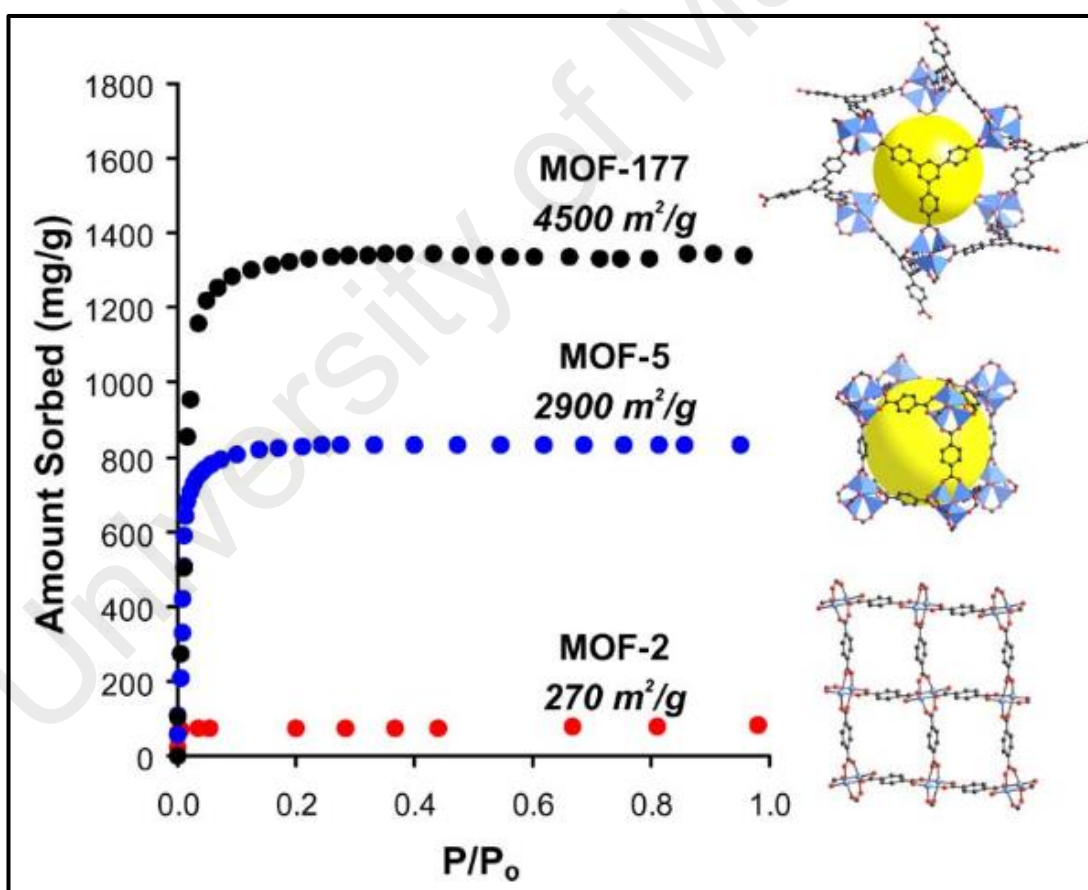


**Figure 2.2:** Nitrogen Sorption Isotherms for MOF-2, MOF-5, MOF-177, Measured at 77K

### 2.3.1 Catalysis by MOFs

All of the MOFs have three main parts including inorganic part (metals), organic part (ligand) and the channel or pore system. Therefore, three different categories are made to describe the MOFs based catalysts.

#### 2.3.1.1 MOFs with Metal Active Sites

In this category of MOFs, catalytic activity is directly linked with the metallic part, either as a single metal center or as metallic clusters, sheets or chain. Here, organic ligand only facilitates for formation of building blocks, channels and cavities, while metal part (M) simultaneously take part in the formation of structural units and also provides the active sites for catalytic activity.

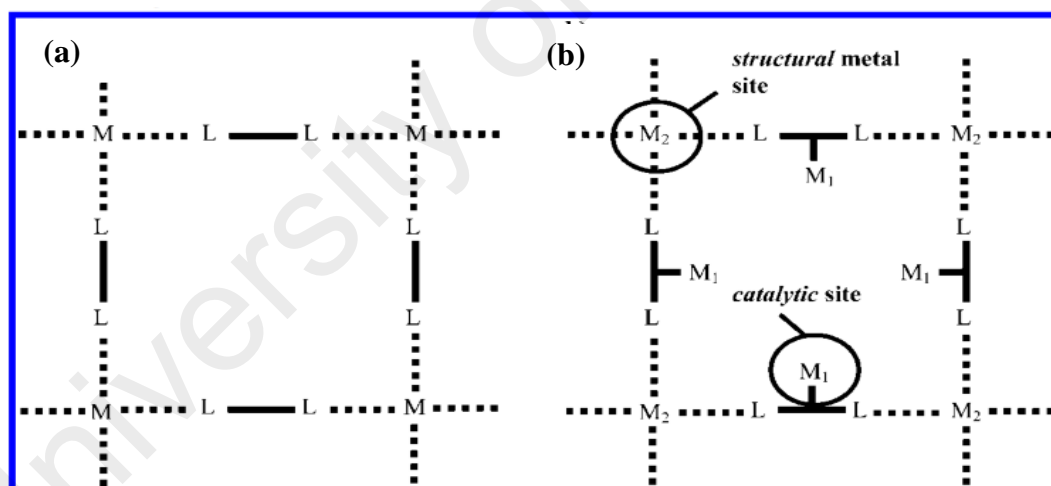


**Figure 2.3:** A Monometallic MOF with Only One Type of Metal Center (M) (a) and A Bimetallic MOF with Both Structural (M<sub>2</sub>) and Catalytic (M<sub>1</sub>) Sites (b)

There are several MOFs which have two dissimilar metals. However, at a time, only one metal (M) can provide active site (M<sub>2</sub>) for catalytic activity, while another metal (M<sub>1</sub>) can play role in the structure formation. Figure 2.3 illustrates the general structure of MOFs with active metal sites. Similarly, Table 2.1 demonstrates the applications of MOFs with metal active sites.

### 2.3.1.2 MOFs with Reactive Functional Groups

In the second class of MOFs, catalytic activity is related with the functional groups of the ligand part. These organic ligands contain different functional groups, which have ability to catalyze the specific reactions. Figure 2.4 illustrates the general structure of MOFs containing the reactive functional groups.

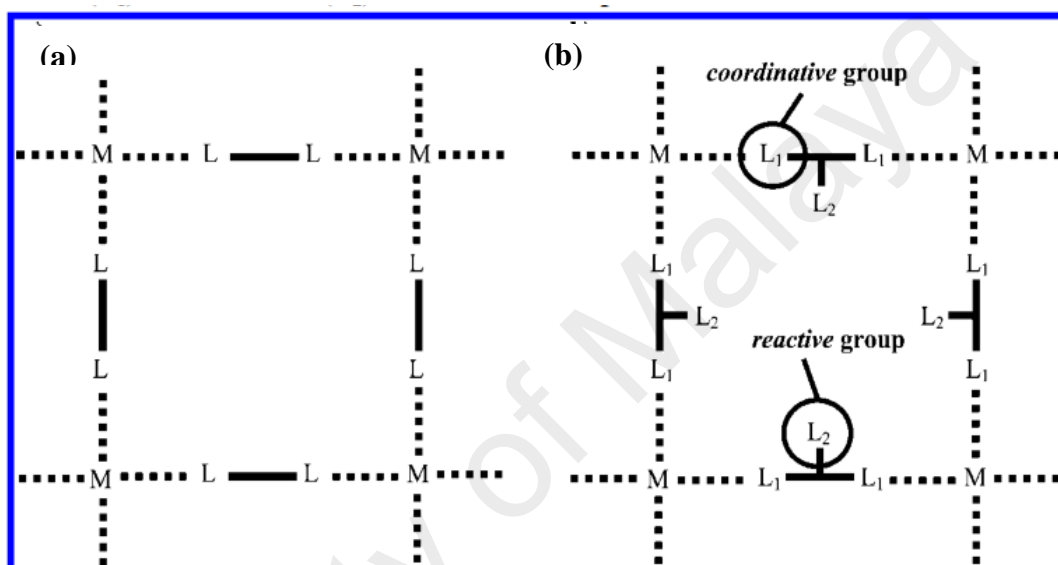


**Figure 2.4:** MOFs with Reactive Functional Groups

Mostly two different types of functional groups involve to synthesize this kind of MOFs. Coordinative groups (L<sub>1</sub>), are practiced for the construction of MOF while reactive groups (L<sub>2</sub>) is the responsible for catalytic activity as presented in Figure 2.4.

Table 2.1 demonstrates the various applications of this class of MOFs.

The number of MOFs with reactive functional groups is quite limited. This is due to requirement of the reactive group (L<sub>2</sub>) need to be available and accessible to react with the desired materials and not to be bonded with metal part of the MOF. Therefore, the synthesis of such type of MOFs is difficult as the functional groups of the organic ligand have natural tendency to make coordination with metals.

### 2.3.1.3 MOFs as Host Matrices or Nanometric Reaction Cavities

In the third scheme, both metal part and ligand part do not take part in catalysis. In this category of MOFs, porosity of the materials plays its role by providing physical space or offers its services as a cage where catalytic sites can be encapsulated.

Reaction medium in terms of hydrogen bonding, viscosity, polarity, hydrophobicity/hydrophilicity and etc. have the prominent effect on the reactivity of a system. However, in most of the cases, it is poorly understood. In a chemical reaction, particularly at molecular level, the surrounding of the reacting moieties is considered as cavity, which can be dynamic and flexible, such as when the chemical reaction is conducted in a solvent, or can be rigid like micro/mesoporous crystalline solids. Earlier, zeolites captured the attention of researchers due to their unique properties which have ability to influence the reactivity of a system in the ground as well as excited states. In this context, it was also revealed that when molecular size of substrate and host matrix have same dimensions, distortion of molecular orbital energy and geometry takes place. Due to this, electronic confinement occurs. Therefore, in case of MOFs, it is highly required to delineate the particularities of the MOFs in terms of its cavities and strength of electric fields and force potentials inside the framework.

Styrene polymerization is an example of reaction carried out inside the MOFs cavities (Uemura et al., 2005). This reaction was carried out using two different MOFs, including  $[\text{Cu}(\text{pzdc})_2(4,4'\text{-bpy})]$  (pzdc = pirazine-2,3-dicarboxylate, 4,4'-bpy= 4,4'-bipyridine) and  $[\text{M}_2(\text{bdc})_2(\text{teda})]$  ( $\text{M} = \text{Cu}^2$  or  $\text{Zn}^{2++}$ , teda = triethylenediamine). Both MOFs contains continuous and regular one dimensional nano sized channels with cross sections of  $0.82 \times 0.60$  and  $0.75 \times 0.75 \text{ nm}^2$ , respectively (Uemura et al., 2005). Figure 2.5 illustrates the process flow diagram.

In spite of attaining similar loadings of styrene, polymerization reaction was not noticed in  $[\text{Cu}(\text{pzdc})_2(4,4'\text{-bpy})]$  even at high temperature (373 K). HNMR spectroscopy was used to study this polymerization. This failure inside pyrazine based MOF may be attributed to the restricted mobility of styrene inside the pores of MOF (very broad NMR peak was detected). However, with benzene-dicarboxylate based MOF, high mobility with rapid rotation around the C1-C4 axis of styrene ring was detected (Uemura et al., 2005). However, anionic polymerization of methyl propiolate was best carried out in  $[\text{Cu}(\text{pzdc})_2(4,4'\text{-bpy})]$ .

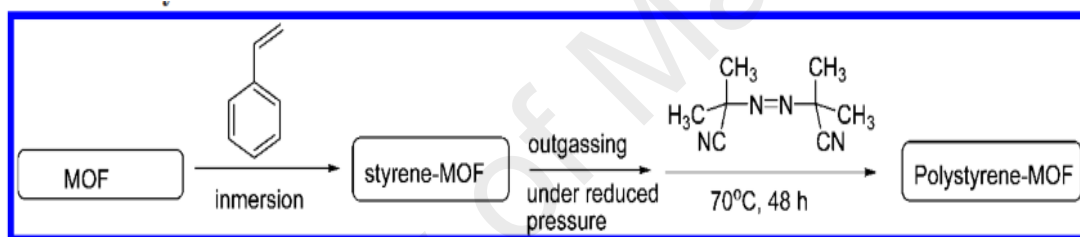


**Figure 2.5:** Styrene Radical Polymerization Procedure Inside MOFs

This may be attributed to the noticeable Lewis basicity of the carboxylate oxygen atoms (Uemura et al., 2005; Uemura et al., 2006). On the other side, when azodiisobutyronitrile (AIBN) as a radical was used to initiate styrene polymerization, the radical polymerization was noticed successful with  $[\text{M}_2(\text{bdc})_2(\text{teda})]$ . The yield of the polymer was about 70%. Beside this no change due to the nature of the  $\text{Cu}^{2+}$  or  $\text{Zn}^{2+}$  metal was noticed (Corma et al., 2010; Uemura et al., 2006).

In the MOFs, metal component can be formed using a variety of transition metals, highly required in Lewis acid based catalysis. In addition to this, the organic part of the MOF can easily support both acid and base or their combination, which have ability to

carry out the cascade reactions. Therefore, there is a lot of potential in the chemical industry in employing MOFs as replacement of other heterogeneous catalysts. An unique feature of MOFs, is that it can be used as enantioselective catalysts, which cannot be possible in zeolites. Normally, asymmetric syntheses are required in the formation of drugs, and these types of reactions are carried out using homogeneous catalysts which have high costs. Through the application of chiral ligands, a variety of newly developed MOFs would be possible to be evaluated in this field.

Bearing in mind the ease of the production of MOFs and their less cost, it will be essential to explore if MOFs can perform in asymmetric reactions or at larger scale, effectively substituting the homogeneous catalysts. Researchers are hopeful that, as like zeolites, gradual introduction of MOFs as industrial catalysts will boost further research in this area. Table 2.1 illustrates the possible potential in the industry for MOFs as replacement of other heterogeneous catalysts (Corma et al., 2010; Rowsell & Yaghi, 2004; Sugikawa et al., 2013; Wijngaarden et al., 2008).

However, despite their higher metal content compared to zeolites, the use of MOFs in heterogeneous catalysis is restricted due to their relatively low stability at elevated temperature and in the presence of water vapor or chemical reagents. In addition, the metal ions in MOFs are often blocked by the organic linker molecules and are therefore not accessible for catalytic reactions.

**Table 2.1:** MOFs with Metal Active Sites (Corma et al., 2010)

MOF	Active metal	Catalyzed Reaction(s)
[RhCl(CO)(1,4-dicb)] [M(4,4'-dicbp) <sub>x</sub> ]	Rh <sup>+</sup> M = Pd <sup>0</sup> ( $x = 1.82 \pm 0.12$ ) M = Pt <sup>0</sup> ( $x = 1.25 \pm 0.2$ )	1-hexene hydrogenation/isomerization 1-hexene hydrogenation/isomerization
[MCl <sub>2</sub> (4,4'-dicbp)]	M = Pd <sup>2+</sup> , Pt <sup>2+</sup>	alkene and alkyne hydrogenation/isomerization
[RhCl(4,4'-dicbp) <sub>2</sub> ]	Rh <sup>+</sup>	1-hexene hydrogenation/isomerization
[RuCl <sub>2</sub> (1,4-dicb) <sub>2</sub> ][RuCl <sub>2</sub> (1,4-dicb) <sub>3</sub> ]	Ru <sup>2+</sup>	1-hexene hydrogenation/isomerization
[Cd(4,4'-bpy) <sub>2</sub> ](NO <sub>3</sub> ) <sub>2</sub>	Cd <sup>2+</sup>	(shape-selective) cyanosilylation of aldehydes/imines
[ <i>cis/trans</i> -(OArO) <sub>x</sub> Ti(py) <sub>y</sub> ] (OArO = aryldioxide)	Ti <sup>4+</sup>	ethylene and propylene polymerization
[Ln(7-H <sub>2</sub> )(7-H <sub>3</sub> )(H <sub>2</sub> O) <sub>4</sub> ]	Ln = La, Ce, Pr, Nd, Sm, Gd, Tb	cyanosilylation of aldehydes ring opening of <i>meso</i> -anhydrides
[Pd(2-pymo) <sub>2</sub> ]	Pd <sup>2+</sup>	(shape-selective) hydrogenation of olefins
IRMOF-3-SI-Au(SIsalicylideneimine)	Au <sup>3+</sup>	oxidation of alcohols Suzuki C-C coupling 3-component coupling and cyclization
MIL-101(Cr)-proline	Cu <sup>2+</sup>	various acid-catalyzed reactions
[Yb(C <sub>4</sub> H <sub>4</sub> O <sub>4</sub> ) <sub>1.5</sub> ]	Fe <sup>3+</sup>	Friedel-Crafts benzylation

**Table 2.1: MOFs with Metal Active Sites (Continued)**

MOF	Active metal	Catalyzed Reaction(s)
IRMOF-3-SI-VO(acac)(SIsalicylideneimine)	V(O)acac <sub>2</sub> (acac = acetylacetonate)	hydrogenation of 1,3-butadiene
		oxidation of cyclohexene
PIZA-3	Mn <sup>3+</sup>	hydroxylation of linear and cyclic alkanes
[Cu(2-pymo) <sub>2</sub> ]	Cu <sup>2+</sup>	oxidation of tetralin (with air)
[Co(bzim) <sub>2</sub> ] (ZIF-9)	Co <sup>2+</sup>	
MIL-101(Cr)	Cr <sup>3+</sup>	oxidation of tetralin (with BuOOH)
[Zn <sub>2</sub> (bpdC) <sub>2</sub> (salenMnCl)]	Mn <sup>3+</sup>	enantioselective olefin epoxidation
[Co(bpb)] (MFU-3)	Co <sup>2+</sup>	cyclohexene oxidation
[Cu <sub>2</sub> (1,4-chdc) <sub>2</sub> ]	Cu <sup>2+</sup>	oxidation of alcohols
V <sub>6</sub> O <sub>13</sub> -Co-MOF	V <sub>6</sub> O <sub>13</sub>	oxidation of thiols
V <sub>6</sub> O <sub>13</sub> -Tb-MOF	V <sub>6</sub> O <sub>13</sub>	oxidation of thiols
RPF-4	Ln = La, Ce, Pr, Nd, Sm, Eu, Gd, Tb, Dy, Er, Yb	oxidation of sulfides
[Yb(C <sub>4</sub> H <sub>4</sub> O <sub>4</sub> ) <sub>1.5</sub> ]	Yb <sup>3+</sup>	acetalization of aldehydes oxidation of sulfides hydrodesulfurization
MIL-101(Cr)-proline	Cu <sup>2+</sup>	various acid-catalyzed reactions

**Table 2.1:** MOFs with Metal Active Sites (Continued)

MOF	Active metal	Catalyzed Reaction(s)
[Zn <sub>2</sub> (bdc)(L-lact)(dmf)]	Zn <sup>2+</sup>	Oxidation of sulfides
MIL-101(Cr)	Cr <sup>3+</sup>	Oxidation of sulfides
[Na <sub>20</sub> (Ni <sub>8</sub> (4,5-IDC) <sub>12</sub> )]	Ni <sup>2+</sup>	CO oxidation to CO <sub>2</sub>
[Cu(5-mipt)]	Cu <sup>2+</sup>	CO oxidation to CO <sub>2</sub>
[Ni <sub>2</sub> (H <sub>2</sub> O) <sub>2</sub> (2,3-pydca) <sub>2</sub> (4,4'-bpy) <sub>2</sub> - U <sub>5</sub> O <sub>14</sub> (H <sub>2</sub> O) <sub>2</sub> (OAc) <sub>2</sub> ] · 2H <sub>2</sub> O	U <sub>5</sub> O <sub>14</sub>	photocatalysis
[Co <sub>2</sub> (4,4'-bpy)(oba) <sub>2</sub> ][Ni <sub>2</sub> (4,4'-bpy) <sub>2</sub> (oba) <sub>2</sub> ]-	Co <sup>2+</sup> /Ni <sup>2+</sup> /Zn <sup>2+</sup>	photocatalysis
[Zn <sub>2</sub> (4,4'-bpy)(oba) <sub>2</sub> ]	Zn <sub>4</sub> O <sub>13</sub>	photocatalysis
[Zn <sub>4</sub> (O)(bdc) <sub>3</sub> ] (MOF-5) IRMOF's	Zn <sub>4</sub> O <sub>13</sub>	photocatalysis
[Cu <sub>3</sub> (btc) <sub>2</sub> ] (HKUST-1)	Cu <sup>2+</sup>	aldehyde cyanosilylation
Mn <sub>3</sub> [(Mn <sub>4</sub> Cl) <sub>3</sub> (btt) <sub>8</sub> (CH <sub>3</sub> OH) <sub>10</sub> ] <sub>2</sub>	Mn <sup>2+</sup>	cyanosilylation of carbonyls
MOF POST-1	Cr <sup>3+</sup>	Mukaiyama-aldol condensation aldehyde cyanosilylation
MOF POST-1	Yb <sup>3+</sup>	hydrodesulfurization

**Table 2.1:** MOFs with Metal Active Sites (Continued)

MOF	Active metal	Catalyzed Reaction(s)
[Yb(C <sub>4</sub> H <sub>4</sub> O <sub>4</sub> ) <sub>1.5</sub> ]	Fe <sup>3+</sup>	Friedel-Crafts benzylation
[Cu <sub>2</sub> (pzdc) <sub>2</sub> (4,4'-bpy)] [Zn <sub>4</sub> (O)(ata) <sub>3</sub> ](IRMOF-3) MIL-101(Cr)-ED	[Cd(4-btapa) <sub>2</sub> (NO <sub>3</sub> ) <sub>2</sub> ] MIL-53(NH <sub>2</sub> ) MIL-101(Cr)-ED	ZnEt <sub>2</sub> addition to aldehydes

**Table 2.2:** MOFs with Reactive Functional Groups (Corma et al., 2010)

MOF	Active metal	Catalyzed Reaction(s)
POST-1	pyridyl group	(size-/enantioselective) transesterification
[Cu <sub>2</sub> (pzdc) <sub>2</sub> (4,4'-bpy)]	carboxylate oxygen	polymerization of acidic acetylenes
[Cd(4-btapa) <sub>2</sub> (NO <sub>3</sub> ) <sub>2</sub> ]	amide	Knoevenagel condensation
[Zn <sub>4</sub> (O)(ata) <sub>3</sub> ](IRMOF-3) MIL-53(NH <sub>2</sub> )	amino	Knoevenagel condensation
MIL-101(Cr)-ED	amino	Knoevenagel condensation
MIL-101(Cr)-proline	proline	asymmetric aldol reaction

## 2.4 Synthesis of MOFs

MOFs are usually synthesized in the liquid phase, either by using a single solvent or a blend of solvents. The produced crystalline frameworks having metal organic coordinate bonding in their structural units. In most of the cases, MOFs are synthesized through the mixing of two solutions containing the organic ligand and metal component, either at ambient conditions or under solvothermal environment. Sometime addition of an secondary molecules is also required. A variety of the metals atoms with their stable oxidation states have been utilized to synthesize MOFs. These metals from the groups include alkaline, alkaline earth, transition metals and even rare earth group. In case of organic ligand, rigid molecules are normally used, since they result into highly crystalline, stable and porous MOFs (Corma et al., 2010; Nazir et al., 2011; Yoon et al., 2011).

Selections for ligands are linked with the some of the nuclei and their derivatives such as bipyridines, polycarboxylic aromatic molecules, polyazaheterocycles and etc. Both charged and neutral molecules can be employed. However, cationic based organic ligands are not used commonly to synthesize the MOFs, because they have less affinity to make coordinate bond with metal cations. Kaes et al. (2000) claimed that the 2,2'-bipyridine is the most widely used ligand, particularly used in the synthesis of 2,2'-bipyridine metal complexes.

Bipyridines also known as bipyridyls, and dipyrindines are a family of chemical compounds with the formula  $C_{10}H_8N_2$ , which are formed by the coupling of two pyridine rings. They are aromatic nitrogen heterocycles that form complexes with most transition metals. They interact with metals via both  $\sigma$ -donating nitrogen atoms and  $\pi$ -accepting molecular orbitals. The 2,2'-bipyridine is widely used as a metal chelating ligand because of its ease of functionalization and robust redox stability (Kaes et al., 2000). As

compared to other available ligands, like catechol (dianionic), and derivatives of acetylacetonate (monoanionic), 2,2' bipyridine is a neutral ligand. Therefore it has ability to form charged complexes having metal cations, and due to this unique property a large number of metal-bipyridine complexes are synthesized for a variety of applications (Kaes et al., 2000).

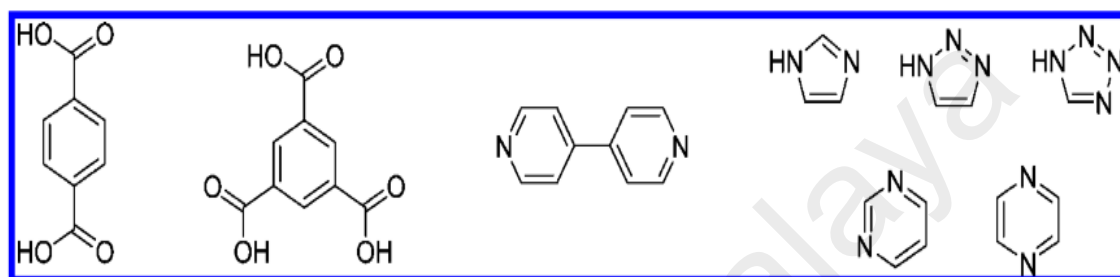


**Figure 2.6:** Polycarboxylic Aromatic Molecules, Bipyridines, and Polyazaheterocycles as linkers for MOFs Preparation

The nature of the solvent, and the presence of other auxiliary molecules also effect the crystal structure of the synthesized MOFs (Corma et al., 2010; Li et al., 2014; Rowsell & Yaghi, 2004; Yoon et al., 2011). Therefore with a same metal-ligand combination, different structures can be formulated using different synthesis parameters. For example, of zinc imidazolate can be synthesized up to seven different frame works having general formula  $[Zn(im)_2 \cdot xG]$  (im = imidazolate, G = guest molecule,  $x = 0.2-1$ ) (Tian et al., 2007). Prior studies were reported with the same organic ligand and metal (imidazolate and  $Zn^{2+}$ ) for the synthesis of all zinc imidazolate based MOFs, and the only parameter, solvent was altered during their synthesis (Corma et al., 2010; Tian et al., 2007). In addition, prominent effect of the secondary molecules on the imidazolate ring was observed for attaining the final crystalline structure (Ren et al., 2008; Wang et al., 2012b). Similarly, most of the researchers used DMF, THF, methanol, ethanol and propanol as solvents. However, DMF was found most powerful

solvent to coordinate a large number of metals. It can simultaneously act as solvent as well as ligand (Bae et al., 2008; Li & Du, 2011; Senkovska & Kaskel, 2006).

Numerous patterns are available in the literature related to MOFs, in which a certain binary metal-ligand system can produce different structures, mainly depending on the specific process conditions (Corma et al., 2010; Deng et al., 2012; Eddaoudi et al., 2001; Farha & Hupp, 2010). Synthesis of MOFs can be classified into three major classes. The detail of each scheme is provided in the following sections.

#### 2.4.1 Synthesis of MOFs with Unsaturated Metal Sites

This includes the preparation of MOFs based materials in which the metal centers are not totally blocked by the organic spacers. To achieve unblocking, usually labile ligands are used, which can be eliminated during the activation stage, before to use these MOFs as catalysts. Labile ligands are solvent based molecules, which provide free coordination positions in the metallic part of MOFs.

$\text{Cu}_3(\text{btc})_2$  (btc = 1,3,5-benzenetricarboxylate) material HKUST-1 is an example of this approach. In this MOF, water molecule is removed from copper sites through thermal activation, thus leaving an accessible coordination vacancy on the Cu (Figure 2.7). An another complex example is revealed with the MOF,  $[\text{Mn}(\text{dmf})_6]@[(\text{Mn}_4\text{Cl})_3(\text{btt})_8(\text{H}_2\text{O})_{12}]_2$  (btt = 1,3,5-benzenetristetrazolate) well explained by Dinca et al. (2006). Here,  $[\text{Mn}(\text{dmf})_6]^{2+}$  complexes are clathrated inside sodalite-type cages formed by square-planar 1,3,5-benzenetristetrazolate(btt) ligand and  $\text{Mn}_4\text{Cl}$  clusters.

By replacing the dmf molecules with methanol and eliminating at 423 K, the subsequently resulted material offers two types of exposed Mn sites: (a) five-coordinated sites I originated from framework  $\text{Mn}^{2+}$  ions of the  $\text{Mn}_4\text{Cl}$  clusters after elimination of a  $\text{H}_2\text{O}$  molecule and (b) two-coordinated sites II which are linked to  $\text{Mn}^{2+}$

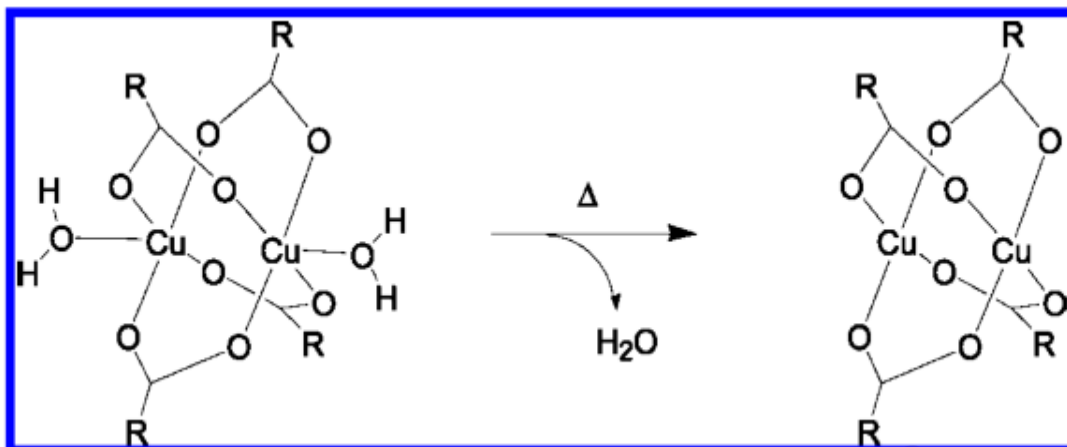


**Figure 2.7:** A Free Coordination Position in the Metal after Removal of H<sub>2</sub>O

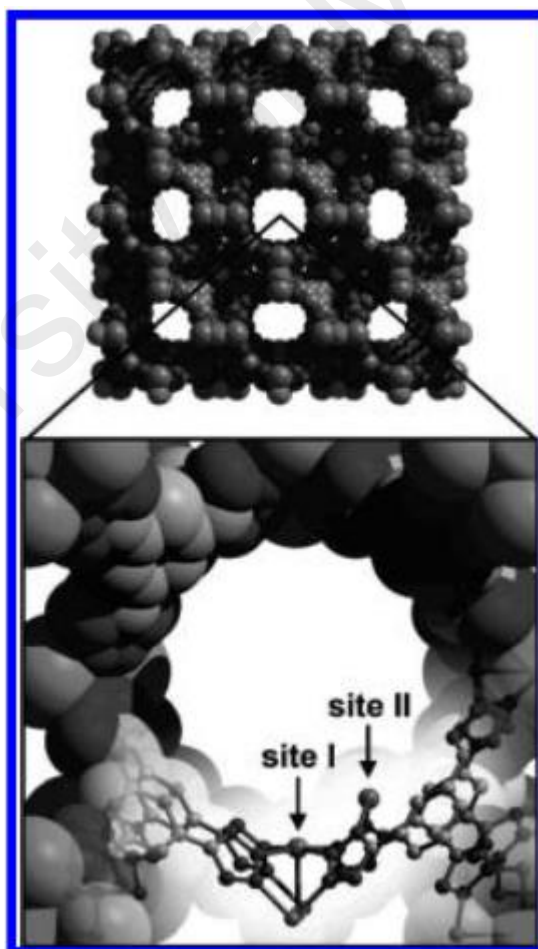


**Figure 2.8:** Material with two types of exposed Mn sites: (a) five-coordinated sites I  
(b) two-coordinated sites II

ions formerly in the additional framework  $[\text{Mn}(\text{dmf})_6]$  complexes, and which continue its coordination with two N atoms belong to neighboring tetrazole rings after elimination of the dmf molecules (Figure 2.8).

Development of MOFs having unsaturated metal centers is particularly used to synthesize materials for gas storage applications (Dinca et al., 2006; Dincă & Long, 2008; Vitillo et al., 2008). Actually, the presence of this open type metal enhances the adsorption and catalysis because it strongly favors the direct interaction between the substrate and metal reactive site (Chowdhury, 2016; Gygi et al., 2016).

#### **2.4.2 Synthesis of MOFs with Metal as Structural Units**

In this scheme, the MOF can be synthesized as an ordered three-dimensional array of metal coordination complexes. Through this scheme a large number of MOFs, have been synthesized.

Noro et al. (2002) and Kitagawa et al. (2006) have focused to synthesize another type of MOF by using a previously prepared  $\text{Cu}(\text{2,4-pydc})_2$  complex (2,4-pydc = pyridine-2,4-dicarboxylate) employing as a metalloligand, which was further allowed to coordinate to  $\text{Zn}^{2+}$  cations through one of the carboxylate clusters to form a three-dimensional structure. Here,  $\text{Zn}^{2+}$  simply plays its role as a structural unit, while  $\text{Cu}^{2+}$  cations were responsible for guest coordination. These researchers have also synthesized a series of MOFs having metal Schiff base complexes,  $\text{M}(\text{H}_2\text{salphdc})$  ( $\text{M} = \text{Cu}^{2+}$ ,  $\text{Ni}^{2+}$ , or  $\text{Co}^{2+}$ , salphdc = N,N'-phenylenebis (salicylidene-imine) dicarboxylate), with  $\text{Zn}^{2+}$  cations at the nodes (Corma et al., 2010; Kitagawa et al., 2006; Noro et al., 2002). However, these researchers did not evaluate the catalytic activity of the prepared materials.

Wu et al. (2005a) have synthesized a homochiral MOF containing  $\text{Cd}^{2+}$  cations and the chiral ligand (R)-6,6'-dichloro-2,2'-dihydroxy-1,1'-binaphthyl-4,4'-bipyridine as the structural unit. The ligand coordinates to  $\text{Cd}^{2+}$  through pyridine nitrogen and chlorine, whereas the two hydroxyl groups of the binaphthyl specie remain unbonded and pointing to the networks. Addition of titanium isopropoxide as post synthesis modification of this MOF, resulted into a titanium containing material, with titanium diisopropoxide grafted to the walls of the MOF through the dihydroxy groups (Corma et al., 2010; Wu et al., 2005b). Several researchers also synthesized bimetallic based MOFs containing Y or Gd ions as building nodes along with  $\text{Pt}^{2+}$  ions as catalytic active sites. In both complexes,  $\text{Pt}^{2+}$  ions have made four-coordination bonds, two with N atoms of 2,2'-bipyridine-4,4'-dicarboxylate (bpydc) (4) and two with Cl, resulting into a mimic structure of homogeneous coordination complexes with  $\text{Pt}^{2+}$  linked to N-containing ligands by electron donation (Corma et al., 2010; Szeto et al., 2006; Szeto et al., 2007). Similarly, use of anionic based diazaheterocycles 2-pymo and bzim organic ligands can produce MOFs having single metal sites linked to four nitrogen atoms and that can be effectively employed in catalysis. This was confirmed through the synthesis of  $[\text{Pd}(2\text{-pymo})_2]$ ,  $[\text{Cu}(2\text{-pymo})_2]$ , and  $[\text{Co}(\text{bzim})_2]$  following the previously described techniques, which were noticed to be active in a large number of reactions linking the metal center and for which analogous homogeneous complexes are known to be active (Navarro et al., 2006; Tabares et al., 2001).

### 2.4.3 Postsynthesis Modifications of MOFs

Post synthesis is basically modification schemes used to synthesize tailored MOFs, with improved features for applications in catalysis and, gas adsorption. In this scheme, covalent attachment is introduced to the organic linker, for the functionalization of the framework. Another approach is the grating is of organic molecules at metal sites

vacancies produced after the removal of solvent (Horike et al., 2013; Li et al., 2012; Madrahimov et al., 2014; Sun et al., 2013). Covalent based post synthesis of the organic linkers are getting prominence in the recent reports (Ezugwu et al., 2016; Karmakar et al., 2016; Wang & Cohen, 2007). An existing MOF containing functional groups not directly linked with the metal sites, was transformed through a covalent reaction subsequently, as opposite to the “pre-synthesis” strategy used. In this synthesis approach, the amino groups of IRMOF-3 (a material with composition  $[Zn_4O(ata)_3]$ , ata = 2-aminoterephthalate) were introduced to react with isocyanates or alkyl anhydrides (Corma et al., 2010; Wang & Cohen, 2007).

This idea was further followed by Costa et al. (2008) to synthesize a MOF containing Gd(III) and 2-aminoterephthalate ligands. The amino group of the organic linker was post-synthesized using two different functionalities, by reacting either with a carboxylic acid or with an isocyanate. Postsynthesis of MOFs is also applied in different scenarios. Goto et al. (2008) used an azide based functionalized ligand that was reacted with organic molecules bearing a terminal alkyne (through a click reaction using CuBr as the catalyst), as revealed in Figure 2.9. Through this, the researchers have presented hanging groups with several functionalities: alcohol, ester, and alkyl chain. However, efforts to react carboxylic acid and amino groups following the same scheme caused the dissolution of the MOF (Corma et al., 2010; Goto et al., 2008).

Ingleson et al. (2008) have explained the synthesis of Brønsted acid sites based material using postsynthesis protonation of the carboxylate ligands of a MOF with anhydrous HCl.

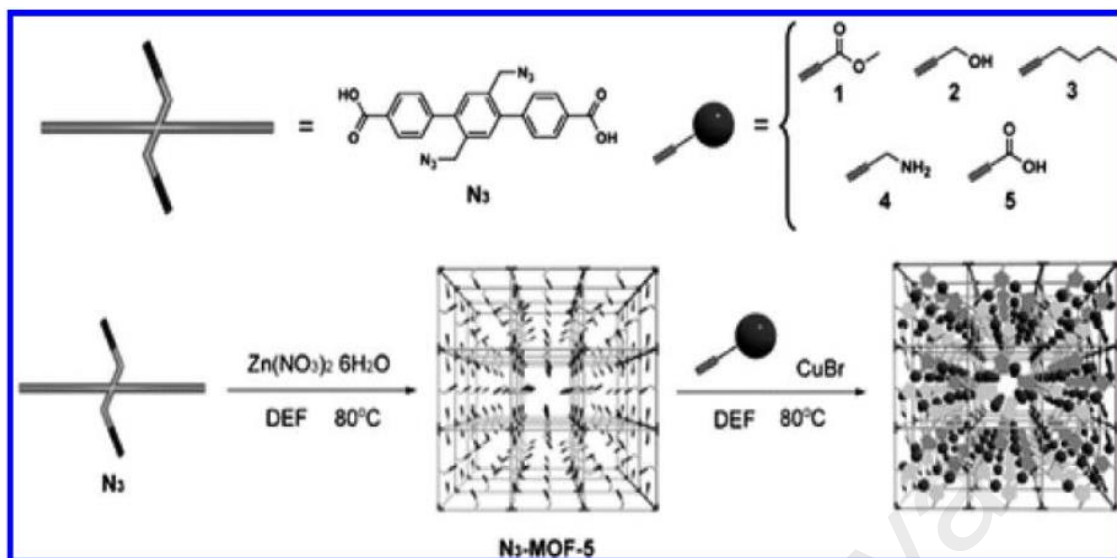


**Figure 2.9:** Postsynthesis Modification of a MOF Bearing an Azide Ligand through Copper Catalyzed Click Reaction

They have also reported the new reform in the amino groups of IRMOF-3 introducing salicylaldehyde to produce corresponding imine. This ligand was utilized to complex metal ions, as validated by covalently anchoring vanadyl acetylacetonate. First, a covalent functionalization of the available amino groups of IRMOF-3 was carried out with salicylaldehyde to form the salicylideneimine, and in a second step, Au(III) sites were coordinated to the Schiff base complex. The two-step process is shown in Figure 2.10.

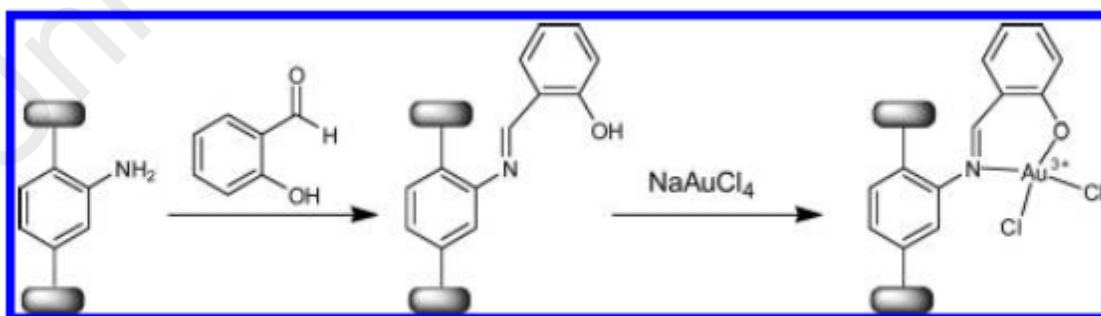


**Figure 2.10:** The modification of the Amino Groups of IRMOF-3 to Form the Imine Leading to Au(III)-Schiff Base Complex

An approach was also introduced to substitute covalent modifications using anchoring to metal coordination vacancies of the MOF organic molecules containing

heteroatoms with lone electron pairs. This scheme was initiated by Hwang et al. (2008), who carried out the grafting of an amine pendant group to the chromium sites of the chromium terephthalate MIL-101, using ethylenediamine. Banerjee et al. (2009) have adopted the anchoring approach to compose chromium sites of MIL-101 proline moiety terminated through a pyridine group, which has facilitated the synthesis of a MOF-based organo-catalyst. Similarly, Demessence et al. (2009) have used this scheme to anchored ethylenediamine to the coordinative unsaturations.

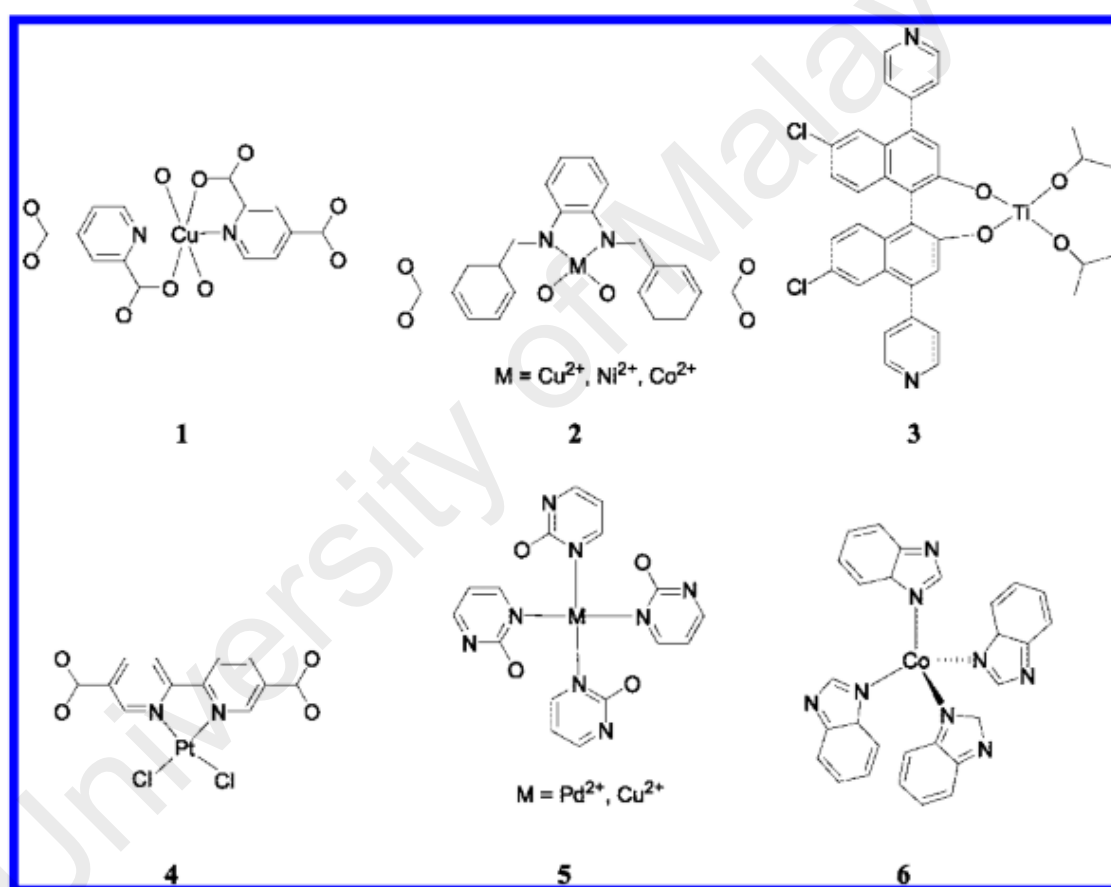


**Figure 2.11:** Isomorphous Substitution in MOFs

A totally different strategy of isomorphous substitution was also introduced as a postsynthesis modification. In this scheme, central metal is replaced with other suitable metal. Das et al. (2009) described the isomorphous substitution, as metathesis exchange process leading to a fully reversible substitution of framework Cd<sup>2+</sup> ions by Pb<sup>2+</sup> in a

MOF single crystal, without disturbing its crystalline integrity (Figure 2.11). This scheme was also confirmed through the exchange of  $\text{Cd}^{2+}$  ions with trivalent lanthanide cations  $\text{Nd}^{3+}$  or  $\text{Dy}^{3+}$ , which formed the positively charged MOFs. This excess charge was compensated by extra framework  $\text{NO}_3^-$  anions. At this time, this specific case of metathesis process does not have an immediate application for catalysis. However, it describes the possibility of tuning the reactivity of a synthesized MOF by postsynthesis choosing the concentration and identity of the metal ions creating the framework.

Overall, MOFs are usually synthesized through the mixing of two solutions containing the organic ligand and metal component, either at ambient conditions or under solvothermal environment. Metals from the groups include alkaline, alkaline earth, transition metals and even rare earth group can be used to synthesize a MOF. In addition, 2,2'-bipyridine is found the most widely used ligand, because of its ease of functionalization and robust redox stability. Similarly, dimethyl formamide (DMF) was found a powerful solvent can be used effectively for metal-ligand coordination. Three different scheme of synthesis are used to synthesize a wide range of MOFs.

#### **2.4.1 MOFs Derived Heterometallic Catalysts Synthesis**

In many industrial applications, direct use of MOFs as catalysts is not possible due to their relatively limited thermal and chemical stability. In addition, the metal ions in MOFs are often blocked by the organic linker molecules and are therefore not accessible for catalytic reactions. The low thermal stability of the crystal structure is certainly a limiting factor for vapor-phase reactions carried out at temperatures above 573 K. Thus, we cannot expect MOFs to play an important role as catalysts for oil-refining or petrochemical processes taking place at temperatures of 573 K. This will be even more so for reactions that are accompanied by formation of coke or heavier residual products that have to be removed by combustion. There is no doubt that, under

these circumstances, zeolites will be preferred over MOFs.

However, several researchers have prepared heterometallic catalysts via MOFs (Mahata et al., 2006; Mansoor et al., 2015; Maza et al., 2014). These methods have significantly improved the efficiency, stability and the reusability of catalysts for environmental and green energy applications (Kim et al., 2013b; Kong et al., 2014). Table 2.3 provides the recently synthesized monometallic and heterometallic catalysts. These involve the 2,2'-bipyridine ligand for metal complex formation, which was eliminated thermally to produce nano size metallic particles (Nazir et al., 2013; Parveen et al., 2013).

Several researchers also tried to combine the MOFs and zeolites. In case of MOFs and zeolites based synthesis, most of the host-guest inclusion complexes in zeolites have been prepared by adsorption of the molecule or species from the exterior to the interior of the zeolite micropores, or in some cases by introducing them as organic structure-directing agents. Polymers, being macromolecules of large kinetic diameter, cannot diffuse inside the zeolite micropores. For this reason, there are numerous studies showing different methodologies to prepare composites in which the organic polymer is hosted inside the zeolite voids. The majority of them are based on the adsorption of a suitable monomer that, in a subsequent step, undergoes polymerization inside the channels (Corma et al., 2010; Yoon et al., 2011). This area is interesting due to combining the features of MOFs and zeolite into single heterometallic; however, it has limited data available.

In addition to synthesis techniques, transformational operations involve also have significant effects on the transformation, yield, and activity MOFs derived catalysts. Numerous methods are used to transform the MOFs into heterometallic catalysts. Mostly, thermal degradation based techniques are used to eliminate the ligand part from

the MOFs (Xu et al., 2012b; Zhang et al., 2015). Thermal degradation or calcination in the presence of air results into formation of metallic oxide. During calcination stage formation of new compounds may occur, particularly if the thermal treatment is performed at higher temperatures (Knozinger & Weitkamp, 1997). Therefore, to avoid formation of oxides or other side materials, inert media (nitrogen, helium and argon) is introduced with controlled flowrates (Nazir et al., 2013; Parveen et al., 2013). The quantity and morphology of the materials is also important in the selection of the furnace. Smaller batches of powdered MOFS based catalysts are calcined in muffle or box furnaces with trays, as like in the case of drying. The gases that are mainly used for heating are in direct contact with the material being calcined. Pellets are calcined in tunnel or belt type furnaces (Knozinger & Weitkamp, 1997).

Alternate techniques frequently used to prepare nano size heterometallic materials via MOFs are chemical vapor deposition (CVD) and aerosol assisted chemical vapor deposition (AACVD) (Ahmed et al., 2014; Liu et al., 2015; Wang et al., 2015c). These methods are also used to transform the gaseous catalyst precursors into catalysts coatings (Bhaviripudi et al., 2010).

**Table 2.3:** MOFs Based Monometallic and Heterometallic Catalysts

MOFs	Target Material/Catalyst	Reference
[Fe(bipy) <sub>3</sub> ]Cl <sub>2</sub>	Fe nano particles	(Nazir et al., 2011)
[Ni(bipy) <sub>2</sub> ]Cl <sub>2</sub>	Ni nano particles	(Parveen et al., 2013)
[Fe(bipy) <sub>3</sub> ]Cl <sub>2</sub> [Mo(bipy)Cl <sub>4</sub> ]	Fe <sub>100-x</sub> Mo <sub>x</sub>	(Nazir et al., 2013)
[Ag <sub>43</sub> (C <sub>5</sub> H <sub>5</sub> N) <sub>2</sub> ] <sub>n</sub> ·nNO <sub>3</sub> ·2nH <sub>2</sub> O	Ag <sub>2</sub> S nanorods	(Sultan et al., 2012)
{[Co <sub>2</sub> (C <sub>10</sub> H <sub>8</sub> N <sub>2</sub> )] [C <sub>12</sub> H <sub>8</sub> O(COO) <sub>2</sub> ] <sub>2</sub> }	Co <sub>3</sub> O <sub>4</sub>	(Mahata et al., 2006)

## 2.5 Summary of Overall Literature Review

Metal Organic Frameworks (MOFs) based new classes of catalysts have shown outstanding potential because of their controllable structure, unique properties and large surface areas. MOFs are usually synthesized through the coordination of the metals with ligands. A large number of metals particularly, transition metals are used to synthesize the MOFs. In addition, 2,2'-bipyridine is found the most widely used ligand, because of its ease of functionalization and robust redox stability. MOFs as catalysts have shown great potential for green energy and environmental applications. However, in many applications, direct use of MOFs as catalysts is not possible due to their relatively limited thermal and chemical stability. To overcome these issues, several researchers have prepared heterometallic catalysts via metal organic frameworks (MOFs). These methods have significantly improved the efficiency, stability and the reusability of catalysts. Beside this, several researchers also tried to combine the MOFs and zeolites. This area is interesting because of the combining the unique features of MOFs to thermal stable zeolite, resulting into a single heterometallic system. However, limited data available is in this respect. In addition, it was also found that the MOFs formation via precipitation based method, followed by impregnation and/or thermal decomposition can produce bulk quantities of heterometallic catalysts. Through this route, synthesis of ultrafine, fine and coarse materials is possible. Therefore, this research would focus on MOFs production via precipitation followed by thermal decomposition to synthesize nano heterometallic catalysts.

## CHAPTER 3: GENERAL METHODOLOGY

### 3.1 Introduction

In this chapter, general methodology for the synthesis of unsupported and supported heterometallic catalysts, and characterization are explained. These catalysts were synthesized by a newly developed 2-step process and decomposed thermally to form heterometallic nano oxides. The specific detail methodology for a particular catalyst has been explained in the respective chapter.

### 3.2 Synthesis of Unsupported Catalysts

Figure 3.1 shows the general process flow diagram for the synthesis of unsupported catalysts. In the first step monometallic complexes were synthesized, filtered, and washed. In the second step, monometallic produced through first step were re-dissolved in DMF separately and then mixed dropwise caused the precipitation of controlled structures of heterometallic complexes. These porous structures can be used in a variety of industrial applications. Thermal decomposition of these complexes was made to produce nano particles. For the unsupported catalysts, initially,  $[\text{Zn}(\text{bpy})_2]\text{Cl}_2$  and  $[\text{Al}(\text{bpy})_3]\text{Cl}_3$  complexes were synthesized and characterized. Then by the reaction of these monometallic complexes, Zn-Al bimetallic complex was prepared and thermally decomposed to produce nano particles.

Influence of the process variables such as temperature ( $^{\circ}\text{C}$ ), time (h) and stirring speed (rpm) were assessed. The optimized conditions were employed to produce Ni-Al bimetallic and Zn-Ni-Al trimetallic nano particles. Synthesized

complexes and nano oxides were characterized by SEM, EDX, XRD, TGA, and FTIR. Detail description of each step is provided in chapters 4 and 5.

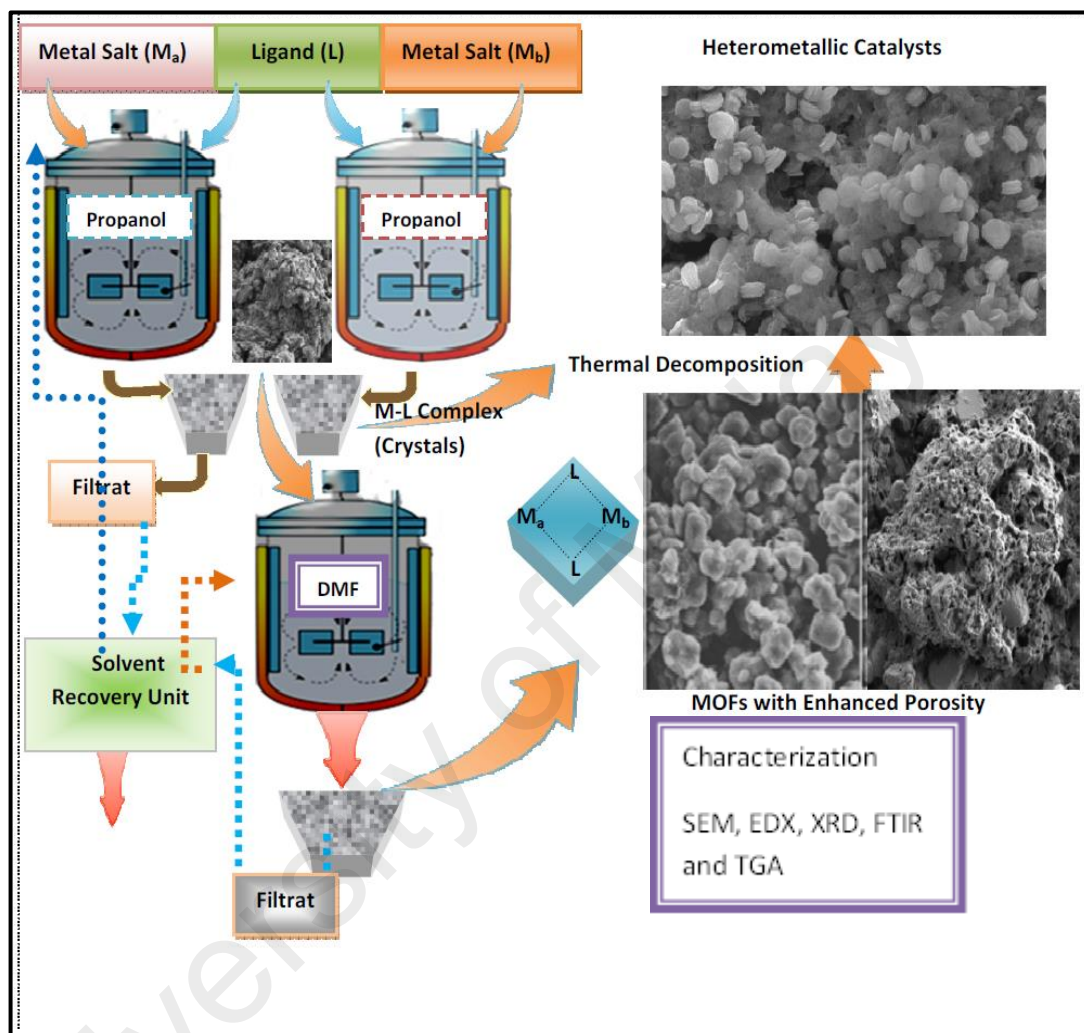


**Figure 3.1:** Process Flow Diagram for the Synthesis of Unsupported Catalysts

### 3.3 Synthesis of Supported Catalysts

For the supported catalysts, ZSM-5 was used as the support. Fe, Zn, Ni and Cu nano oxides were supported using two-step process to synthesize Fe-ZSM-5, Fe-Zn-ZSM-5, Fe-Zn-Cu-ZSM-5 and Fe-Zn-Ni-Cu-ZSM-5 heterometallic catalysts. Figure 3.2 illustrates the main steps for the synthesis of supported catalysts. In this scheme, ZSM-5 was impregnated with monometallic or heterometallic complexes

produced from previous section (Figure 3.1), filtered and dried. Calcination of impregnated zeolite at 650 °C completely removed the ligand part from zeolite matrix. Nano heterometallic oxides were grown at the support surface and also in pores of the support. Detail of the ratio of components used is provided in the chapters 7 and 8.

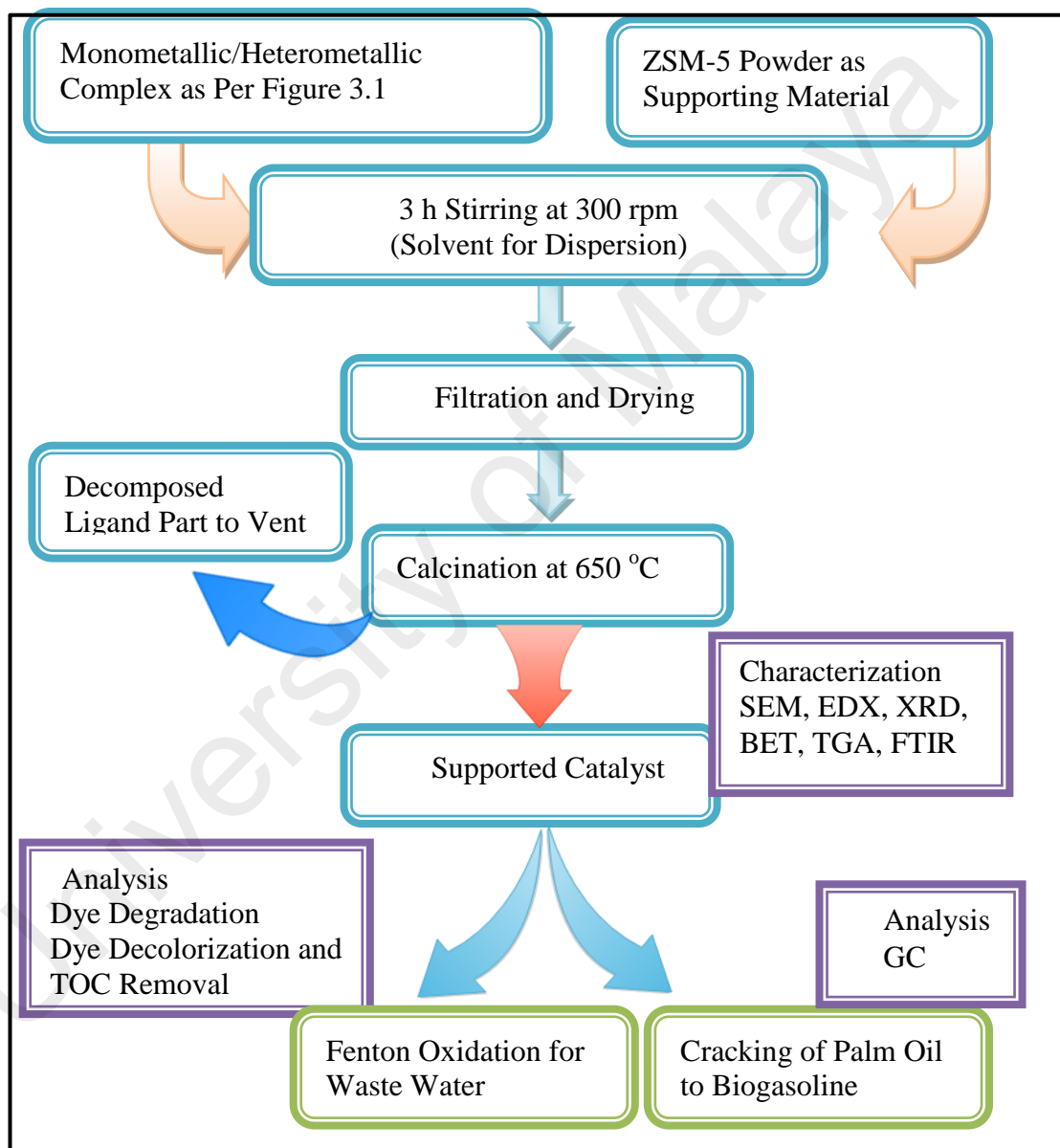


**Figure 3.2:** Process Flow Diagram for Supported Catalysts

### **3.4 Characterization**

In this work, synthesized materials were characterized by field emission scanning electron microscopy (FESEM), high resolution transmission electron microscopy (HRTEM), energy-dispersive X-ray spectroscopy (EDX), fourier transform infrared spectroscopy (FTIR), X-ray powder diffraction (XRD), differential scanning calorimetry (DSC), thermal gravimetric analysis (TGA) and Brunauer-Emmett-Teller (BET) analysis. Detail of the analysis conditions are provided in their respective chapters. Similarly, total organic carbon (TOC), high performance liquid chromatography (HPLC), and UV spectroscopy were used to analyze the treated samples of waste water. Detail of the analysis conditions are provided in chapters 6 and 7. In addition, gas chromatography (GC) technique was used to analyze the produced biogasoline. Detail is provided in chapter 8.

### **3.5 Application of the Synthesized Catalysts**

As there is high demand of heterometallic catalysts (approximately 65 –70% of totally produced) in petrochemical companies (including refineries) and environmental protection agencies. Therefore, recently synthesized catalysts have been used in both of these sectors. However, keeping in mind the scope of this work, only supported type catalyst were used for applications due to added characteristics of ZSM-5 support and ease of recovery and regeneration.

For the wastewater treatment, the activity of synthesized FE-ZSM-5 catalyst was evaluated in Fenton Oxidation process based on the degradation of the model azo dyes, Acid Blue 113, Methyl Orange, and Reactive Black. Detail has been provided in chapters 6 and 7. Similarly, for the biofuel production, ZSM-5 based catalysts integrated with heterometallic nano oxides of Fe, Zn, Cu and Ni were used for the palm oil cracking to produce biogasoline. Detail has been provided in chapter 8.

### 3.6 Optimization Techniques

There were two main part of this research including catalysts synthesis and their applications. Synthesis part involves the precipitations of metal–organic frameworks (MOFs) and their efficient mixing followed by filtration and thermal decomposition. Precipitation of MOFs was the major part of the whole process. Therefore, Response Surface Methodology (RSM) was used to optimize the synthesis of monometallic and bimetallic precipitations. RSM with Central Composite Design (CCD), employs lower-order polynomial and it has proven to be a reliable statistical method for chemical process optimization (Asghar et al., 2014a; Shahrezaei et al., 2012). A set of preliminary experiments and available reliable literature were used to select parameters and their range for this research (Nazir et al., 2013; Parveen et al., 2013). In this work, Design Expert software (Version: 6.0.8) was used. Temperature ( $^{\circ}\text{C}$ ), time (h) and stirring speed (rpm) were chosen as independent variables, while yield (%) of the crystalline MOFs was set as the output response. Detailed experimental design with actual and predicted values is summarized in chapter 4.

The synthesized catalysts have been used for waste water treatment and biogasoline production. Since, each application studied was further influenced by several process parameters, requiring a lot of experiments. To overcome these issues, Taguchi method was used to design and optimize these experiments. Minitab 16 was used to program a Taguchi orthogonal array in order to design the application experiments. This method significant reduces the number of experiments that would be required to fully test each factor with relation to the others (Asghar et al., 2014d). For the wastewater treatment using Fenton oxidation, effects of initial dye concentration, dye/catalyst (wt/wt), catalyst/ $\text{H}_2\text{O}_2$  (wt/wt), reaction time, pH, and temperature were considered and

optimized. TOC removal, decolorization, and degradation were selected as the output responses. Detail has been provided in chapter 6. Similarly, for palm cracking to biogasoline, influence of the independent process variables including amount of catalysts (g/mL), temperature ( $^{\circ}\text{C}$ ) and time (h) were considered and optimized to maximize the yield of biogasoline. Detail has been described in chapter 8.

### **3.7 Process Safety Measures and Material Safety Data Sheet**

Since, used solvents, metal salts and ligand were belong to hazardous class, therefore, safety measure were the important. Purchased chemicals were properly stored under controlled temperature conditions (below  $30\text{ }^{\circ}\text{C}$ ). During the synthesis and application processes, exhaust ventilation were used to keep the airborne concentrations of vapors below their respective threshold limit value. In addition, lab coat, splash goggles, vapor respirator were used as personnel protective equipments (PPE).

## CHAPTER 4: DEVELOPMENT OF A TWO-STEP PROCESS

### 4.1 Introduction

Nano heterobimetallic catalysts are used for many industrial applications. Organic precursors are widely used to induce uniform distribution of metal atoms and enhance the porosity of catalysts. In this chapter, a novel chemical process is developed and optimized to synthesize Zn-Al bimetallic catalyst. 2, 2'-bipyridine was used as a ligand to interlink Zn-Al metal atoms in 2-Propanol and Dimethylformamide (DMF) environment. Central Composite Design (CCD) method was employed to optimize the yield of monometallic and heterobimetallic clusters. The crystalline products were then characterized by FTIR, FESEM, EDX, TGA, DSC and XRD. The produced heterobimetallic complex and nano particles deposited by aerosol-assisted chemical vapour deposition (AACVD) on the stainless steel (SS) substrate were analyzed for change in the porosity and crystal morphology. In addition to it, the optimized experimental yield for Zn-complex, Al-complex and Zn-Al complex were compared with the predicted yield by CCD. Possibility of using this newly developed "Two-Step" process for production of advanced heterometallic complexes, catalysts and composite materials with enhanced porosity and specific composition has been briefly discussed.

### 4.2 Background

Crystal morphology and size selectivity are important aspects to consider for almost all the industrial catalytic processes. These are normally accomplished by employing heterometallic catalysts of controlled and porous structures (Chang et al., 2012; Czaja et al., 2009; Fechete et al., 2012a; Guo et al., 2013; Javad et al., 2012). Nano-sized porous structures provide high surface area and significantly improve product yields (Bell, 2003; Guisnet et al., 1987; Xie et al., 2011). Porosity of the material normally depends on the method by which it is produced (Kumar et al., 2012; Thomas et al., 2003).

Catalysts with highly ordered structures, which are composed of building blocks that contain multiple channels, have higher porosity compared to catalysts with less ordered structures. These unique porous structures of the polymetallic catalysts are important for many industrial applications (Czaja et al., 2009; Jiang & Xu, 2011; Li & Xu, 2013b; Morozan & Jaouen, 2012).

To-date, various methods have been developed and introduced to design microporous and mesoporous materials and their nano particles (Barrios et al., 2014; Bazer-Bachi et al., 2014; Jiao et al., 2011; Patete et al., 2011b; Yang & Xiaohong, 2014). These materials can be synthesized in mother liquor or solution (Samaele et al., 2010; Yin et al., 2012), in vapor phase and in a template (Amin et al., 2009; Kumar et al., 2012; Qian & Yang, 2008) or deposited on a substrate (Sreekanth et al., 2006; Wang et al., 2012a). These synthesis techniques can be categorized as physical or chemical methods (Liu et al., 2014b). Physical methods such as alloying, milling and etc. are effective in producing catalysts and alloys even at room temperature without toxic solvent or reducing agents (Ferrando et al., 2008; Nayak et al., 2010). However, it is not possible to precisely control the mixing of solids particles and their narrow size distribution. Physical methods also require highly sophisticated equipments and complex accessories with high maintenance cost. Due to these problems, chemical methods (e.g., chemical reduction, precipitation, crystallization, thermal decomposition, electrochemical method and sol-gel) have attracted the attention of researchers. Desired size, porosity and elemental distribution can be controlled up to certain extent in chemical methods (Hong et al., 2009; Salavati-Niasari et al., 2011) which are the main requirements of the advanced catalysts for their effective use (Sankar et al., 2012). However, almost all the chemical methods require toxic chemicals and long reaction time for their completion (Parveen et al., 2012; Sankar et al., 2012). In addition, adsorption of surfactants on the active sites of nano particles (NPs) and oxidation of metallic NPs reduce their available

surface areas and effectiveness (Parveen et al., 2012). Therefore, recent researches have focused on improving the porosity, morphology and effective costs of crystalline materials that are to be used as catalysts.

There is a high demand for a suitable chemical method that can be used to fabricate porous heterometallic complexes and catalysts to improve the quality and yield of industrial processes (Kim & Nair, 2013; Vinod et al., 2011). In this respect, metal-organic frameworks (MOFs) have shown outstanding potential because of their controllable structure, unique electrochemical properties and large surface areas (Feng et al., 2013; Kusgens et al., 2009; Rowsell & Yaghi, 2004). Use of MOFs for clean energy production has been widely considered. Particular emphasis is given to selection and utilization of MOFs as potential platforms for storage and/or; production of hydrogen, separation of CH<sub>4</sub>/CO<sub>2</sub> mixtures, solar cells, fuel cells, and other green energy applications (Ho et al., 2014; Prajapati et al., 2009).

Therefore, this chapter aimed at development of a lab-scale process to synthesize heterometallic catalysts via MOFs clusters with porosity enhancement. Analytical grade 2, 2'-bipyridine was used as a ligand to bridge metal atoms while continuous stirring was applied to control the size and elemental distribution during the precipitation process. The heterobimetallic cluster was further decomposed thermally to produce a thin film of nano particles, supported on a stainless steel (SS) substrate. The main focus of this work was to evaluate the performance of a newly developed process to fabricate heterobimetallic catalysts with desired crystal morphology and yield optimization through CCD scheme. Option to employ the same approach for the synthesis of special heterometallic alloys and advanced nano materials for green energy process was considered. This approach is of wide research interest due to availability of required ligand, solvents and relevant information.

### **4.3 Methodology**

#### **4.3.1 Materials**

Analytical grade feed materials were purchased and used without further treatment or purification. Zinc chloride, aluminum chloride, 2, 2'-bipyridine, 2-propanol, n,n-dimethylformamide (DMF) and ethanol were purchased from MERCK. The synthesized heterobimetallic clusters and thin film were characterized by using EDX, FTIR, FESEM, TGA, DSC and XRD.

#### **4.3.2 Synthesis of Monometallic Complex**

3.13g of  $ZnCl_2$  and 7.0g of 2, 2'-bipyridine ligand were dissolved in 10mL of 2-propanol separately and mixed dropwise in a round-bottom lab-scale crystallizer. The mixture was stirred for 2-3 hours (at 300 rpm) and temperature was maintained at  $38 \pm 2$  °C. As a result, fine crystals of  $[Zn(bpy)_2]Cl_2$  complex were obtained which were separated from the solution and washed with ether to remove impurities. The yield of the monometallic crystalline material was 78%.

For the synthesis of  $[Al(bpy)_3]Cl_3$  complex, 2.5g of  $AlCl_3$  and 8.8g of 2, 2'-bipyridine ligand were used and same conditions as those of  $[Zn(bpy)_2]Cl_2$  complex were maintained. Fine crystals of  $[Al(bpy)_3]Cl_3$  complex were separated from the solution and washed with ether to remove impurities. The yield of the crystalline material was 76%.

#### **4.3.3 Synthesis of Heterobimetallic Complex**

For the synthesis of heterobimetallic complex, 0.5g of synthesized Al-Complex and 0.8g of Zn-Complex were dissolved in 10mL of DMF solvent separately. The resultant solutions were mixed dropwise in a round-bottom lab-scale crystallizer

and stirred for one hour at  $38\pm 2$  °C. Fine crystals of Zn-Al-complex were separated from the solution and washed with ether to remove impurities. The yield was 74.5%. The complex was further decomposed at 450°C thermally to produce nano particles.

#### **4.3.4 Deposition of Heterobimetallic Thin Film**

A thin film of produced heterobimetallic was deposited by AACVD on a stainless steel (SS) substrate. Literature revealed that ligand part containing 2, 2'-bipyridine can be easily removed through controlled heating up to 450°C (Parveen et al., 2012). The substrate was washed with distilled water and acetone before being loaded into the reactor chamber and heated up to 450°C for 15 minutes prior to deposition. 10 mg of Zn-Al-complex was dissolved in 10mL of DMF solvent. The well-mixed precursor solution was then transferred into a flask placed over a piezoelectric modulator of an ultrasonic humidifier fitted with the assembly (Figure 4.1) for thin film formation. The aerosol formed in the precursor solution was passed through the furnace tube with the temperature maintained at 450°C. Argon gas was used to direct the aerosol droplets into the reactor tube at a flow rate of 1mL/min. The exhaust from the reactor tube was directed toward a fume cupboard for ventilation. Deposition was allowed for 45 minutes for the formation of thin film. Then, the aerosol transmission was stopped and the SS substrate was cooled to room temperature by passing argon gas slowly through the substrate. The deposited thin film of Zn-Al was analyzed through EDX, FESEM and XRD. The EDX analysis confirmed the presence of Zn and Al as nano particles in the thin film. The XRD and FESEM studies showed that the products had high degree of crystallinity and nano size.

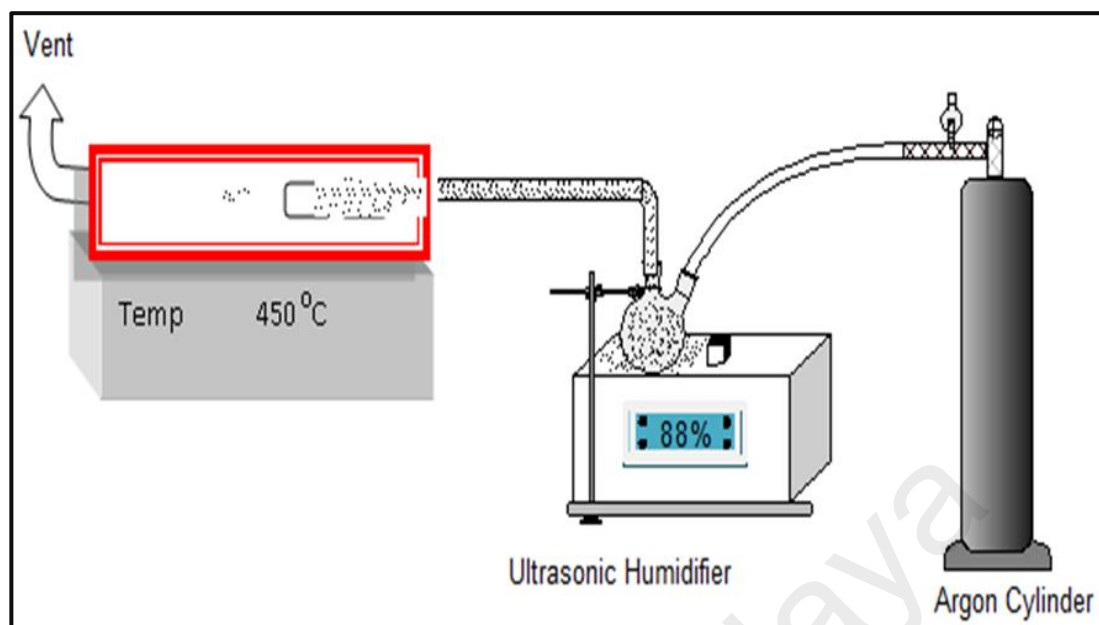


**Figure 4.1:** Aerosol-Assisted Chemical Vapor Deposition (AACVD) Detail Assembly

#### 4.3.5 Characterization

Porosity, surface morphology and composition of the heterobimetallic complex and thin film were analyzed by using FESEM, FEI Quanta 450 coupled with energy dispersive X-ray spectrometer EDX (INCA Energy 200 (Oxford Inst.)) under vacuumed condition with a working distance of 6mm. Surface area method was used to calculate the percentage composition. FTIR studies were conducted using Perkin Elmer FTIR-Spectrum 400. Thermal decomposition behavior of the heterobimetallic complex in the inert medium was studied using TGA (Q500) and DSC (Berth A/700/447). Degree of crystallinity and phase identification were analyzed through PANalytical X-ray diffractometer (model EMPYREAN) with primary monochromatic high intensity Cu-K $\alpha$  ( $\lambda = 1.54060 \text{ \AA}$ ) radiation. A range of  $2\theta$  (from 10.00 to 90.00) was scanned.

#### 4.4 Process Optimization

The developed process involved the precipitations of metal–organic frameworks (MOFs) and their efficient mixing followed by filtration and thermal decomposition. Precipitation of MOFs was the major part of the whole process. The objective was to optimize the process parameters with more influence. In the first stage of this work, suitability of precipitation was determined and the products were characterized completely through FTIR, EDX, XRD, TGA and DSC. A set of preliminary experiments and available reliable literature were used to select parameters and their range for this research (Nazir et al., 2013; Parveen et al., 2013). In the current study, temperature ( $^{\circ}\text{C}$ ), time (h) and stirring speed (rpm) were considered while some other parameters such as concentration, pH, pressure and etc were neglected. In the second stage, experiments were conducted and the response values were obtained to perform optimization through Response Surface Methodology (RSM).

**Table 4.1:** Process Parameter for Zn/Al Monometallic Precipitation Process

Process Parameters	Code	Low Actual Value	High Actual Value
Temperature ( $^{\circ}\text{C}$ )	A	30	46
Time (h)	B	1	5
Stirring Speed (rpm)	C	150	300

Response Surface Methodology (RSM) was used to optimize the synthesis of monometallic and bimetallic precipitations. RSM with Central Composite Design (CCD), employs lower-order polynomial and it has proven to be a reliable statistical method for chemical process optimization (Asghar et al., 2014a; Shahrezaei et al., 2012). In the present study, all experiments required for precipitation processes were designed using CCD with the help of Design Expert (Version: 6.0.8). Temperature ( $^{\circ}\text{C}$ ), time (h) and stirring speed (rpm) were chosen

**Table 4.2:** Experimental Design and Response of Zn-complex Precipitation Process

Standard Order	Run No.	Temperature (°C)	Time (h)	Stirring Speed (rpm)	Actual Value (Yield %)	Predicted Value (Yield %)
1	14	46	5	150	78.0	77.7
2	15	46	1	300	59.0	58.7
3	13	30	5	300	66.0	65.7
4	10	30	1	150	36.0	35.7
5	3	27	3	225	45.0	45.3
6	12	49	3	225	77.0	77.3
7	6	38	1	225	30.0	30.3
8	1	38	6	225	83.0	83.3
9	2	38	3	119	79.0	79.3
10	5	38	3	331	83.5	83.8
11	9	38	3	225	80.5	80.7
12	4	38	3	225	80.5	80.7
13	7	38	3	225	81.0	80.7
14	11	38	3	225	81.0	80.7
15	8	38	3	225	81.0	80.7

**Table 4.3:** Experimental Design and Response of Al-complex Precipitation Process

Standard Order	Run No.	Temperature (°C)	Time (h)	Stirring Speed (rpm)	Actual Value (Yield %)	Predicted Value (Yield %)
1	9	46	5	150	71.0	71.4
2	3	46	1	300	52.0	52.4
3	5	30	5	300	48.0	48.4
4	8	30	1	150	42.0	42.4
5	12	27	3	225	45.0	44.6
6	1	49	3	225	74.0	73.6
7	4	38	1	225	35.0	34.6
8	13	38	6	225	77.0	76.6
9	14	38	3	119	62.0	61.6
10	10	38	3	331	79.0	78.6
11	6	38	3	225	78.0	77.7
12	15	38	3	225	78.0	77.7
13	11	38	3	225	76.0	77.7
14	7	38	3	225	78.0	77.7
15	2	38	3	225	78.0	77.7

as independent variables, while yield (%) of the crystalline MOFs was the output response. Low and high values of the chosen parameters are given in Table 4.1. Detailed experimental design with actual and predicted values is summarized and provided in Table 4.2 to Table 4.5. These predictions are briefly described and discussed in the following sections

**Table 4.4:** Process Parameter for Zn-Al Heterobimetallic Precipitation Process

Process Parameters	Code	Low Actual Value	High Actual Value
Temperature (°C)	A	35	45
Time (h)	B	1	5
Stirring Speed (rpm)	C	150	300

The temperature range for the bimetallic precipitation was slightly changed considering the experimental results of the monometallic precipitations, complexes solubilities and high boiling point of DMF

**Table 4.5:** Experimental Design and Response of Zn-Al-complex Precipitation Process

Standard Order	Run No.	Temperature (°C)	Time (h)	Stirring Speed (rpm)	Actual Value (Yield %)	Predicted Value (Yield %)
1	15	45	5	150	76.0	76.7
2	3	45	1	350	37.0	37.7
3	9	35	5	350	77.0	77.7
4	11	35	1	150	33.0	33.7
5	1	33	3	250	51.0	50.3
6	5	47	3	250	74.0	73.3
7	14	40	1	250	30.0	29.3
8	13	40	6	250	81.5	80.8
9	7	40	3	109	71.0	70.3
10	8	40	3	391	81.0	80.3
11	4	40	3	250	79.0	79.3
12	2	40	3	250	79.0	79.3
13	10	40	3	250	79.0	79.3
14	12	40	3	250	79.0	79.3
15	6	40	3	250	79.0	79.3

## 4.5 Results and Discussion

### 4.5.1 Confirmation of Crystalline Products

The FTIR spectra of  $[\text{Zn}(\text{bpy})_2]\text{Cl}_2$ ,  $[\text{Al}(\text{bpy})_3]\text{Cl}_3$ , and Zn-Al-complex have given the under stable picture of the coordinate bridging of metal atoms with the ligand atoms. The 2,2'-bipyridine spectra was used as a reference to observe several shifts due to coordinate bridging. Strong ring stretching vibrations  $\nu(\text{C}=\text{C})$  and  $\nu(\text{C}=\text{N})$  were detected at  $1553$  and  $1579\text{cm}^{-1}$  for free phase of bipyridine ligand. In the monometallic and bimetallic complexes (Figure 4.2), slight shift in vibrations were detected in the range of  $1561\text{-}1563$  and  $1592\text{-}1595\text{ cm}^{-1}$ , respectively.

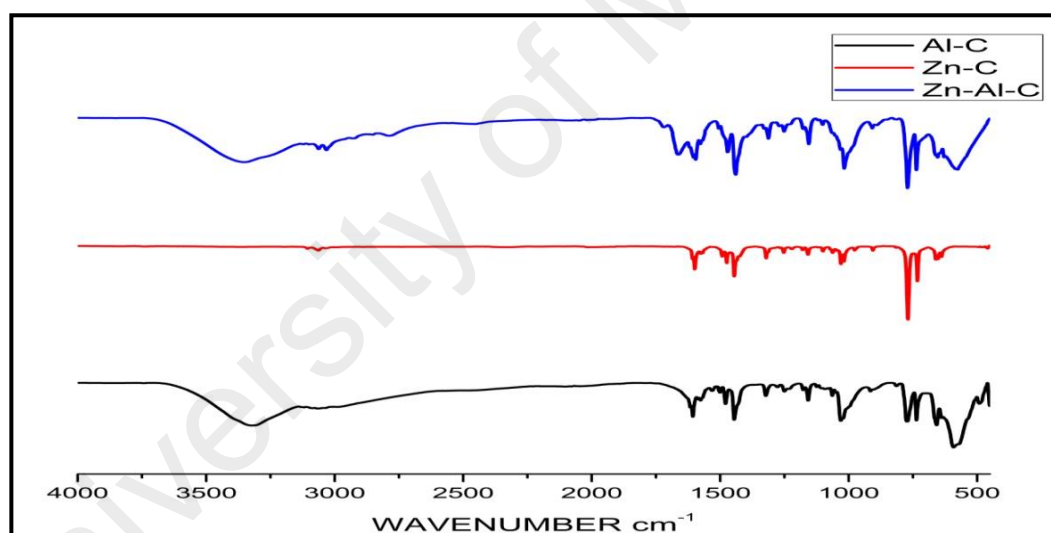


**Figure 4.2:** FTIR of the Monometallic and Bimetallic Complexes

Breathing frequency was shifted from  $991\text{cm}^{-1}$  to  $1019\text{-}1029\text{ cm}^{-1}$ . An increase of about  $20\text{-}29\text{ cm}^{-1}$  in frequencies was observed in the complexes. Bending mode for ring-H (out of plane) in free bipyridine was reported at  $753\text{ cm}^{-1}$ , but the same was observed at  $768\text{ cm}^{-1}$  for  $[\text{Zn}(\text{bpy})_2]\text{Cl}_2$ ,  $772\text{ cm}^{-1}$  for  $[\text{Al}(\text{bpy})_3]\text{Cl}_3$  and  $774\text{ cm}^{-1}$  for Zn-Al-bimetallic complex. Besides, appearance of the new bands in the range of  $812\text{-}816$  and

1313–1319  $\text{cm}^{-1}$  indicated an infrared inactive ring mode. All these shifts and observations indicated the coordination of 2, 2' bipyridine with metal atoms (Laik et al., 2007).

The size and morphology of the monometallic and heterobimetallic clusters together with their thin film grown on SS substrates by AACVD were investigated using FESEM (Figure 4.3 and Figure 4.4). The FESEM study showed that there was a great improvement in crystal structure and porosity in heterobimetallic clusters (Figure 4.4) compared to monometallic (Figure 4.3).

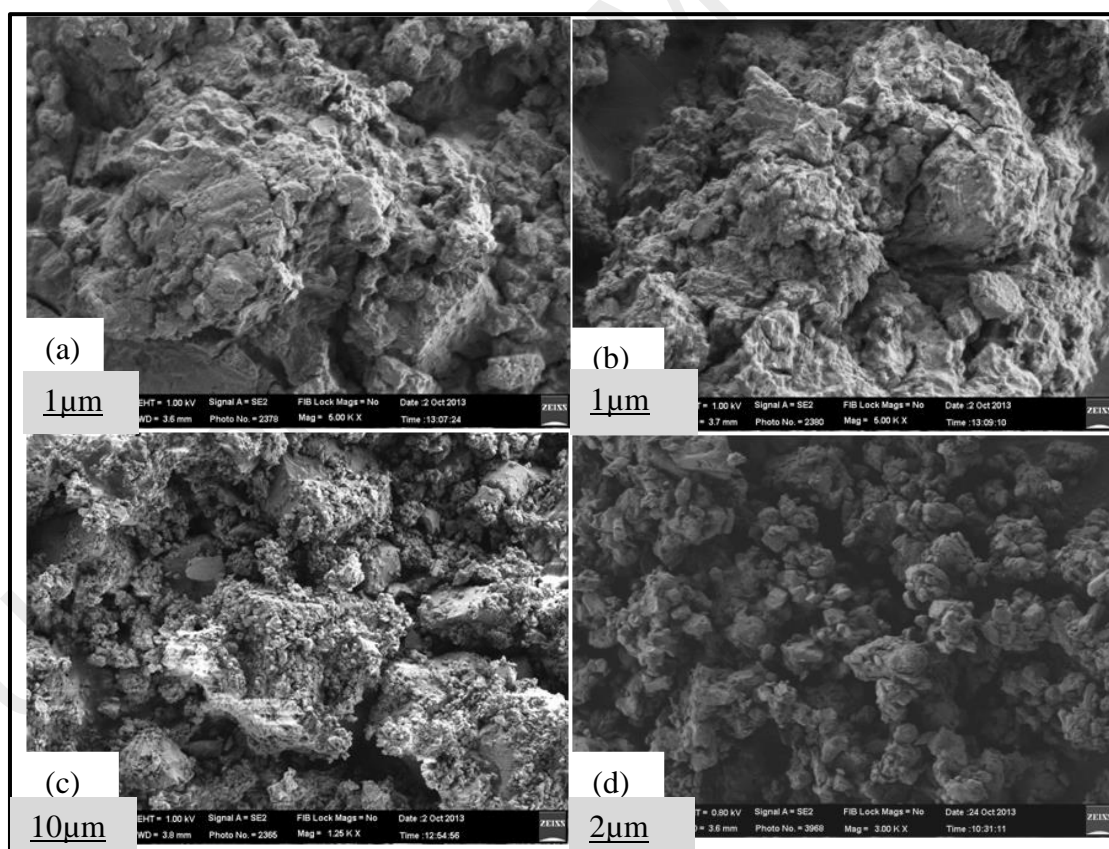


**Figure 4.3:** FESEM Images of Al-Complex (a, b) and Zn-Complex (c, d)

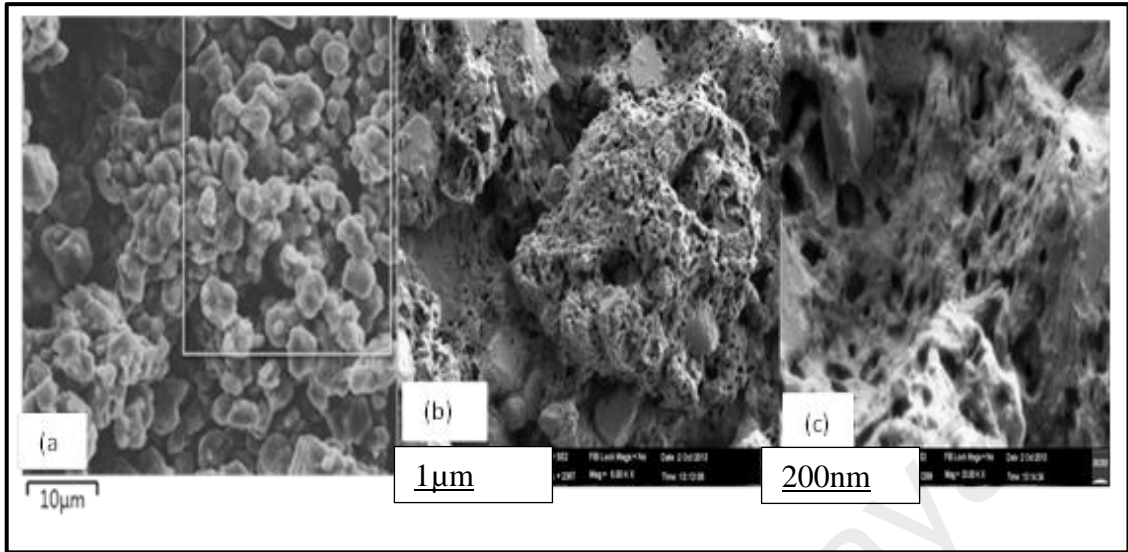


**Figure 4.4:** Zn-Al Bimetallic Complex (a, b and c) with Enhanced Porosity and Better Crystal Morphology

Aerosol assisted chemical vapor deposition (AACVD) led to formation of finer nano balls with clearer boundaries (Figure 4.5). Thin film was smooth.

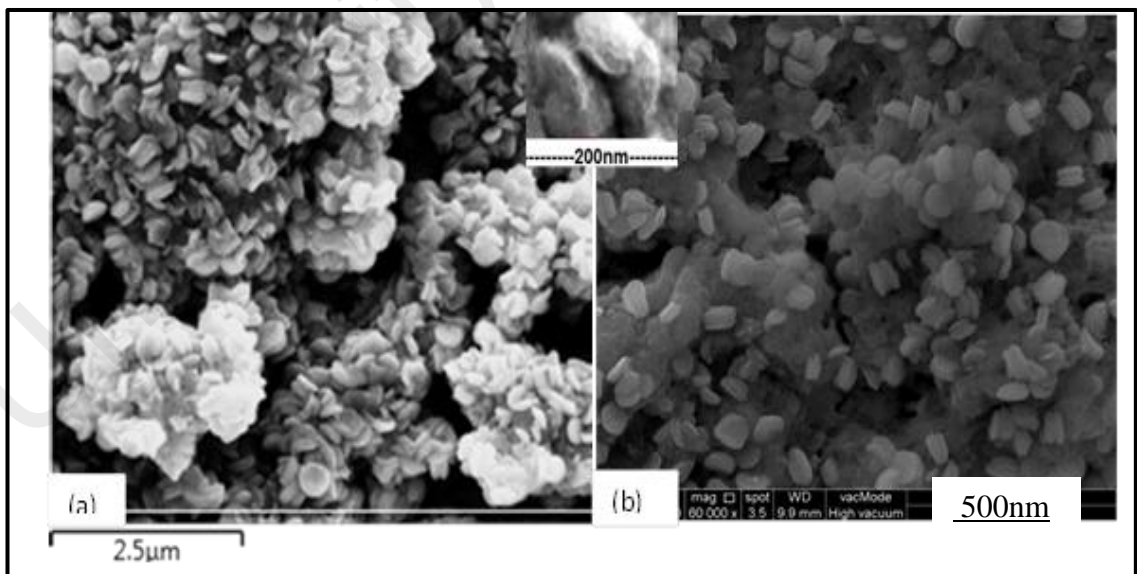


**Figure 4.5:** Zn-Al Thin Film Supported on SS Substrate

Elemental mapping of the coordinated heterobimetallic complex clearly illustrated the uniform distribution of zinc, aluminum, carbon, nitrogen and

chlorine atoms inside the complex. Presence of Zn atoms was most prominent comparative to Al atoms (Figure 4.6). This was occurred due to relatively larger size and high concentration of Zn-complex used for the formation of heterobimetallic complex, which led to the formation of  $\text{Al}_2\text{O}_3\text{Zn}_6$  and ZnO nano balls. EDX analysis (Table 4.6), FESEM study (Figure 4.5) and XRD results (Figure 4.9) have strongly supported the elemental mapping.

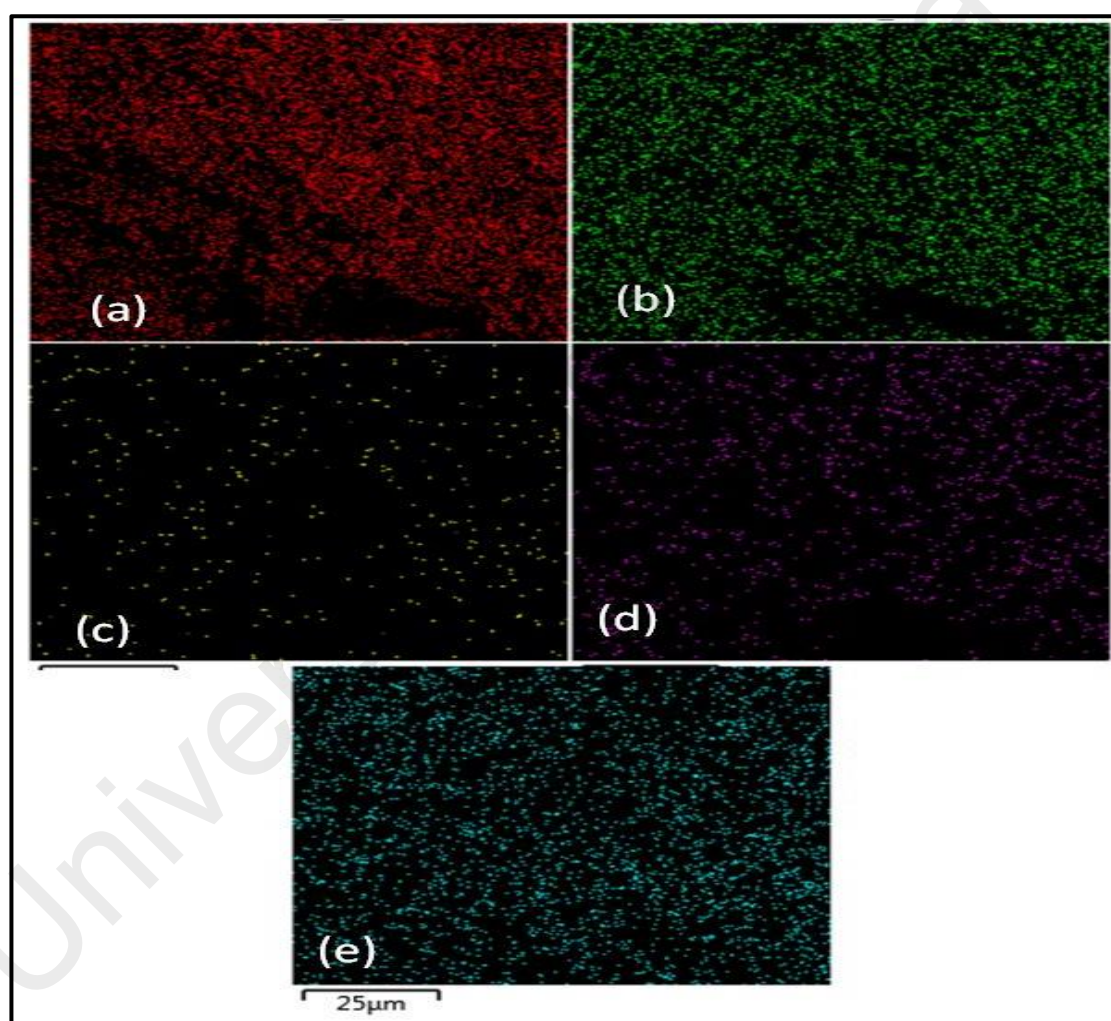


**Figure 4.6:** Elemental Distribution of C (a), Zn (b), Al (c), N (d) and Cl (e) atoms inside the Zn-Al Bimetallic Complex

EDX was used to calculate the percentage composition in the monometallic and heterobimetallic complexes. Table 4.6 summarizes the composition of metals within the

complexes. Significant amount of carbon, nitrogen and chlorine was present in the monometallic and heterobimetallic complexes. However, coordinated ligand atoms were wiped out from thin film due to thermal decomposition supported with Argon flow through the reaction chamber. With the increase in gas flowrate, wiping of the ligand atoms increased.

**Table 4.6:** EDX Analysis of the Synthesized MOFs

Catalyst Clusters	Weight Composition (%)					
	Zn	Al	O	C	Cl	N
[Zn (bipy) <sub>2</sub> ]Cl <sub>2</sub>	15.96		0.00	53.50	14.95	12.98
[Al (bipy) <sub>3</sub> ]Cl <sub>3</sub>	-	4.76	2.96	62.20	17.09	12.99
Zn-Al-Complex	13.84	2.91	0.81	53.41	16.91	12.02
Zn-Al (Thin Film on SS)	68.00	3.00	31.65	-	-	-

Thermal decomposition behavior of the Zn-Al-bimetallic complex was examined by thermogravimetric and differential scanning calorimetry (TGA/DSC). This analysis was carried out under inert nitrogen gas, flowing at 50mL/min and heating rate of 10°C/min. Thermogravimetric data (Figure 4.7) suggested that the complex was eventually degraded to Zn-Al bimetallic nano particles. Besides, the TGA and DSC curves indicated five stages of heat gain at 94, 195, 220, 280 and 405°C, which resulted in a weight loss of 11.55, 18.19, 7.85, 17.32 and 29.16 % respectively. These decomposition stages were not well defined, indicating that unstable intermediate moieties were formed during the thermal decomposition process (Parveen et al., 2012). A possible explanation for early decomposition (at <200°C) is release of volatile material and DMF vapors (Nazir et al., 2012). The final pyrolysis step that produced stable residual mass of 14.51% occurred within the temperature range of 380-505°C. Further heating did not

cause any change or loss in residual mass, which was a clear indication of formation of stable Zn-Al composite.

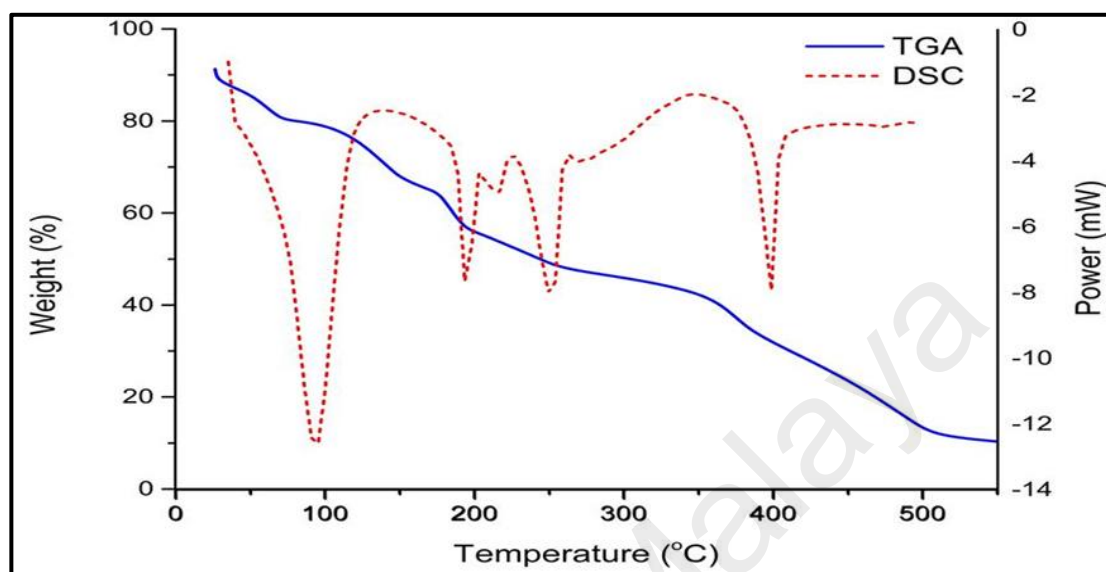


**Figure 4.7:** TGA/DSC Curves Showing Pyrolysis of Zn-Al Bimetallic Complex at A Heating Rate of 10°C/min

Degree of crystallinity of the monometallic and heterometallic complexes, and the deposited thin film were examined by scanning a range of  $2\theta$  from 10.00 to 90.00. Figure 4.8 illustrates the powder diffraction pattern of the  $[\text{Zn}(\text{bipy})_2]\text{Cl}_2$  and Zn-Al bimetallic complex. No clear evidence of free 2,2' bipyridine (Ref. Code 00-015-1119), metals atoms (Al and Zn) and/or; salts was observed. It was believed that the metal salts reacted completely with the ligand to form the complex and the amounts of unreacted quantities were too little to be detected by XRD (Buitrago et al., 2012).

The powder diffraction pattern of the composite Zn-Al thin films (Figure 4.9) deposited on the SS substrate matched very well with that of the spinel phase  $\text{Al}_2\text{O}_3\text{Zn}_6$  (Ref. Code 00-051-0037). There were three intense peaks at  $2\theta = 32.15, 34.38$  and  $36.63$  and other less intense peaks at higher  $2\theta$  values. These peaks increased in intensity with increasing the ZnO (Ref. Code 01-079-0207) loading. The broadness of the peaks indicated small crystal size of the spinel phase.

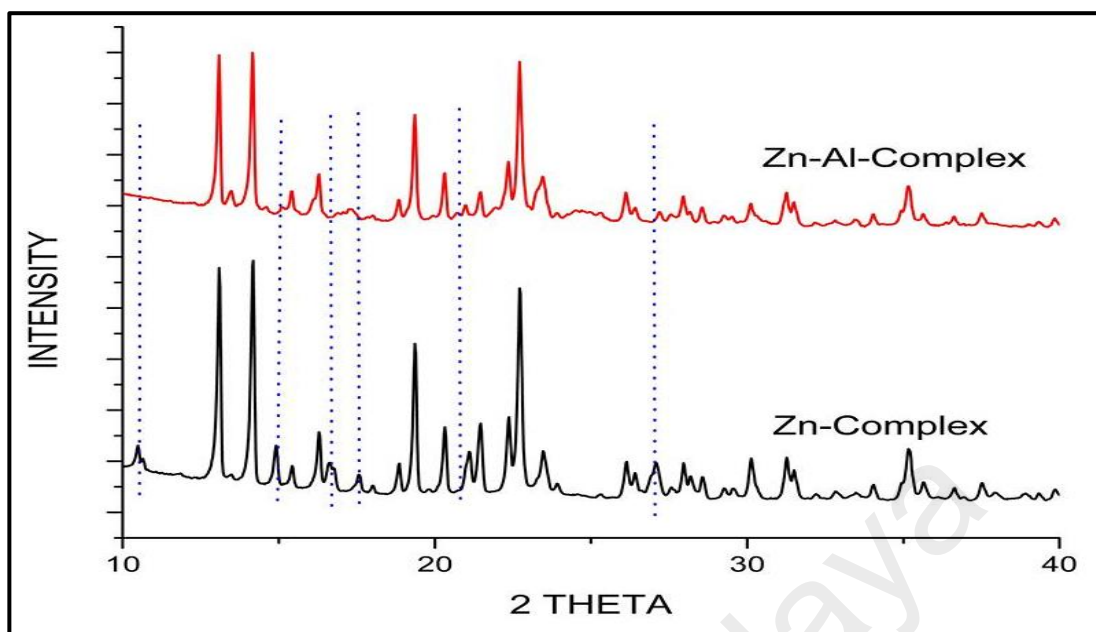


**Figure 4.8:** XRD Patterns of Mono-Metallic and Polymetallic Complexes

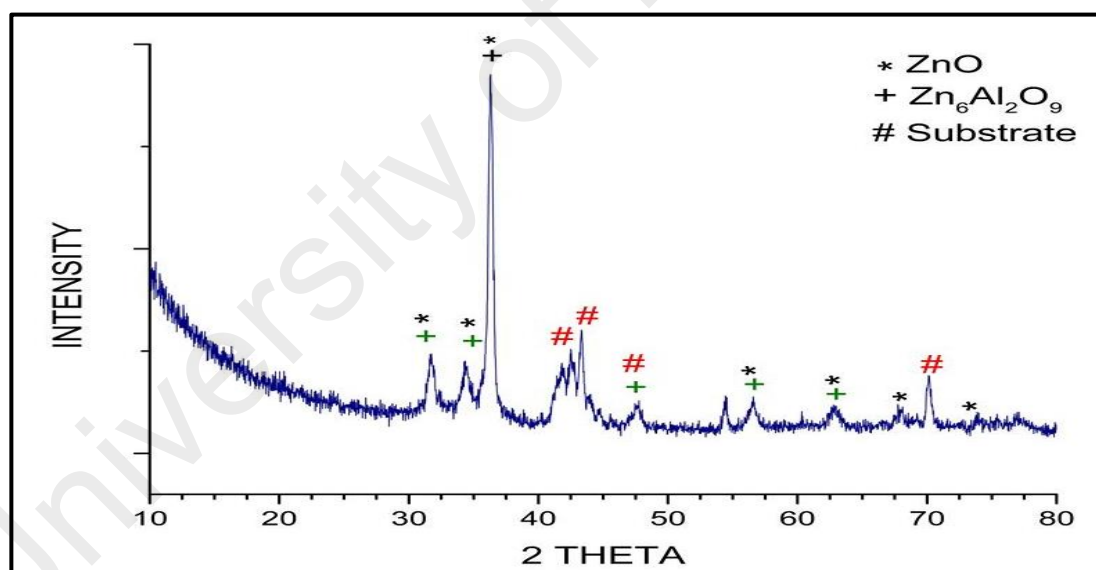


**Figure 4.9:** XRD Patterns of the Thin Film, Deposited on SS Substrate

The XRD results confirmed that the particles in all samples were highly crystalline. Debye–Scherrer equation was used to calculate the average crystal size. The results showed that the particles were nano sized (19.6 to 120 nm). It was observed that these nano sized particles had cluster-making trend. Therefore, the FESEM study focused on cluster’s morphology and porosity.

#### 4.5.2 ANOVA Analysis of Monometallic Complex Precipitation

The monometallic complex precipitations were carried out according to the design described in the equations 4-1 and 4-2 . Yield was selected as response. Based on the experimental results, the following empirical second order polynomial equations (in terms of coded factors) were developed showing the interactions between the proposed independent variables to obtain the precipitation yield.

Yield of Zn-Complex =

$$80.69+11.31A+18.74B+1.59C-9.70A^2-11.95B^2+0.43C^2-1.16AB+6.49AC+2.56BC \quad 4-1$$

Yield of Al-Complex =

$$77.74+10.25A+14.85B+6.01C-9.30A^2-11.05B^2-3.80C^2+9.26AB+8.60AC+2.006BC \quad 4-2$$

These empirical models describe the interaction of independent variables influencing the process yield. The experimental and predicted yields are summarized and compared. The experimental yields of Zn and Al monometallic MOFs varied between 30–81% and 35–78%, respectively, which were in good agreement with the predicted values. The developed mathematical models, after fitting the data into the function, may provide deceptive results. That is why ANOVA, an integral and reliable approach, is mostly used to confirm the suitability and significance of a model (Asghar et al., 2014a). Table 4.7 and Table 4.8 show the ANOVA results for the yields of monometallic complexes.

**Table 4.7:** ANOVA Analysis of Zn-Complex Precipitation

Source	Sum of Squares	Degree of Freedom	Mean Square	F Value	Prob > F
Model	4,639.54	9	515.50	2,166.32	< 0.0001 (Significant)
A (Temperature)	512.00	1	512.00	2,151.59	< 0.0001
B (Time)	1,404.50	1	1404.50	5,902.17	< 0.0001
C (Stirring Speed)	10.12	1	10.12	42.54	0.0013
A2	725.69	1	725.69	3,049.62	< 0.0001
B2	1,101.44	1	1,101.44	4,628.65	< 0.0001
C2	1.39	1	1.39	5.88	0.0597
AB	2.68	1	2.68	11.29	0.0201
AC	84.19	1	84.19	353.82	< 0.0001
BC	13.14	1	13.14	55.24	0.0007
Residual	1.189	5	0.23	R <sup>2</sup> =0.9997	
Pure Error	0.30	4	0.075	R <sup>2</sup> Adj=0.9993	
Cor Total	4,640.73	14		Adeq Precision=134.32	

F-value indicates the reliability and suitability of a model. A variable with Prob> F less than 0.05 has significant effects on the response. The greater the F value for a particular variable more would be the effect of that particular variable on the specific response. In the present study, F-values of 2166.32 and 434.11 indicated that the precipitation models for Zn and Al complexes were suitable. The quality of fit of both models was also confirmed through determination coefficient (R<sup>2</sup>). The R<sup>2</sup> values were 0.9997 and 0.9987 for both models, which were in reasonable agreement with the adjusted R<sup>2</sup>. Adequate precision (AP) is normally used to

**Table 4.8:** ANOVA Analysis of Al-Complex Precipitation

Source	Sum of Squares	Degree of Freedom	Mean Square	F Value	Prob > F
Model	3,545.20	9	393.91	434.11	< 0.0001 (significant)
A (Temperature)	420.50	1	420.50	463.41	< 0.0001
B (Time)	882.00	1	882.00	972.00	< 0.0001
C (Stirring speed)	144.50	1	144.50	159.24	< 0.0001
A2	666.68	1	666.68	734.71	< 0.0001
B2	941.30	1	941.30	1,037.35	< 0.0001
C2	111.18	1	111.18	122.52	0.0001
AB	171.51	1	171.51	189.01	< 0.0001
AC	147.89	1	147.89	162.99	< 0.0001
BC	8.02	1	8.02	8.84	0.031
Residual	4.54	5	0.91	R <sup>2</sup> =0.9987	
Pure Error	3.20	4	0.80	R <sup>2</sup> Adj=0.9964	
Cor Total	3,549.73	14		Adeq Precision=56.57	

determine signal to noise (S/N) ratio to examine the validity of a model and a ratio greater than 4 is recommended. In the present study, AP values of 134.3 and 56.57 indicated adequate signal to noise (S/N) ratios for the models. These values also showed that models were suitable and can be used to optimize the design space.

#### 4.5.2.1 Effect of Variables on Yield

The perturbation plots as shown in Figure 4.10 and Figure 4.11 were used to compare the combined effects of all the three variables on a single point. The slope of the curve indicates the influence of a variable and the steepest curve was the main center of attention. It was noticed that factor B (Process time) was the most influencing factor towards the yield. The second most influencing factor was A (Temperature) while C (Stirrer speed) was the least influencing. However, for precipitation of Al-complex

(Figure 4.11), increase in stirrer speed showed positive effects on the yield. Increasing the mixing time and impeller speed, the suspension of the particles increased, which led to maximum exposure of the available surface area to solution for mass transfer (Ferrando et al., 2008).

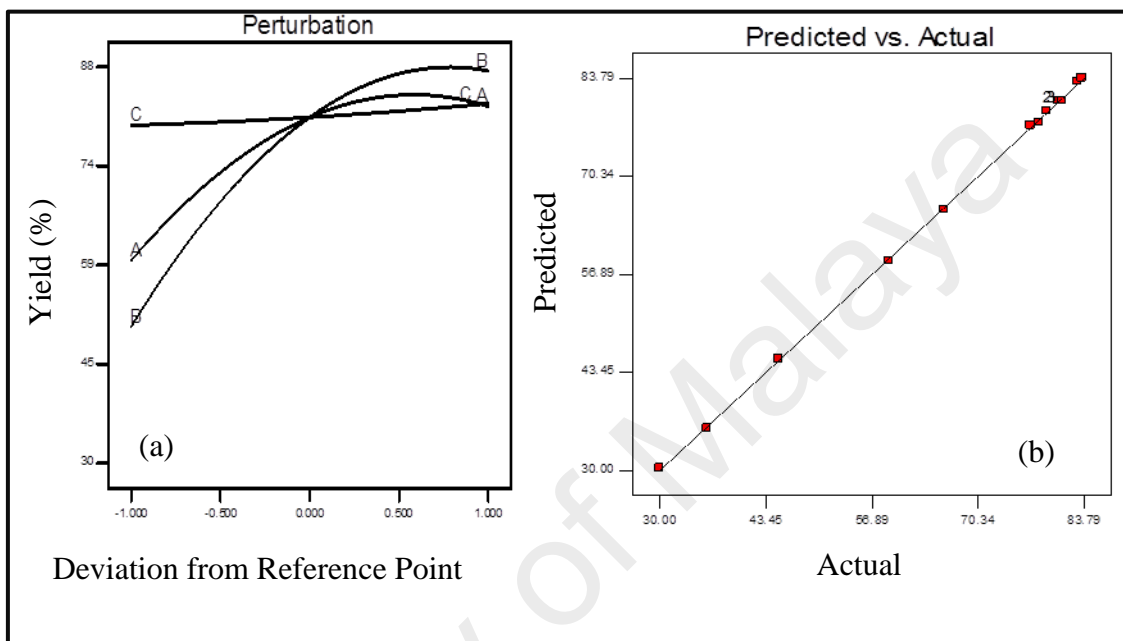


**Figure 4.10:** Perturbation Plot (a), A is Temperature, B is Reaction Time, C is Stirring Speed, and Comparison Plot (b) for Zn-complex

Figure 4.10 and Figure 4.11 illustrate the comparison between the experimental and predicted values. From both the figures, it is clear that the experimental values are in linear relationship with the predicted ones, indicating that the predicted values were close to the experimental values.

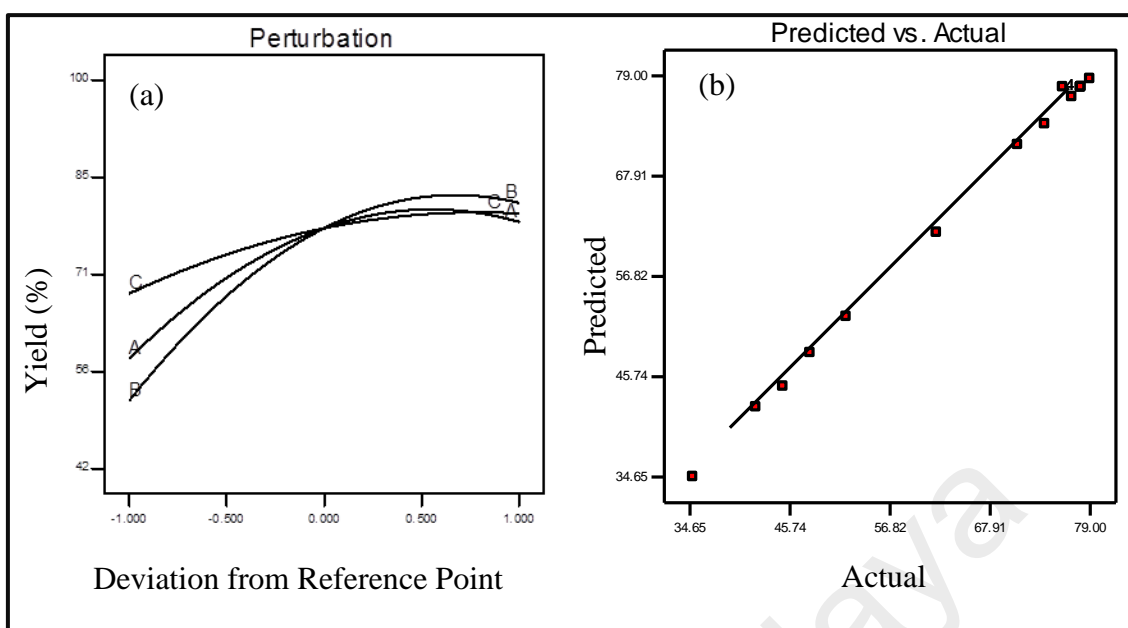


**Figure 4.11:** Perturbation Plot (a), A is Temperature, B is Reaction Time, C is Stirring Speed, and Comparison Plot (b) for Al-Complex

Optimization study of the experimental results was carried out by keeping all responses within the desired ranges by using Response Surface Methodology (RSM). Yield was targeted to the maximum while the other variables were kept within the range. The suggested optimized values of temperature ( $38^{\circ}\text{C}$ ), time (4 h) and stirrer speed (260 rpm) were validated through the experiment. The approximate yields were 80 % and 78% for Zn and Al complexes, respectively. There was a good agreement between the experimental and predicted results under optimized conditions.

### 4.5.3 ANOVA Analysis of Heterobimetallic Complex Precipitation

The heterobimetallic complex precipitation was completed by following the by following the same experimental design as earlier. DMF was used as the solvent instead of 2-propanol in order to improve the metal-ligand coordinate bridging. Following empirical second-order polynomial equation (in terms of coded factors) showing the

interactions between the proposed independent variables to obtain the precipitation yield was developed.

*Heterobimetallic Complex Yield =*

$$79.28+8.13A+18.21B+3.54C-8.74A^2-12.11B^2-1.99C^2+2.29AB-$$

4-3

$$2.54AC+7.38BC$$

The experimental yield of heterobimetallic complex varied from 30–82%, which was in good agreement with the predicted values. Table 4.9 shows the ANOVA analysis of variance for the yield of heterometallic complex.

**Table 4.9:** ANOVA analysis of Zn-Al Heterobimetallic Complex Precipitation

Source	Sum of Squares	Degree of Freedom	Mean Square	F Value	Prob > F
Model	5,047.89	9	560.88	538.44	< 0.0001 (Significant)
A (Temperature)	264.50	1	264.50	253.92	< 0.0001
B (Time)	1,326.13	1	1,326.13	1,273.08	< 0.0001
C (Stirring Speed)	50.00	1	50.00	48.00	0.0010
A <sup>2</sup>	588.75	1	588.75	565.20	< 0.0001
B <sup>2</sup>	1,131.52	1	1,131.52	1,086.26	< 0.0001
C <sup>2</sup>	30.43	1	30.43	29.21	0.0029
AB	10.45	1	10.45	10.03	0.0249
AC	12.92	1	12.92	12.41	0.0169
BC	108.98	1	108.98	104.62	0.0002
Residual	5.21	5	1.04	R <sup>2</sup> =0.9990	
Pure Error	0.00	4	0.00	R <sup>2</sup> Adj =0.9971	
Cor Total	5,053.10	14		Adeq Precision=61.80	

The model F-value represents the reliability of the model and the variance of the output response. In the present case, F-value of 538.44 implies that the model is significant. The R<sup>2</sup> value of 0.9990 was also in good agreement with the adjusted R<sup>2</sup>. Furthermore, adequate Precision (AP) value of 61.80 for the response indicated an adequate signal to noise (S/N) ratio.

### 4.5.3.1 Effect of Variables on Heterobimetallic Complex Yield

Perturbation plots (Figure 4.12) compared the combined effects of all the three variables on a single point. In this case, factor B (Process time) was seen the most influencing factor towards the yield. However, effects of two other factors, A (Temperature) and C (Stirrer speed) were also significant. Crystal growth and yield were significantly influenced by long reaction and mixing time at high impeller speed. Long reaction and mixing time allowed complete suspension, which provides maximum surface area and particle-particle interaction inside the magma for enhanced mass transfer. However, at higher values of A (In the range of 46-49 °C), less yield was obtained. It might be occurred due to crystal breakage and dissolution at higher temperature and stirring speed (Ferrando et al., 2008). The experimental values were in a linear relationship with the predicted values, which indicates that the model is appropriate. These plots provide clear pictures of the precipitation processes.

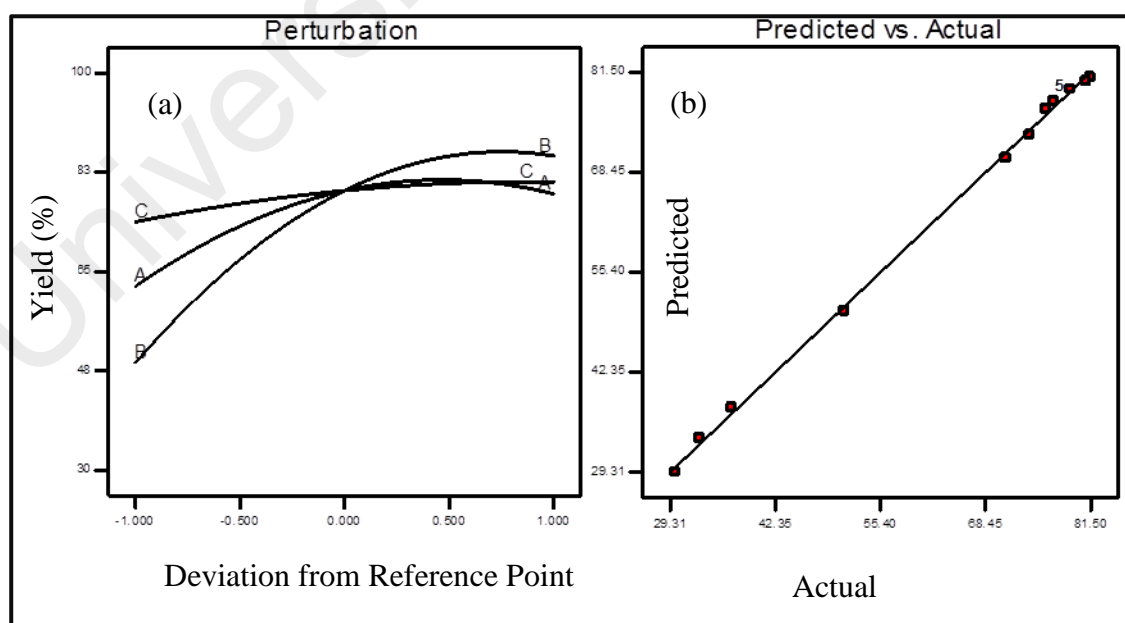


**Figure 4.12:** Perturbation Plot (a), A is Temperature, B is Reaction Time, C is Stirring Speed, and Comparison Plot (b) for Zn-Al-Complex

Optimization of heterobimetallic precipitation was relatively more challenging due to formation of more complicated complex compared to optimization of monometallic precipitation. The experiments were performed based on precise measurements in inert condition to avoid any by-products. During the CCD optimization studies, maximum yield was targeted while all the variables were kept within the desired range. The recommended optimized values of temperature (40 °C), time (4 h) and stirrer speed (240 rpm) were validated through the experiment. Approximate yield was 78.5%. There was a good agreement between the experimental and predicted results under optimized conditions.

#### **4.6 Summary**

In this work, a newly developed two-step chemical process was developed and used to synthesize bimetallic catalyst by suitably distributing the metal atoms inside the Zn-Al bimetallic complex. The crystalline products were characterized by FTIR, FESEM, EDX and XRD. Central Composite Design (CCD) method was employed to optimize process yields, while ANOVA was used to analyze the data to obtain the interaction among the process variables (temperature, time and stirrer speed).

The developed heterobimetallic nano particles showed enhanced porosity and better crystal morphology. The Optimized yields of Zn- complex, Al-complex and Zn-Al complex were 80%, 78% and 78.5% which were in a good agreement CCD predicted values. Process time was seen as the most influencing variable in both monometallic and bimetallic precipitations. Effect of temperature and stirrer speed was also significant towards the crystalline yields. The produced heterometallic complexes and their alloys have great potential for green energy applications.

## CHAPTER 5: SYNTHESIS OF NANO HETEROMETALLIC CATALYSTS

### 5.1 Introduction

Heterometallic crystalline particles with controlled size and morphology are widely used for many industrial applications. To achieve specific crystal morphology and desired quantities of heterometallic catalysts, different synthesis approaches are in use. Among them, precipitation followed by thermal decomposition is one of the most prominent option to produce catalysts and their nano particles even at industrial scale.

In this chapter, a newly developed two-step process was evaluated for the synthesis of trimetallic (Ni-Zn-Al) nano particles (NPs) at low temperature (35°C) and pressure. 2,2'-bipyridine was used as ligand to interlink metal atoms. Crystalline products were characterized by FTIR, FeSEM, EDX and XRD. Ni, Zn NPs. heterometallic synthesis and yields have been briefly discussed and compared to develop an avenue for the synthesis of industrial scale heterometallic catalysts with improved features.

### 5.2 Background

Heterometallic catalysts are frequently used in chemical, pharmaceutical and refinery processes. Approximately ninety percent of chemical processes utilize heterogeneous catalysts and the value created by utilizing catalysts is approximately three orders of magnitude higher than the amount invested in them (Czaja et al., 2009; Fechete et al., 2012b). Moreover, morphology, size and selectivity of the catalysts are the essential considerations for almost all the industrial catalytic processes and are usually accomplished by employing polymetallic catalysts of nano porous structures (Gomez & Tigli, 2013; Guo et al., 2013). Uniform porosity can be possible by fabricating highly ordered structures, in which channels/pores are the part of the building blocks (i.e.,

repetitive units). These unique structures of the polymetallic catalysts are beneficial for various industrial applications (Czaja et al., 2009; Li & Xu, 2013a; Montes et al., 2014; Morozan & Jaouen, 2012).

Numerous methods of synthesizing heterometallic catalysts and their nano particles (NPs) have been recently reported (Dai et al., 2014; Patete et al., 2011a). Polymetallic catalysts and their nano particles (NPs) can be synthesized via two main categories; physical and chemical methods (Liu et al., 2014a). Physical techniques are mainly based on the mechanical alloying of the materials. Both categories were also employed to synthesize nano size polymetallic NPs. Physical methods are effective to produce catalysts even at room temperature without toxic solvent or reducing agents (Ferrando et al., 2008). However, these methods need complicated equipments and their accessories with their huge maintenance cost. Moreover the morphology of the synthesized NPs and their narrow size distribution are not possible to control. Therefore chemical methods attracted the attention of researchers as attractive alternates (Guo et al., 2014; Hosoya et al., 2014; Moezzi et al., 2012). These are easy to perform and the synthesized polymetallic catalysts with desired size and morphology which are the main requirements of the NPs or their clusters to be used as catalyst (Salavati-Niasari et al., 2011). Each chemical method has specific advantages (Sankar et al., 2012). However, chemical methods mostly require toxic solvents and reducing agents as well as a synthesis process that is often energy and time consuming (Parveen et al., 2012). Moreover, adsorption of the surfactants on the active sites of the NPs is also a common problem, which reduces their effectiveness in industrial applications. In addition to these, several metallic NPs or their clusters are easily prone to oxidation (Parveen et al., 2012). So, compromise is made either on the quality of the crystalline material or its cost, when it is produced at industrial scale.

To overcome these problems and induced specific properties, several researchers have focused MOFs derived materials. MOFs have shown excellent potential due to their high surface areas, controllable structures and versatile electrochemical properties (Burrows, 2011). In addition, these methods have significantly improved the efficiency, stability and the reusability of heterometallic catalysts for the heterogeneous processes (Yang et al., 2011). Significant advances in the development of MOFs for clean energy applications are also reviewed and special emphases are shown to the applications of MOFs as platforms for hydrogen production and storage, fuel cells, Li-ion rechargeable batteries and solar cells (Burrows, 2011; Cukrowski et al., 2014; Li & Xu, 2013a).

Present study offers preparation of bimetallic and trimetallic nano particles via thermal decomposition of MOFs. This work is the extension of researcher's previous published chapter in which Zn-Al bimetallic nano particles were synthesized using newly developed 2-step process. Influence of the independent process variables such as temperature ( $^{\circ}\text{C}$ ), time (h) and stirring speed (rpm) were assessed and optimized. Results were highly engorging. A great improvement in crystal morphology and yield were achieved. In this work, addition of Ni into Zn-Al composite has been carried out using 2-Step process. In the first step, monometallic, bimetallic and trimetallic complexes of Ni, Zn and Al were prepared and characterized. 2,2'-bipyridine was used as ligand to interlink metal atoms while continuous stirring is applied to control crystal size distribution (CSD) inside the crystallizer. In the second step, AACVD method was employed to produce nano particles.

The main focus was to extend the application of the newly developed two-step process to produce a wide range of heterometallic crystalline catalysts and their NPs. Major part of the production process (precipitation) was carried out at low temperature ( $35\text{-}38\text{ }^{\circ}\text{C}$ ) and atmospheric pressure, without releasing toxic fumes. Therefore, the

process is environmentally friendly. Moreover, synthesis process was divided into two parts to optimize time, energy and product cost. 2-proapnol and DMF were effectively used for monometallic and polymetallic systems to produce desire materials. Availability of ligand, solvents and their data were also considered here. A wide range of reliable data regarding 2,2'-bipyridine and its complexes is available (Cukrowski et al., 2014; Nazir et al., 2011; Parveen et al., 2012). Solvents; ethanol, 2-proapnol and DMF are also available at commercial scale. Temperature range of the major operational part (precipitation) is very low as compared to other process. All these make this an attractive process for the production of a variety of catalysts. Moreover, with the addition and employment of efficient solvent recovery system, developed process would be the more cost effective and environmentally safe. This study explores new avenues for the industrial scale production of heterometallic complexes, catalysts and special alloys for a variety of industrial applications.

### **5.3 Experimental Details**

In this study, optimization conditions of previous work (chapter 2) were used to synthesize the monometallic, bimetallic and trimetallic MOFs. Detail of the synthesis for each MOF is provided in the following sections.

#### **5.3.1 Materials**

In this study, Nickel chloride hexahydrate was used along with the previously described reagents (in chapter 4). Nickel chloride hexahydrate was also purchased from MERCK and used to synthesize bimetallic and trimetallic clusters and thin films. Crystalline products were confirmed by characterizing them using FTIR, EDX, FeSEM and XRD.

### 5.3.2 Synthesis of Monometallic Complexes

Stoichiometric ratios were used for the synthesis of the mono-metallic complexes. Optimized conditions of the previous chapter were used to get maximized yields. 3.13g of  $ZnCl_2$  and 7.0g of 2,2'-bipyridine ligand were dissolved in 2-propanol 10 mL and 100 mL separately and dropwise mixed in a round bottom lab scale crystallizer with a flow rate of 0.33 mL/min. Solution stirred for 2 hours and temperature was maintained at  $38 \pm 2$  °C. Fine crystals of Zn-complex were separated, washed with ether to remove impurities. The yield was 80%.

Similar environment was employed for  $[Ni(bpy)]Cl_2$  and  $[Al(bpy)_3]Cl_2$ . 6.4g of 2,2'-bpy ligand and 2.6g of  $NiCl_2 \cdot H_2O$  were used to synthesize  $[Ni(bpy)]Cl_2$  while 2.5g of  $AlCl_3$  and 8.8g of 2,2'-bpy ligand were used to synthesize  $Al(bpy)_3Cl_3$ .

Fine crystals of  $[Ni(bpy)]Cl_2$  and  $[Al(bpy)_3]Cl_3$  were separated, washed with ether to remove impurities. The yields were 81% and 78% respectively.

### 5.3.3 Synthesis of Bimetallic Complexes

0.8g of Zn-complex and 0.5g of Ni-complex were dissolved in 10 mL DMF solvent separately and dropwise mixed in a round bottom lab scale crystallizer with a flow rate of 0.33 mL/min. Solution stirred for one hour and temperature was maintained at  $38 \pm 2$  °C. Fine crystals of Zn-Ni-complex were separated, washed with ether to remove impurities. The yield was 85%.

Similar conditions were employed for the synthesis of bimetallic complexes of the Zn-Al. For this system, 0.8g of Zn-complex and 0.5g of Al-complex were used and fine crystals of Zn-Al-complex separated, washed with ether to remove impurities. The yield was 78.5%.

### 5.3.4 Synthesis of Trimetallic Complex

0.52g of Zn-Complex, 0.48g of Ni-Complex and 0.40g of Al-complex were dissolved in 10 mL DMF solvent separately and dropwise mixed. Solution stirred for one hour and temperature was maintained at  $38\pm 2$  °C. Fine crystals of Zn-Ni-Al-complex were separated, washed with ether to remove impurities. The yield was 77%.

### 5.3.5 Deposition of Thin Films by AACVD

Thin films were deposited by AACVD on a stainless steel (SS) and fluorine-doped tin oxide (FTO) coated glass substrates. Substrates were washed with distilled water, ethanol and acetone. 10mg of Zn-Ni-Al-complex was dissolved in 10mL DMF solvent. The well mixed solution was poured into a round bottom flask, placed in the sonicator bath (PIFCO air humidifier) fitted with the assembly for thin film formation. SS substrate was kept first followed by FTO coated glass substrates. Small mist/aerosol produced in the solution, directed toward the furnace, kept at 400°C. This was slightly lower than the temperature of previous study (Chapter 4), to investigate the behavior of film formation at different temperatures. Argon was passed through the aerosol mist at a flow rate of 1mL/min, to force the aerosol droplets into the reactor chamber. The exhaust from the reactor was vented directly into the extraction system of a fume cupboard. Depositions were conducted for 40 min for the formation of thin film. After that aerosol line was closed, and furnace was allowed to cool up to 40°C before substrate and films were removed from the reaction chamber for structural studies.

Similar procedure was adopted for Zn-Al thin film on SS substrate, kept at 400°C. However, for Zn-Al bimetallic system, only SS substrate was used to compare the synthesized Zn-Al material with the previous work (chapter 4). Thin films of Zn-Ni-Al and Zn-Al, showing high homogeneity and smooth feature were analyzed through

FeSEM, EDX and XRD. EDX analysis (Table 5.1) confirms presence of Zn, Ni and Al oxides in the thin films. FeSEM and XRD results have further supported the results in term of crystallinity and nano-size.

#### 5.4 Results and Discussion

The formation of complexes occurred due to metal-ligand bridging (---C-N-M-N-C--). The infrared spectra for  $[\text{Zn}(\text{bpy})_2]\text{Cl}_2$ ,  $[\text{Ni}(\text{bpy})_2]\text{Cl}_2$ ,  $[\text{Al}(\text{bpy})_3]\text{Cl}_3$ , Ni- Zn - complex, Zn-Al-complex and Ni-Zn-Al-complex were analyzed and comparison was made with free 2,2'-bipyridine spectra (NIST). A range between  $2000\text{--}450\text{ cm}^{-1}$  was given focus. Figure 5.1 represents several shifts and differences. For example, in free 2,2'-bipyridine stretching vibrations at  $1553$  and  $1579\text{ cm}^{-1}$  appear for  $\nu(\text{C}=\text{C})$  and  $\nu(\text{C}=\text{N})$  respectively. In monometallic and polymetallic complexes, these vibrations appeared in the range  $1561\text{--}1563$  and  $1592\text{--}1595\text{ cm}^{-1}$ , respectively. The characteristic pyridine ring breathing frequency at  $991\text{ cm}^{-1}$  is shifted by  $21\text{--}29\text{ cm}^{-1}$  to higher frequencies in the complexes. Bending mode (for ring-H, out-of-plane ) in the uncoordinated bipyridine, was reported at  $753\text{ cm}^{-1}$ , but the same was observed at  $766\text{ cm}^{-1}$  for  $[\text{Zn}(\text{bpy})_2]\text{Cl}_2$ ,  $777\text{ cm}^{-1}$  for  $[\text{Ni}(\text{bpy})_2]\text{Cl}_2$ ,  $772\text{ cm}^{-1}$  for  $[\text{Al}(\text{bpy})_3]\text{Cl}_3$ ,  $771\text{ cm}^{-1}$  for Ni-Zn-complex and  $774\text{ cm}^{-1}$  for Ni-Zn-Al-complex. Besides these, new bands in the range  $813\text{--}816$  and  $1313\text{--}1319\text{ cm}^{-1}$  were also appeared. These results reveal that the ligand is coordinated to the metal atom (Laïk et al., 2007).

EDX analysis of the particles showed presence of carbon, nitrogen and chlorine containing coordinated ligand. During decomposition these coordinated ligand atoms were removed from the metal complex in the presence of argon flow, which has provided inert atmosphere and also wiped out the decomposed by-products from the reaction zone. Table 5.1 summarizes the metals with their organic or oxides clusters.

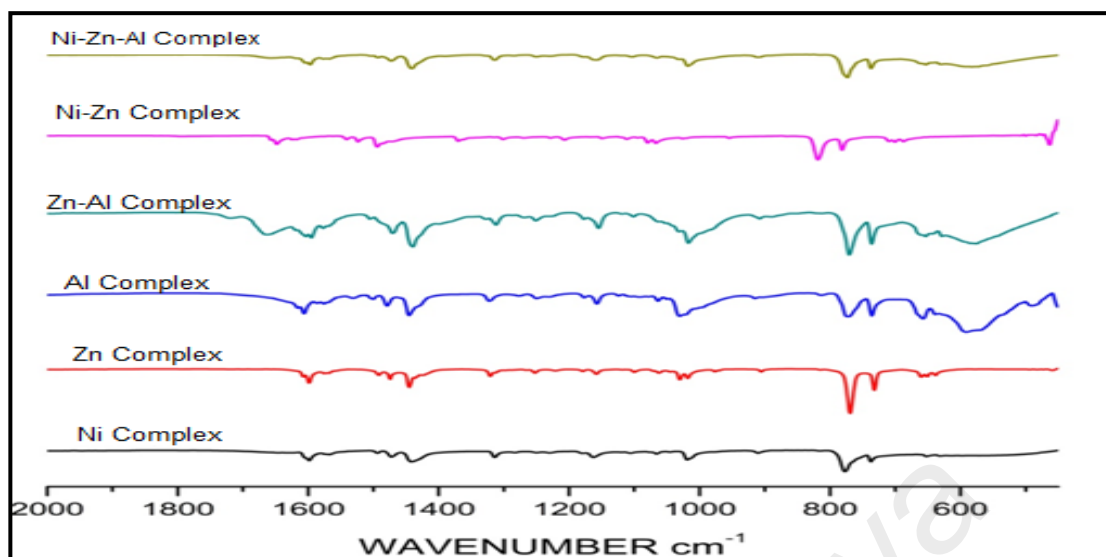


**Figure 5.1:** IR Spectra of Monometallic and Polymetallic Complexes

The morphology of the bimetallic and trimetallic clusters was investigated using FESEM. Samples were collected from their magma solutions, dried and then analyzed without dispersion of the crystalline particles Figure 5.2 and Figure 5.3 illustrate the understandable features of these complexes.

**Table 5.1:** EDX Analysis of the Clusters and Thin Films

Catalyst Clusters	Weight composition (%)						
	Ni	Zn	Al	O	C	Cl	N
[Ni(bpy) <sub>2</sub> ]Cl <sub>2</sub>	15.35	-	-	1.50	53.95	16.06	12.98
[Zn(bpy) <sub>2</sub> ]Cl <sub>2</sub>		15.96		0.00	53.50	14.95	12.59
[Al(bpy) <sub>3</sub> ]Cl <sub>3</sub>	-	-	4.76	2.96	62.20	17.09	12.99
Ni-Zn-complex	3.9	6.74	-	2.06	61.47	13.84	12.03
Zn-Al-complex	-	7.84	5.10	0.81	55.52	17.76	12.02
Ni-Zn-Al-complex	4.58	4.48	3.69	4.65	57.48	15.46	9.69
Zn-Al (Thin Film on SS)	-	68.00	3.00	31.60	-	-	-
Zn-Ni-Al (Thin Film on SS )	1.50	76.33	7.26	14.96	-	-	-
Zn-Ni-Al (Thin Film on FTO Glass)	11.1	3.7	0.10	20.4	-	-	-

The particles in polymetallic clusters (Figure 5.3) have better defined boundaries as compared to monometallic cluster. In all clusters, particles have shown tendency of sintering together to make linked microporous structures. Figure 5.4 shows the Zn-Al thin film grown on both SS substrate by AACVD. The FeSEM results reveal that grown particles are mesoporous nano balls.

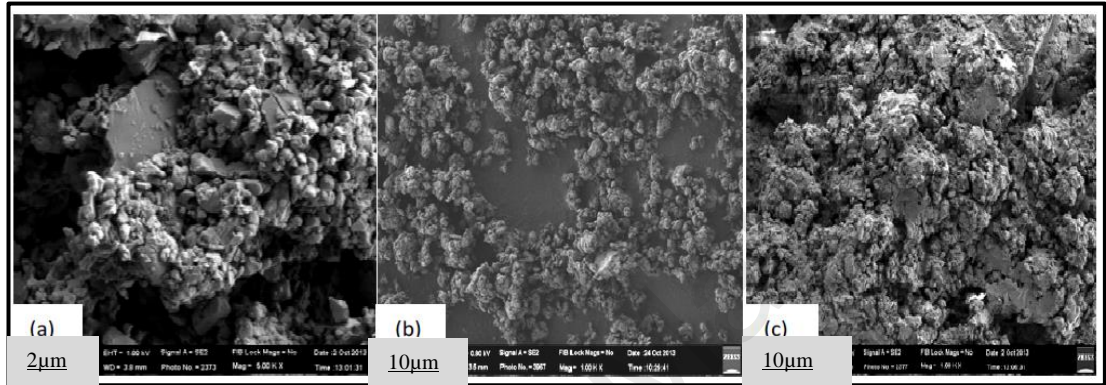


**Figure 5.2:** Ni (a), Zn (b) and Al (c) Monometallic Complexes

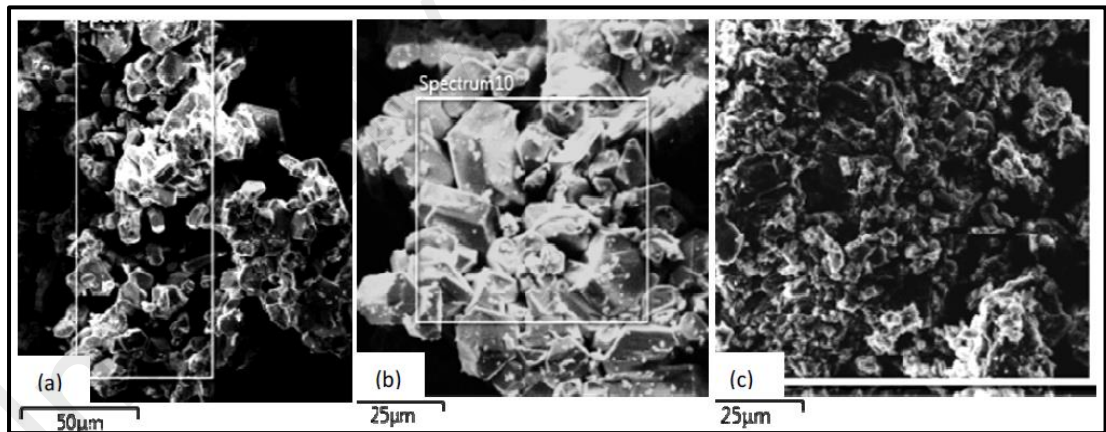


**Figure 5.3:** Zn-Ni (a), Zn-Al (b) and Zn- Ni-Al (c) Heterometallic Complexes

For trimetallic films, deposition pattern of the nano particles of the metal atom on SS substrate was slightly different as compared with FTO substrate (Figure 5.5 and Figure 5.6). Addition of Ni atoms caused the growth of needle like crystals instead of nano balls. However, material of construction and location of the substrate also affected the

particle size and quality of the crystalline material. In this case, Zn-deposition was noted more on the SS substrate (placed first), followed by FTO glass substrate, while the deposition of Ni was increased at FTO glass substrate. Average particle size of the SS-substrate based film was also greater than other.

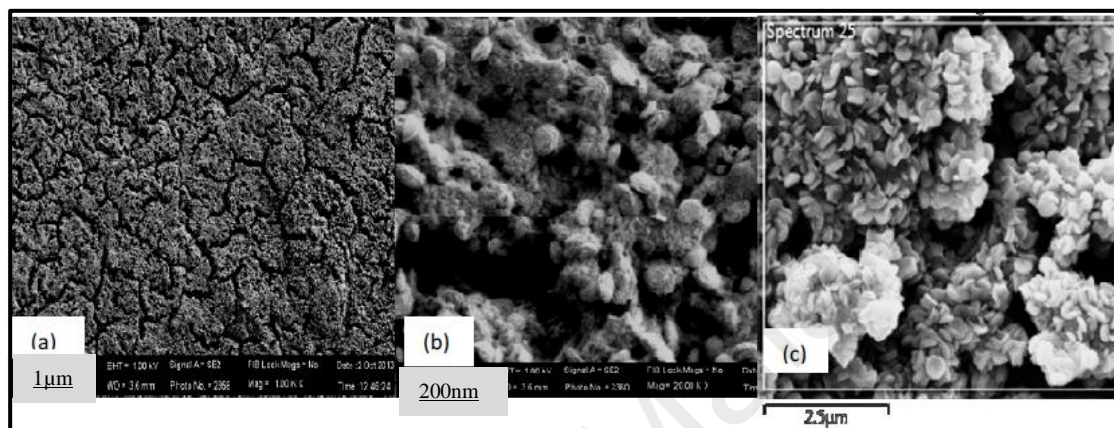
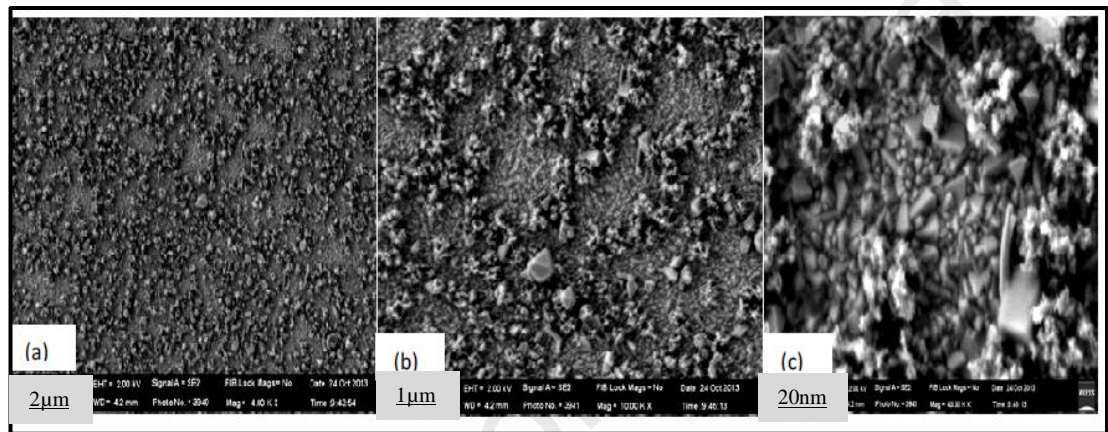


**Figure 5.4:** FeSEM Images (a & b) and Electron Image (c) of Zn-Al Thin Film Supported On SS Substrate

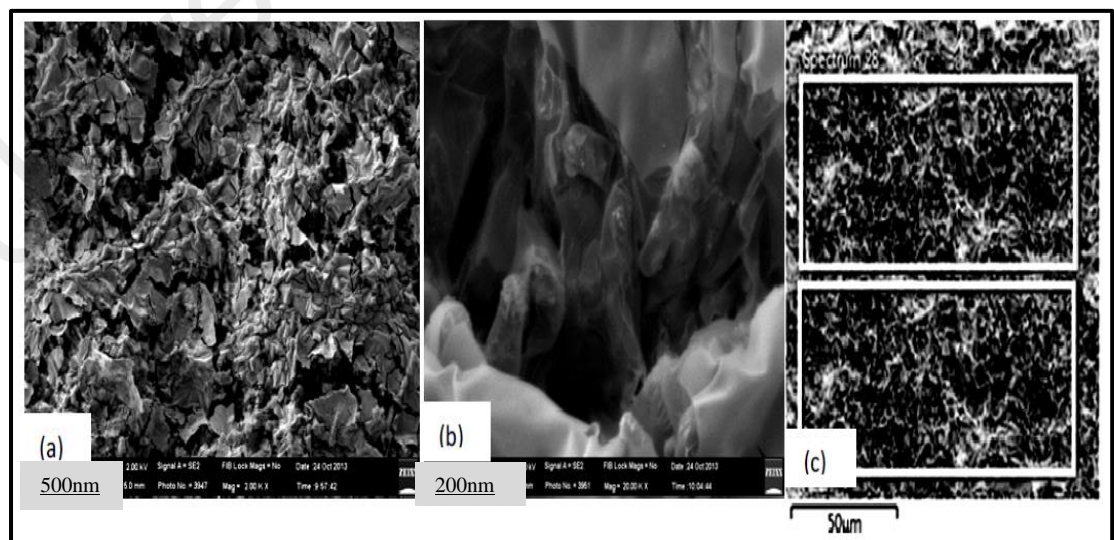
The identity of the phase and the degree of crystallinity of the crystalline materials and the deposited thin films were examined by scanning a range of  $2\theta$  from  $10^\circ$  to  $90^\circ$ . Figure 5.7 shows the XRD patterns of the  $[\text{Ni}(\text{bpy})_2]\text{Cl}_2$ ,  $[\text{Zn}(\text{bpy})_2]\text{Cl}_2$ ,  $[\text{Al}(\text{bpy})_3]\text{Cl}_3$ , Ni-Al-complex and Ni-Zn-Al-complex. No clear evidence of the presence of metal (Ni, Al and Zn) salts can be observed, this is due to both the fact that reactants have completely reacted with ligand to form the complex phase and that the unreacted quantities are very small as to be detected by XRD (Buitrago-Sierra et al., 2012).

Figure 5.8 shows the XRD patterns of thin films, deposited on SS and FTO glass substrate. For bimetallic system, the presence of spinel phase  $\text{Al}_2\text{O}_3\text{Zn}_6$  (Ref. Code 00-051-0037), characterized by three intense peaks at  $2\theta = 32.15$ ,  $34.38$  and  $36.63$  and other less intense peaks at higher  $2\theta$  values, is clearly evidenced. These peaks increase

in intensity with increasing the ZnO (Ref. Code 01-079-0207) loading (Buitrago-Sierra et al., 2012). The broadness of the peaks indicates a small crystal size of the spinel phase. The broadness of the XRD peaks was used to calculate the average crystalline size using the Debye–Scherrer equation. The results showed that the particles in all the tested samples were nano sized with size between 104.8 and 103 nm (Zhang et al., 2012).



**Figure 5.5:** Zn-Ni-Al Thin Film Supported On FTO Glass Substrate



**Figure 5.6:** Zn-Ni-Al Thin Film on SS Substrate

For trimetallic system, presence of  $\text{Al}_2\text{Ni}_{0.4}\text{O}_4\text{Zn}_{0.6}$  (Ref. Code 01-080-1685) characterized by two intense peaks at  $2\theta = 31.30, 36.90$  and other less intense peaks at higher  $2\theta$  values, is clearly evidenced. The presence of the  $\text{Ni}_{0.8}\text{OZn}_{0.2}$  (Ref. Code 01-075-0271), characterized by two intense peaks at  $2\theta = 37.28, 43.30$  and other less intense peaks at higher  $2\theta$  is also detected. It may be due to the insufficient amount of Al atoms required to produce  $\text{Al}_2\text{Ni}_{0.4}\text{O}_4\text{Zn}_{0.6}$ . The XRD results confirmed that particles in all the samples were highly crystalline. Using the Debye–Scherrer equation, the particles were found in the range of 112.8 and 105 nm (Zhang et al., 2012). However, in FeSEM study, cluster’s morphology and porosity were given the main focus. Moreover, oxygen content can be minimized by employment of the inert atmosphere; passing argon gas during crystallization, deposition and cooling the thin films.

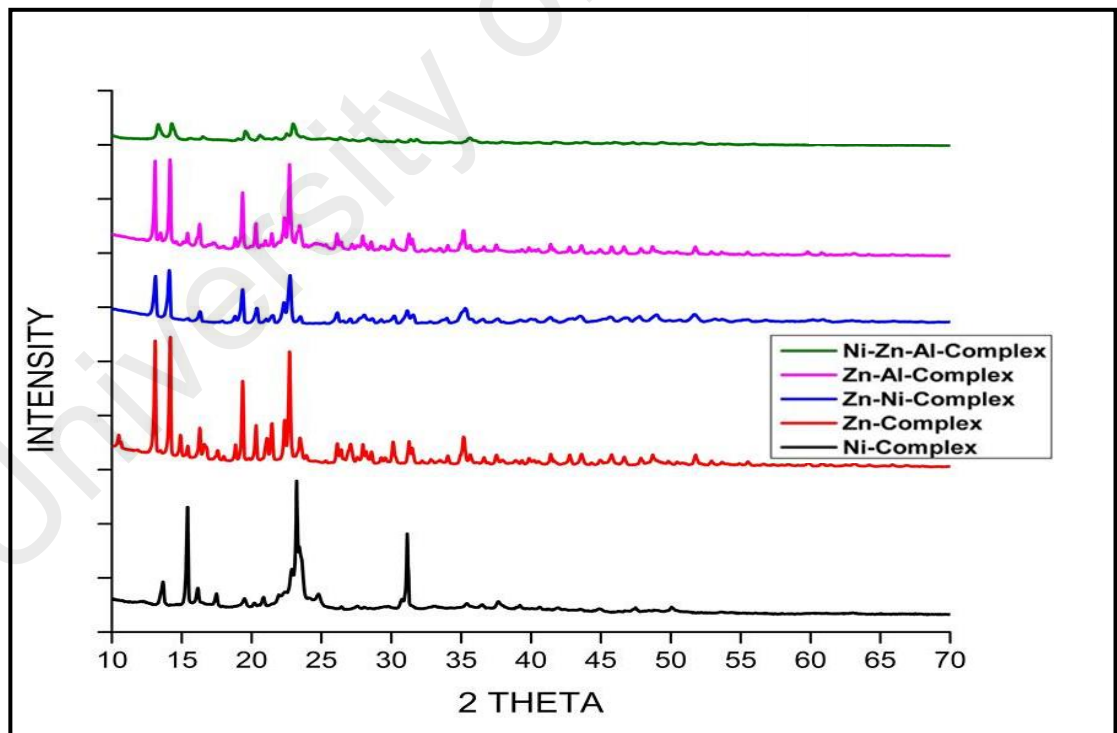


**Figure 5.7:** XRD Patterns of Monometallic and Heterometallic Complexes

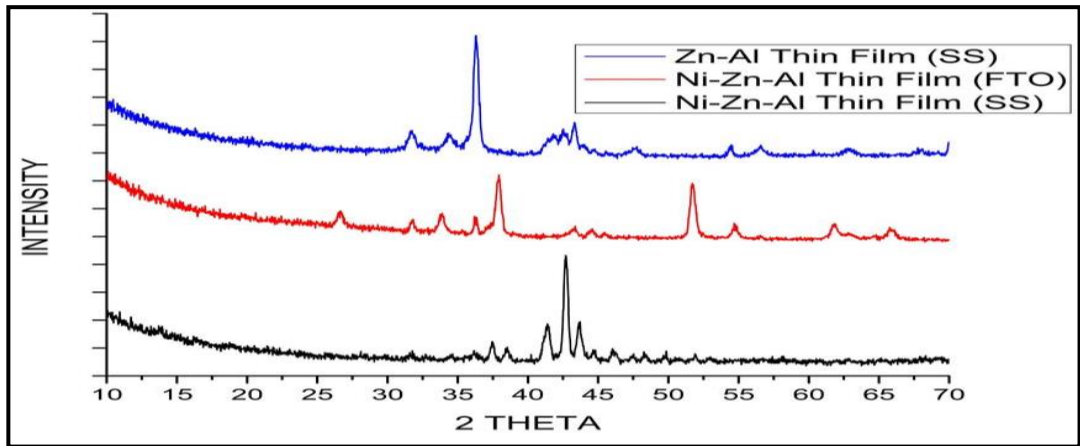


**Figure 5.8:** XRD Patterns of Thin Films

In addition to better crystal morphology, narrow crystal size distribution; yield of the synthesized materials was remarkable. Figure 5.9 illustrates the percent yield of the crystalline material produced by the proposed process. Ni and Zn clusters have shown better yield (above 80%), while Al-cluster was the least in production (77%).

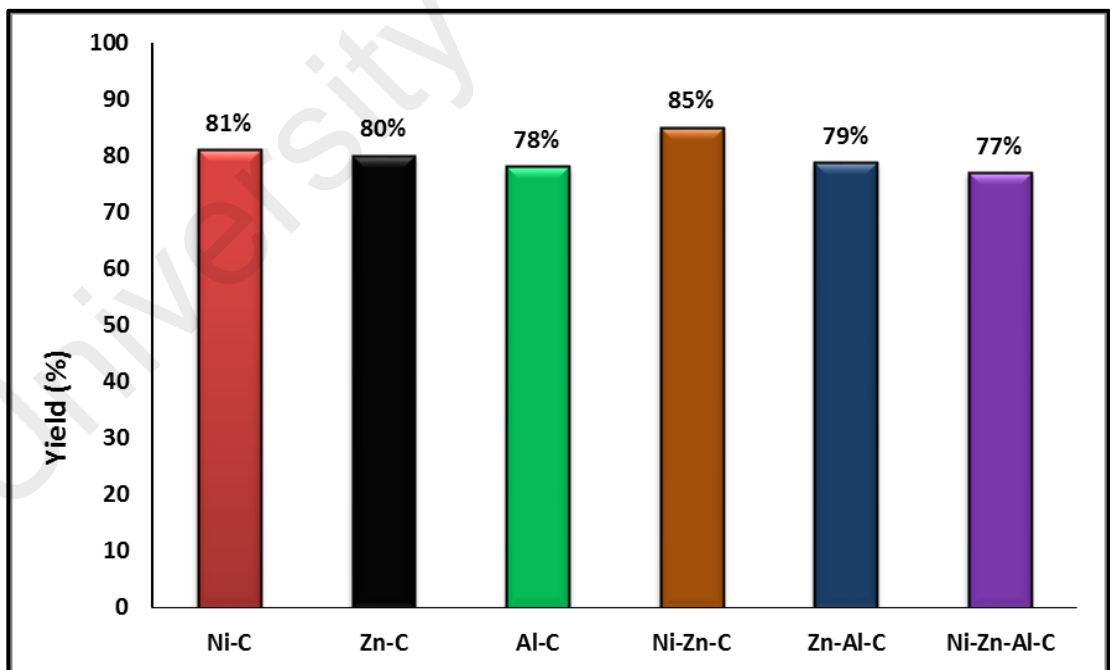


**Figure 5.9:** Yield of the Crystalline Materials

It might be due to the loss of ultra-fine particles during filtration stage. With efficient filtration systems, yield can be increased up to 85-90%. From the results it is clear that 2-Step process has shown excellent potential for the production of a wide range of industrial catalysts and composite materials

## **5.5 Summary**

A 2-step process was used for the synthesis of heterometallic MOFs and their thermal decomposition to form nano sized clusters. In the first stage, precipitation process was effectively employed to produce monometallic and polymetallic complexes. 2,2'-bipyridine was used as the ligand to interlink metal atoms (Ni, Zn and Al). In the second stage, heterometallic complexes were thermally decomposed to produce nano clusters. The crystalline products were characterized by FTIR, FeSEM, EDX and XRD. The developed process was found to greatly improve the size, morphology and porosity of the crystalline materials.

The yield of Ni, Zn and Al clusters were above 81%, 80% and 78% respectively, while the yield of Ni-Zn, Zn-Al and Ni-Zn-Al complexes were 85%, 78.5% and 77% respectively. Addition of Ni metal-atoms to Zn-Al composites changed the size and morphology of the crystalline particles. Thermal decomposition of Zn-Al complex produced mesoporous nano balls. However, Zn-Ni-Al complex caused formation of needle like crystals.

The synthesized materials can be used in a variety of industrial applications. In addition, availability of ligand (2,2'-bipyridine), solvents (ethanol, 2-proapnol and DMF) and their relevant information in the literature make this 2-step process an attractive process for the production of a variety of catalysts and special alloys.

## CHAPTER 6: SYNTHESIS AND APPLICATION OF A SUPPORTED CATALYST

### 6.1 Introduction

Fenton oxidation, an advanced oxidation process, is an efficient method for the treatment of recalcitrant wastewaters. Unfortunately, it utilizes  $H_2O_2$  and iron-based homogeneous catalysts, which lead to the formation of high volumes of sludge and secondary pollutants. To overcome these problems, alternate option is the usage of heterogeneous catalyst, particularly the supported type metallic catalysts.

In this chapter, a supported type catalyst was developed to provide an alternative solution for homogeneous Fenton oxidation. Fe-ZSM-5 was synthesized using a new two-step process. Next, the catalyst was characterized by EDX, SEM, FTIR and BET to explore the morphological changes occurred at the zeolitic matrix. Furthermore, efficiency of the developed catalyst was evaluated by performing heterogeneous Fenton oxidation to degrade the azo dyes.

Optimize conditions for the catalyst's synthesis and heterogeneous Fenton oxidation conditions both are important. However, in the present chapter, in addition to synthesis of Fe-ZSM-5 catalyst, only Fenton process was optimized. In order to assess and optimize mineralization efficiency, Taguchi method was coupled with principal component analysis. Under optimized conditions, synthesized catalyst was further evaluated to degrade higher concentrations of a dye as well as the dye mixture. In addition to these activities, the developed catalyst was evaluated for its stability and reusability.

## 6.2 Background

Wastewater discharge from the energy, mineral processing, paper, plastic, textile, and cosmetic industries contains toxic organic compounds, dyestuffs, and other recalcitrant materials which adversely affect the environment and the quality of water reservoirs (Roberts et al., 2013). The textile industry is particularly wasteful, with 125-150 L of discharged wastewater for every 1 kg of product (Körbahti & Tanyolaç, 2008). The situation is further complicated by the fact that there are approximately 100,000 commercial dyes and pigments, available in the market and 10-15% of which find their way into the environment during the dyeing process (Inoue et al., 2006). This discharged wastewater has high levels of suspended solids and organic compounds, both toxic and otherwise, resulting in turbid, colored solutions with a wide pH range of 5-12 that in turn increase chemical and biochemical oxygen demand (Akan et al., 2009; Faryal & Hameed, 2005; Qin et al., 2014; Savin & Butnaru, 2008).

Commercial synthetic dyes are grouped into 20-30 classes based on their chemical structures or chromophores (Lucas & Peres, 2006), with azo dyes accounting for 60-70% of these overall (Vinodgopal & Peller, 2003). These dyes are characterized by one or more azo groups (-N=N-) and have poor biodegradability (Karthikeyan et al., 2011) that proceeds slowly (Ulson et al., 2010). As a result, these toxic and carcinogenic substances are always found in wastewater (Meric et al., 2003; Shu et al., 2010), necessitating intricate treatment prior to disposal.

Fenton oxidation, one of several advanced oxidation processes, is an efficient wastewater treatment method for recalcitrant wastewater. Use of iron salts and H<sub>2</sub>O<sub>2</sub> under acidic conditions produces hydroxyl radicals (HO<sup>•</sup>) (Eq 6.1) non-selective and highly oxidative species with a redox potential of 2.80 eV, making it capable of mineralizing a wide range of recalcitrant organic contaminants (Matta et al., 2007; Uslu

& Balcioglu, 2009). This process is advantageous because it is characterized by high mineralization efficiency, simple operation, and short reaction times. However, the required pH and high cost of H<sub>2</sub>O<sub>2</sub> and the excess Fenton reagents required limit the application of this process. Besides, high concentration of iron results in production of a large volume of sludge during the neutralization stage of process, which is undesirable as the concentration of iron ions in waste discharge should not exceed 2 ppm, according to limits established by the European Union (Dukkanci et al., 2010b; Navalon et al., 2010).



6-1

Heterogeneous solid catalysts have been developed to overcome these issues. In the heterogeneous Fenton process, the active phase is generally immobilized on a porous support. A wide range of solid catalysts have been developed for this process, such as Fe-Cu, Al-Fe, Al-Cu, MnO<sub>2</sub>, Ni<sub>2</sub>O<sub>3</sub>, Pt, Fe, and Cu, which in turn can be supported on pillared clays, zeolites, or CuO, ZnO, and TiO<sub>2</sub>, supported on Al<sub>2</sub>O<sub>3</sub>/Al-MCM-41 have been used for heterogeneous Fenton process. However, among all these combinations, iron particles supported on a zeolite or activated carbon matrix are the most effective (Chang et al., 2009; Dong et al., 2010; Pirkanniemi & Sillanpaa, 2002; Qiu et al., 2005b). Moreover, among all the promising supports for heterogeneous process, ZSM-5 has captured the attention of many researches due to its high stability, large surface area, remarkable porosity, and unique surface chemistry. Iron particles suppress the reaction between iron and H<sub>2</sub>O<sub>2</sub> and the produced Fe<sup>+2</sup>/Fe<sup>+3</sup> complexes on the surface of ZSM-5 react with H<sub>2</sub>O<sub>2</sub> to initiate the Fenton catalytic cycle (Tekbaş et al., 2008).

Fe-ZSM-5 activity depends on the concentration, size, morphology, and surface area of the iron particles, and these parameters can normally be controlled through careful

dispersion of fine iron particles through the controlled, porous structure (Szostak et al., 1987). To date, various methods have been developed and introduced to design microporous and mesoporous Fe-ZSM-5 (Karthikeyan et al., 2012), including ion exchange (Kusic et al., 2006), hydrothermal processes (Dukkancı et al., 2010a), chemical vapor deposition (Battiston et al., 2003), and incipient wetness impregnation (Yan et al., 2014). Fe-ZSM-5 produced by hydrothermal process has shown better activity compared to that produced by other methods (Kiss et al., 2006); however, in all cases, metal leaching reduces catalyst activity, particularly in acidic media and at high temperature (Dukkancı et al., 2010a; Karthikeyan et al., 2012; Yan et al., 2014). These issues must be addressed if viable catalysts for the oxidation of wastewater are to be developed (Dantas et al., 2006).

The objective of this work was to study the stability and specific properties of Fe-ZSM-5 synthesized using a newly developed 2-step process with respect to heterogeneous Fenton oxidation. This method is based on a previous one used to synthesize heterometallic nanoparticles at low temperatures, and relies on the development of a metal-organic framework and its thermal decomposition in order to produce fine iron oxide particles. The efficiency of the synthesized Fe-ZSM-5 was tested against the decolorization of Acid Blue 113 and Total Organic Carbon (TOC) removal. Dye degradation trend was also evaluated at higher concentrations and in a mixture of dyes. Up to our knowledge, no one has used Fe-ZSM-5 for the degradation of Acid Blue 113.

Multiple process parameters, specifically initial dye and H<sub>2</sub>O<sub>2</sub> concentrations, initial pH value, catalyst amount, time, and temperature, were assessed and optimized. This method improves the efficiency, stability, and reusability of the catalyst (Banerjee et al., 2012; Yang et al., 2011).

## 6.3 Materials and Methodology

### 6.3.1 Reagents

Acid Blue 113 was chosen as the model dye because the two azo bonds in its chemical structure, as shown in Figure 6.1, make it particularly recalcitrant. To make dye mixture, Methyl Orange and Reactive Black 5 were selected. Dyes were procured from Sigma-Aldrich while 30% (wt/wt)  $\text{H}_2\text{O}_2$  was purchased from Merck. Iron chloride, 2,2'-bipyridine, 2-propanol, and ethanol were obtained from Merck and used for the preparation of the heterogeneous catalysts. ZSM-5 ( $\text{SiO}_2/\text{Al}_2\text{O}_3$  mole ratio: 50) was purchased from Zeolyst International. The initial pH of the synthetic dye solution was adjusted using 0.5 M  $\text{H}_2\text{SO}_4$  and 1 M  $\text{NaOH}$  (Merck). Quantitative estimation of  $\text{H}_2\text{O}_2$  concentration at the end of the experiment was accomplished using peroxide strips.

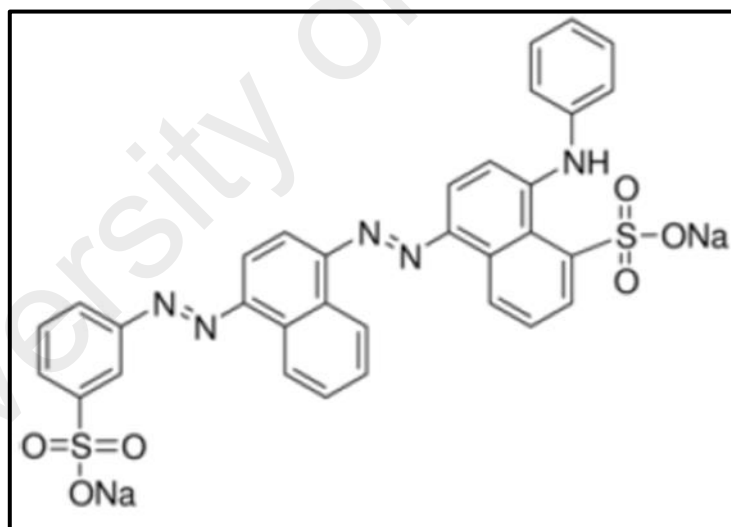


**Figure 6.1:** Chemical Structure of Acid Blue 113

### 6.3.2 Catalyst Preparation

Fe-ZSM-5 was prepared using two-step process, involving precipitation and thermal decomposition. In the first step, a mono-metallic complex was prepared by reacting iron chloride with 2,2'-bipyridine in 2-propanol. Then, 3.6 g of  $\text{FeCl}_2 \cdot 4\text{H}_2\text{O}$  and 8.5 g of 2,2'-

bipyridine were each separately dissolved in 20 mL of 2-propanol and mixed dropwise in a round bottom lab-scale crystallizer. The mixture was stirred for 2-3 h at  $38\pm 2$  °C. Fine crystals of  $[\text{Fe}(\text{byp})_2]\text{Cl}_2$  were then separated from the solution and washed with ether to remove impurities and yield the target at 78%. The produced monometallic complex showed enhanced features, indicating that it could be used directly in a variety of clean energy applications.

In the second step, the Fe-complex was impregnated with ZSM-5 zeolite particles. The concentration of the Fe-complex was adjusted to obtain a 3% Fe (wt/wt) catalyst. After impregnation, the crystalline particles were dried at 100 °C for 12 h and then calcined in air at 700 °C for 7 h. The temperature was ramped slowly to completely remove the ligand.

**Table 6.1:** EDX analysis of ZSM-5 and Fe-ZSM-5

Catalyst Clusters	Weight Composition (%)				
	Si	Al	O	C	Fe
Fe-ZSM-5	31.9	1.7	63.3	0.0	3.1
ZSM-5	41.4	2.2	54.3	0.0	-

Characterization of both the Fe-complex and Fe-ZSM-5 was performed using EDX, SEM, and FTIR. Surface morphology and composition were additionally analyzed using the Phenom ProX SEM. The surface area method was used to calculate the percentage composition of ZSM-5 and Fe-ZSM-5; the corresponding data is provided in Table 6.1. Thermal decomposition of the complex caused the formation of nano-sized iron particles on the ZSM-5 matrix.

FTIR studies were conducted using a Perkin Elmer FTIR Spotlight 400. The FTIR spectra for  $[\text{Fe}(\text{bpy})_2]\text{Cl}_2$ , ZSM-5, and Fe-ZSM-5 were analyzed for shifts due to coordinate bridging in  $[\text{Fe}(\text{bpy})_2]\text{Cl}_2$  and for the formation of the new complex.

The surface area, pore volume, and pore width of the ZSM support and the Fe-ZSM-5 catalyst are presented in Table 6.2. The Brunauer-Emmett-Teller (BET) method was employed to calculate specific surface areas and average pore width.  $\text{N}_2$  adsorption-desorption isotherms were used to calculate the total pore volume. Finally, the t-plot method was employed to calculate the micropore volume.

**Table 6.2:** Pore Structure Characteristics of the ZSM-5 and Fe-ZSM-5 Catalyst

Sample	$S_{\text{BET}}$ ( $\text{m}^2/\text{g}$ )	$S_{\text{micro}}$ ( $\text{m}^2/\text{g}$ )	$S_{\text{ext}}$ ( $\text{m}^2/\text{g}$ )	$V_t$ ( $\text{cm}^3/\text{g}$ )	$V_{\text{micro}}$ ( $\text{cm}^3/\text{g}$ )	Pore width (nm)
ZSM-5	293.59	241.75	51.85	0.17	0.11	2.40
Fe-ZSM-5	243.93	112.35	131.57	0.16	0.06	2.68

$S_{\text{BET}}$  is the specific surface area,  $S_{\text{ext}}$  is the external surface area,  $V_t$  is the total pore volume, and  $V_{\text{micro}}$  is the micropore volume.

### 6.3.3 Experimental Design

In this work, Minitab 16 was used to program a Taguchi orthogonal array in order to design the oxidation experiments.  $[\text{Dye}]_{\text{ini}}$ , Dye/catalyst (wt/wt), catalyst/ $\text{H}_2\text{O}_2$  (wt/wt), pH, reaction time, and temperature were chosen as the control factors while TOC removal, decolorization, and degradation were selected as the responses. This method recommended a total of 27 experiments, a significant improvement over the 729 that would have been required to fully test each factor with relation to the others (Asghar et al., 2014d).

Preliminary experiments to determine concentration ranges for the input variables followed the design used in researcher's previous study. For this purpose, 100 mL of

dye solution (100 mg/L) was treated with different amounts of the iron catalyst and H<sub>2</sub>O<sub>2</sub>. The amount of catalyst and H<sub>2</sub>O<sub>2</sub> ranged from 100 to 200 mg and 2 to 5 mL, respectively. The reaction temperature was kept constant at 30 °C and the pH was maintained at 3. The initial concentration of the dye and operating range determined for the previously stated variables are provided in Table 6.3. The L<sub>27</sub> orthogonal array for the experimental design is given in Table 6.4.

**Table 6.3:** Taguchi Design Factors and Their Levels

<b>Operating Parameters</b>	<b>Level 1</b>	<b>Level 2</b>	<b>Level 3</b>
Dye (mg/L)	100	150	200
Dye: Catalyst (wt/wt)	0.75	1.00	1.50
H <sub>2</sub> O <sub>2</sub> : Catalyst (wt/wt)	1	1.7	2.5
pH	3	5	9
Temperature (°C)	30	40	50
Time (h)	1	2.5	4

**Table 6.4:** L27 Orthogonal Design, Experimental Results, and Taguchi Analysis

Run	Dye (mg/L)	Dye/Catalyst wt/wt	H <sub>2</sub> O <sub>2</sub> /Catalyst wt/wt	pH	Time h	Temperature (°C)	Decolorization %	Dye Removal %	TOC %
1	1	3	1	1	1	1	91.35	92.76	46.80
2	1	3	1	1	2	2	97.16	97.73	51.32
3	1	3	1	1	3	3	99.63	99.83	58.30
4	1	2	2	2	1	1	91.63	93.01	37.28
5	1	2	2	2	2	2	99.26	99.52	77.40
6	1	2	2	2	3	3	99.75	99.94	63.96
7	1	1	3	3	1	1	79.24	82.43	51.50
8	1	1	3	3	2	2	95.37	96.19	52.14
9	1	1	3	3	3	3	97.53	98.04	60.24
10	2	3	2	3	1	2	48.84	49.23	26.90
11	2	3	2	3	2	3	72.20	72.32	18.19
12	2	3	2	3	3	1	65.55	65.65	22.19
13	2	2	3	1	1	2	99.07	99.17	48.59
14	2	2	3	1	2	3	99.84	99.94	60.49
15	2	2	3	1	3	1	99.91	99.99	70.50
16	2	1	1	2	1	2	66.15	66.24	22.21

**Table 6.4:** L27 Orthogonal Design, Experimental Results, and Taguchi Analysis (Continued)

Run	Dye	Dye/Catalyst	H <sub>2</sub> O <sub>2</sub> /Catalyst	pH	Time	Temperature	Decolorization	Dye Removal	TOC
	(mg/L)	wt/wt	wt/wt		h	(°C)	%	%	%
17	2	1	1	2	2	3	97.70	97.80	46.10
18	2	1	1	2	3	1	75.47	76.03	27.90
19	3	3	3	2	1	3	58.32	61.71	24.67
20	3	3	3	2	2	1	89.34	90.27	26.37
21	3	3	3	2	3	2	99.07	99.22	54.73
22	3	2	1	3	1	3	65.71	68.51	29.13
23	3	2	1	3	2	1	70.61	73.02	22.29
24	3	2	1	3	3	2	85.78	86.99	18.50
25	3	1	2	1	1	3	98.71	98.89	54.85
26	3	1	2	1	2	1	99.56	99.67	54.38
27	3	1	2	1	3	2	99.79	99.88	67.81

## 6.4 Experimentation

Experiments were performed in 500 mL Erlenmeyer flasks equipped with magnetic stirrers. In each experiment, 100 mL of the dye solution was introduced to the flask and adjusted for pH accordingly. The desired amount of catalyst and H<sub>2</sub>O<sub>2</sub> solution was then added and the resulting mixture was stirred at 250 rpm. The start time was marked as the point when H<sub>2</sub>O<sub>2</sub> was added. At the end of the experiment, samples were collected from the treated solution, filtered with 0.20 μm Millipore syringe filters, and immediately analyzed.

### 6.4.1 Analysis

A digital pH meter (Cyberscan pH 300, Eutectic Instruments) was used to measure pH values. Quantitative measurement of residual H<sub>2</sub>O<sub>2</sub> in the treated wastewater was carried out using peroxide test strips (Merck).

All of the raw and treated samples were analyzed using a UV spectrophotometer (Spectroquant Pharo 300, Merck), after which the decolorization and degradation efficiency of the samples was calculated.

$$\text{Decolorization}(\%) = \left(1 - \frac{Abs_t}{Abs_i}\right) \times 100 \quad \text{6-2}$$

$$\text{Degradation}(\%) = \left(1 - \frac{C_t}{C_o}\right) \times 100 \quad \text{6-3}$$

Where Abs<sub>i</sub>, and Abs<sub>t</sub>, are the UV absorption determined at λ<sub>max</sub> for each dye and mixture at initial and at a certain time t. λ<sub>max</sub> for the Acid Blue 113, Reactive Black 5

and Methyl Orange were 566 nm, 598 nm and 462 nm, respectively. Similarly  $C_0$  and  $C_t$  are the dye concentrations, calculated at initial and at a certain time  $t$ .

In addition to the decolorization measurements, TOC values of the treated samples were analyzed using a TOC Analyzer (SHIMADZU-00077). TOC was calculated as the difference between the total carbon content and inorganic carbon content in the treated sample. TOC removal was calculated as follows:

$$TOC(\%) = \left( 1 - \frac{TOC_f}{TOC_0} \right) \times 100 \quad 6-4$$

Treated samples at optimized conditions were also examined by high performance liquid chromatography (HPLC) using an Agilent technology 1200 series. This analysis has given further details about the degradation intermediates and final products. C18 column (4.6mm  $\times$  150 mm  $\times$  5 $\mu$ m) at 25 °C was used as the separation column for finally produced compounds, with the mobile phase acetonitrile/water (v/v) operated at 60/40 ratio and a flow rate of 1 ml/min. To identify compounds generated from the Fenton degradation of Acid Blue 113, the HPLC system was calibrated using standard analytical reagents namely benzene, phenol, aniline, hydroquinone, benzoquinone, catechol, formic acid, malic acid and oxalic acid. The Fenton-oxidation compounds were identified by comparing their retention times with those of calibrated runs under similar conditions.

#### 6.4.2 Taguchi Optimization Steps

The Taguchi method is a robust statistical technique that employs orthogonal arrays for designing experiments. Use of orthogonal arrays allows for an evaluation of factors using the minimum number of experiments, thereby reducing cost and time. The main

feature of this method is that it relies on the signal-to-noise (S/N) ratio instead of the precise experimental results. Here, 'signal' implies the mean value while 'Noise' shows the standard deviation term. Lower variability is ensured by maximizing this ratio. The Taguchi method classifies S/N ratios as smaller is better, normal is better, and larger is better. The formulas representing these ratios are provided in Table 6.5.

The application of this method is limited to single response processes, and situation gets complicated with multi-response processes like the one analyzed in this study, potentially increasing time and cost. However, it can be combined with other statistical techniques to overcome this limitation; in this case, PCA is especially applicable [35,36].

PCA is a multivariate statistical technique that uses the S/N ratio obtained from the Taguchi analysis. It reduces the dimensionality of a data set consisting of a number of interrelated variables while retaining variation as much as possible in the data sheet (Gu et al., 2014), and is effected by converting data into components whose contribution to the variability of the original data is easy to identify, so-called principal components. Table 6.5 outlines the integration of these two methods (Dubey & Yadava, 2008; Gauri & Chakraborty, 2009).

**Table 6.5:** Theoretical Framework of the Taguchi Method Coupled With Principle Component Analysis (PCA)

<b>Taguchi Method</b>		
<b>Step</b>	<b>Detail</b>	<b>Equation</b>
Step: Computing S/N ratios	Smaller is better	$\frac{S}{N} = -10 \log \left( \frac{1}{n} \sum_{k=1}^n y_i^2 \right)$
	Larger is better	$\frac{S}{N} = -10 \log \left( \frac{1}{n} \sum_{k=1}^n \frac{1}{y_i^2} \right)$
	Normal is better	$\frac{S}{N} = -10 \log \left( \frac{1}{n} \sum_{k=1}^n \frac{\mu^2}{\sigma^2} \right)$
<b>Principal Component Analysis</b>		
Step 1: Normalizing S/N ratios	<ul style="list-style-type: none"> <li>• Normalization of S/N ratios (output of Taguchi method) prior to PCA transformation</li> </ul>	$\bar{x}_i(n) = \frac{x_i(k) - \mu_i}{\sigma_i}$
Step 2: Finding covariance matrix (Cx)	<ul style="list-style-type: none"> <li>• Computation of covariance matrix to decorrelate S/N ratio</li> <li>• Obtained by multiplying the transpose of matrix <math>\bar{X}</math> with the original matrix</li> </ul>	$C_x = \frac{1}{n-1} \begin{pmatrix} \bar{x}_1 \bar{x}_1^T & \bar{x}_1 \bar{x}_2^T & \dots & \bar{x}_1 \bar{x}_m^T \\ \bar{x}_2 \bar{x}_1^T & \bar{x}_2 \bar{x}_2^T & \dots & \bar{x}_2 \bar{x}_m^T \\ \vdots & \vdots & \ddots & \vdots \\ \bar{x}_n \bar{x}_1^T & \bar{x}_n \bar{x}_2^T & \dots & \bar{x}_n \bar{x}_m^T \end{pmatrix}$
Step 3: Eigenvalue	<ul style="list-style-type: none"> <li>• Eigenvalue (<math>\lambda_i</math>) corresponding to each response can be computed by solving the determinant of <math>C_x</math></li> <li>• In PCA, these are used to find the Eigenvector</li> </ul>	$\det(C_x - \lambda_i I) = 0$
Step 4: Eigenvector	<ul style="list-style-type: none"> <li>• Eigenvector (<math>A_i</math>) provides information about the data pattern</li> </ul>	$C_x A_i = \lambda_i A_i$
Step 5: Principal component	<ul style="list-style-type: none"> <li>• Principal Component (<math>Y_i</math>) is computed to decrease the variance in the reported data.</li> </ul>	$Y_i = X * A_i,$
Total Principal index (TPCI)	TPCI is computed to find out the average factor effect at each level corresponding to each experimental run	$[TPCI] = P_i Y_i *$

\* Where  $P_i$  represents the proportion explained with the principal component

### **6.4.3 Leaching and Deactivation of Fe-ZSM-5**

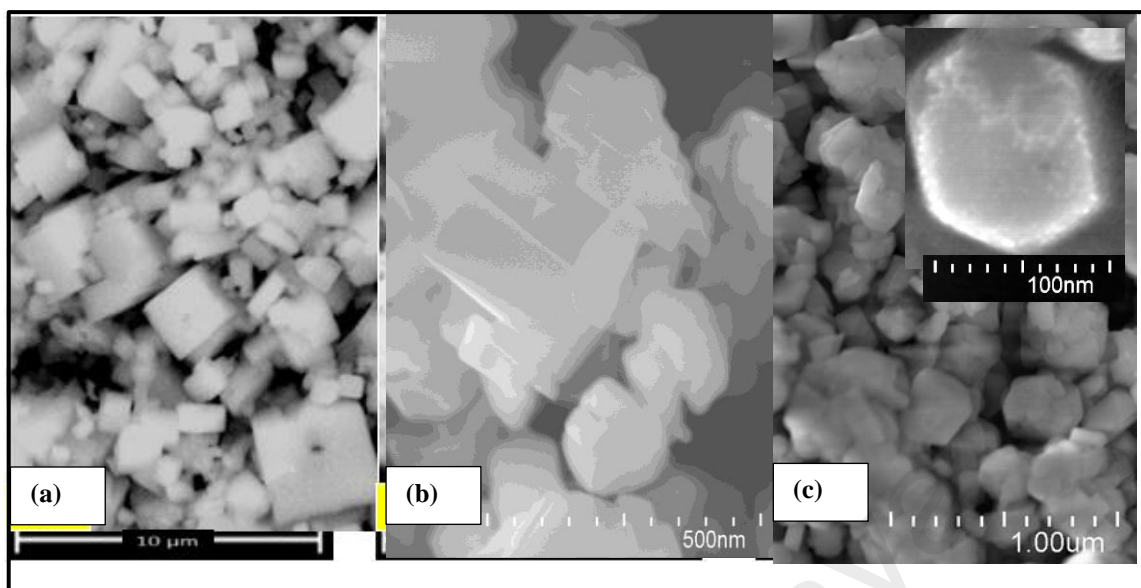
Fe-ZSM-5 stability was determined by EDX, SEM, and FTIR. Ten different samples of the catalyst were separated from the treated dye solutions through filtration, washed with aqueous methanol, and dried at temperatures up to 200 °C. EDX, SEM, and FTIR were then used to examine changes in composition, chemical structure, and morphology caused by metal leaching and in-situ transformation. Catalyst reusability was also assessed.

## **6.5 Results and Discussion**

### **6.5.1 Characterization of Fe-ZSM-5**

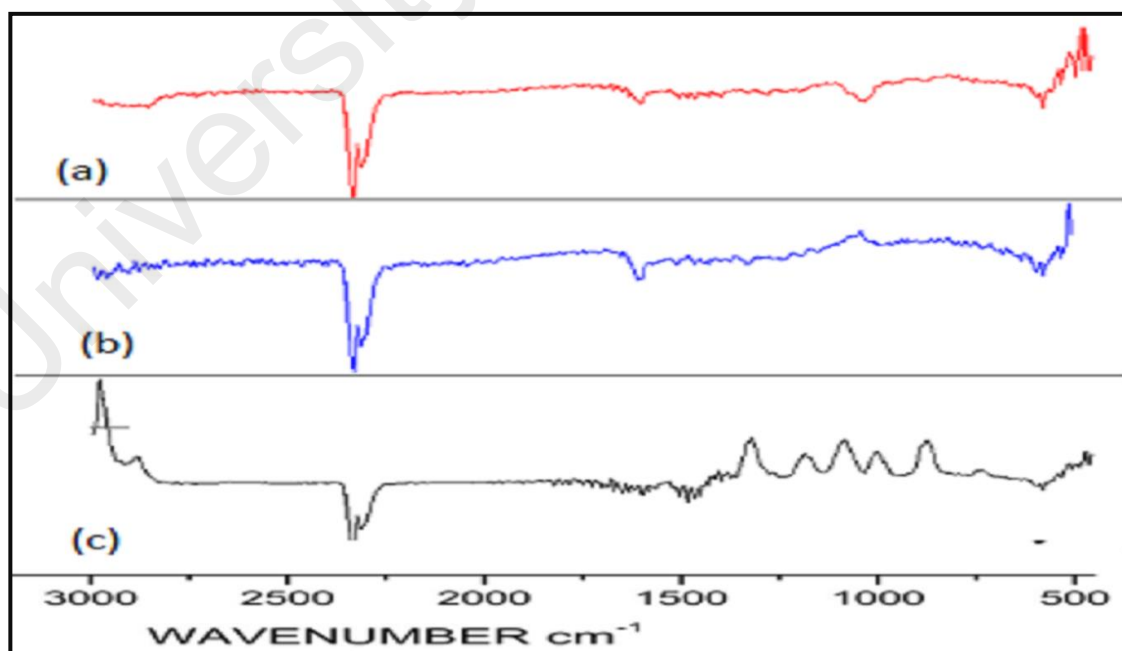
The surface area method was used to calculate the percentage composition of ZSM-5 and Fe-ZSM-5. A significant amount of carbon, nitrogen, and chlorine was present in the monometallic Fe-complex. However, after impregnation with ZSM-5, the coordinated ligand atoms were eliminated through thermal decomposition and calcination (Table 6.1). In addition, elemental mapping clearly illustrated a uniform distribution of silicon, aluminum, iron, and oxygen atoms inside the catalyst cluster. Silicon and oxygen were the most prominent, while aluminum was the least; however, their distribution was nearly homogenous.

Figure 6.2 provides SEM data. The crystal morphology of the Fe-complex was significantly changed after calcination. Thermal decomposition of the complex caused the formation of nano-sized iron particles in the ZSM-5 matrix.



**Figure 6.2:** FESEM images of (a) the Fe(byp) complex, (b) ZSM-5, and (c) Fe-ZSM-5

The FTIR spectra of the  $[\text{Fe}(\text{bpy})_2]\text{Cl}_2$  complex (Figure 6.3) was studied using 2,2'-bipyridine as a reference in order to track shifts due to coordinate bridging (Nazir et al., 2011).



**Figure 6.3:** FTIR Data for (a) the ZSM-5, (b) Fe-ZSM-5, and (c) Fe(byp) Complex

The major ring stretching vibrations  $\nu(\text{C}=\text{C})$  and  $\nu(\text{C}=\text{N})$  of the free ligand were detected at 1553 and 1579  $\text{cm}^{-1}$ , respectively. In the Fe-complex, slight shifts lead to corresponding vibrations in the range of 1561-1563 and 1592-1595  $\text{cm}^{-1}$ , respectively, while the breathing frequency shifted from 991 to 1012  $\text{cm}^{-1}$ . Similarly, new bands appeared in the range of 1094-1136 and 2886–2888  $\text{cm}^{-1}$  for Fe-ZSM-5.

The surface area, pore volume, and pore width of the ZSM support and Fe-ZSM-5 catalyst are presented in Table 6.2. The BET-surface area of the synthesized Fe-ZSM-5 decreased from 293.59 to 243.93  $\text{m}^2/\text{g}$ , while total pore volume decreased from 0.17 to 0.11  $\text{cm}^3/\text{g}$ . This change is due to the presence of iron oxide nanoparticles, which filled the ZSM-5 pores and effectively reduced the specific area and pore volume (Yan et al., 2014). The average particle size of the loaded material was 12.29 nm.

### **6.5.2 Process Optimization by Coupling the Taguchi Method with PCA**

The dye degradation, decolorization, and TOC removal efficiency data, as determined by the combined Taguchi and PCA method employed in this study, are provided in Table 6.4. A detailed analysis of the tabulated results shows that Fe-ZSM-5 can achieve 99% degradation and 77% mineralization for the selected 100 mg/L dye solution using 1 and 1.7 wt/wt ratios of catalyst and  $\text{H}_2\text{O}_2$  with respect to the dye, respectively. This result is similar to that obtained in researcher's previous work (Asghar et al., 2014c), and suggests that iron-based heterogeneous Fenton oxidation could be as efficient as the homogeneous equivalent. Furthermore, at higher dye concentrations of 200 mg/L, the selected protocol gave 68% mineralization and nearly 100% decolorization and dye degradation, respectively.

The responses obtained as a result of Fenton oxidation were then converted to S/N ratios. High degradation efficiency is desirable in Fenton oxidation; therefore, the larger the better S/N ratio was chosen (Table 6.5). These values were maximized for runs 5, 14, and 15. Because obtaining optimized values for each individual response was not viable, the S/N ratio at each level was optimized and converted to single component called “Total Principal Component Index” by using Principal Component Analysis (PCA).

University of Malaya

**Table 6.6:** The Obtained S/N Ratios, Normalized S/N Ratios, and TPCI Values

Run	S/N ratio			Normalized S/N ratio			TPCI
	Decolorization	Dye Removal	TOC	Decolorization	Dye Removal	TOC	
1	39.21	39.35	33.40	0.35	0.38	0.33	0.55
2	39.75	39.80	34.21	0.65	0.65	0.53	0.95
3	39.97	39.99	35.31	0.78	0.76	0.81	1.22
4	39.24	39.37	31.43	0.36	0.40	-0.18	0.27
5	39.94	39.96	37.77	0.76	0.75	1.43	1.56
6	39.98	39.99	36.12	0.78	0.77	1.01	1.34
7	37.98	38.32	34.24	-0.36	-0.22	0.54	0.02
8	39.59	39.66	34.34	0.56	0.57	0.56	0.88
9	39.78	39.83	35.60	0.67	0.67	0.88	1.16
10	33.78	33.84	28.60	-2.76	-2.88	-0.89	-3.30
11	37.17	37.19	25.19	-0.82	-0.90	-1.76	-1.85
12	36.33	36.34	26.92	-1.30	-1.40	-1.32	-2.09
13	39.92	39.93	33.73	0.75	0.73	0.41	0.96
14	39.99	39.99	37.03	0.79	0.77	1.24	1.48
15	39.99	40.00	35.56	0.79	0.77	0.87	1.27

**Table 6.6:** The Obtained S/N Ratios, Normalized S/N Ratios, and TPCI Values (Continued.)

Run	S/N ratio			Normalized S/N ratio			TPCI
	Decolorization	Dye Removal	TOC	Decolorization	Dye Removal	TOC	
16	36.41	36.42	26.93	-1.26	-1.35	-1.32	-2.04
17	39.80	39.81	33.27	0.68	0.66	0.29	0.83
18	37.55	37.62	28.91	-0.60	-0.64	-0.81	-1.08
19	35.32	35.81	27.84	-1.88	-1.71	-1.09	-2.40
20	39.02	39.11	28.42	0.24	0.24	-0.94	-0.30
21	39.92	39.93	34.76	0.75	0.73	0.67	1.11
22	36.35	36.72	29.29	-1.29	-1.18	-0.72	-1.63
23	36.98	37.27	26.96	-0.93	-0.85	-1.31	-1.63
24	38.67	38.79	25.34	0.03	0.05	-1.72	-0.94
25	39.89	39.90	34.78	0.73	0.71	0.67	1.10
26	39.96	39.97	34.71	0.77	0.75	0.66	1.13
27	39.98	39.99	36.63	0.78	0.76	1.14	1.42

First, the S/N ratio at each level was normalized. Subsequently, PCA was applied to the normalized data, using matrix  $\bar{X}$ . After the stepwise execution, matrix  $\bar{X}$  was converted into covariance matrix  $C_x$ , which was used to compute Eigenvalues for these responses.

Eigenvalues of the three principal components and the corresponding Eigenvectors are given in Table 6.7. The Eigenvalues obtained by PCA were 2.69, 0.31, and 0.002. This procedure transformed the normalized S/N ratios into a set of uncorrelated principal components; the value with an Eigenvalue greater than 1 was then chosen (Liao, 2004).

**Table 6.7:** Eigenvalues Obtained Through PCA Processing of the Normalized S/N Ratios

Principal Component	Eigenvalue	Proportion (%)	Cumulative (%)	Eigenvector
First	2.69	89	89	[0.595, 0.596, 0.539]
Second	0.31	10	99.9	[0.383, -0.38, 0.842]
Third	0.002	1	100	[-0.706, 0.708, -0.0002]

The Eigenvalue of the first principal component can be used to explain the performance characteristics of the Fenton oxidation. In this case, the first two Eigenvalues were used to compute the TPCI, since together they accounted for 99% of the observed variance. Larger TPCI values imply better process performance; based on the obtained values, it was therefore observed that pH significantly contributed to efficiency. Overall, the following trend was observed for influence of the assessed parameters:

$$\text{pH} > \text{Dye} > \text{Time} > \text{Dye/Fe}^{+2} > \text{H}_2\text{O}_2/\text{Fe}^{+2} > \text{Temperature}$$

The TPCI values listed in Table 6.8 and the corresponding data in Figure 6.4 could be used to optimize the operating parameters. In this vein, those parameters that provided the maximum TPCI values were selected (Table 6.8). The optimized values showed that consumption of iron catalyst was reduced by 90% in comparison with researcher's previous work (Asghar et al., 2014c); however, energy requirements increased. Since TPCI analysis ranked temperature at the lowest number in the list, therefore 30 °C was selected as the optimized value instead of 50 °C.

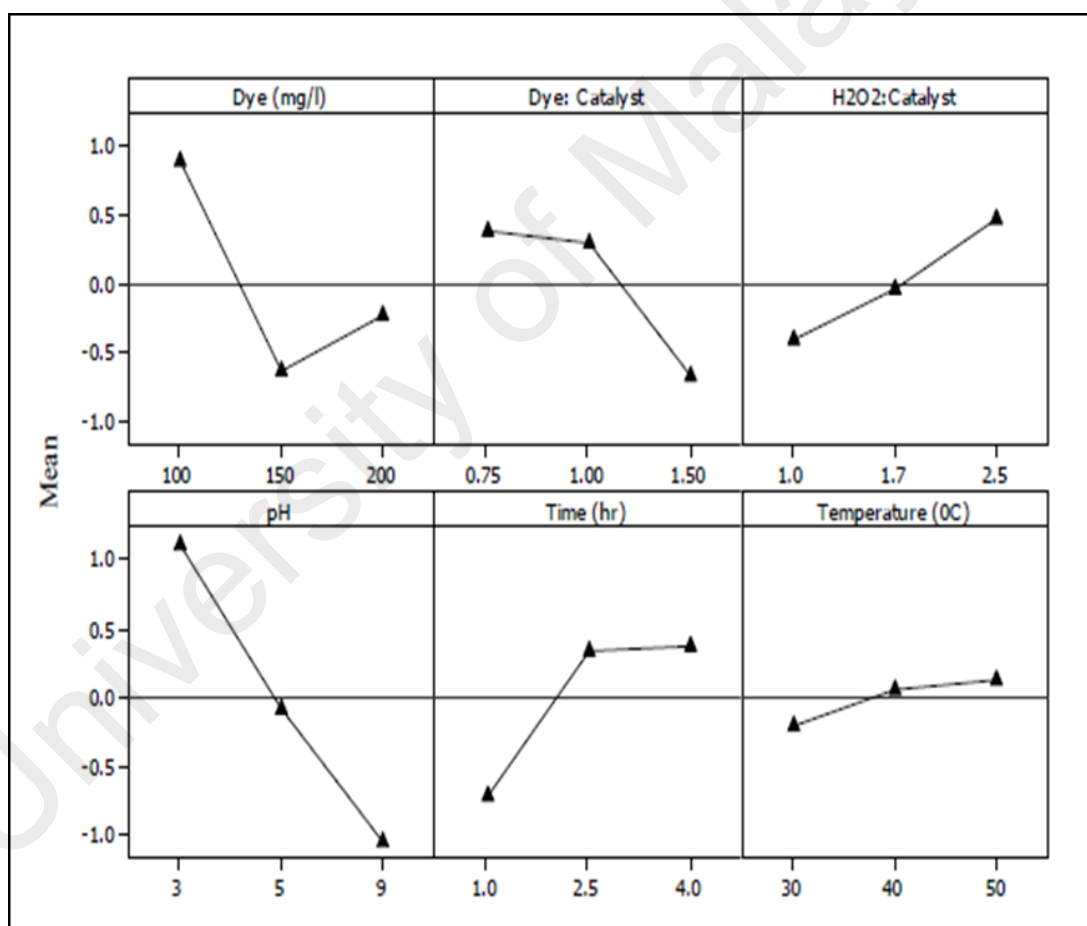


**Figure 6.4:** Mean TPCI Plots with Respect to Parameter Changes

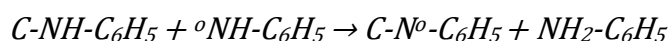
Reaction efficiency was then assessed at the optimized conditions. These experiments were also repeated at higher dye concentrations; the results are

summarized in Table 6.9. At higher dye concentrations, decrease in TOC removal was observed. This is because at higher concentration, degradation rate is low due to non-availability of hydroxyl radicals (Gomathi Devi et al., 2009).

**Table 6.8:** List of TPCI responses

Level	Dye	Dye: Fe	H <sub>2</sub> O <sub>2</sub> :Fe <sup>+2</sup>	pH	Time (h)	Temperature (°C)
1	0.88401	0.37928	-.41912	1.11866	-0.71866	-0.20613
2	-0.64688	0.29935	-0.04612	-0.07721	0.33794	0.06688
3	-0.2370	-0.67857	0.46530	-1.04139	0.38078	0.13931
Delta	1.53089	1.05784	0.88442	2.16005	1.09944	0.34545
Rank	2	4	5	1	3	6

Overall, it was confirmed that the heterogeneous reaction performs just as well as the homogeneous one, with the added advantage that it reduces consumption of the iron catalyst (Prihod'ko et al., 2011). To identify different compounds generated at optimized conditions, the HPLC system was employed. Traces of carboxylic acid, benzoquinone and aniline were detected corresponding to the peaks at ca. 1.92 min, 2.420 min and 5.97 min, respectively. Aniline formation would be in agreement with the oxidative hemolytic splitting of dye amino benzene moiety making a <sup>o</sup>NH-C<sub>6</sub>H<sub>5</sub> radical which could then abstract an amino hydrogen atom from other dye molecule (Zayani et al., 2008).



**6-5**

The other identified compound was benzoquinone which is often found in the degradation of benzene and phenol(Ajeel et al., 2015; Zayani et al., 2008).

Further oxidation and splitting of benzoquinone ring resulted into formation of carboxylic acids, particularly maleic acid and fumaric acid (Ajeel et al., 2015).

These results highlight the utility of this analytical method, which clearly can be used for the systematic investigation and optimization of multiresponse systems.

University of Malaya

**Table 6.9:** Optimized values for heterogeneous Fenton oxidation

Dye	Dye/Catalyst	H <sub>2</sub> O <sub>2</sub> /Catalyst	pH	Time	Temperature	Decolorization	Dye Removal	TOC
(mg/L)	wt/wt	wt/wt		h	(°C)	%	%	%
100	0.75	2.5	3	4	30	99.7	99.8	77
200	0.75	2.5	3	4	30	99.6	99.7	69
250	0.75	2.5	3	4	30	99.2	99.3	70
500	0.75	2.5	3	4	30	99.4	99.5	71
1,000	0.75	2.5	3	4	30	99.1	99.1	71.5

**Table 6.10:** ANOVA Analysis for Fenton Oxidation Parameters

Factor	Degree of Freedom	Sum of Squares	Mean Squares	F-ratio	p-value	Percent Contribution (%)
Dye	2	11.31	5.65	3.02	0.068	20.08
Dye/Catalyst	2	6.25	3.12	1.50	0.244	11.09
H <sub>2</sub> O <sub>2</sub> /Catalyst	2	3.55	1.77	0.81	0.458	6.30
pH	2	21.08	10.54	7.18	0.004	37.44
Time	2	6.98	3.49	1.70	0.204	12.40
Temperature	2	0.60	0.30	0.13	0.880	1.06

### 6.5.3 Analysis of Variance (ANOVA)

ANOVA is used in the Taguchi method to evaluate the experimental results and to determine the contribution of each factor to their overall variance (Asghar et al., 2014c). ANOVA is similar to regression analysis, which is employed to determine the relationship between response variables and one of more responses. These results are provided in Table 6.10.

Again, pH was the most significant variable, with a contribution of 37.44%; meanwhile, temperature was the least significant, with a contribution of 1.06%. The ANOVA results are in agreement with the TPCI results listed in Table 6.8. Based on the TPCI values, the regression analysis equation was calculated as follows:

$$TPCI = 2.61 - 0.0112 A - 1.49 B + 0.591 C - 0.343 D + 0.366 E + 0.0173 F \quad \mathbf{6-6}$$

Where A, B, C, D, E and F are dye (mg/L), dye/catalyst, H<sub>2</sub>O<sub>2</sub>/catalyst, pH, time (h) and temperature (°C).

### 6.5.4 Interaction of Operating Parameters

Fenton oxidation efficiency strongly depends not only on the process parameters themselves, but on the interaction between them. This section addresses the effect of that interaction and their effects on TOC removal and dye degradation.

#### 6.5.4.1 Interaction Between Operating Parameters with Respect to TOC

##### Removal

An interaction plot between the parameters Dye and Dye/Catalyst shows that an increase in the Dye/Catalyst ratio reduced mineralization efficiency for a constant dye concentration (Figure 5.5). Higher values of both of these parameters resulted in a significant decrease in mineralization efficiency. Maximum mineralization efficiency

was achieved at a dye concentration of 150 mg/L and a Dye/Catalyst ratio of 1.00. On the other hand, at constant dye concentrations, an increase in the H<sub>2</sub>O<sub>2</sub>/Catalyst ratio reduced TOC removal. Similar trends were observed between the Dye/Catalyst and H<sub>2</sub>O<sub>2</sub>/Catalyst ratios.

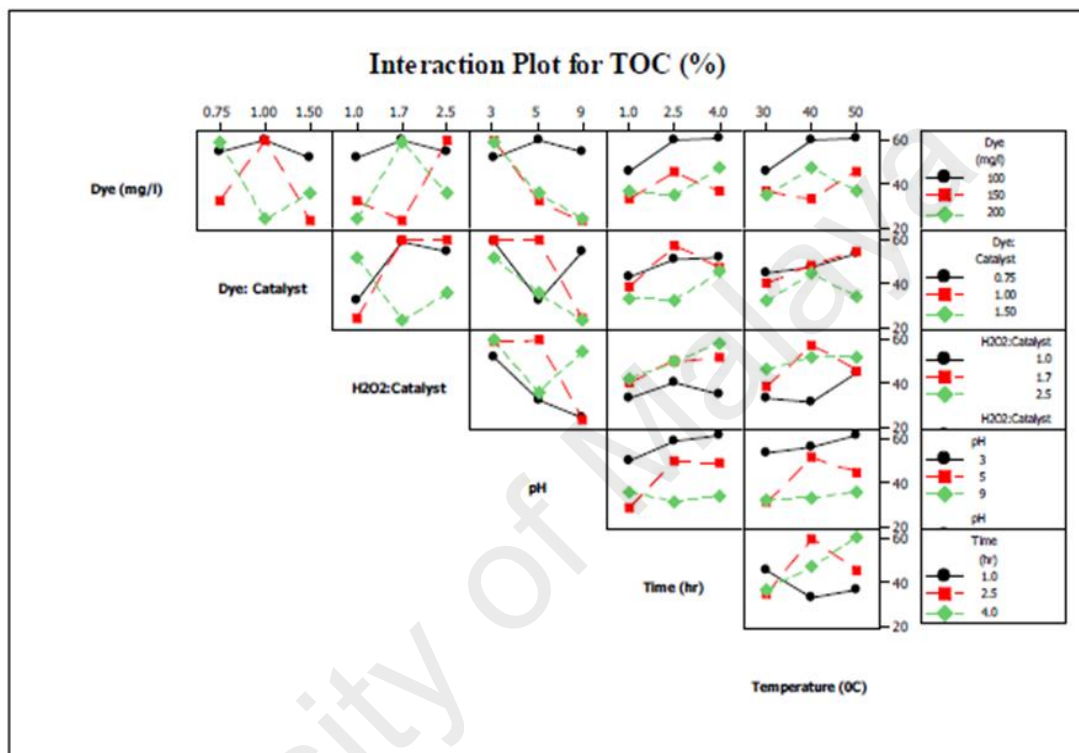
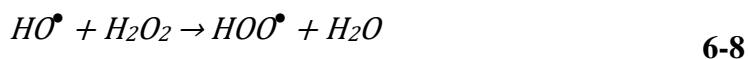
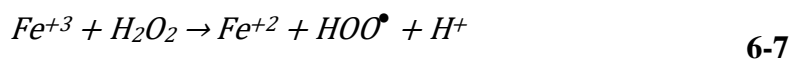


**Figure 6.5:** Interaction of Parameters with Respect to TOC

These results are consistent with the observation that at higher values for the Dye, Dye/Catalyst, and H<sub>2</sub>O<sub>2</sub>/Catalyst parameters, the amount of catalyst added is greatly reduced compared to added H<sub>2</sub>O<sub>2</sub>. This means that less amounts of the catalyst are available to interact with the H<sub>2</sub>O<sub>2</sub>, such that residual H<sub>2</sub>O<sub>2</sub> will react with the oxidized form of Fe<sup>+3</sup> or scavenge hydroxyl radicals through the following reactions (Neyens & Baeyens, 2003):



This results in a significant decrease in mineralization efficiency. This also makes the effect of pH on mineralization efficiency even more obvious than it already was; for all values studied of the operating parameters, lower pH values were favored, while higher pH values decreased mineralization efficiency. This is because ferrous ions are easily converted into ferric ions, which have a tendency to produce ferric-hydroxo complexes with H<sub>2</sub>O<sub>2</sub> at higher pH (Tekin et al., 2006).

Another parameter that is commonly addressed is the time required to elicit Fenton oxidation. In this process, reaction time is influenced by the rate of HO radical formation, which is in turn produced by the interaction between iron salt and H<sub>2</sub>O<sub>2</sub>. As observed from the graph in Fig. 5, at lower values for Dye and Dye/Catalyst, mineralization efficiency slowly increased with time as more H<sub>2</sub>O<sub>2</sub> was made available. In addition, excess amounts of H<sub>2</sub>O<sub>2</sub> may react with ferric salts after complete consumption of Fe<sup>+2</sup>; however, this reaction is slow, which is why at the end of reaction, mineralization efficiency decreased. However, at higher operating parameters, with the exception of the H<sub>2</sub>O<sub>2</sub>/Catalyst ratio, mineralization efficiency decreased with time. This was attributed to the fact that with excess amounts of H<sub>2</sub>O<sub>2</sub>, residual H<sub>2</sub>O<sub>2</sub> reacts with ferric iron present on the surface of the heterogeneous catalyst and degrades the intermediate products formed as a result of the initial degradation reaction (Li & Zhang, 2014). On the other hand, mineralization efficiency increased with temperature, with an approximate 20% increase observed when temperature rose from 30 to 50 °C. However, again, this increase was minimal at higher temperatures, since such a change increases the reaction rate between H<sub>2</sub>O<sub>2</sub> and the iron catalyst and thus decreases the

concentration of hydroxyl radicals (Sun et al., 2007). Finally, in several experimental runs, such as run 6 and 11, reduction in TOC removal efficiency was observed with an increase in temperature. This may be due to decomposition of  $H_2O_2$  at high temperatures.

#### 6.5.4.2 Interaction of Factors with Respect to Dye Decolorization Efficiency

Fenton oxidation induces rapid decolorization (Chang et al., 2009). This is because the color content of the dye is linked to the chromophore, or the conjugated unsaturated double bond present in the dye structure. The azo bonds in particular are active and can be easily broken by highly oxidative hydroxyl radical (Tantak & Chaudhari, 2006; Turhan et al., 2012). This explains why decolorization efficiency is generally higher than mineralization efficiency. As seen in Table 4.4, over 99% dye degradation was achieved in runs 14 and 15.

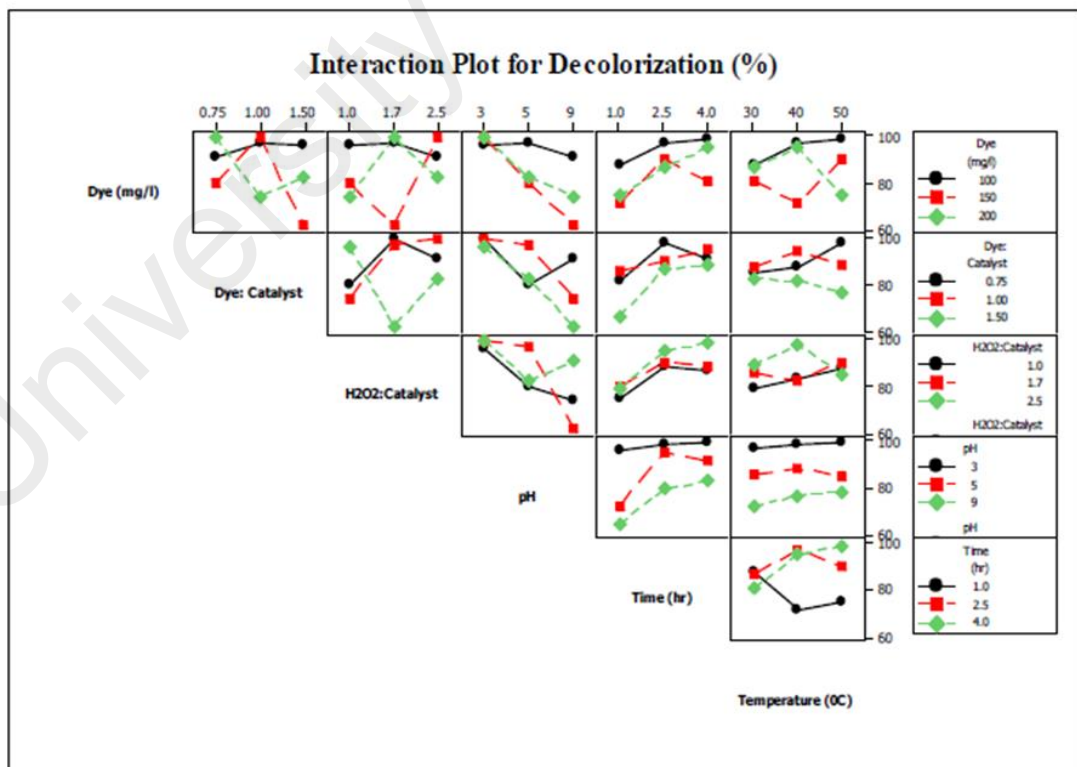


**Figure 6.6:** Interaction of Parameters with Respect to Decolorization

Nevertheless, the degree of decolorization varies with changes in the operating parameters. Interaction plots for dye degradation and decolorization efficiencies are shown in Figure 6.6 and Figure 6.7, respectively. Similar trends to those observed for TOC removal efficiency are present here; as dye degradation and decolorization efficiencies are directly linked with each other, this section treats the observed phenomenon for only dye degradation.

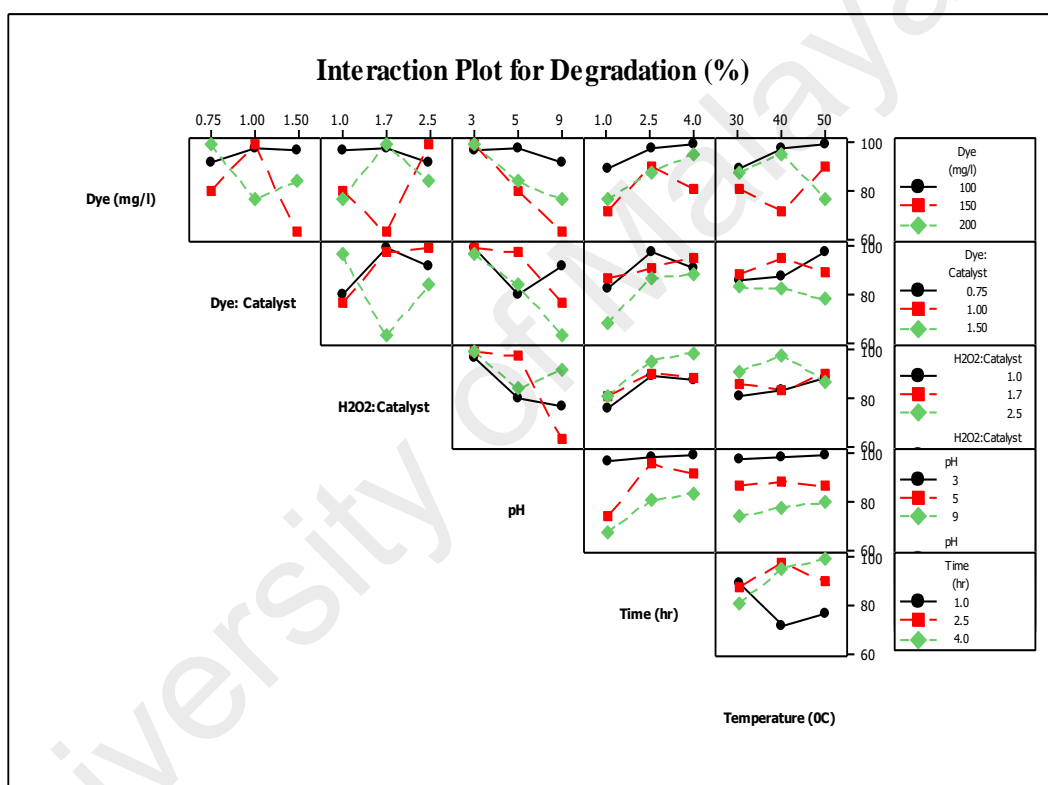


**Figure 6.7:** Interaction of Parameters with Respect to Degradation

Overall, dye degradation efficiency was higher at lower dye concentrations and Dye/Catalyst ratios. This is due to the fact that at higher dye concentrations and lower Dye/Catalyst ratios, the amount of catalyst added is higher, which may result in rapid production of hydroxyl radicals and adsorption of dye during the neutralization stage. On the other hand, an increase in dye concentration and the H<sub>2</sub>O<sub>2</sub>/Catalyst ratio reduced

decolorization efficiency. This observation can be supported by the fact that at higher  $\text{H}_2\text{O}_2$ /Catalyst ratios, excess amounts of  $\text{H}_2\text{O}_2$  are added in comparison with the amount of catalyst. This results in reduced production of hydroxyl radicals, which eventually leads to the observed effect.

As observed in Figure 6.6, pH had an inverse relationship with dye decolorization efficiency. This is because at higher pH values,  $\text{H}_2\text{O}_2$  decomposes to  $\text{O}_2$  and ferrous ions are converted into ferric-hydroxo complexes. Previous research shows that the decolorization process is rapid in nature and that complete decolorization can be achieved within 10 min. It is also evident from the Figure 6.6 that increase in time has no significant effect on dye decolorization efficiency. Although temperature was still found to be the least significant, its effect on dye decolorization efficiency was obvious in most cases. For instance, at higher dye concentration and temperature, dye degradation increased with time, though this effect may be due to thermal decomposition of the dye. On the other hand, lower dye concentrations and higher levels of the  $\text{H}_2\text{O}_2$ /Catalyst and Dye/Catalyst ratios resulted in decreased dye degradation efficiency. This is because higher temperatures thermally decompose  $\text{H}_2\text{O}_2$ , thus reducing the availability of  $\text{H}_2\text{O}_2$  for hydroxyl radical production.

#### **6.5.5 Long Term Stability and Reusability of Fe-ZSM-5**

In addition to the heterogeneous catalytic activity of the synthesized catalyst, it is important to consider stability and reusability as well. The decreased leaching of iron ions from zeolites during wastewater treatment is an indication of catalyst stability (Yan et al., 2014), so this parameter was tracked by EDX, SEM, and FTIR.

Ten different samples of the spent Fe-ZSM-5 were collected from the treated wastewater at the same temperature at which the reaction was performed. The samples

were then washed with methanol and dried at 200 °C before being analyzed by EDX. This method allows indirect measurement of the presence of iron ions leached into solution. In the majority of cases, less than 2% of leaching was observed; however, at a pH of 3 and at 30 °C, this value increased to 2-3%, further jumping to 6-7% once temperature was increased to 50 °C. This shows that catalysis mainly on the surface of the particles, instead of on the leached iron although a small amount of iron was present in the aqueous phase. Furthermore, SEM data (Figure 6.8) shows no significant difference in the crystal morphology between the fresh and spent catalysts.

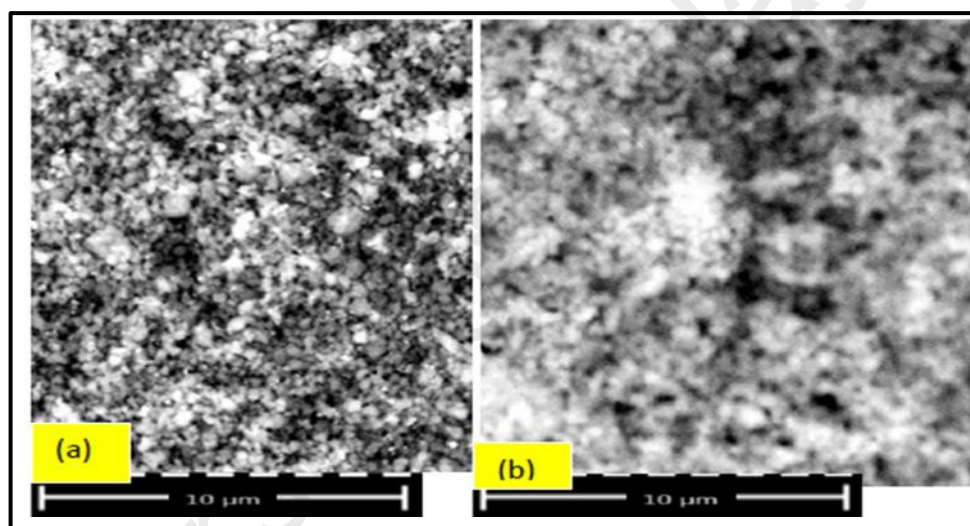


**Figure 6.8:** SEM Images of the (a) Fresh and (b) Spent Fe-ZSM-5

In addition, the FTIR spectra of the fresh and spent catalysts were also observed (Figure 6.9), yet showed no significant change in the chemical structure. To test the reusability, the recovered catalyst was subjected to the same process conditions after being dried at 200 °C for 3 h. Three trials were carried out, all of which indicated continued stability.

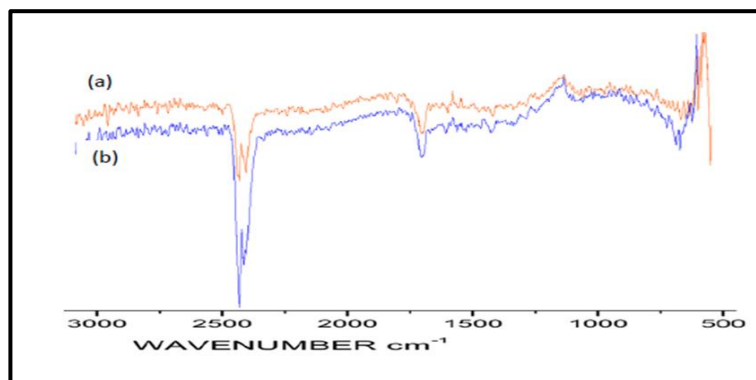


**Figure 6.9:** FTIR Spectra of the (a) Fresh Fe-ZSM-5 and (b) Spent Fe-ZSM-5

This indicated that the catalytic behavior of the developed catalyst was reproducible in consecutive experiments without a significant drop in its efficiency. This shows that catalyst deactivation, either due to iron leaching or in-situ transformation is insignificant.

#### 6.5.6 Efficiency of Synthesized Fe-ZSM-5 for Mixture of Dyes

A set of experiments were performed for the mixtures of three dyes containing 50%, 25% and 25% of Acid Blue 113, Reactive Black 5 and Methyl Orange, respectively. Two stock solutions with net concentrations of 50mg/L and 100mg/L were prepared and treated at optimized values (Table 6.9). Decolorization and dye removal was combined as dye degradation, and was measured by recording average variations in absorbance at  $\lambda_{\max}$  corresponding to each dye.  $\lambda_{\max}$  for the Acid Blue 113, Reactive Black 5 and Methyl Orange were 566 nm, 598 nm and 462 nm, respectively. Figure 6.10 illustrates the clear picture of degradation and TOC removal.

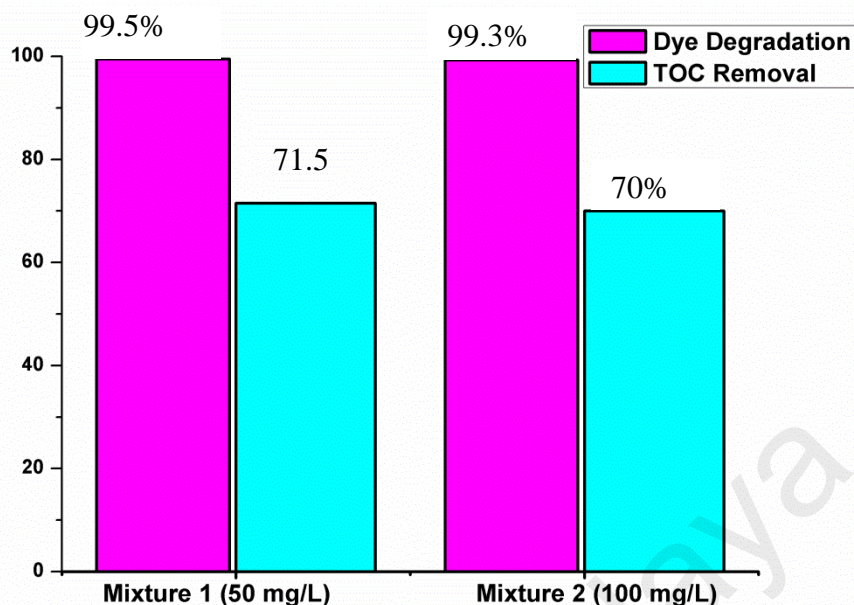


**Figure 6.10:** Degradation and TOC Removal of Mixture of Dyes Using Fe-ZSM-5

The measured values of dye degradation were 99.5% and 99.3%, while TOC removals were 71.5% and 70%. A reduction of 6-7% in TOC removal indicates that the mixture mineralization is relatively complex phenomena. Other reason may be the presence of Methyl Orange, the degradation of which is favored by alkaline medium particularly at pH 9 (Kaur et al., 2013). However, overall performance of the synthesized catalyst was remained excellent for the dyes mixtures.

## 6.6 Summary

In this study, Fe-ZSM-5 was synthesized using a newly developed 2-step process, after which the catalyst was characterized by SEM, EDX, FTIR, and BET. The performance of the developed catalyst was analyzed by performing Fenton oxidation on the azo dye Acid Blue 113. The catalyst has enhanced shown activity, yielding over 99% degradation and decolorization and 77% mineralization efficiency under optimized conditions (Dye/Catalyst=1 and  $H_2O_2$ /Catalyst=1.7 (wt/wt)). Furthermore, at higher dye concentrations (200 - 1,000 mg/L), and in mixture of dyes, the mineralization efficiency

was in the range of 69-71%. Applying Fe-ZSM-5 heterogeneous Fenton oxidation is economical, as 90% consumption of catalyst was reduced. Stability testing with respect to metal leaching and reusability showed that less than 2ppm of the iron was leached. Thus, the present study proved that the developed catalyst is efficient and economical.

University of Malaya

## CHAPTER 7: PROCESS OPTIMIZATION FOR SUPPORTED CATALYSTS

### 7.1 Introduction

In this chapter, influence of the independent process variables such as temperature ( $^{\circ}\text{C}$ ), time (h) and stirring speed (rpm) were considered to optimize the supported type Fe-ZSM-5 catalyst's synthesis. Metal Organic Framework (MOF) derived iron nano oxide particles were supported on ZSM-5 Zeolite using two step processes. Central Composite Design (CCD) was used to optimize the yield of the catalyst and ANOVA was used to analyse the data to obtain the interaction between the selected process variables.

The catalyst, synthesized at optimized conditions was then characterized using EDX, SEM, HRTEM, FTIR and BET. The optimized experimental yield was compared with the CCD predicted. Subsequently, the catalytic activity of the catalyst in Fenton Oxidation process was evaluated based on the degradation of the model azo dyes, Acid Blue 113, Methyl Orange, and Reactive Black. Apart from catalyst's yield, obtained mineralization efficiency was compared with other heterogeneous catalysts and discussed briefly to the synthesize a promising Fe-ZSM-5 catalyst for Fenton oxidation process

### 7.2 Background

Treatment of industrial wastewaters to remove the effluents before their discharge into any water streams is of utmost importance and environmental regulations strictly guideline the quality of the water discharged. These wastewaters contain recalcitrant contaminants including toxic organic compounds and dyes which significantly pollute the environment as well as poses threat to the aquatic life(Korbahti & Tanyolac, 2008). Conventional treatment methods such as homogenous advanced oxidation treatments

using iron based catalysts are used to degrade and decolorize recalcitrant contaminants (Innocenti et al., 2014). In addition to conventional methods, Fenton oxidation, an advanced and efficient oxidation process is used for the treatment of recalcitrant wastewaters (Luo et al., 2014; Nidheesh, 2015; Zhou et al., 2014). It utilizes  $H_2O_2$  and iron-based catalysts, to produce highly oxidative and non-selective species with a redox potential of 2.80eV which lead to the degradation of recalcitrant organic contaminants.

These methods are demonstrated to be very efficient and fast. However, the high cost associated with the use of oxidizing agent (especially  $H_2O_2$ ) as well as the use of stoichiometric amount of catalysts are the major disadvantages of AOPs based water treatment. Besides, these processes tend to release high concentration of iron, which is consumed during the treatment of wastewater and this causes the formation of secondary metal pollutants in the form of sludge which is not desirable. The European Union limited the concentration of discharged iron ions in treated effluents up to 2 ppm (Dukkancı et al., 2010b; Navalon et al., 2010).

To overcome these difficulties, heterogeneous processes were considered as viable and attractive alternatives. In heterogeneous Fenton process, generally a porous matrix is used to hold the active catalyst phase (Hartmann et al., 2010; Singh et al., 2014; Yu et al., 2015). A variety of catalytic materials such as Fe, Cu,  $MnO_2$ ,  $Ni_2O_3$ , ZnO, Pt, and  $TiO_2$  supported on pillared clay, zeolites or activated carbons have been used as heterogeneous catalysts (Akolekar & Bhargava, 1998; Gupta et al., 2011; Lucking et al., 1998; Nidheesh, 2015; Pirkanniemi & Sillanpaa, 2002; Rahim Pouran et al., 2015; Shen et al., 2015). Iron based catalysts supported on zeolites supports have been found more efficient compared to the other supported iron catalysts (Fajerweg et al., 1997; Pirkanniemi & Sillanpaa, 2002; Qiu et al., 2005a; Xu et al., 2012a; Yan et al., 2016).

Iron oxides supported on the ZSM-5 zeolites have shown high surface area, extraordinary stability, and remarkable porosity (Gonzalez-Olmos et al., 2011; Queiros et al., 2015; Yan et al., 2016). Fine-size iron oxide particles cause to suppress reaction between  $\text{H}_2\text{O}_2$  and iron, and the formed  $\text{Fe}^{+3}/\text{Fe}^{+2}$  complexes on the support (ZSM-5) surface (Tekbaş et al., 2008; Yan et al., 2016). Activity of Fe-ZSM-5 catalyst is normally controlled by the concentration and morphology of the iron particles dispersed on the porous support of ZSM-5 (Szostak et al., 1987). Normally, Fe-ZSM-5 catalyst is synthesized using hydrothermal process (Dukkancı et al., 2010a), ion exchange method (Kusic et al., 2006), incipient wetness impregnation (Yan et al., 2014) and chemical vapor deposition techniques (Battiston et al., 2003). Fe-ZSM-5 synthesized through ion-exchange method has shown lesser activity compared to that prepared by hydrothermal process (Kiss et al., 2006). However, many studies have shown that due to the acidic mediums and high temperature, leaching of metal occurs from the support matrix, which leads to deactivation of Fe-ZSM-5 catalyst (Dukkancı et al., 2010a; Karthikeyan et al., 2012; Yan et al., 2014).

Metal organic frameworks (MOFs) consist of iron as a metal in the ligand framework can potentially overcome the afore-mentioned disadvantages associated with the zeolites supported iron particles. These MOF based catalysts have significantly improved the efficiency, stability and the reusability of catalysts used for the heterogeneous oxidation processes (Banerjee et al., 2012; Cleveland et al., 2014; Yang et al., 2011).

The main objective and scope of this work was to optimize the synthesis of an efficient Fe-ZSM-5 catalyst using two-step process. In researcher's previously published work (chapter 6), MOF based Fe-ZSM-5 catalyst was synthesized using 2-step process, characterized and evaluated for the degradation and decolorization of

mixture of dyes. The results were encouraging, and 100% of dye degradation and 77% of total carbon content (TOC) removal were achieved at optimized conditions. These results had motivated authors to optimize the catalyst yield for larger scale production. Therefore, in this work, influence of the independent process variables such as temperature ( $^{\circ}\text{C}$ ), time (h) and stirring speed (rpm) were considered and optimized. CCD was used to design the experiments and ANOVA was used to analyse the data to obtain the interaction between the selected process variables. The quality of the predicted model was confirmed through determination coefficient ( $R^2$ ), the model F-value and adequate precision (AP).

In addition to optimized catalyst's yield, catalytic activity of the catalyst, synthesized at optimized conditions in terms of adsorption and oxidation were need to be explored further. Therefore, three set of experiments (including adsorption and oxidation) were carried to cover these objectives. In these experiments, three dyes, Acid Blue 113, Methyl Orange and Reactive Black 5, were used individually and in the mixture form.

### **7.3 Materials and Methodology**

Detail of the used chemicals including 2,2'-bipyridine, iron chloride, ethanol 2-propanol, Acid Blue 113, Methyl Orange, and Reactive Black 5 is provided in the chapter 6. All chemicals were used without any additional purification.

#### **7.3.1 Catalyst Synthesis**

Fe-ZSM-5 catalyst was synthesized using "two-Step" process. This process involves precipitation of an iron based mono metallic-organic framework (MOF), followed by impregnation and thermal decomposition.

##### **7.3.1.1 Synthesis of Fe-Monometallic Complex**

A mono metallic-organic framework (MOF) was synthesized by reacting 2,2'-bipyridine with iron chloride using 2 propanol as solvent. For this, 3.6 g of  $\text{FeCl}_2 \cdot 4\text{H}_2\text{O}$  and 8.5g of bipyridine ligand were dissolved in 25 mL of solvent separately and reacted in a lab-scale reactor. The reaction mixture was continuously stirred at  $38 \pm 2$  °C. Fine crystalline material containing  $[\text{Fe}(\text{byp})_2]\text{Cl}_2$  complex was then filtered, and washed with ether solution to eliminate impurities. The yield of the crystalline material was 77%.

### **7.3.1.2 Impregnation**

In this step, ZSM-5 zeolite and Fe-complex were separately dispersed in the methanol solvent, and then mixed dropwise to impregnate the fine particles of Fe-complex for 2 h. The concentration of Fe-MOF was set to get a 3% Fe on the ZSM-5 (wt/wt). Due to impregnation, color of the crystalline material became reddish-brown. After impregnation, the crystalline material was dried for 2 h (at 100 °C) and in the presence of air, calcined at 650 °C for 7 h. These conditions of temperature ( 650 °C) and time (7 h) were selected on the basis of available literature for the complete elimination of the ligand part of MOF (Deutschmann et al., 2009; Parveen et al., 2013).

### **7.3.1.3 Characterization**

ZSM-5 support and the synthesized materials were characterized through EDX, SEM, FTIR, HRTEM and BET techniques. Composition and surface morphology of the ZSM-5, Fe-complex, and Fe-ZSM-5 were studied using Phenom ProX SEM. HRTEM was performed using the instrument having model number “JEOL JEM2100-F”. FTIR analysis was carried out through Perkin Elmer FTIR-spectrum 400 to observe shifts due to coordinate bonding in Fe-complex, and formation of the new chemical structure of Fe-ZSM-5.

Surface area of ZSM matrix and synthesized Fe-ZSM- catalyst were studied using Surface Area and Porosity Analyzer (ASAP 2020). The BET method was used to determine the surface area and pore width. N<sub>2</sub> adsorption-desorption curves were employed to estimate the pore volume. Similarly, the t-plot scheme was used to calculate the micropore volume.

### 7.3.2 Process Optimization

The developed process involved precipitation of MOF followed by its impregnation with ZSM-5 and calcination. Precipitation of Fe based MOF was the major part of the whole process compared to the impregnation and calcination parts of the catalyst synthesis. Therefore, this work aimed at accessing and optimizing process parameters that play the vital part in synthesising the Fe-complex.

In the first step, suitable conditions for the precipitation and impregnation were determined and the synthesized Fe-ZSM-5 was characterized completely through FTIR, EDX, SEM and BET. In the second step, experiments were conducted for the synthesis of Fe-complex and the optimized response values were obtained from Response Surface Methodology (RSM). Formations of complex and crystals yields were confirmed through FTIR and weight analysis.

RSM was used to optimise the synthesis of monometallic precipitations. RSM with Central Composite Design (CCD) uses lower-order polynomial and has shown its reliability for the optimization of many chemical processes (Alslaibi et al., 2013; Asghar et al., 2014b). In the present study, all experiments that required for Fe-complex precipitation were designed using CCD with the help of Design Expert (Version: 6.0.8). Temperature (°C), time (h) and stirring speed (rpm) were

chosen as independent process variables, while the yield (%) of the Fe-complex was the output response. A specified range of the selected parameters is given in Table 7.1. Details of the experimental design with the actual and predicted values are summarised in Table 7.2.

**Table 7.1:** Process Parameters for Fe Monometallic Precipitation Process

<b>Process Parameters</b>	<b>Code</b>	<b>Low Actual Value</b>	<b>High Actual Value</b>
Temperature (°C)	A	30	40
Time (h)	B	1	5
Stirring Speed (rpm)	C	150	300

University of Malaya

**Table 7.2:** Experimental Design and Response of Fe-MOF's Precipitation Process

<b>Standard Order</b>	<b>Run No.</b>	<b>Temperature (°C)</b>	<b>Time (h)</b>	<b>Stirring Speed (rpm)</b>	<b>Actual Value (Yield %)</b>	<b>Predicted Value (Yield %)</b>
1	6	40	5	150	75.00	75.03
2	5	40	1	300	45.00	45.03
3	14	30	5	300	75.00	75.03
4	9	30	1	150	41.00	41.03
5	8	28	3	225	72.50	72.47
6	4	42	3	225	77.00	76.97
7	11	35	0.2	225	10.00	9.97
8	2	35	6	225	82.00	81.97
9	15	35	3	119	71.00	70.97
10	7	35	3	331	79.00	78.97
11	1	35	3	225	78.00	77.61
12	10	35	3	225	77.00	77.61
13	13	35	3	225	78.00	77.61
14	3	35	3	225	78.00	77.61
15	12	35	3	225	77.00	77.61

### 7.3.3 Efficiency Evaluation of the Synthesized Fe-ZSM-5

Experiments were carried out to determine the efficiency of the Fe-ZSM-5 catalyst, synthesized at optimized conditions. Three dyes, Acid Blue 113, Methyl Orange, and Reactive Black 5 and their mixtures were used for this purpose. The efficiency was evaluated based on dye decolorization, degradation and Total Organic Carbon (TOC) removal.

All of the experiments were performed in a laboratory-scale stirred tank reactor (500 mL capacity) equipped with a magnetic stirrer. Two solutions (0.5M sulfuric acid and 1M sodium hydroxide) were employed to regulate the initial pH of dye solution. Earliest set of experiments were carried out to evaluate the adsorption rate of the selected dyes. Three stock solutions containing Acid Blue 113, Methyl Orange, and Reactive Black 5 were prepared and treated individually under dark for 4h. Each solution had starting concentration of 100mg/L. Continuous stirring was applied during adsorption experiments. Optimized value of catalyst was used in each experiment. These values were selected based on the finding of researcher's previous work, which aimed at determining the effects of process factors such as starting concentration of dye and H<sub>2</sub>O<sub>2</sub>, starting pH value, catalyst amount, time and temperature for Fenton heterogeneous process. The treated samples were centrifuged, filtered and examined for decolonization.

The next set of experiments was done to examine the degradation of Acid Blue 113 with higher concentrations. In every experiment, 100ml of solution having known dye concentration was used and the pH of the dye solution was adjusted prior to be transferred into the stirred reactor. A stirring speed of 250 rpm was used for solution mixing and particles distribution. A desired amount of Fe-ZSM-5 and H<sub>2</sub>O<sub>2</sub> (33.3 g/L) were introduced into the reactor after stabilizing the reactor's temperature and the

process time monitored after the addition of  $\text{H}_2\text{O}_2$ . After the reaction, samples were taken from the solution, filtered through syringe filters ( $0.20\mu\text{m}$  Millipore) and analyzed directly.

The treated samples were examined employing a Merck UV-spectrophotometer and TOC analyzer. The degradation and TOC removal of the samples were estimated using the equations 6-2 to 6-4 (chapter 6).

In addition to UV and TOC analysis, high performance liquid chromatography (HPLC) was used to examine the treated dye solutions. This study has illustrated the clear picture of the degradation products. Detail of HPLC and separation column is provided in chapter 6. To identify different compounds and intermediate moieties generated from the Fenton degradation of selected dyes, the HPLC unit was calibrated using standard analytical reagents namely benzene, phenol, aniline, hydroquinone, catechol, benzoquinone, formic acid, oxalic acid, and malic acids. The compounds produced during Fenton-oxidation were identified through comparing retention times with those of calibrated runs under similar conditions (Ajeel et al., 2015).

In the third set, degradation of Methyl Orange, and Reactive Black 5 individually, and in mixture form with Acid Blue 113 were studied. Table 7.6. Illustrates the different prepared compositions (V/V) of the mixtures containing Acid Blue 113, Methyl Orange, and Reactive Black 5. All of these four mixtures were treated at optimized conditions.

#### **7.3.4 Deactivation of Synthesized Fe-ZSM-5**

It is common practice that the catalyst's deactivation occurs due to the leaching of metal ions from the support matrix. In this study, leaching was directly measured using ICP. Instrument was calibrated using six standard solutions containing 0, 5, 10, 20, 50,

100 ppm of the iron. Leaching was also indirectly measured through the EDX analysis to support and confirm the ICP study. After the specified reaction time, the solid particles of Fe-ZSM-5 catalyst were filtered, washed with methanol and dried at 200 °C. EDX analysis was used to study the change in the composition. Similarly, the FTIR and SEM studies were used to examine the change in linkage and morphology of Fe-ZSM-5 due to metal leaching or in-situ transformation

## 7.4 Results and Discussions

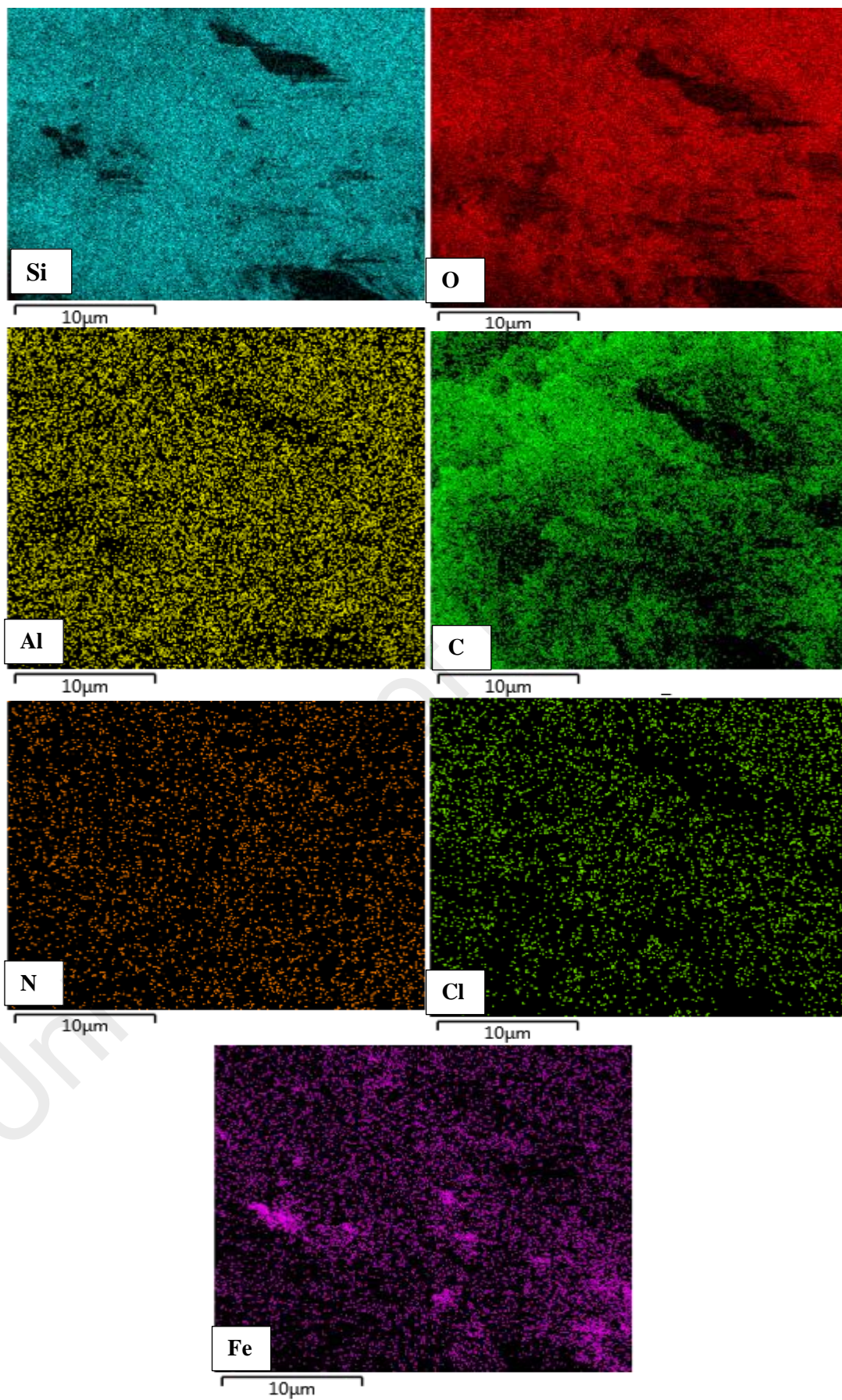
### 7.4.1 Characterization of Synthesized Fe-ZSM-5 Catalyst

EDX results of the ZSM-5 support and prepared Fe-ZSM-5 are provided in Table 3. Percentage compositions were determined using surface area method. Elemental mapping of Fe-ZSM-5 clearly illustrated the presence of aluminum, silicon, iron and oxygen atoms inside the solid cluster (Figure 7.1). The ratios of silicon and oxygen were prominent as compared to iron and aluminum atoms. It was found that the calcination caused the complete removal of the ligand part from the supported monometallic Fe-complex, producing nano oxides on the surface of the support.

**Table 7.3:** EDX Analysis of the ZSM-5 Support and Synthesized Fe-ZSM-5

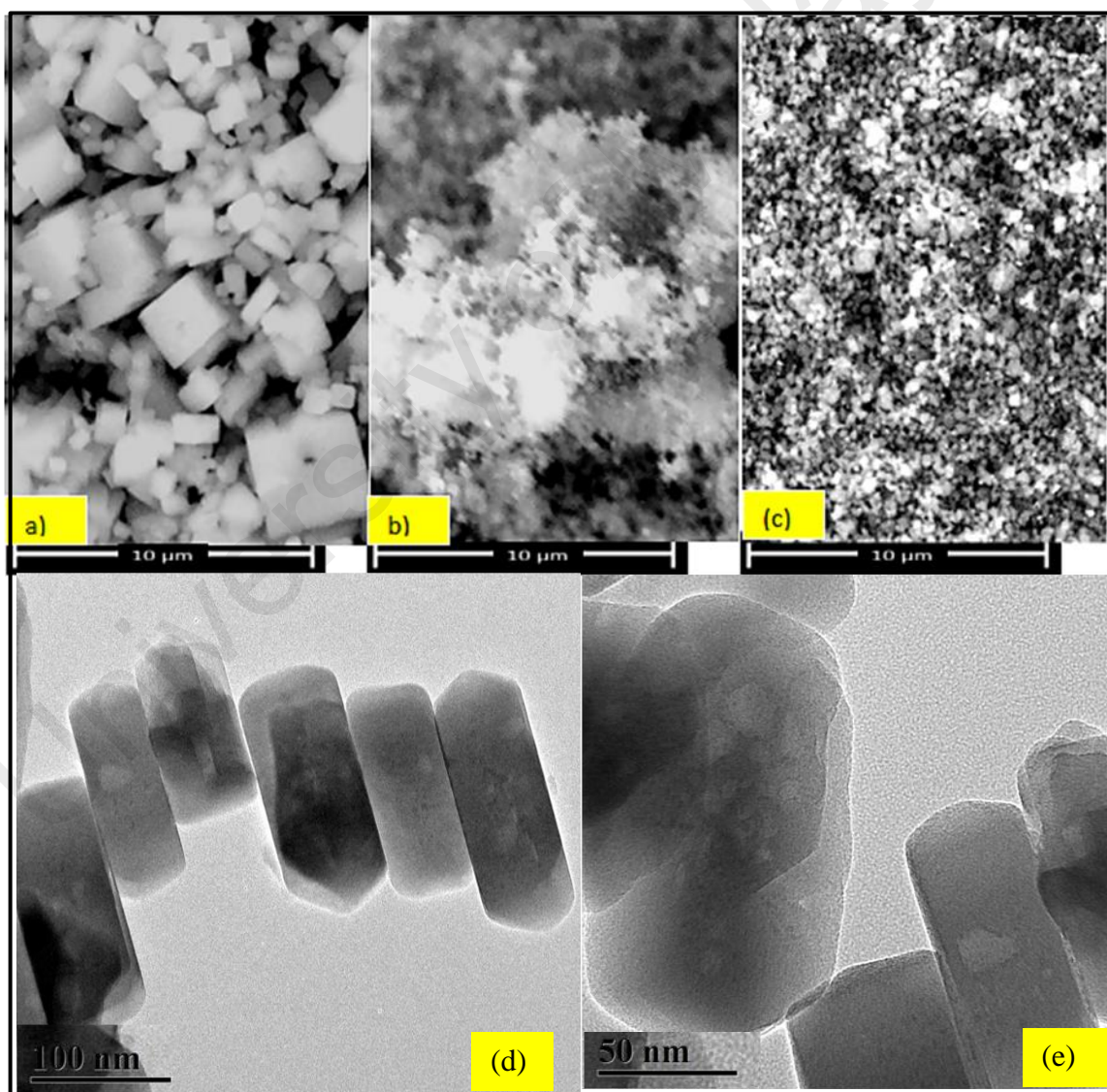
Catalyst Clusters	Weight Composition (%)				
	Si	Al	O	C	Fe
Fe-ZSM-5	31.7	1.7	63.3	0.0	3.2
ZSM-5	41.4	2.2	54.3	0.0	-

Figure 7.2 illustrates the SEM and HRTEM images of iron oxides supported catalyst. Surface morphology of the synthesized Fe-complex was significantly transformed after calcination. Initially, the particles were relatively larger before calcination. However,



**Figure 7.1:** Elemental Compositions of the Fe-ZSM-5 Prior to Calcination

after thermal decomposition of the impregnated Fe-complex, nano-sized particles of iron oxides were formed on the matrix of ZSM-5. The specific surface area of the support and catalyst (in  $\text{m}^2/\text{g}$ ) was determined by measuring the volume of  $\text{N}_2$  gas, using the BET (Brunauer-Emmett-Teller) method. BET results confirmed the findings of previously published work (chapter 6). Again the presence of nano sized iron particles changed the specific surface area, pore size and pore volumes. These results clearly confirmed the findings of previously published work (chapter 6) and also well supported by the relevant literature (Dukkancı et al., 2010b; Yan et al., 2014).



**Figure 7.2:** SEM Images of Fe(byp) Complex (a), ZSM-5 (b), Fe-ZSM-5(c), and HRTEM Images of Fe-ZSM-5(d & e).

The FTIR spectra of the  $[\text{Fe}(\text{bpy})_2]\text{Cl}_2$  complex was studied by using the spectra of 2,2'-bipyridine as a reference to study the shift in the wave number as a result of coordinate bonding (Nazir et al., 2011). The main ring stretching vibrations  $\nu(\text{C}=\text{N})$ , and  $\nu(\text{C}=\text{C})$  were observed at 1553 and 1579  $\text{cm}^{-1}$  for the bipyridine ligand. In the Fe-complex, a slight shift in vibrational frequency was observed in the range of 1592-1595 and 1561-1563  $\text{cm}^{-1}$ . In addition, breathing mode of Bipyridine was found to be shifted from 991  $\text{cm}^{-1}$  to 1012  $\text{cm}^{-1}$  when it formed coordination compound with iron. Similarly, in the case of synthesized Fe-ZSM-5, new bands appeared in the range of 2886–2888, and 1094-1136  $\text{cm}^{-1}$ , which had distinguished it from the FTIR spectra of ZSM-5. These shifts and observations confirmed the formation of a chemical linkage between the iron and ZSM-5 in Fe-ZSM-5.

XRD analysis of the synthesized Fe-ZSM-5 and the ZSM-5 support is provided in the Figure 7.3. Synthesized catalyst has shown the distinctive diffractograms of the supporting matrix (ZSM-5,  $2\theta = 7 - 9^\circ$  and  $23 - 25^\circ$ ) provided in the literature (Cihanoglu et al., 2015). This analysis revealed that the loading of Fe MOFs in accessible positions insight the zeolite matrix had not damaged the crystallinity of the matrix. However, intensities of characteristic peaks were reduced due to filling of metallic nano oxides into the zeolite matrix of ZSM-5. This indicated that the X-ray absorption was fevered by the presence of Fe nano oxide particles (Cihanoglu et al., 2015). In addition, the size of integrated Fe oxide particles was observed in a range of 2-5 nm.

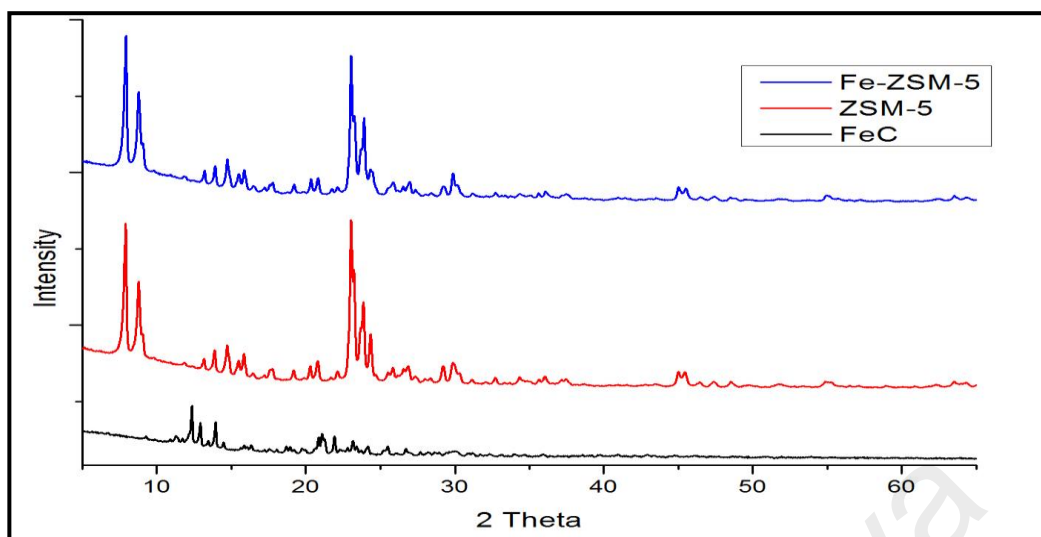


**Figure 7.3:** XRD Analysis of Fe-ZSM-5, ZSM-5, and Fe(byp)-Complex(c)

#### 7.4.2 Process Optimization and ANOVA Analysis

The Fe-complex precipitations were carried out according to the design described in Table 7.1 with ‘yield’ as the response factor. On the basis of the experimental results, an empirical model (Eq 7-1) was developed. This was a second order polynomial (in terms of coded factors), showing the interactions among the independent variables to achieve the precipitation yield.

*Yield of Fe-Complex=*

$$77.61+1.59A+25.46B+2.83C-1.44A^2-15.82B^2 \quad 7-1$$

$$1.32C^2+1.83AB+9.46AC+0.59BC$$

This empirical model showed the interaction among independent variables and their influence on the response yield. The predicted and experimental values were summarized and compared in Table 7.2. The experimental values of the Fe-complexes varied between 10–82%, which were in good agreement with the predicted values.

ANOVA, an integral and reliable approach, was further employed to confirm the suitability and significance of a model (Asghar et al., 2014b). Table 4 illustrates the ANOVA results for the processed values.

F-value indicates the reliability and suitability of a model. A variable with Prob> F of less than 0.05 is considered to have significant effects on the response. The greater the F value for a particular variable, the more significant the effect of that particular variable on the specific response.

**Table 7.4:** ANOVA Analysis of Fe-MOF's Precipitation

Source	Sum of Squares	Degree of Freedom	Mean Square	F Value	Prob > F
Model	4,639.54	9	622.97	2,577.79	< 0.0001 (significant)
A (Temperature)	512.00	1	10.13	41.90	0.0013
B (Time)	1,404.50	1	2,592.00	10,725.52	< 0.0001
C (Stirring Speed)	10.12	1	32.00	132.42	< 0.0001
A <sup>2</sup>	725.69	1	16.10	66.60	0.0004
B <sup>2</sup>	1,101.44	1	1,930.54	7,988.43	< 0.0001
C <sup>2</sup>	1.39	1	13.43	55.57	0.0007
AB	2.68	1	6.69	27.67	0.0033
AC	84.19	1	178.83	739.97	< 0.0001
BC	13.14	1	0.70	2.89	0.1498
Residual	1.189	5	0.24	R <sup>2</sup> =0.9998	
Pure Error	1.20	4	0.30	R <sup>2</sup> Adj=0.9994	
Cor Total	5,607.90	14	Adeq Precision=179.38		

In the present work, F-values of 4,639 indicated that the precipitation model for the Fe-complexes was suitable. The quality of fit of both models was also confirmed through determination coefficient (R<sup>2</sup>). The R<sup>2</sup> value was 0.9998, which was in good agreement with the adjusted R<sup>2</sup>. Adequate precision (AP) is usually used to get the signal to noise (S/N) ratio to confirm the validity of a model and a ratio greater than 4 is

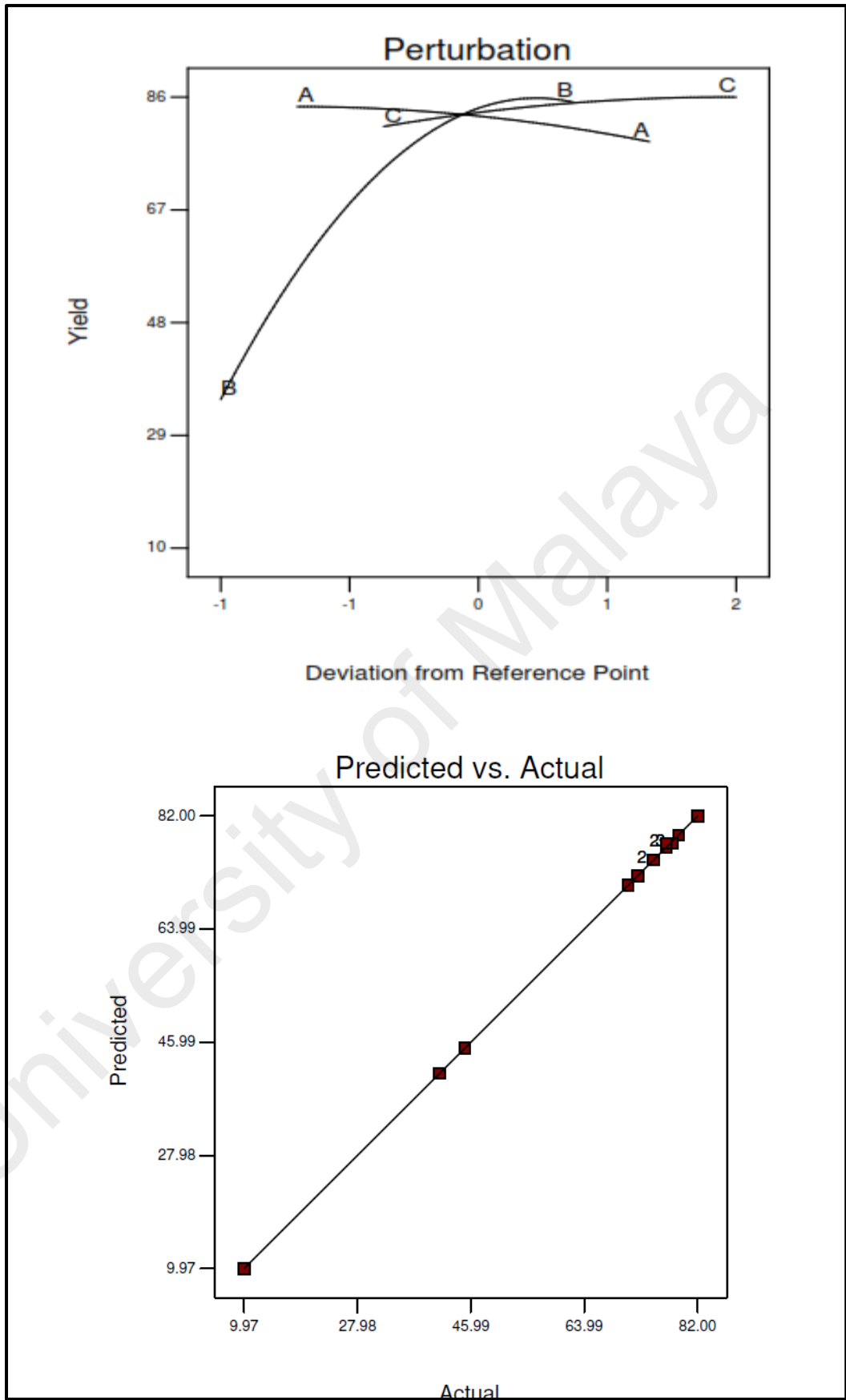
recommended. In the present case, an AP value of 179.38 indicated that there was adequate signal to noise (*S/N*) ratio for the model. These values confirmed that the model was suitable and could be used to optimize the design space.

### 7.4.3 Effect of Process Variables on Yield

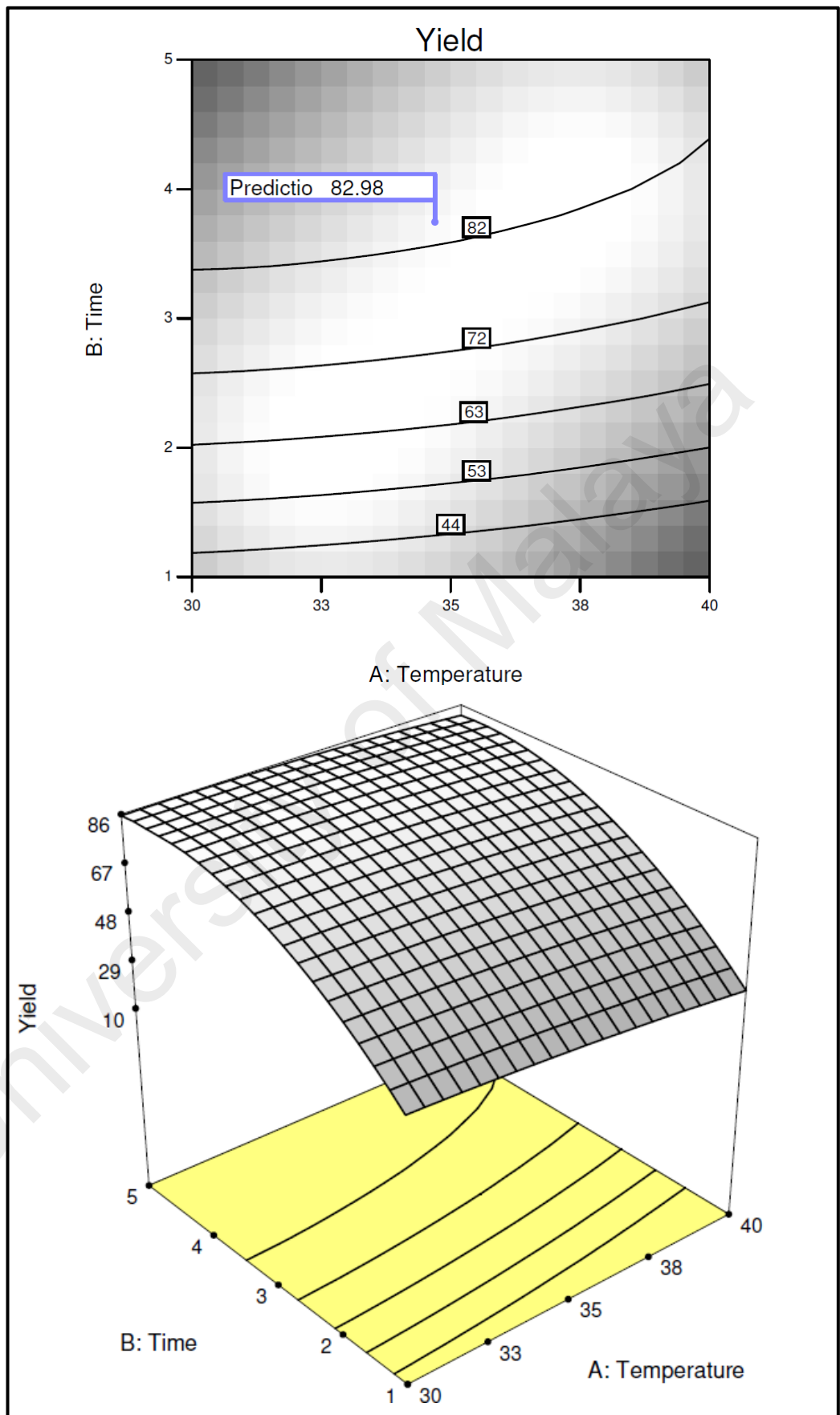
The perturbation plots (Figure 7.4a) compares the combined effects of all the three variables. The slope of the curve showed the influence of a variable and the steepest curve was the main focus of attention. It was observed that process time (Factor B) was the most influencing factor on the yield. Process temperature (factor A) was the second most influencing factor while stirring speed (Factor C) was the least influencing. Increasing the process time and impeller speed increased the suspension of crystals which led to maximum exposure of the available surface area to the solution for mass transfer (Ferrando et al., 2008). However, at high temperature, increasing stirring caused dissolution of the crystalline material.

Figure 7.4(b) illustrates the comparison between the experimental and predicted values. From the plot, it is clear that the experimental values were in a linear relationship with the predicted values, indicating that the predicted values were close to the experimental values. The 2D and 3D contour plots (Figure 7.5 and Figure 7.6) present a clear and understandable analysis of the process.

The optimization of the results obtained through experiments was carried out using Response Surface Methodology (RSM). Responses were kept within the desired ranges while the maximum yield was targeted. The suggested optimized values of temperature (33 °C), time (4 h) and stirrer speed (245 rpm) were validated through the experiment. The approximate yield of the Fe-complexes was 81.5%. There was a good agreement between the predicted and experimental results under optimized environment.



**Figure 7.4:** Perturbation Plot (A is Temperature, B is Reaction Time, and C is Stirring Speed) and Comparison Plot for Fe-MOFs



**Figure 7.5:** Contour Plot and Three Dimensional Plot Showing Combine Effect of Time and Temperature on Fe-MOF's Yield

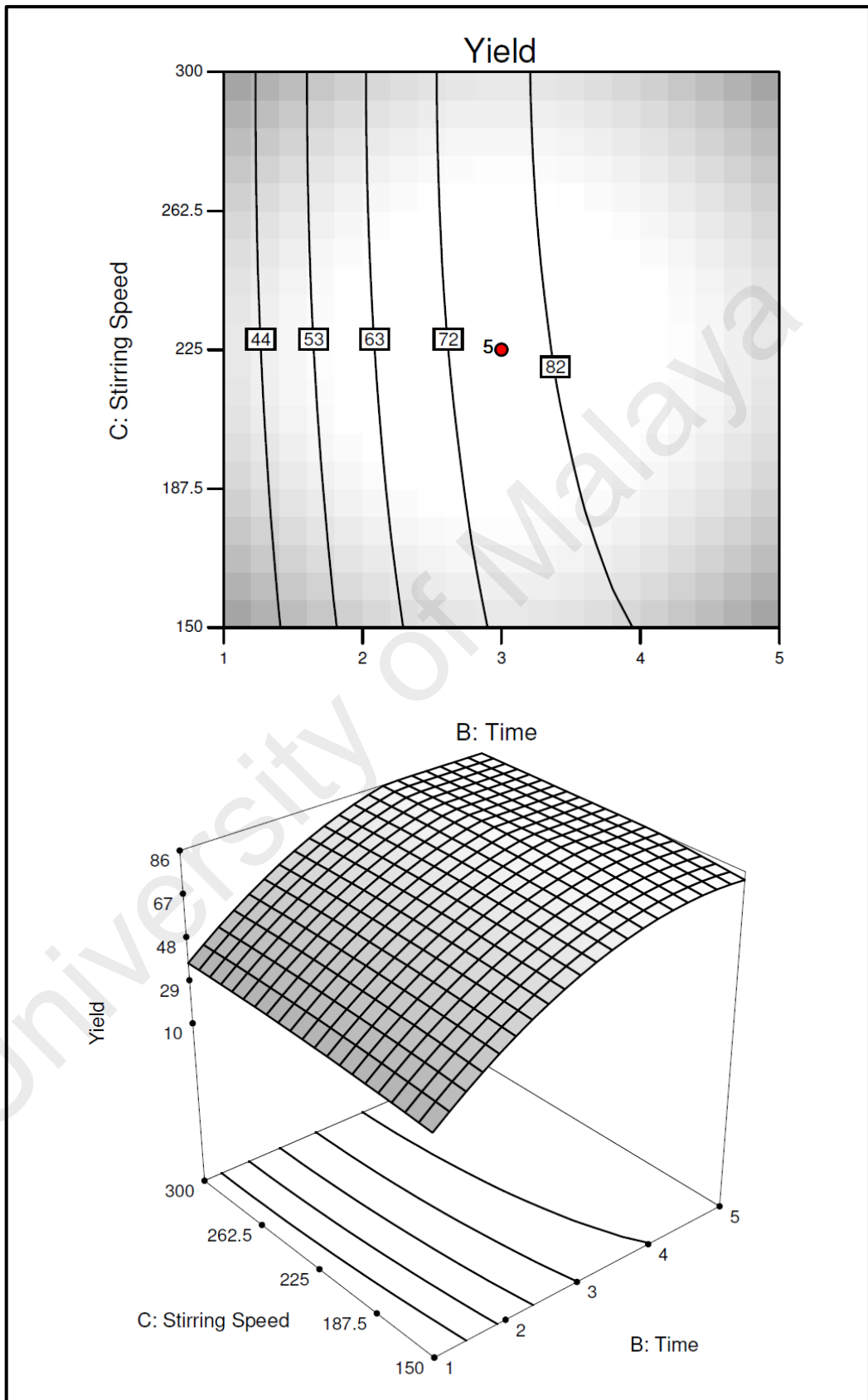


**Figure 7.6:** Contour Plot and Three Dimensional Plot Showing Combine Effect of Time and Stirring Speed on Fe-MOF's Yield

Furthermore, in the impregnation step, 82-84% yield of Fe-ZSM-5 was observed. The yield can be further increased up to 90% with an efficient filtration system.

#### **7.4.4 Efficiency and Stability Evaluation of the Fe-ZSM-5 catalyst**

Experiments exhibiting Fenton oxidation were carried out to degrade and decolorize three selected dyes. In order to examine the adsorption, the preliminary study was conducted with 100 mg/L of dye concentration. After four hours, percentage of adsorbed Acid Blue 113, Methyl Orange, and Reactive Black 5 were 78%, 71%, and 63%, respectively. All the obtained results imply that the adsorption equilibrium was achieved and no further change was detected. The synthesized Fe-ZSM-5 illustrated more adsorption performance for Acid Blue 113 than Methyl Orange, and Reactive Black 5. Difference in adsorption rate was due to the dissimilar organic structures, which had made difficulties to approach surface of the catalyst. The other reason was the different binding affinities with the surface of Fe-ZSM-5. Normally, binding affinities are affected by different functional groups such as  $-\text{NH}_2$ ,  $\text{SO}_3^-$ ,  $-\text{OH}$  (Shirzad-Siboni et al., 2014; Zhou et al., 2013). Similarly the Methyl Orange molecules were more easily adsorbed than Reactive Black 5, which can be related to smaller molecule size of the Methyl Orange (Zhou et al., 2013).

The adopted optimized values for the second set of experiments are provided in Table 6.9. These values are based on researcher's previous results in which effects of initial dye concentration, dye/catalyst (wt/wt), catalyst/ $\text{H}_2\text{O}_2$  (wt/wt), reaction time, pH, and temperature were considered and optimized. The finding of previous work includes that the pH had significant effect on the treatment efficiency. At pH 3, the degradation rate of dye was found maximum as compared to pH 5 and pH 9. Effects of other parameters were also significant as described below:

pH > Initial Dye Conc. > Time > Dye/Fe<sup>+2</sup> > H<sub>2</sub>O<sub>2</sub>/Fe<sup>+2</sup> > Temperature

The efficiency was evaluated based on Acid Blue 113 decolorization, degradation and TOC removal (Table 7.5). For 100 mg/L of initial dye concentration, 99.7% of degradation, 99.8% of decolorization and 77% of TOC removal were achieved. However, the TOC removal was reduced to 69% when the dye concentrations increased to 200 mg/L. It indicated that less amount of the catalyst was available to interact with H<sub>2</sub>O<sub>2</sub> or the residual H<sub>2</sub>O<sub>2</sub> scavenged hydroxyl radicals (Neyens & Baeyens, 2003). These results reflected and supported the findings of researcher's previous work. However, at higher concentrations, the degradation efficiency slightly increased (Table 7.5).

Treated samples were examined by HPLC. Traces of carboxylic acid, aniline, and benzoquinone were sensed corresponding to the calibrated peaks at ca. 1.92 min, 5.97 min, and 2.420 min, respectively. Formation of aniline may be attributed to the oxidative splitting of the dye amino benzene moiety forming a °NH-C<sub>6</sub>H<sub>5</sub> radical which has potential to abstract an amino hydrogen atom from dye molecules (Zayani et al., 2008).

The other detected moiety was benzoquinone. This compound is frequently detected in the degradation of phenol and benzene (Ajeel et al., 2015; Gomathi Devi et al., 2009; Zayani et al., 2008). Further oxidation has caused the splitting of benzoquinone ring into maleic and formic acids (Ajeel et al., 2015). These results also reflected the findings of researcher's previous work.

**Table 7.5:** Efficiency of the Synthesized Catalyst at Optimized Conditions

<b>Dye</b>	<b>Dye/Catalyst</b>	<b>H<sub>2</sub>O<sub>2</sub>/Catalyst</b>	<b>pH</b>	<b>Time</b>	<b>Temperature</b>	<b>Decolorization</b>	<b>Dye Removal</b>	<b>TOC</b>
(mg/L)	wt/wt	wt/wt		h	(°C)	%	%	%
100	0.75	2.5	3	4	30	99.7	99.8	77
200	0.75	2.5	3	4	30	99.6	99.7	69
300	0.75	2.5	3	4	30	99.3	99.2	69.5
600	0.75	2.5	3	4	30	99.2	99.3	70
900	0.75	2.5	3	4	30	99.1	99.1	71.5

#### 7.4.5 Catalyst's Evaluation for Mixture of Dyes

In the third set, degradation of Methyl Orange and Reactive Black 5 individually, and in mixture forms were studied. Figure 7.7 illustrates the comparison of these experiments. In all cases, color was completely removed in less than an hour. However, the noted TOC removal values were 68% and 71% for Reactive Black 5, and Methyl Orange, respectively. A decrease of 6-8% in the TOC removal indicates that the degradation rate depends on the structures of organic molecules (Shirzad-Siboni et al., 2014). Beside this, some study also reveals that degradation of Methyl Orange type azo dye is favored by alkaline medium (Kaur et al., 2013).

Table 7.6 illustrates the composition of mixtures, their percentage degradation and TOC removal. In all cases, color was completely removed in the less than an hour. However, mineralization efficiency for mixtures 1- 4 was 70%, 73%, 69%, and 72%. Due to the presence of Acid Blue 113, in mixture 2 and 4, mineralization efficiency was remained maximum. The catalyst has shown relatively less mineralization efficiency for mixture 3 containing Methyl Orange and Reactive Black 5 (Figure 7.7). It can be attributed to different structures of dye molecules, or different functional group such as  $-NH_2$ ,  $SO_3^-$ ,  $-OH$  (Shirzad-Siboni et al., 2014; Zhou et al., 2013). Overall the efficiency of the catalyst against different dyes and their mixture was remained excellent.

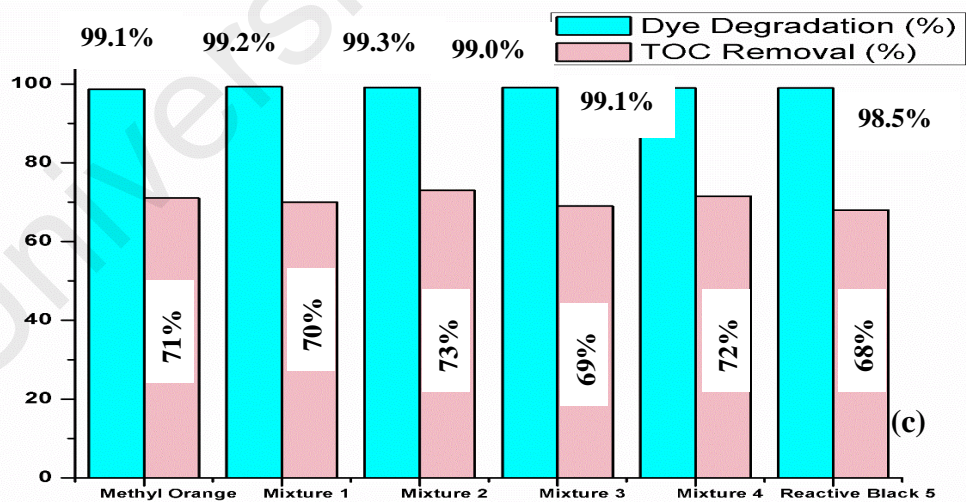
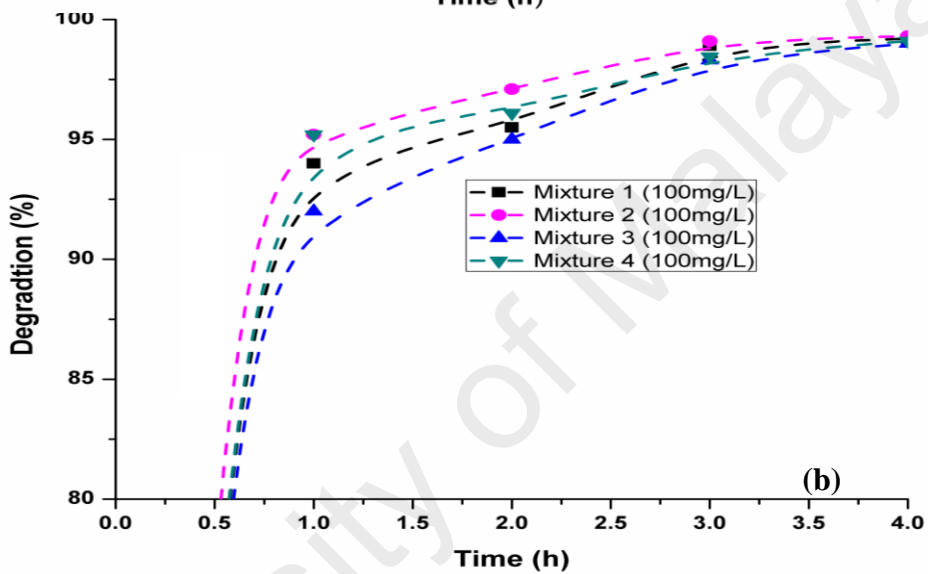
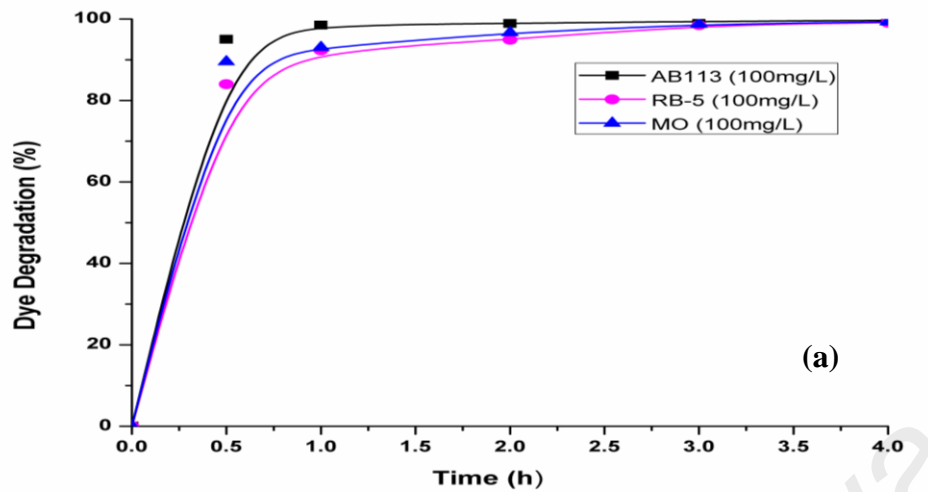


**Figure 7.7:** Degradation of Individual Dye (a), in Mixture Form (b), and TOC Reduction for Reactive Black 5, Methyl Orange, Mixture1, Mixture 2, Mixture 3, and Mixture 4 (c)

**Table 7.6:** Mixtures of Three Dyes, Their Degradation and TOC Removal

Name	Dye Conc.	AB113	RB-5	MO	Degradation	TOC Removal
	(mg/L)	(%)	(%)	(%)	%	%
Mixture 1	100	50	50	0	99.2	70
Mixture 2	100	50	0	50	99.3	73
Mixture 3	100	0	50	50	99.0	69
Mixture 4	100	50	25	25	99.1	72

AB113 (Acid Blue 113), MO (Methyl Orange), and RB-5 (Reactive Black- 5)

#### 7.4.6 Comparison of the Fe-ZSM-5 with Existing Catalysts

Apart from catalytic activity, efforts were made to compare the performance of the synthesized Fe-ZSM-5 with other frequently used catalysts for the degradation of textile dyes. However, it was revealed that no one had used the Fe-ZSM-5 for the degradation of Acid Blue 113 and Reactive Black 5 (up to authors' knowledge). Therefore, it was an additional novelty of this work. Beside this, for third selected dyes "Methyl Orange", limited degradation data was available with Fe-ZSM-5. The existing data for the degradation of Methyl Orange, was based on the utilization of UV to enhance the degradation rate (Zhou et al., 2013), which significantly increased the process cost. It was found that the degradation of several other textile dyes were also carried out using Fe-ZSM-5 catalysts, synthesized from different ion exchange and hydrothermal methods. However, each researcher had used different process conditions, and reactor type. Therefore, it was not possible to repeat all the experiments for efficiency comparison. To overcome this issue, an alternate option was considered by setting one liter of dye solution as basis and assessing different factors (e.g dye initial concentration, catalyst used, H<sub>2</sub>O<sub>2</sub> required), efficiencies of catalysts

synthesized through different methods were compared (Table 7.7). Comparative study has given an understandable picture of color and TOC removals from dye solutions.

Table 7.7 illustrates that Fe-ZSM-5 synthesized using ion exchanged techniques are suitable for the degradation of azo dyes (Bolova et al., 2012; Queiros et al., 2015; Yaman & Gunduz, 2015). Queiros et al. (2015) consumed smaller quantity of their synthesized catalyst as compared to this study. Similarly, Queiros et al. (2015), Bolova et al. (2012), Unnu et al. (2015), and Grcic et al. (2009) used lower initial concentrations of the selected dye (50mg/L and 35 mg/L) to assess the activities of Fe-ZSM-5 catalysts. It is common practice that with smaller dye concentration, degradation rate increases due to more available hydroxyl radicals and their interaction with organic molecules (Gomathi Devi et al., 2009). However, even with smaller initial concentrations, the obtained results of TOC reduction were considerably lesser than this work (Table 6). Chen et al. (2008) used high catalyst concentration (4,000mg/L) to decolorize KN-R dye and maximum 90% of decolorization was achieved. Zhou et al. (2013) synthesized different types of Fe-ZSM-5 catalysts and evaluated against Methyl Orange. Using UV-visible irradiation, TOC reduction was noted in the range of 8-64%. With excess amount of catalyst and H<sub>2</sub>O<sub>2</sub>, and comparatively increased temperature (333K), Yaman and Gunduz (2015) achieved 81% of COD reduction for the selected dye, Reactive Red 141. However, when researchers used ambient conditions for dye treatment, the degradation rate was significantly reduced (even up to 0% of COD reduction). Similarly, lowering the catalyst amount (1.0 g/L) also caused the decrease in the COD reduction (52%).

In addition to these, Prihod'ko et al. (2011) synthesized Fe-ZSM-5 (improved) and evaluated against Rodamine G dye. Significant TOC reduction (80%) was reported in a comparatively shorter time (2.5 h). High concentration of H<sub>2</sub>O<sub>2</sub> (5.44-6.8 g/L) was used

in those experiments, which is nearly two time of this work. Beside higher amounts of H<sub>2</sub>O<sub>2</sub>, catalyst synthesis process for improved Fe-exchanged zeolites is complicated and requires longer time (3- 4 days) as compared to currently used process.

On the basis of this comparative study, it is clear that newly developed two-step process can be used to synthesize, efficient and economical Fe-ZSM-5 catalysts for advance oxidation processes to achieve the treatment targets.

Apart from the optimization and catalytic activity, stability of the catalyst is also a key factor in oxidation processes. It is a common practice that leaching of metal ions from supporting matrix causes deactivation of the catalyst (Yan et al., 2014). A catalyst showing a minimal amount of leaching is considered as a stable catalyst.

In researcher's previous study (chapter 6), the stability of Fe-ZSM-5 was analyzed through EDX, SEM and FTIR and it was confirmed that the leaching was below 2ppm.

In the present case, leaching was measured by ICP techniques. Leaching of iron was observed below 2ppm for all dyes at higher pH values. However, at pH 3, the measured values of leaching were 2.7, 2.1, 4.1, and 2.8 for mixture 1 to 4. This indicates that catalysis mainly occurred on the active sites, although a slight traces of iron was available in the solution phase. For the mixture 3, the leaching rate (4.1ppm) was relatively higher as compared to other mixtures. In the present case, fresh and spent samples were also analyzed by EDX to confirm the ICP results. Samples of the used catalysts were obtained from the treated solutions, washed with methanol and heated upto 200 °C prior to EDX analysis. Difference in iron content was used estimate the iron ions leached into the treated water.

From comparison, it is revealed that ICP values are little higher side than the EDX results. Similarly the mostly ICP values are in the range of 2-3 ppm, which are slightly

increased from the permissible limit (<2ppm). However the present leaching results are better than most of the reported values (Chen et al., 2008; Dukkancı et al., 2010b; Grcic et al., 2009; Yan et al., 2016). This has confirmed the stability of the catalyst as reported in previous work.

University of Malaya

**Table 7.7:** Comparative Study of the Synthesized Catalyst with Other Available Catalysts

Dye	Dye Conc.	Fe-ZSM-5	H <sub>2</sub> O <sub>2</sub>	pH	Time	Decolorization	TOC/COD Removal	Reference
	(mg/L)	Wt (mg/L)	Wt (mg/L)		h	%	%	
AB113	100	1,330	3,333	3	4	99.7	77 (TOC)	Present study
RB-5	100	1,330	3,333	3	4	99.1	68 (TOC)	
MO	100	1,330	3,333	3	4	99.3	71 (TOC)	
RG	100	1,000	5,440	4	2.5	99.0	80 (TOC)	(Prihod'ko et al., 2011)
OII	35	333	680	3	3	91.0	36 (TOC)	(Queiros et al., 2015)
MO	200	1,000	1020	5.8	2	99.0	64 (TOC)	(Zhou et al., 2013)
RR141	100	2,000	9,078	3.5	2	100	81 (COD)	(Yaman & Gunduz, 2015)
RR141	100	1,000	1,122	3.5	2	57	0 (COD)	(Yaman & Gunduz, 2015)
OII	50	Not available	9,067	7	2	99.9	55 (COD)	(Bolova et al., 2012)
KN-R	250	4,000	1,020	2.5	0.5	90	Not available	(Chen et al., 2008)
CV	25	1,000	1,700	3.5	2	98	53 (COD)	(Unnu et al., 2015)
ATZ	1	500	567	3	0.5	84	Not available	(Grcic et al., 2009)

AB113 (Acid Blue 113), OII (Orange II), RG (Rodamine G), MO (Methyl Orange), RR141 (Reactive Red 141), KN-R (Reactive Brilliant Blue KN-R), CV (Crystal Violet), and ATZ (Atrazine)

## 7.5 Summary

In this study, synthesis, optimization and activity evaluation of Fe-ZSM-5 in advanced oxidation process were conducted. The present study proved that MOF derived Fe-ZSM-5 can be used as a preferred catalyst in Fenton oxidation process for the industrial wastewater treatments containing recalcitrant contaminants.

Catalyst was synthesized using a 2-Step process and characterized by EDX, SEM, HRTEM, FTIR and BET. CCD method was used to optimize the yield and interactions among the process variables (temperature, time and stirrer speed). The quality of fit of the polynomial models were confirmed through determination coefficient ( $R^2$ ), the model F-value, probability value (Prob>F), and adequate precision (AP).

Process time was seen as the most influencing variable in catalyst preparation. Effects of temperature and stirrer speed on the yield were also significant. The optimized experimental yield was 81.5%, which was in good agreement with the CCD predicted value. Furthermore, the efficiency of the catalyst, produced at optimized environment was also evaluated against three dyes and their mixtures. Total Organic Carbon (TOC) removal was achieved up to 77%, 71 % and 68% for Acid Blue 113, Methyl Orange, and Reactive Black 5, respectively. For the mixtures, TOC removal was observed in the range 69 to 72%, which possesses an excellent mineralization efficiency range. Besides, it was observed that leaching of iron metal was below 2ppm.

## **CHAPTER 8: NANO OXIDE INTEGRATED CATALYSTS FOR BIOGASOLINE PRODUCTION**

### **8.1 Introduction**

Biofuels produced from palm oil have shown great potential as a useful fossil fuel substitute and are environmental friendly. Utilization of palm oil as biofuel requires zeolite based catalytic technology that facilitates selective conversion of substrates to desired products, including biogasoline and biodiesel. However, the synthesis and integration of suitable zeolite based supported catalysts for the desired products are the key challenges in biofuel production. The alternative to overcome these problems is to use nano heterometallic materials supported on zeolite catalysts.

In this chapter, Zeolite Socony Mobile-5 (ZSM-5) based catalysts loaded with heterometallic nano oxides were synthesized and characterized by SEM, EDX, HRTEM, FTIR and BET. Next, the catalysts were used for the palm oil cracking to produce biogasoline. Taguchi method was used to assess and optimize the catalytic cracking process. The catalytic cracking results were also compared under optimized conditions. Effect of loaded metal oxides was also investigated to synthesis an efficient and economical catalyst for producing biogasoline from cracking of palm oil.

### **8.2 Background**

The available oil reservoirs of the world are depleting due to increasing demand of the fuels. On the other side, utilization of fossil fuels has caused severe environmental pollution through release of carbon oxides, sulphur and nitrogen that lead to greenhouse effects, and global warming. Therefore, there is a high demand for alternative energy resources to replace fossil fuels. Biofuels have been found to have a great potential as a fossil fuel substitute. Biofuels include gaseous fuels and liquid fuels, and usually

produced from renewable resources (Chew & Bhatia, 2008; Choi et al., 2015; Lin & Cheng, 2012; Ong & Bhatia, 2010). Gaseous biofuels such as methane and hydrogen, as well as liquid biofuels such as biogasoline and biodiesel are primarily used by vehicles. In addition, they are also used for the production of electricity (Ong & Bhatia, 2010).

Biofuels can be produced from plant oil based feed stock (vegetable oils and palm oil), waste materials (agriculture, wood, and crop residue), aquatic biomass (algae, and water weed), energy crops (sugar, barley, wheat, and etc., containing starch) and forest products (trees, shrubs and wood) (Ong & Bhatia, 2010; Taufiqurrahmi & Bhatia, 2011; Twaiq et al., 2004a; Venderbosch & Prins, 2010; Wang et al., 2015a). Plant oil based feed stock mainly contains triglycerides, which can be easily reformed into liquid biofuels compared to other available biomass containing cellulose and starch. Several countries such as Malaysia are producing a large amount of palm oil and have sustained concern in the use of palm oil and its other residues for the synthesis of biofuels. These fuels are environmental friendly and carbon neutral. Therefore, utilization of biofuels produced from palm oil can significantly contribute to reduce the global warming (Chew & Bhatia, 2008; Kim et al., 2013a; Ong & Bhatia, 2010).

Currently, several methods are available and more methods are being developed or modified to produce biofuels (Biswas et al., 2013; Buzetzki et al., 2011; Chen et al., 2003; Dickerson & Soria, 2013; Iliopoulou et al., 2007; Taufiqurrahmi & Bhatia, 2011). These methods include transesterification, fermentation, ecofining, thermal and catalytic cracking. Amongst all, catalytic cracking has several advantages compared to the others (da Mota et al., 2014; Kadrmas et al., 2015; Vu et al., 2015b). Higher yields of gasoline, kerosene and diesel fractions from non-edible and edible oils are achievable at relatively lower temperature range (350-550 °C). In addition to feed stock, the choice of catalysts is also important in catalytic cracking (Dickerson & Soria, 2013; Suyanta & Izul, 2012;

Zhao et al., 2015). Catalysts with ordered structures and acidic sites promote cracking with the option of selectivity. Currently, zeolites based catalysts are effectively used for most of the cracking processes (Farshi & Abri, 2012; Galadima & Muraza, 2015; Ishihara et al., 2014). A variety of zeolite catalysts are synthesized and used for the cracking of palm oils, vegetable oils and used palm oil. ZSM-5 is normally employed as a catalyst additive to enhance the yield of light olefins and to increase the gasoline octane number (Farshi & Abri, 2012; Ishihara et al., 2014; Ngo et al., 2010; Ong & Bhatia, 2010; Yigezu & Muthukumar, 2014). Apart to synthesize heterometallic and zeolitic catalysts separately, development of the multifunctional catalysts is also gaining attention as these type of catalysts can give promising results though simultaneously enhancing the catalytic cracking and hydrodeoxygenation of the bio feed stock. In this regard, zeolites doped with heterometallic nano catalysts have captured the researchers' attention (Dickerson & Soria, 2013; Vu et al., 2015b). Multifunctional catalysts are able to give a selective product stream and also to provide shed light on the complex mechanisms of catalytic reforming and cracking, which are still not well defined. Several efforts were also made to integrate the doped zeolites into the cracking equipment and in situ upgradation of the catalysts (Dickerson & Soria, 2013; Vu et al., 2015b). However, the synthesis and integration of suitable zeolite supported catalysts to produce the desired products are the main challenges in bio refineries (Dickerson & Soria, 2013; Vu et al., 2015a; Zhao et al., 2015).

In the present study, ZSM-5 based catalysts loaded with heterometallic nano oxides were synthesized and used for palm oil cracking to produce biogasoline. This work is based on the synthesis procedures developed from researcher's previously published work (chapters 6 and 7) in which Fe-ZSM-5 was prepared using a newly developed process, characterized and evaluated for environmental applications to treat the industrial effluents. The main objective and scope of this work was to extend the

application of the newly developed 2-step process for the synthesis of efficient catalysts for green energy application. In the present work, refined palm oil was used as the model feed stock for the biogasoline production. In addition to palm cracking, influence of the independent process variables such as the amount of catalysts (g), temperature ( $^{\circ}\text{C}$ ) and time (h) were considered and optimized to maximize the yield of biogasoline. Taguchi method was used to design the experiments and analyze the data to obtain the interaction among the selected process variables.

### **8.3 Materials**

Detail specifications of used materials including, 2,2'-bipyridine, zinc chloride, iron chloride, copper chloride, ethanol, 2-propanol, n,n-dimethyl formamide (DMF) and ZSM-5 is provided in chapter 3 and 6. In addition to these, palm oil was purchased from Eon Big (Malaysia) and used to produce biogasoline through catalytic cracking process.

#### **8.3.1 Catalyst Preparation**

Heterometallic loaded catalysts were synthesized using a two-step process. This process comprises precipitation, impregnation and thermal decomposition. In the current work, initially metallic organic frameworks (MOFs) were prepared by reacting chlorides of Fe, Zn, Cu, and Ni with 2,2'-bipyridine in 2-propanol. For Fe-MOF, 8.5 g of 2,2'-bipyridine and 3.6 g of  $\text{FeCl}_2 \cdot 4\text{H}_2\text{O}$  were dissolved (separately) in 30 mL of solvent and slowly mixed in a lab-scale stirred tank reactor. Temperature of the mixture was maintained at  $36^{\circ}\text{C}$  and continuous stirring was employed for 2-3 h to complete the reaction. Fine precipitates of  $[\text{Fe}(\text{bpy})_2]\text{Cl}_2$  were then filtered and washed with ethanol and ether to remove impurities and yield the target at 80%. Similar condition was employed for the synthesis of  $[\text{Zn}(\text{bpy})_2]\text{Cl}_2$ ,  $[\text{Cu}(\text{bpy})]\text{Cl}_2$ , and  $[\text{Ni}(\text{bpy})]\text{Cl}_2$  complexes. For  $[\text{Zn}(\text{bpy})_2]\text{Cl}_2$ , 7.0g of 2, 2'-bipyridine ligand and 3.13g of  $\text{ZnCl}_2$  were used while 3.77g of  $\text{CuCl}_2 \cdot 2\text{H}_2\text{O}$  and 7.0g of 2,2'-bipyridine ligand were used to synthesize

[Cu(bpy)]Cl<sub>2</sub>. In addition to these, 6.4g of 2,2'- bipyridine ligand and 2.6g of NiCl<sub>2</sub>.6H<sub>2</sub>O were used to synthesize [Ni(bpy)]Cl<sub>2</sub>. Fine crystals of [Zn(bpy)<sub>2</sub>]Cl<sub>2</sub>, [Cu(bpy)]Cl<sub>2</sub>, and [Ni(bpy)]Cl<sub>2</sub> complexes were filtered and washed with ethanol and ether to eliminate contaminations. The yields of the synthesized complexes were 81%, 79%, and 82% respectively.

In the next step, impregnation of ZSM-5 matrix with the previously synthesized MOFs ([Fe(bpy)<sub>2</sub>]Cl<sub>2</sub>, [Zn(bpy)<sub>2</sub>]Cl<sub>2</sub>, [Cu(bpy)]Cl<sub>2</sub>, and [Ni(bpy)]Cl<sub>2</sub>) crystalline particles was carried out. The concentrations of the monometallic complexes were adjusted to obtain the desired loading (wt/wt) of Fe, Zn, Cu, and Ni on ZSM-5 (Table 8.1). After impregnation, the impregnated material was separated from the solution, and continuously heated for 12 h (at 100 °C) to evaporate the solvent. Dried material was then calcined in air for 7 h. Furnace temperature was increased slowly and finally maintained at temperature 650 °C to fully remove the ligand part.

The synthesized catalysts were given codes as ZSM-5 (30), Fe-Zn-Cu-ZSM-5(31), Fe-Zn-Cu-ZSM-5 (32) and Fe-Zn-ZSM-5 (33) for easy understanding of readers. ZSM-5 (30) is not an integrated catalyst while Fe-Zn-Cu-ZSM-5(31), Fe-Zn-Cu-ZSM-5 (32) and Fe-Zn-ZSM-5 (33) are integrated nano oxides catalysts. The detailed compositions of the integrated nano oxides catalysts are provided in Table 8.1.

### 8.3.2 Characterization

Characterization of the synthesized materials was performed using FeSEM, EDX, HRTEM, FTIR, and BET methods. Detail of used instruments including, Phenom ProX SEM, Perkin Elmer FTIR-spectrum 400, JEOL JEM2100-F, PANalytical X-ray diffractometer is provided in chapter 3 and 6.

**Table 8.1:** Composition of ZSM-5(30) Support and Synthesized Catalysts (31-33)

Catalyst	Weight Composition (%)						
	<i>Si</i>	<i>Al</i>	<i>O</i>	<i>Fe</i>	<i>Zn</i>	<i>Cu</i>	<i>Ni</i>
ZSM-5 (30)	41.4	2.2	54.3	-	-	-	-
Fe-Zn-Cu-ZSM-5 (31)	48.6	2.2	34.1	5.9	2.5	6.6	-
Fe-Zn-Cu-ZSM-5 (32)	39.3	1.9	56.2	0.9	0.8	0.9	0.8
Fe-Zn-ZSM-5 (33)	34.5	1.9	56.5	3.0	4.2	-	-

ZSM-5 (30) is unintegrated catalyst while Fe-Zn-Cu-ZSM-5(31), Fe-Zn-Cu-ZSM-5 (32) and Fe-Zn-ZSM-5 (33) are integrated nano oxides catalysts.

Table 8.1 illustrates the corresponding data of EDX. The BET technique was used to analyze specific surface area of ZSM-5 and the changes occurred due to integration of nano oxides on the ZSM-5 matrix. N<sub>2</sub> adsorption-desorption plots were considered to estimate the pore volume. Similarly, micropore volume was calculated using the t-plot method. Table 8.2 shows the corresponding data of the ZSM-5 support and the synthesized catalysts. XRD patterns were analyzed selecting a range of 2θ values (from 5.0 to 70.0) was scanned.

**Table 8.2:** BET analysis of the ZSM-5 support (31) and synthesized catalysts (31-33)

Sample	SBET (m <sup>2</sup> /g)	S <sub>micro</sub> (m <sup>2</sup> /g)	S <sub>ext</sub> (m <sup>2</sup> /g)	V <sub>t</sub> (cm <sup>3</sup> /g)	V <sub>micro</sub> (cm <sup>3</sup> /g)	Pore Size (nm)
ZSM-5 (30)	297.59	241.75	51.85	0.17	0.11	2.40
Fe-Zn- Cu-ZSM-5 (31)	243.93	112.35	131.57	0.16	0.06	2.68
Fe-Zn- Cu-ZSM-5 (32)	295.33	167.68	129.64	0.18	0.08	2.47
Fe-Zn-ZSM-5 (33)	208.68	82.84	125.83	0.13	0.04	2.53

S<sub>BET</sub> is the specific surface area, V<sub>t</sub> is the total pore volume, S<sub>ext</sub> is the external surface area, and V<sub>micro</sub> is the micropore volume. ZSM-5 (30) is unintegrated catalyst while Fe-Zn-Cu-ZSM-5(31), Fe-Zn-Cu-ZSM-5 (32) and Fe-Zn-ZSM-5 (33) are integrated nano oxides catalysts.

#### 8.4 Experimental Design for Palm Oil Cracking Process

In the present work, Taguchi method was used to program all the experiments. For this, Minitab 16 software was used. In case of fluid catalytic cracking, catalyst loading, temperature, time, reactor size, geometry, feed flow, inlet position, preheating and reflux play important role. However, in the present case, aim of the research was to develop process for catalysts and evaluate the activity of the synthesized materials in suitable applications. For palm oil cracking, a batch reactor was used, in which, reactor size is already fixed. In addition, there were also no possibilities to change flow or flow locations, therefore only, in order to design the palm oil cracking experiments, temperature ( $^{\circ}\text{C}$ ), catalyst loading (wt of oil/wt of catalyst) and time (min) were chosen as the independent variables, while yield (%) of the gasoline fractions was selected as the output response. Low and high values of the chosen parameters are given in Table 8.3. Selection of these values was considered on the basis of available literature (Twaiq et al., 2003a; Twaiq et al., 2003b; Twaiq et al., 2004b) and few preliminary experiments. This method had suggested a set of 9 experiments, a notable reduction over the 128 experiments that would had been required to evaluate each independent parameter with relation to another selected parameters. Table 8.4 represents the suggested  $L_9$  orthogonal array for the palm oil cracking experiments.

**Table 8.3:** Process Factors with Their Three Level Values Used for Taguchi Design

Process Parameters	Level 1	Level 2	Level 3
Temperature ( $^{\circ}\text{C}$ )	350	400	450
Catalyst loading (wt %)	1	2	3
Time (min)	30	45	60

### 8.4.1 Experimentation

Initially, a set of experiments (Table 8.4) were performed to evaluate and optimize the cracking of palm oil using the Fe-Zn-ZSM-5(33) catalyst. Experiments were conducted in a 500mL-lab-scale reactor equipped with a heating mantle, magnetic stirrer, dean stark and condenser. In all of the experiments, 50 mL of palm oil was introduced to the reactor. The desired amount of catalyst (wt/wt) was added and the oil-catalyst mixture was stirred at the specified temperature (Table 8.4).

A continuous stirring (400 rpm) was employed in each experiment. Samples were obtained from the dean stark, filtered using syringe filter (0.20  $\mu\text{m}$  Millipore), and examined through gas chromatography (GC). Using the optimized values, performance of parent ZSM-5(30), and the other synthesized catalysts: Fe-Zn-Cu-ZSM-5 (30) and Fe-Zn-Cu-ZSM-5 (32) were evaluated in terms of conversion of palm oil and yield of biogasoline fractions. The organic liquid products analyzed through GC, revealed details about the cracked products.

**Table 8.4:** Experimental Results of Palm Oil Cracking and Taguchi Analysis

Run. No	Temperature (°C)	Catalyst Loading (%)	Time (min)	Gasoline Yield (%)
1	350	1	30	8.11
2	350	2	45	27.20
3	350	3	60	44.18
4	400	1	45	45.30
5	400	2	60	48.29
6	400	3	30	41.11
7	450	1	60	44.65
8	450	2	30	44.05
9	450	3	45	55.91

The GC system was initially calibrated using standard analytical reagents namely iso-octane, n-heptane, cyclohexane, n-hexane, n-pentane, toluene, benzene, phenol and ethanol to identify moieties produced from the cracking process. The cracked compounds were recognized by matching their retention times with standard reagents. The conversion and gasoline yield are defined as follows:

$$\text{Conversion (wt \%)} = \frac{C}{P} \times 100 \quad \mathbf{8-1}$$

$$\text{Gasoline (wt \%)} = \frac{Y}{P} \times 100 \quad \mathbf{8-2}$$

Where C is the total organic liquid product, P is the palm oil feed (g) and Y is the total gasoline fractions (equations 8-1 and 8-2). The scope of this study was conversion of palm oil to gasoline using the synthesized catalysts. Therefore, other liquid and gaseous products were not considered in this work.

## **8.5 Results and Discussions**

### **8.5.1 Characterization of Synthesized Catalysts**

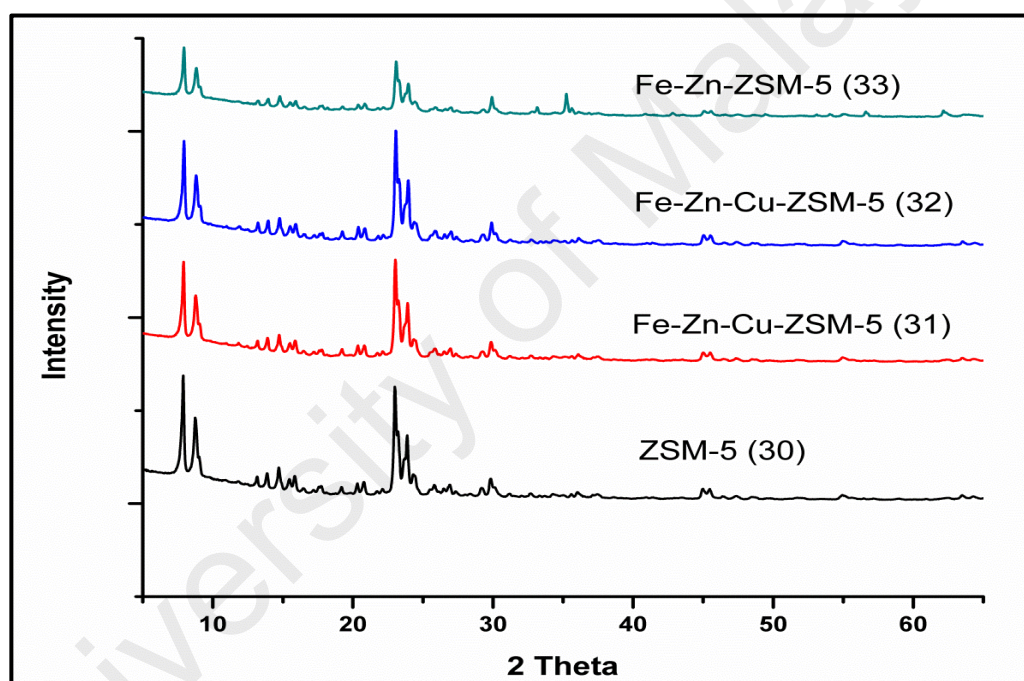
The corresponding data related to percentage composition of support, ZSM-5 and synthesized catalysts is provided in Table 8.1. These percentage compositions were observed using surface area method. Elemental mapping of synthesized materials clearly illustrated the presence of aluminum, silicon, iron and oxygen atoms inside the solid cluster. The ratios of silicon and oxygen were prominent as compared to aluminum and integrated atoms. It was found that the calcination caused the complete removal of the ligand part from the supporting matrix, producing nano oxides on the surface of the support. The EDX values of the loaded moieties were in agreement with the theoretical values.

Figure 8.1 shows the XRD patterns of the synthesized catalysts together with ZSM-5 for comparison purpose. The synthesized catalysts exhibited the distinctive diffractograms of the ZSM-5 ( $2\theta = 7 - 9^\circ$  and  $23 - 25^\circ$ ) provided in the literature (Cihanoglu et al., 2015). This analysis revealed that the loading of Fe, Zn, Ni and Cu MOFs and their nano oxides in accessible positions insight the zeolite matrix had not damaged the crystallinity of the matrix. However, intensities of characteristic peaks were changed due to filling of metallic nano oxides into the zeolite matrix of ZSM-5. The characteristic peak intensities were reduced significantly with Fe and Zn. This indicated that the X-ray absorption was fevered by the presence of Fe and Zn nano oxide particles (Cihanoglu et al., 2015).

In addition, the reduction in the peak intensities may be attributed to the decrease in the particle size of the ZSM-5 as a consequence of the mixing step and with growth of the non-uniform zones linked with washing away aluminum atoms from the matrix of ZSM-5. The other reason may be the amorphous oxides phases on the zeolite surface, caused the decrease in the peak intensities (Cihanoglu et al., 2015; Dukkancı et al., 2010b). However, addition of Cu along with Fe, Zn, and Ni nano oxide particles slightly increased the peak intensities which was best matched with the finding of Dukkancı et al. (2010b).

SEM and HRTEM study (Figure 8.2) illustrated the surface microstructures of all the synthesized catalysts and the morphology of the parent ZSM-5. The morphology of the parent ZSM-5 (Figure 8.2 (a, b)) was significantly changed after the addition of metallic oxides via impregnation of MOFs and their thermal degradation (Figure 8.2 (c, e, and g)). The HRTEM results (Figure 8.2 (d, f, and h)) clearly illustrated that calcination caused thermal decomposition of MOFs, resulting in the formation of nano-sized heterometallic oxides on the zeolitic matrix (Chen et al., 2009).

The specific surface areas of the synthesized catalysts and ZSM-5 support are provided in Table 8.2. As presented in the table, the parent ZSM-5 and synthesized catalysts had relatively smaller surface area compared to the literature value, but they were still in the reported region (Sang et al., 2004; Sani et al., 2015). Addition of nano oxides via impregnation of MOFs and their thermal decomposition reduced the surface area. This variation was due to the filling of nanoparticles (metallic oxides), inside the pores and also on the surface of the matrix and decreased the pore volume, and specific area (Yan et al., 2014).



**Figure 8.1:** XRD Analysis of Synthesized Catalysts

The size of integrated oxide particles was observed in a range of 2-5 nm. The smaller surface area of the synthesized catalysts was also caused by the presence of amorphous materials (Sang et al., 2004). The synthesized catalysts had a greater pore size (2.68 nm) than the parent ZSM-5 (2.40 nm). Changes occurred in the specific surface area and pore size (4V/A by BET) are well supported by the literature (Dukkancı et al., 2010b; Yan et al., 2014).

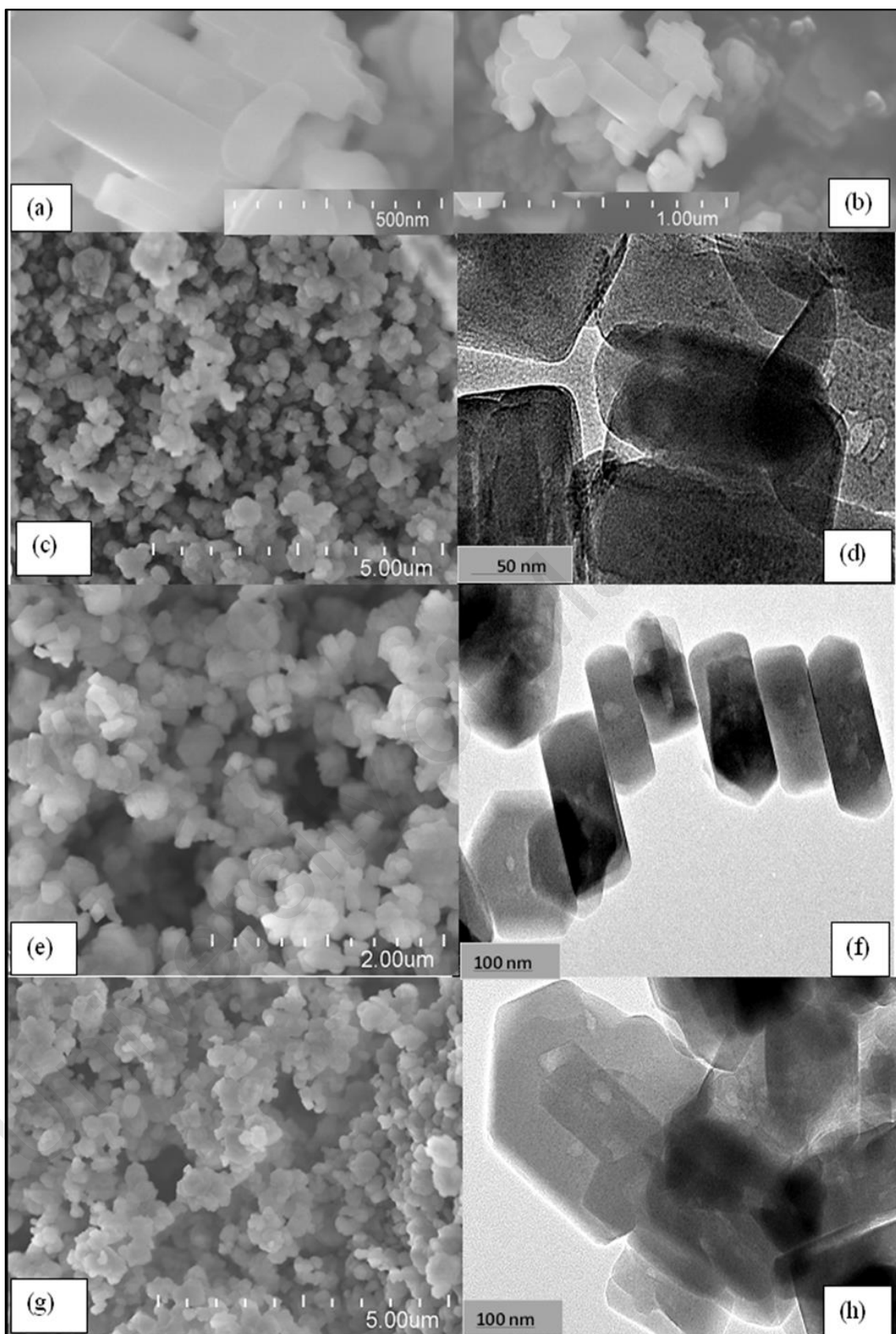


**Figure 8.2:** FeSEM (a, b, c, e, & g) and HRTEM (d, f, & h) Images of the Synthesized Catalysts

### 8.5.2 Palm Oil Catalytic Cracking

In this work, the amount of the heat supplied was well controlled by the temperature of the heating mantle, fitted with the lab scale reactor. At the same time, catalysts were added to lower the activation energy of the cracking process. The presence of catalysts reduced the energy needed to crack long-chain hydrocarbons and thus products were formed in a more energy-efficient way. Table 8.4 lists the biogasoline yield from 9 experimental runs. The influence of the process variables on the yield is provided in the following sections.

Available literature best support this process and cracking mechanism. Ramya et al. (2012) have described a detailed mechanism for the cracking of the vegetable oil using ZSM-5 based catalysts. Authors claimed that both the acidity and catalysts structure had significant effect on the catalytic cracking, oligomerization and aromatization. Presence of Brønsted acid sites as well as Lewis acids sites promote cracking while the structure of ZSM-5 facilitates in modifying the cracked fragments to form branched hydrocarbons such as gasoline and diesel. In the present case, nano size integrated ZSM-5 favored the yield of gasoline fractions. This may be attributed to the metallic oxide particles. Wang et al. (2015b) and Ni et al. (2011) earlier well described the effect of different nano size oxides such as Zn, Ga, Fe and Cu supported on ZSM-5. Ni et al. (2011) further revealed that the nano structures offer more resistance to coke. In addition, the life time of nano sized ZSM-5 based catalysts are longer than those of micro sized catalysts. In some cases, although the amount of coke was high for ZnO/ZSM-5, however, the conversion of methanol into petroleum products was found higher. The influence of the process variables on the yield is provided in the following sections.

### 8.5.2.1 Effect of Catalyst Loadings

The range of catalyst loading was set between 1-3% (Table 8.3) to study the effects of the synthesized catalyst on the yield of the organic liquid fractions. With smaller amount of catalyst in the feed oil, the conversion of palm oil was faster; however the gasoline yield was relatively low. The cracking rate increased and there was a steep curve (Figure 8.3) by increasing the catalyst loading from 1 to 3% in the feed oil. Increase in the biogasoline yield with the increase in amount of catalyst was due to an increase in the number of active sites on the heterogeneous catalyst surface (Chew & Bhatia, 2008; Farshi & Abri, 2012). Solid acid catalysts are effective for catalytic cracking of palm oil. Zeolitic catalysts such as ZSM-5 are normally used to reduce the oxygenates in liquid products (Dickerson & Soria, 2013; Ong & Bhatia, 2010; Vu et al., 2015b). The acidic properties are very important in catalyzing the cracking, decarboxylation, isomerization, dehydration, and oligomerization-aromatization reactions. The selectivity and activity of ZSM-5 depend on the number of the available acid sites, and the nature (Lewis or Bronsted), and strength of these sites (Chew & Bhatia, 2008; Iliopoulou et al., 2007). As reported in some literature, loading of metallic oxides nano particles on ZSM-5 significantly enhances the Lewis and Bronsted acidities (Cihanoglu et al., 2015; Taufiqurrahmi & Bhatia, 2011). In this study, metallic oxides nano particles significantly increased the liquid products, particularly the gasoline fractions from 8 to 44%.

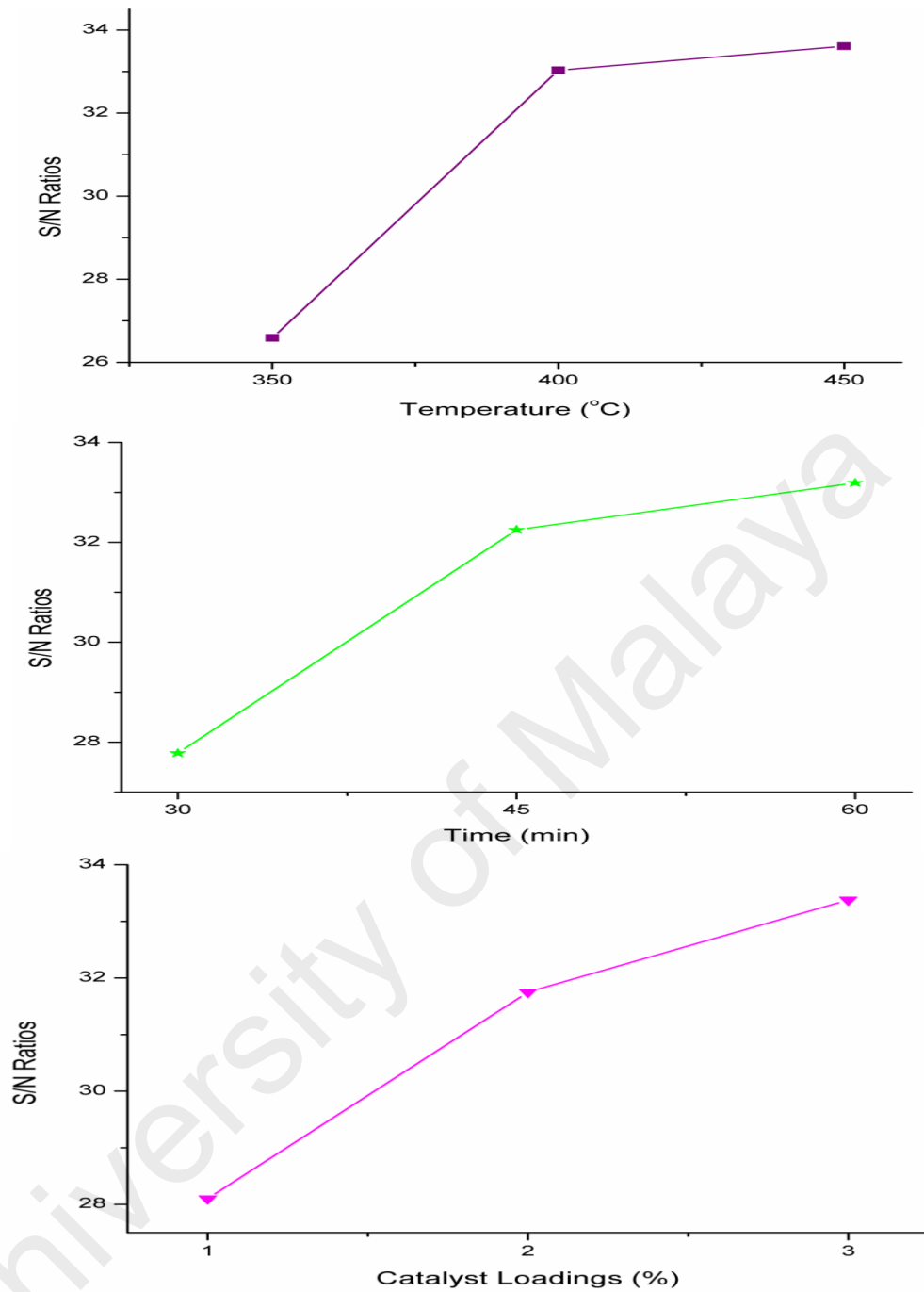


**Figure 8.3:** Effect of Process Parameters on Yield Of Biogasoline, Calculated on the Basis of S/N Ratios

### 8.5.2.2 Effect of Cracking Temperature

Reaction temperature is one of the significant parameters in the cracking process (Vu et al., 2015a; Yigezu & Muthukumar, 2014). In this study, range was set between 350-

450 °C (Table 8.3). The effect of temperature was significant in runs 3 and 5 (Table 8.4). Conversion of palm oil increased (Figure 8.3) with temperature.

It was noted that the cracking rate increased and the curve was steep by increasing the temperature from 350 to 400 °C. However, the curve became flat when the temperature was changed from 400°C to 450°C. Normally, lower temperature (400-550 °C) and high heating rate have yielded of liquid products containing oxygenated aromatic and aliphatic compounds. However, at higher temperature (500-850 °C), production of fuel gas containing CO, CO<sub>2</sub>, CH<sub>4</sub>, C<sub>2</sub>H<sub>4</sub>, C<sub>2</sub>H<sub>6</sub>, and slight amount of water vapors became prominent (Chen et al., 2003; Chew & Bhatia, 2008; Galadima & Muraza, 2015).

#### **8.5.2.3 Effect of Cracking Time**

Time is one of the most significant parameters in the cracking process (Yigezu & Muthukumar, 2014). Apart of cracked products were refluxed back after condensation of vapours via the top line of the dean stark. In this study, the time range was set between 30-60 min (Table 8.3). By increasing the time from 30 to 45 min, the yield of the gasoline fractions increased sharply. The increment rate reduced when the time was increased up to 60 min (Figure 8.3). This was because long-chain hydrocarbon was further cracked to produce smaller hydrocarbon and this increased the yield of gasoline significantly. However, increasing the time up to 60 min increased the yield of lighter products such as methane and ethane etc. (Farshi & Abri, 2012; Ngo et al., 2010).

#### **8.5.2.4 Interaction of Process Variables with Respect to Biogasoline Yield**

An interaction graph between temperature and catalyst loadings showed that increasing the catalyst increased the yield of biogasoline at a constant temperature (Figure 8.4). Increased values of these variables resulted in a notable increase in the product yield. The maximum yield was obtained at 450 °C using 3% of catalyst loading.

Similar trend was observed between the time, and temperature, when the temperature was in the range of 350-400°C. However, at higher temperature (450 °C), increasing the

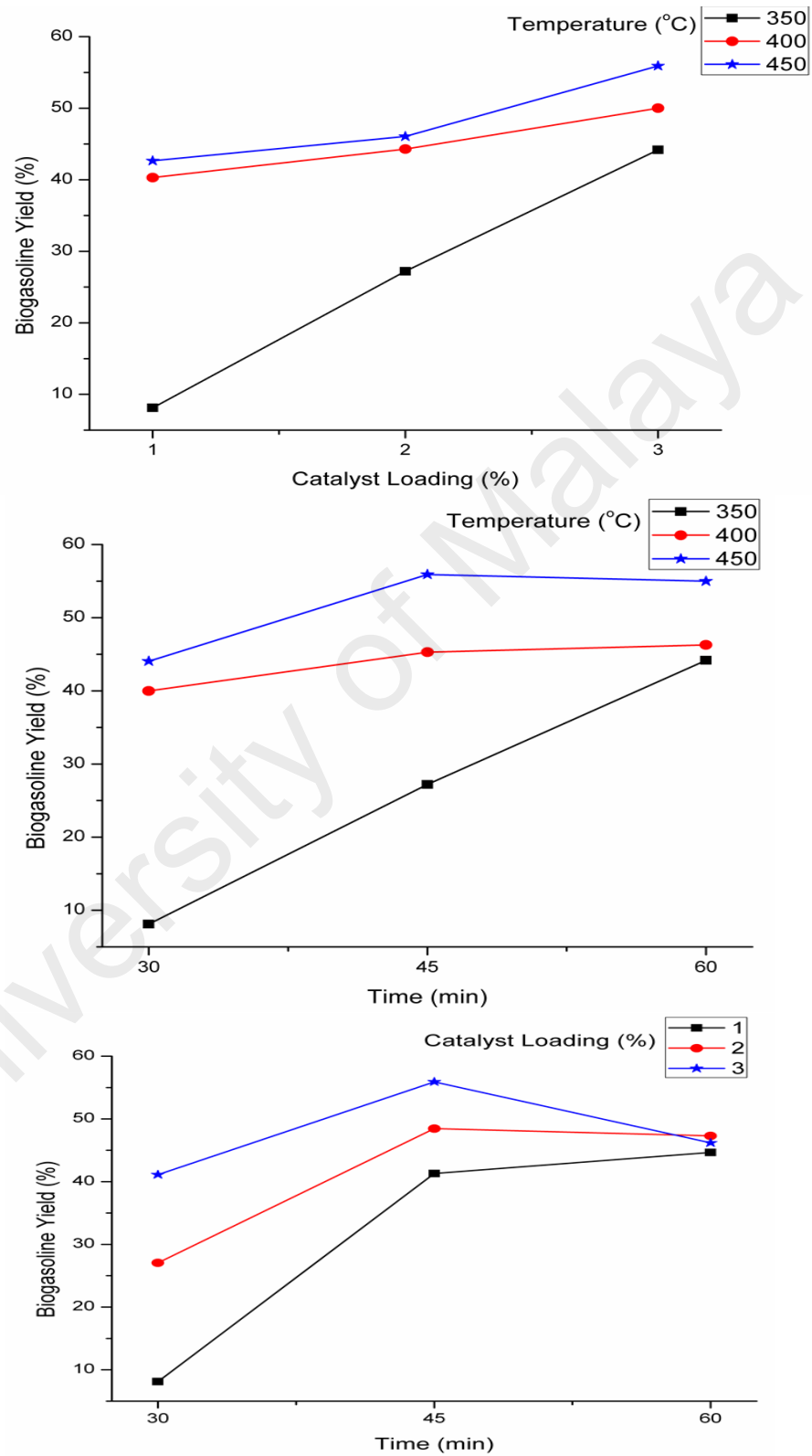


**Figure 8.4:** Interaction of Parameters with Respect to Gasoline Yield (%)

time from 45 min to 60 min reduced the biogasoline yield. This might be due to the production of gaseous or smaller hydrocarbon. On the other side, an increase in the time up to 45 min increased the yield of biogasoline, when the catalyst loading was kept constant. However, increasing the values of these factors resulted in a reduced product yield. This might be attributed to the presence/ formation of gaseous hydrocarbons(Vu et al., 2015a).

### 8.5.3 Optimization Study

Cracking of palm oil was optimized by Taguchi method. Details of all the steps are summarized and provided in previous chapter (Table 6.5). The response obtained as a result of the cracking was transformed to S/N ratios. In this study, high yield of gasoline is desirable in the cracking process. Therefore, option; “larger the better” S/N ratio was chosen. These values remained the highest for runs 3 and 8. The present study dealt with the production of gasoline only. However, real processes also include other organic products such as biodiesel, kerosene and etc. Therefore, it would not be feasible to optimize response individually. The S/N ratio must be optimized and transformed to a single component called “Total Principal Component Index” using Principal Component Analysis (PCA) (French & Czernik, 2010). To achieve this, the S/N ratio at each level must be normalized, followed by applying PCA to the normalized data using matrix  $\bar{X}$ . Next the matrix  $\bar{X}$  is transformed into covariance matrix  $C_x$ , which is further used to calculate Eigen values for considered responses. This method transforms the S/N ratios (normalized) into a set of un-correlated major components. Larger than 1 “Eigen value” is selected for these calculations. The theoretical detail of each step is available in the chapter 6.

In the present study, it was found that the synthesized Fe-Zn-ZSM-5 could achieve 56% of the biogasoline yield. The results are provided in Table 8.5. The effect of

temperature on the biogasoline yield was more significant, while catalyst loading had less influence compared to the other two parameters. Generally, all the parameters had significant effects on the biogasoline yield.

**Table 8.5:** Response Table for Signal to Noise Ratios

Level	Temperature (°C)	Catalyst Loading (%)	Time (min)
1	26.59	28.10	27.78
2	33.03	31.75	32.25
3	33.61	33.38	33.19
Delta	7.02	5.28	5.41
Rank	1	3	2

ANOVA was employed in the Taguchi method to assess the catalytic cracking results and find the influence of every factor on product yield. ANOVA is just like to the regression analysis, used to access the relationship among the response variable (Asghar et al., 2014c)s. Table 8.6 illustrates the ANOVA analysis.

**Table 8.6:** ANOVA Analysis for Process Parameters

Factor	Degree of Freedom	Sum of Squares	Mean Squares	F-ratio	p-value	Percent Contribution (%)
Temperature (°C)	2	821	410	3.21	0.113	61
Catalyst Loading( % )	2	310	155	0.73	0.521	18
Time (min)	2	359	180	0.88	0.463	21

Again, the effect of temperature (61%) was the most prominent; meanwhile, the catalyst loading had the least effect, with a contribution of 18%. The S/N ratio results,

listed in Table 8.5 were in a good agreement with the ANOVA results. Based on the S/N ratios, the regression analysis equation for the biogasoline yield was calculated as follows:

$$S/N \text{ Ratio} = -10.4 + 0.0702 A + 2.64 B + 0.180 C \quad \mathbf{8-3}$$

Where A, B and C are temperature ( $^{\circ}\text{C}$ ), catalyst loading (wt %) and time (min), respectively. The efficiency of the synthesized catalysts was assessed at the optimized conditions. The process conditions are summarized in Table 8.7. The results indicated that the system improved the biogasoline yield with a significant increment of 8-10%. Overall, it was concluded that the synthesized catalysts can be used effectively for the cracking process to yield green energy.

### **8.6 Efficiency of Other Integrated Catalysts**

A series of experiments were performed to evaluate the efficiency of the parent ZSM-5 (30), and synthesized Fe-Zn-Cu-ZSM-5 (31), and Fe-Zn-Cu-ZSM-5 (32) catalysts using the optimized values. The results are provided in Table 8.7. At optimized conditions, the gasoline yield was maximized up to 59% by the Fe-Zn-Cu-ZSM-5 (31) catalyst. However, ZSM-5 (30) and Fe-Zn-Cu-ZSM-5 (32) yielded 14% and 49% of biogasoline, respectively. Higher efficiency of Fe-Zn-Cu-ZSM-5 (31) might be attributed to higher content of loaded metal oxides compared to Fe-Zn-Cu-ZSM-5 (32). The other reason was the presence of copper oxide nano particles, which significantly increased the yield of biogasoline compared to Fe-Zn-Cu-ZSM-5 (33). Therefore, Fe-Zn-Cu-ZSM-5 (31) was found to be suitable for this cracking process.

STA analyses carried out to study the coke deposition on the synthesized catalysts. These values were well supported and confirmed by EDX values. Observed values were 8%, 12%, 9%, and 10% for ZSM-5 (30), Fe-Zn-Cu-ZSM-5 (31), Fe-Zn-Cu-ZSM-5 (32)

and Fe-Zn-ZSM-5 (33), respectively. The coke deposition increased with the metal contents (Wang et al., 2015b). The increased coke deposition might be attributed to the secondary cracking reactions over the metallic oxides (Wang et al., 2015b). In addition, high porosity and uniform distribution of metal oxides on the zeolite matrix makes feasible the deposition and growth of the coke molecules on the catalysts surface (Al-Khattaf et al., 2014; Galadima & Muraza, 2015; Twaiq et al., 2003a).

Fe-Zn-Cu-ZSM-5 (31) was further analyzed with long reaction time. It was revealed that, with increasing the time from 1h to 24 h, the coke deposition rate was increased from 12% to 55%. The residual coke was also analyzed using STA. It contained 83.3% of carbon, which was oxidized completely in the range of 400-580 °C. Detail of coke deposition analysis is provided in the Appendix A.

**Table 8.7:** At Optimized Values, Efficiencies of the ZSM-5 and Synthesized Catalysts

Catalyst	Temperature (°C)	Catalyst Loading (%)	Time (min)	Gasoline Yield (%)
ZSM-5 (30)	450	3	45	14
Fe-Zn- Cu-ZSM-5 (31)	450	3	45	59
Fe-Zn- Cu-ZSM-5 (32)	450	3	45	49

## 8.7 Summary

Utilization of palm oil as biofuel requires zeolite based catalytic technology that may facilitate selective conversion of oil into desired products, including biogasoline and biodiesel. However, development of suitable catalysts for the desired products is a key challenge in the biofuel production, which may be overcome through the usage of nano heterometallic materials supported on zeolite catalysts.

In this chapter, Zeolite Socony Mobile-5 (ZSM-5) based catalysts loaded with heterometallic nano oxides of Fe, Zn, Cu and Ni were synthesized, characterized and used for the palm oil cracking to produce biogasoline. Taguchi method was used to assess and optimize the catalytic cracking process. The optimized values of temperature, catalyst loading, and time were 450 °C, 3%, and 45 min, respectively.

Under optimized conditions, ZSM-5 (30), Fe-Zn-Cu-ZSM-5 (31), Fe-Zn-Cu-ZSM-5 (32) and Fe-Zn-Cu-ZSM-5 (33) yielded 14%, 59%, 49% and 56% of biogasoline, respectively. Higher efficiency of Fe-Zn-Cu-ZSM-5 (31) might be attributed to higher content of loaded metal oxides compared to the other synthesized catalysts. The yield of biogasoline through Fe-Zn-Cu-ZSM-5 (31) was 8% more than the literature values. Therefore, the present study proved that the integrated heterometallic Fe-Zn-Cu-ZSM-5 (31) was efficient and economical to produce biogasoline from cracking of palm oil.

## CHAPTER 9: CONCLUSIONS AND RECOMMENDATIONS FOR FUTURE WORK

In this research, a two-step chemical process was developed and used for the synthesis of heterometallic metal organic frame works (MOFs) and their thermal decomposition to form nano sized clusters. Overall, the produced heterometallic catalysts have shown great potential for waste water treatments and green energy applications. In addition, availability of ligand (2,2'-bipyridine), solvents (ethanol, 2-proapnol and DMF) and their relevant information in the literature make this 2-step process an attractive process for the production of a variety of heterometallic catalysts and special alloys.

In the first stage, precipitation process was effectively employed to produce monometallic and polymetallic complexes. 2,2'-bipyridine was used as the ligand to interlink metal atoms (Ni, Zn and Al). In the second stage, heterometallic complexes were thermally decomposed to produce nano clusters. Central Composite Design (CCD) method was employed to optimize process yields, while ANOVA was used to analyze the data to obtain the interaction among the process variables (temperature, time and stirrer speed). The crystalline products were characterized by FTIR, FeSEM, EDX, TGA and XRD.

The yield of Ni, Zn and Al clusters were above 81%, 80% and 78% respectively, while the yield of Ni-Zn, Zn-Al and Ni-Zn-Al complexes were 85%, 78.5% and 77% respectively. Addition of Ni metal-atoms to Zn-Al composites changed the size and morphology of the crystalline particles. Thermal decomposition of Zn-Al complex produced mesoporous nano balls. However, Zn-Ni-Al complex caused formation of

needle like crystals. These synthesized materials can be used in a variety of industrial applications.

Two-step process was further utilized to produce supported type catalyst. Zeolite Socony Mobile-5 (ZSM-5) matrix was integrated with heterometallic nano oxides of Fe, Zn, Cu and Ni. Synthesized catalysts were characterized using FeSEM, EDX, FTIR, HRTEM, BET and XRD, and coded as Fe-ZSM-5, ZSM-5 (30), Fe-Zn-Cu-ZSM-5 (31), Fe-Zn-Cu-ZSM-5 (32) and Fe-Zn-Cu-ZSM-5 (33). Synthesized supported catalysts were used in two sectors including wastewater treatment and biofuel production.

For the wastewater treatment, synthesized Fe-ZSM-5 heterometallic catalyst was effectively used to degrade and decolorize the textile based effluents, containing organic recalcitrant contaminants through Fenton oxidation process. Acid Blue 113, Methyl Orange, and Reactive Black 5 were used as the model dyes. The catalyst has yielded over 99% degradation of the selected dyes, individually and in the mixture form. Similarly, the total organic carbon (TOC) removal was achieved up to 77%, 71 % and 68% for Acid Blue 113, Methyl Orange, and Reactive Black 5, respectively. For the mixtures, TOC removal was observed in the range 69 to 72%, which was better than the reported values in the literature. With detail comparison to available literature, it was found that applying Fe-ZSM-5 heterogeneous Fenton oxidation is economical, as 90% consumption of catalyst was reduced. In addition to this, stability testing with respect to metal leaching and reusability showed that less than 2ppm of the iron was leached, which was an indication of high stability and reusability of the synthesized catalyst.

For the biofuel production, synthesized ZSM-5 (30), Fe-Zn-Cu-ZSM-5 (31), Fe-Zn-Cu-ZSM-5 (32) and Fe-Zn-Cu-ZSM-5 (33) were used to crack the palm oil. Taguchi method was used to assess and optimize the catalytic cracking process. Under optimized conditions (450 °C, 3% of catalyst loading, and 45 min), ZSM-5 (30), Fe-Zn-

Cu-ZSM-5 (31), Fe-Zn-Cu-ZSM-5 (32) and Fe-Zn-Cu-ZSM-5 (33) yielded 14%, 59%, 49% and 56% of biogasoline, respectively. Higher efficiency of Fe-Zn-Cu-ZSM-5 (31) might be attributed to higher content of loaded metal oxides compared to the other synthesized catalysts. The yield of biogasoline through Fe-Zn-Cu-ZSM-5 (31) was approximately 8% more than the literature values. Therefore, the present study proved that the integrated heterometallic Fe-Zn-Cu-ZSM-5 (31) was efficient and economical to produce biogasoline from cracking of palm oil.

Overall, the produced heterometallic catalysts have shown great potential for waste water treatments and green energy applications. In addition, availability of ligand (2,2'-bipyridine), solvents (ethanol, 2-propanol and DMF) and their relevant information in the literature make this 2-step process an attractive process for the production of a variety of heterometallic catalysts and special alloys.

### **9.1 Recommendations for Future Work**

This work has enabled the development of a chemical process to synthesize a wide range of heterometallic materials via MOFs for environmental and green energy applications. Findings of this work have resulted into a patent along with ten publications, which have added useful information to available literature, required to transform MOFs into heterometallic materials. Researcher believes that this study will make an original contribution to both industry as well as human development. In addition, it is anticipated that this study will provide an exciting opportunity to advance the researchers' knowledge about the heterometallic materials via MOFs and will cause to open new research avenues in this field.

In the future, the efficiencies of the catalysts produced by two-step process can be evaluated against other organic pollutants and also for the production of biofuels from

non-edible oils. However, the major recommendation for this work is to scale up this process for the larger scale productions. Scale up can be considered either as design, fabrication and installation of the larger scale equipments or modifications in the existing units for the larger scale heterometallic production.

### **9.1.1 Scale up of the Two-Step Process**

Development of a new process or a new material at the laboratory scale is the first step to perform prior to scale up applications. However, the production of nano-sized materials at industrial scale is challenging and requires expertise and sophisticated equipments for production and separation processes. This is because; the process conditions, such as mixing, temperature, pressure and etc are difficult to maintain at larger scale production as compared to lab scale.

Computational fluid dynamics (CFD) based modelling and simulation has made it possible to capture and enlarge the true picture of the process. Therefore, scale-up of the developed process would be worth consideration using CFD based modelling and scale up. Reaction kinetics, mixing environment and product features of the developed materials (at optimized conditions) can be used as the main inputs for this modelling and scale up.

Utilization of the existing industrial scale plant or unit is also possible for this scale up. Figure illustrates a novel approach to scale up of the two-step process. CFD methods can be used to simulate mixing and reaction environment at larger scale for the maximized yield. Figure 9.1 illustrates the systematic scale up for the two-step process.

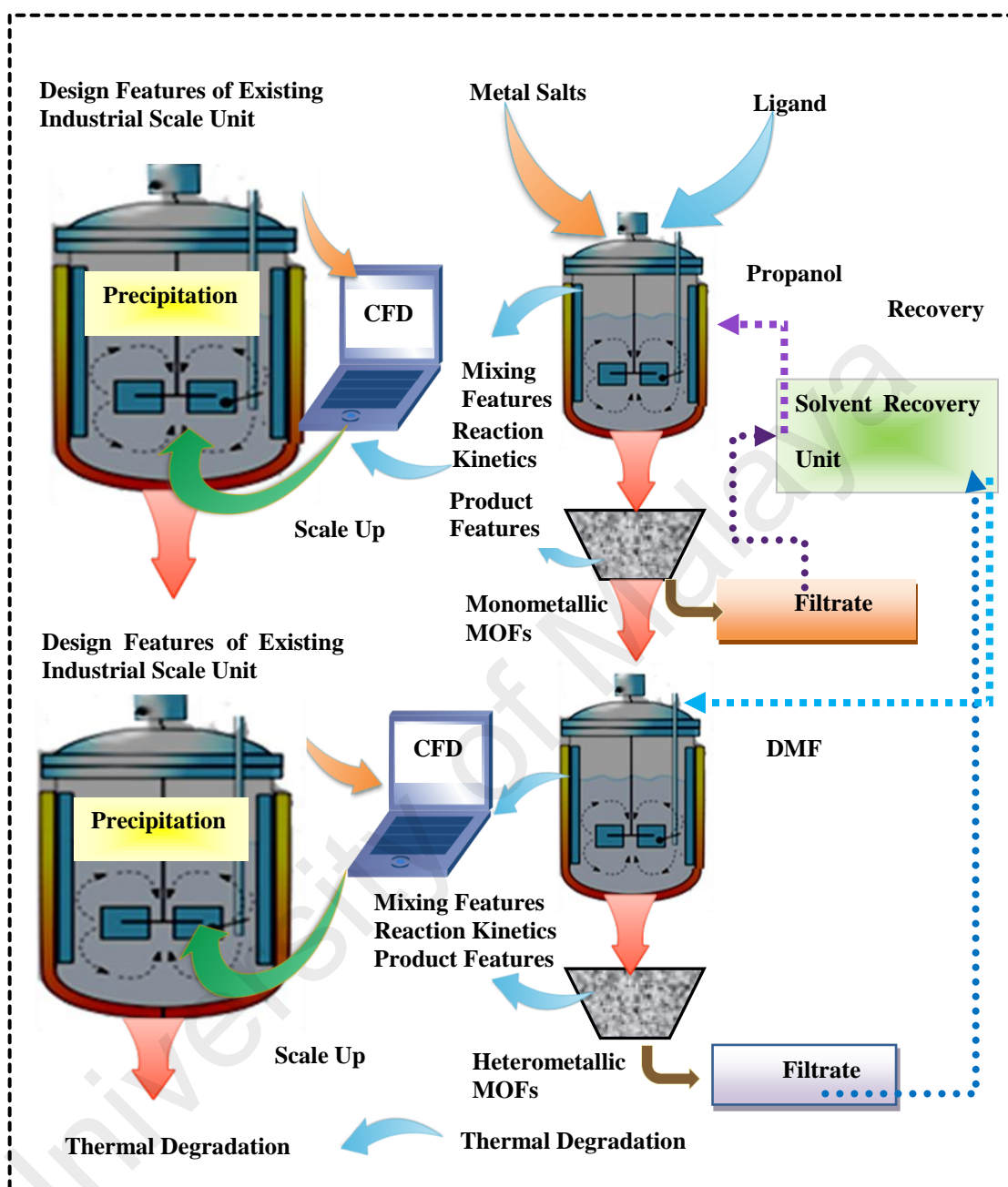


**Figure 9.1:** Process Flow Diagram for the Scale Up of Two-Step Process

### 9.1.2 Design of an Efficient Solvent Recovery System

Design of an efficient solvent recovery system is the other main recommendation for the scale up of the developed two-step process. Normally, recovery of the solvent is considered as an important aspect to make the process cost effective and environment

friendly. Industrial solvents are mostly recovered through distillation and solvent-solvent extraction or their combination (Bremner & Keeney, 1965; Capello et al., 2007; Crook et al., 1975; Earle et al., 2006). These methods are able to recover bulk quantities.

Figure 9.2 illustrates the proposed process flow diagram of the recovery system with compact design for the recovery of different solvents, would be used in the developed two-step process. Variable feed inlets and modified the design of column bottom can significantly enhance the solvent recovery and quality. This system would able to handle a variety of the industrial solvents like ethanol, propanol, DMF, acetone, propanol and acetic acid.

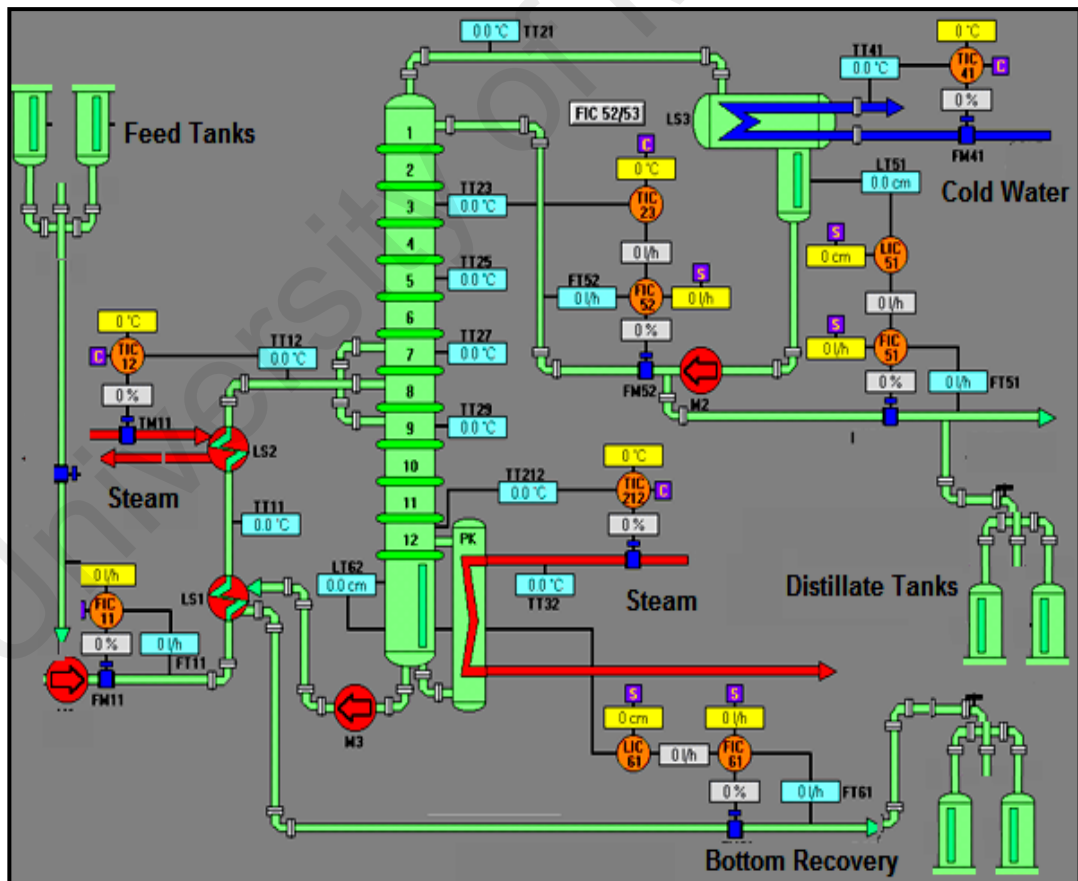


**Figure 9.2:** Two-Step Process with Proposed Recovery of Solvent

## REFERENCES

- Abdullah, A. H., & Wong, W.-Y. (2010). Decolorization of Reactive Orange 16 Dye by Copper Oxide System. *Sains Malaysiana*, 39(4), 587-591.
- Ahmed, S., Mansoor, M. A., Basirun, W. J., Sookhajian, M., Huang, N. M., Mun, L. K., et al. (2015). The synthesis and characterization of a hexanuclear copper–yttrium complex for deposition of semiconducting  $\text{CuYO}_{2-0.5} \text{Cu}_2\text{O}$  composite thin films. *New Journal of Chemistry*, 39(2), 1031-1037.
- Ahmed, S., Mansoor, M. A., Mazhar, M., Söhnle, T., Khaledi, H., Basirun, W. J., et al. (2014). Semiconducting composite oxide  $\text{Y}_2\text{CuO}_4\text{-5CuO}$  thin films for investigation of photoelectrochemical properties. *Dalton Transactions*, 43(22), 8523-8529.
- Ajeel, M. A., Aroua, M. K., & Daud, W. M. A. W. (2015). Preparation and characterization of carbon black diamond composite electrodes for anodic degradation of phenol. *Electrochimica Acta*, 153, 379-384.
- Akan, J. C., Abdulrahman, F. I., Ayodele, J. T., & Ogugbuaja, V. O. (2009). Impact of tannery and textile effluent on the chemical characteristics of Challawa River, Kano State, Nigeria. *Australian Journal of Basic and Applied Sciences*, 3(3), 1933-1947.
- Akolekar, D. B., & Bhargava, S. K. (1998). FTIR investigations of the adsorption and disproportionation of NO on Cu exchanged silicoaluminophosphate of type 34. *J.Chem.Soc.Faraday Trans.*, 94 155.
- Al-Khattaf, S., D'Agostino, C., Akhtar, M. N., Al-Yassir, N., Tan, N. Y., & Gladden, L. F. (2014). The effect of coke deposition on the activity and selectivity of the HZSM-5 zeolite during ethylbenzene alkylation reaction in the presence of ethanol. *Catalysis Science & Technology*, 4(4), 1017-1027.
- Alslaibi, T. M., Abustan, I., Ahmad, M. A., & Foul, A. A. (2013). Application of response surface methodology (RSM) for optimization of  $\text{Cu}^{2+}$ ,  $\text{Cd}^{2+}$ ,  $\text{Ni}^{2+}$ ,  $\text{Pb}^{2+}$ ,  $\text{Fe}^{2+}$ , and  $\text{Zn}^{2+}$  removal from aqueous solution using microwaved olive

stone activated carbon. *Journal of Chemical Technology & Biotechnology*, 88(12), 2141-2151.

Amin, S. A., Pazouki, M., & Hosseinnia, A. (2009). Synthesis of TiO<sub>2</sub>-Ag nanocomposite with solgel method and investigation of its antibacterial activity against E. coli. *Powder Technology*, 196(3), 241-245.

Asghar, A., Abdul Raman, A. A., & Daud, W. M. (2014a). A comparison of central composite design and taguchi method for optimizing fenton process. *ScientificWorldJournal*, 2014, 869120.

Asghar, A., Abdul Raman, A. A., & Daud, W. M. A. W. (2014b). A Comparison of Central Composite Design and Taguchi Method for Optimizing Fenton Process. *The Scientific World Journal*, 2014.

Asghar, A., Abdul Raman, A. A., & Daud, W. M. A. W. (2014c). A Comparison of Central Composite Design and Taguchi Method for Optimizing Fenton Process. *The Scientific World Journal*, 2014, 14.

Asghar, A., Abdul Raman, A. A., & Daud, W. M. A. W. (2014d). A Comparison of Central Composite Design and Taguchi Method for Optimizing Fenton Process. *The Scientific World Journal*, 2014, 14.

Bae, Y.-S., Farha, O. K., Spokoyny, A. M., Mirkin, C. A., Hupp, J. T., & Snurr, R. Q. (2008). Carborane-based metal-organic frameworks as highly selective sorbents for CO<sub>2</sub> over methane. *Chem. Commun.*(35), 4135-4137.

Banerjee, A., Gokhale, R., Bhatnagar, S., Jog, J., Bhardwaj, M., Lefez, B., et al. (2012). MOF derived porous carbon-Fe<sub>3</sub>O<sub>4</sub> nanocomposite as a high performance, recyclable environmental superadsorbent. *Journal of Materials Chemistry*, 22(37), 19694-19699.

Banerjee, M., Das, S., Yoon, M., Choi, H. J., Hyun, M. H., Park, S. M., et al. (2009). Postsynthetic modification switches an achiral framework to catalytically active homochiral metal-organic porous materials. *Journal of the American Chemical Society*, 131(22), 7524-7525.

- Barrios, C. E., Baltanas, M. A., Bolmaro, R., & Bonivardi, A. L. (2014). Preparation and structural characterization of ZnO and CeO<sub>2</sub> nanocomposite powders as 'active catalytic supports'. *Powder Technology*, 267(0), 180-192.
- Battiston, A., Bitter, J., De Groot, F., Overweg, A., Stephan, O., Van Bokhoven, J., et al. (2003). Evolution of Fe species during the synthesis of over-exchanged Fe/ZSM5 obtained by chemical vapor deposition of FeCl<sub>3</sub>. *Journal of catalysis*, 213(2), 251-271.
- Bazer-Bachi, D., Assie, L., Lecocq, V., Harbuzaru, B., & Falk, V. (2014). Towards industrial use of metal-organic framework: Impact of shaping on the MOF properties. *Powder Technology*, 255(0), 52-59.
- Bell, A. T. (2003). The Impact of Nanoscience on Heterogeneous Catalysis. *Science*, 299(5613), 1688-1691.
- Bhavioripudi, S., Jia, X., Dresselhaus, M. S., & Kong, J. (2010). Role of kinetic factors in chemical vapor deposition synthesis of uniform large area graphene using copper catalyst. *Nano letters*, 10(10), 4128-4133.
- Biswas, S., Mohanty, P., & Sharma, D. K. (2013). Studies on synergism in the cracking and co-cracking of Jatropha oil, vacuum residue and high density polyethylene: Kinetic analysis. *Fuel Processing Technology*, 106, 673-683.
- Bolova, E., Gunduz, G., & Dukkanci, M. (2012). Heterogeneous Fenton-like degradation of orange II in water using FeZSM-5 zeolite catalyst. *International Journal of Chemical Reactor Engineering*, 10(1).
- Bolova, E., Gunduz, G., Dukkanci, M., Yilmaz, S., & Yaman, Y. C. (2011). Fe containing ZSM-5 zeolite as catalyst for wet peroxide oxidation of Orange II. *International Journal of Chemical Reactor Engineering*, 9(1).
- Bremner, J. M., & Keeney, D. R. (1965). Steam distillation methods for determination of ammonium, nitrate and nitrite. *Analytica Chimica Acta*, 32(0), 485-495.

- Buitrago-Sierra, R., Ruiz-Martínez, J., Serrano-Ruiz, J. C., Rodríguez-Reinoso, F., & Sepúlveda-Escribano, A. (2012). Ethanol steam reforming on Ni/Al<sub>2</sub>O<sub>3</sub> catalysts: Effect of the addition of Zn and Pt. *Journal of Colloid and Interface Science*, 383(1), 148-154.
- Buitrago, S. R., Ruiz, M. J., Serrano, R. J. C., Rodriguez, R. F., & Sepulveda, E. A. (2012). Ethanol steam reforming on Ni/Al<sub>2</sub>O<sub>3</sub> catalysts: Effect of the addition of Zn and Pt. *Journal of Colloid and Interface Science*, 383(1), 148-154.
- Burrows, A. D. (2011). Mixed-component metal–organic frameworks (MC-MOFs): enhancing functionality through solid solution formation and surface modifications. *CrystEngComm*, 13(11), 3623.
- Buzetzkí, E., Sidorová, K., Cvengrošová, Z., & Cvengroš, J. (2011). Effects of oil type on products obtained by cracking of oils and fats. *Fuel Processing Technology*, 92(10), 2041-2047.
- Cao, N., Yang, L., Dai, H., Liu, T., Su, J., Wu, X., et al. (2014). Immobilization of Ultrafine Bimetallic Ni–Pt Nanoparticles Inside the Pores of Metal–Organic Frameworks as Efficient Catalysts for Dehydrogenation of Alkaline Solution of Hydrazine. *Inorganic Chemistry*, 53(19), 10122-10128.
- Capello, C., Fischer, U., & Hungerbühler, K. (2007). What is a green solvent? A comprehensive framework for the environmental assessment of solvents. *Green Chemistry*, 9(9), 927-934.
- Chae, H. K., Siberio-Pérez, D. Y., Kim, J., Go, Y., Eddaoudi, M., Matzger, A. J., et al. (2004). A route to high surface area, porosity and inclusion of large molecules in crystals. *Nature*, 427(6974), 523-527.
- Chang, C. C., Hsu, C. C., Chang, C. T., Chen, Y. P., Liaw, B. J., & Chen, Y. Z. (2012). Effect of noble metal on oxidative steam reforming of methanol over CuO/ZnO/Al<sub>2</sub>O<sub>3</sub> catalysts. *International Journal of Hydrogen Energy*, 37(15), 11176-11184.

- Chang, J. H., Ellis, A. V., Hsieh, Y. H., Tung, C. H., & Shen, S. Y. (2009). Electrocatalytic characterization and dye degradation of Nano-TiO<sub>2</sub> electrode films fabricated by CVD. *Science of The Total Environment*, 407(22), 5914-5920.
- Chen, A., Ma, X., & Sun, H. (2008). Decolorization of KN-R catalyzed by Fe-containing Y and ZSM-5 zeolites. *Journal of Hazardous Materials*, 156(1), 568-575.
- Chen, G., Andries, J., & Spliethoff, H. (2003). Catalytic pyrolysis of biomass for hydrogen rich fuel gas production. *Energy Conversion and Management*, 44(14), 2289-2296.
- Chen, H., Chen, J., & Wang, R. (2009). A structural study of the Fe/ZSM-5 catalyst by through-focus exit-wavefunction reconstruction in HRTEM. *Microporous and Mesoporous Materials*, 120(3), 472-476.
- Chew, T. L., & Bhatia, S. (2008). Catalytic processes towards the production of biofuels in a palm oil and oil palm biomass-based biorefinery. *Bioresour Technology*, 99(17), 7911-7922.
- Choi, I.-H., Hwang, K.-R., Han, J.-S., Lee, K.-H., Yun, J. S., & Lee, J.-S. (2015). The direct production of jet-fuel from non-edible oil in a single-step process. *Fuel*, 158, 98-104.
- Chowdhury, P. (2016). CO, CO<sub>2</sub> and CH<sub>4</sub> Gas Adsorption (Pure and Binary) on Cu-BTC and MIL-101 Metal Organic Frameworks (MOFs). *une*, 13, 15.
- Cihanoglu, A., Gunduz, G., & Dukkancı, M. (2015). Degradation of acetic acid by heterogeneous Fenton-like oxidation over iron-containing ZSM-5 zeolites. *Applied Catalysis B: Environmental*, 165(0), 687-699.
- Cleveland, V., Bingham, J.-P., & Kan, E. (2014). Heterogeneous Fenton degradation of bisphenol A by carbon nanotube-supported Fe<sub>3</sub>O<sub>4</sub>. *Separation and Purification Technology*, 133(0), 388-395.

- Corma, A., Garcia, H., & Llabrés i Xamena, F. (2010). Engineering metal organic frameworks for heterogeneous catalysis. *Chemical Reviews*, 110(8), 4606-4655.
- Costa, J. S., Gamez, P., Black, C. A., Roubeau, O., Teat, S. J., & Reedijk, J. (2008). Chemical modification of a bridging ligand inside a metal–organic framework while maintaining the 3D structure. *European Journal of Inorganic Chemistry*, 2008(10), 1551-1554.
- Crook, E. H., McDonnell, R. P., & McNulty, J. T. (1975). Removal and Recovery of Phenols from Industrial Waste Effluents with Amberlite XAD Polymeric Adsorbents. *Product R&D*, 14(2), 113-118.
- Cukrowski, I., de Lange, J. H., & Mitoraj, M. (2014). Physical nature of interactions in Zn(II) complexes with 2,2'-bipyridyl: quantum theory of atoms in molecules (QTAIM), interacting quantum atoms (IQA), noncovalent interactions (NCI), and extended transition state coupled with natural orbitals for chemical valence (ETS-NOCV) comparative studies. *J Phys Chem A*, 118(3), 623-637.
- Czaja, A. U., Trukhan, N., & Muller, U. (2009). Industrial applications of metal-organic frameworks. *Chem Soc Rev*, 38(5), 1284-1293.
- da Mota, S., Mancio, A., Lhamas, D., de Abreu, D., da Silva, M., dos Santos, W., et al. (2014). Production of green diesel by thermal catalytic cracking of crude palm oil (*Elaeis guineensis* Jacq) in a pilot plant. *Journal of Analytical and Applied Pyrolysis*, 110, 1-11.
- Dai, L., You, W., Li, Y., Liu, L., Ge, X., & Che, W. (2014). A new Keggin-templated heterometal-oxide-based organic–inorganic hybrid compound. *Inorganica Chimica Acta*, 413, 208-213.
- Dantas, T. L. P., Mendonça, V. P., José, H. J., Rodrigues, A. E., & Moreira, R. F. P. M. (2006). Treatment of textile wastewater by heterogeneous Fenton process using a new composite Fe<sub>2</sub>O<sub>3</sub>/carbon. *Chemical Engineering Journal*, 118(1–2), 77-82.

- Das, S., Kim, H., & Kim, K. (2009). Metathesis in Single Crystal: Complete and Reversible Exchange of Metal Ions Constituting the Frameworks of Metal–Organic Frameworks. *Journal of the American Chemical Society*, *131*(11), 3814-3815.
- Demessence, A., D’Alessandro, D. M., Foo, M. L., & Long, J. R. (2009). Strong CO<sub>2</sub> binding in a water-stable, triazolate-bridged metal– organic framework functionalized with ethylenediamine. *Journal of the American Chemical Society*, *131*(25), 8784-8786.
- Deng, H., Grunder, S., Cordova, K. E., Valente, C., Furukawa, H., Hmadeh, M., et al. (2012). Large-pore apertures in a series of metal-organic frameworks. *science*, *336*(6084), 1018-1023.
- Deutschmann, O., Knözinger, H., Kochloefl, K., & Turek, T. (2009). *Heterogeneous catalysis and solid catalysts*.
- Dickerson, T., & Soria, J. (2013). Catalytic fast pyrolysis: a review. *Energies*, *6*(1), 514-538.
- Dinca, M., Dailly, A., Liu, Y., Brown, C. M., Neumann, D. A., & Long, J. R. (2006). Hydrogen storage in a microporous metal-organic framework with exposed Mn<sup>2+</sup> coordination sites. *Journal of the American Chemical Society*, *128*(51), 16876-16883.
- Dincă, M., & Long, J. R. (2008). Hydrogen storage in microporous metal–organic frameworks with exposed metal sites. *Angewandte Chemie International Edition*, *47*(36), 6766-6779.
- Dong, Y., Han, Z., Liu, C., & Du, F. (2010). Preparation and photocatalytic performance of Fe (III)-amidoximated PAN fiber complex for oxidative degradation of azo dye under visible light irradiation. *Science of The Total Environment*, *408*(10), 2245-2253.

- Dubey, A. K., & Yadava, V. (2008). Multi-objective optimization of Nd:YAG laser cutting of nickel-based superalloy sheet using orthogonal array with principal component analysis. *Optics and Lasers in Engineering*, 46(2), 124-132.
- Dukkancı, M., Gunduz, G., Yılmaz, S., & Prihodko, R. (2010a). Heterogeneous Fenton-like degradation of Rhodamine 6G in water using CuFeZSM-5 zeolite catalyst prepared by hydrothermal synthesis. *Journal of Hazardous Materials*, 181(1), 343-350.
- Dukkancı, M., Gunduz, G., Yılmaz, S., Yaman, Y. C., Prihod'ko, R. V., & Stolyarova, I. V. (2010b). Characterization and catalytic activity of CuFeZSM-5 catalysts for oxidative degradation of Rhodamine 6G in aqueous solutions. *Applied Catalysis B: Environmental*, 95(3-4), 270-278.
- Earle, M. J., Esperanca, J. M. S. S., Gilea, M. A., Canongia Lopes, J. N., Rebelo, L. P. N., Magee, J. W., et al. (2006). The distillation and volatility of ionic liquids. *Nature*, 439(7078), 831-834.
- Eddaoudi, M., Moler, D. B., Li, H., Chen, B., Reineke, T. M., O'Keeffe, M., et al. (2001). Modular Chemistry: Secondary Building Units as a Basis for the Design of Highly Porous and Robust Metal–Organic Carboxylate Frameworks. *Accounts of Chemical Research*, 34(4), 319-330.
- Ezugwu, C. I., Kabir, N. A., Yusubov, M., & Verpoort, F. (2016). Metal–organic frameworks containing N-heterocyclic carbenes and their precursors. *Coordination Chemistry Reviews*, 307, 188-210.
- Fajerwerg, K., Foussard, J., Perrard, A., & Debellefontaine, H. (1997). Wet oxidation of phenol by hydrogen peroxide: the key role of pH on the catalytic behaviour of Fe-ZSM-5. *Water Science and Technology*, 35(4), 103-110.
- Farha, O. K., & Hupp, J. T. (2010). Rational Design, Synthesis, Purification, and Activation of Metal–Organic Framework Materials. *Accounts of Chemical Research*, 43(8), 1166-1175.

- Farshi, A., & Abri, H. (2012). The Addition of ZSM-5 to a Fluid Catalytic Cracking Catalyst for Increasing Olefins in Fluid Catalytic Cracking Light Gas. *Petroleum Science and Technology*, 30(12), 1285-1295.
- Faryal, R., & Hameed, A. (2005). Isolation and characterization of various fungal strains from textile effluent for their use in bioremediation. *Pakistan Journal of Botany*, 37(4), 1003-1008.
- Fechete, I., Wang, Y., & Védrine, J. C. (2012a). The past, present and future of heterogeneous catalysis. *Catalysis Today*, 189(1), 2-27.
- Fechete, I., Wang, Y., & Védrine, J. C. (2012b). The past, present and future of heterogeneous catalysis. *Catalysis Today*, 189(1), 2-27.
- Feng, Y., Jiang, H., Chen, M., & Wang, Y. (2013). Construction of an interpenetrated MOF-5 with high mesoporosity for hydrogen storage at low pressure. *Powder Technology*, 249(0), 38-42.
- Ferrando, R., Jellinek, J., & Johnston, R. L. (2008). Nanoalloys: From Theory to Applications of Alloy Clusters and Nanoparticles. *Chemical Reviews*, 108(3), 845-910.
- French, R., & Czernik, S. (2010). Catalytic pyrolysis of biomass for biofuels production. *Fuel Processing Technology*, 91(1), 25-32.
- Furukawa, H., Cordova, K. E., O'Keeffe, M., & Yaghi, O. M. (2013). The chemistry and applications of metal-organic frameworks. *Science*, 341(6149), 1230444.
- Galadima, A., & Muraza, O. (2015). In situ fast pyrolysis of biomass with zeolite catalysts for bioaromatics/gasoline production: A review. *Energy Conversion and Management*, 105, 338-354.

- Gauri, S., & Chakraborty, S. (2009). Multi-response optimisation of WEDM process using principal component analysis. *The International Journal of Advanced Manufacturing Technology*, 41(7-8), 741-748.
- Geyer, F. L., Rominger, F., Vogtland, M., & Bunz, U. H. F. (2015). Interpenetrated Frameworks with Anisotropic Pore Structures from a Tetrahedral Pyridine Ligand. *Crystal Growth & Design*, 15(7), 3539-3544.
- Gomathi Devi, L., Girish Kumar, S., Mohan Reddy, K., & Munikrishnappa, C. (2009). Photo degradation of Methyl Orange an azo dye by Advanced Fenton Process using zero valent metallic iron: Influence of various reaction parameters and its degradation mechanism. *Journal of Hazardous Materials*, 164(2-3), 459-467.
- Gomez, J., & Tigli, O. (2013). Zinc oxide nanostructures: from growth to application. *Journal of Materials Science*, 48(2), 612-624.
- Gonzalez-Olmos, R., Holzer, F., Kopinke, F. D., & Georgi, A. (2011). Indications of the reactive species in a heterogeneous Fenton-like reaction using Fe-containing zeolites. *Applied Catalysis A: General*, 398(1-2), 44-53.
- Goto, Y., Sato, H., Shinkai, S., & Sada, K. (2008). "Clickable" Metal-Organic Framework. *Journal of the American Chemical Society*, 130(44), 14354-14355.
- Grcic, I., Muzic, M., Vujevic, D., & Koprivanac, N. (2009). Evaluation of atrazine degradation in UV/FeZSM-5/H<sub>2</sub>O<sub>2</sub> system using factorial experimental design. *Chemical Engineering Journal*, 150(2-3), 476-484.
- Gu, F., Hall, P., Miles, N. J., Ding, Q., & Wu, T. (2014). Improvement of mechanical properties of recycled plastic blends via optimizing processing parameters using the Taguchi method and principal component analysis. *Materials & Design*, 62(0), 189-198.
- Guisnet, M., Alvarez, F., Giannetto, G., & Perot, G. (1987). Hydroisomerization and hydrocracking of n-heptane on Pth zeolites. Effect of the porosity and of the distribution of metallic and acid sites. *Catalysis Today*, 1(4), 415-433.

- Guo, D., Sato, K., Hibino, S., Takeuchi, T., Bessho, H., & Kato, K. (2014). Low-temperature preparation of transparent conductive Al-doped ZnO thin films by a novel sol-gel method. *Journal of Materials Science*, 49(14), 4722-4734.
- Guo, W., Stamatakis, M., & Vlachos, D. G. (2013). Design Principles of Heteroepitaxial Bimetallic Catalysts. *ACS Catalysis*, 3(10), 2248-2255.
- Gupta, V., Gupta, B., Rastogi, A., Agarwal, S., & Nayak, A. (2011). A comparative investigation on adsorption performances of mesoporous activated carbon prepared from waste rubber tire and activated carbon for a hazardous azo dye-Acid Blue 113. *Journal of Hazardous Materials*, 186(1), 891-901.
- Gygi, D., Bloch, E. D., Mason, J. A., Hudson, M. R., Gonzalez, M. I., Siegelman, R. L., et al. (2016). Hydrogen Storage in the Expanded Pore Metal-Organic Frameworks M<sub>2</sub>(dobpdc)(M= Mg, Mn, Fe, Co, Ni, Zn). *Chemistry of Materials*.
- Hartmann, M., Kullmann, S., & Keller, H. (2010). Wastewater treatment with heterogeneous Fenton-type catalysts based on porous materials. *Journal of Materials Chemistry*, 20(41), 9002-9017.
- Hasan, Z., & Jhung, S. H. (2015). Removal of hazardous organics from water using metal-organic frameworks (MOFs): plausible mechanisms for selective adsorptions. *Journal of hazardous materials*, 283, 329-339.
- Ho, T. M., Howes, T., & Bhandari, B. R. (2014). Encapsulation of gases in powder solid matrices and their applications: A review. *Powder Technology*, 259(0), 87-108.
- Hong, R., Li, J., Chen, L., Liu, D., Li, H., Zheng, Y., et al. (2009). Synthesis, surface modification and photocatalytic property of ZnO nanoparticles. *Powder Technology*, 189(3), 426-432.
- Horike, S., Kamitsubo, Y., Inukai, M., Fukushima, T., Umeyama, D., Itakura, T., et al. (2013). Postsynthesis modification of a porous coordination polymer by LiCl to

enhance H<sup>+</sup> transport. *Journal of the American Chemical Society*, 135(12), 4612-4615.

Hosoya, T., Sakamoto, W., & Yogo, T. (2014). In situ synthesis of manganese zinc ferrite nanoparticle/polymer hybrid nanocomposite from metal organics. *Journal of Materials Science*, 49(14), 5093-5099.

Hwang, Y. K., Hong, D. Y., Chang, J. S., Jung, S. H., Seo, Y. K., Kim, J., et al. (2008). Amine grafting on coordinatively unsaturated metal centers of MOFs: consequences for catalysis and metal encapsulation. *Angewandte Chemie International Edition*, 47(22), 4144-4148.

Iliopoulou, E., Antonakou, E., Karakoulia, S., Vasalos, I., Lappas, A., & Triantafyllidis, K. (2007). Catalytic conversion of biomass pyrolysis products by mesoporous materials: Effect of steam stability and acidity of Al-MCM-41 catalysts. *Chemical Engineering Journal*, 134(1), 51-57.

Ingleson, M. J., Barrio, J. P., Bacsa, J., Dickinson, C., Park, H., & Rosseinsky, M. J. (2008). Generation of a solid Brønsted acid site in a chiral framework. *Chemical Communications*(11), 1287-1289.

Innocenti, I., Verginelli, I., Massetti, F., Piscitelli, D., Gavasci, R., & Baciocchi, R. (2014). Pilot-scale ISCO treatment of a MtBE contaminated site using a Fenton-like process. *Science of The Total Environment*, 485-486(0), 726-738.

Inoue, M., Okada, F., Sakurai, A., & Sakakibara, M. (2006). A new development of dyestuffs degradation system using ultrasound. *Ultrasonics Sonochemistry*, 13(4), 313-320.

Ishihara, A., Fukui, N., Nasu, H., & Hashimoto, T. (2014). Hydrocracking of soybean oil using zeolite-alumina composite supported NiMo catalysts. *Fuel*, 134, 611-617.

Jauhar, S., Singhal, S., & Dhiman, M. (2014). Manganese substituted cobalt ferrites as efficient catalysts for H<sub>2</sub>O<sub>2</sub> assisted degradation of cationic and anionic dyes:

Their synthesis and characterization. *Applied Catalysis A: General*, 486, 210-218.

Javad, M., Sara, M., & Saeed, K. (2012). The Influence of Morphology on Photocatalytic Activity and Optical Properties of Nano-crystalline ZnO Powder. *Nano-Micro Letters*, 4(4), 197-201.

Jiang, H. L., & Xu, Q. (2011). Porous metal-organic frameworks as platforms for functional applications. *Chem Commun (Camb)*, 47(12), 3351-3370.

Jiao, Q., Chunqiu, L., & Qiao, C. (2011). Synthesis of Multi-walled Carbon Nanotubes/ZnO Nanocomposites using Absorbent Cotton. *Nano-Micro Letters*, 3(2), 115-120.

Kadrmaz, C., Khambete, M., Kubátová, A., Kozliak, E., & Seames, W. (2015). Optimizing the Production of Renewable Aromatics via Crop Oil Catalytic Cracking. *Processes*, 3(2), 222-234.

Kaes, C., Katz, A., & Hosseini, M. W. (2000). Bipyridine: the most widely used ligand. A review of molecules comprising at least two 2, 2'-bipyridine units. *Chemical reviews*, 100(10), 3553-3590.

Karmakar, A., Desai, A. V., & Ghosh, S. K. (2016). Ionic metal-organic frameworks (iMOFs): Design principles and applications. *Coordination Chemistry Reviews*, 307, 313-341.

Karthikeyan, S., Priya, M. E., Boopathy, R., Velan, M., Mandal, A., & Sekaran, G. (2012). Heterocatalytic Fenton oxidation process for the treatment of tannery effluent: kinetic and thermodynamic studies. *Environmental Science and Pollution Research*, 19(5), 1828-1840.

Karthikeyan, S., Titus, A., Gnanamani, A., Mandal, A. B., & Sekaran, G. (2011). Treatment of textile wastewater by homogeneous and heterogeneous Fenton oxidation processes. *Desalination*, 281(0), 438-445.

- Kaur, J., Bansal, S., & Singhal, S. (2013). Photocatalytic degradation of methyl orange using ZnO nanopowders synthesized via thermal decomposition of oxalate precursor method. *Physica B: Condensed Matter*, 416(0), 33-38.
- Kim, S. W., Koo, B. S., Ryu, J. W., Lee, J. S., Kim, C. J., Lee, D. H., et al. (2013a). Bio-oil from the pyrolysis of palm and Jatropha wastes in a fluidized bed. *Fuel Processing Technology*, 108, 118-124.
- Kim, T. K., Lee, K. J., Cheon, J. Y., Lee, J. H., Joo, S. H., & Moon, H. R. (2013b). Nanoporous metal oxides with tunable and nanocrystalline frameworks via conversion of metal-organic frameworks. *Journal of the American Chemical Society*, 135(24), 8940-8946.
- Kim, W.-g., & Nair, S. (2013). Membranes from nanoporous 1D and 2D materials: A review of opportunities, developments, and challenges. *Chemical Engineering Science*, 104(0), 908-924.
- Kiss, E., Vulic, T., Reitzmann, A., & Lazar, K. (2006). Photo-Fenton catalysis for wet peroxide oxidation of phenol on Fe-ZSM-5 catalyst. *Revue Roumaine de Chimie*, 51(9), 931.
- Kitagawa, S., Noro, S.-i., & Nakamura, T. (2006). Pore surface engineering of microporous coordination polymers. *Chemical Communications*(7), 701-707.
- Knozinger, H., & Weitkamp, J. (1997). *Handbook of heterogeneous catalysis* (Vol. 1): Wiley-VCH.
- Kong, A., Lin, Q., Mao, C., Bu, X., & Feng, P. (2014). Efficient oxygen reduction by nanocomposites of heterometallic carbide and nitrogen-enriched carbon derived from the cobalt-encapsulated indium-MOF. *Chemical Communications*, 50(98), 15619-15622.
- Korbahti, B. K., & Tanyolac, A. (2008). Electrochemical treatment of simulated textile wastewater with industrial components and Levafix Blue CA reactive dye: Optimization through response surface methodology. *Journal of Hazardous Materials*, 151(2), 422-431.

- Körbahti, B. K., & Tanyolaç, A. (2008). Electrochemical treatment of simulated textile wastewater with industrial components and Levafix Blue CA reactive dye: Optimization through response surface methodology. *Journal of Hazardous Materials*, 151(2–3), 422-431.
- Kumar, R. T., Selvam, N. C. S., Ragupathi, C., Kennedy, L. J., & Vijaya, J. J. (2012). Synthesis, characterization and performance of porous Sr(II)-added ZnAl<sub>2</sub>O<sub>4</sub> nanomaterials for optical and catalytic applications. *Powder Technology*, 224(0), 147-154.
- Kusgens, P., Rose, M., Senkovska, I., Frode, H., Henschel, A., Siegle, S., et al. (2009). Characterization of metal-organic frameworks by water adsorption. *Microporous and Mesoporous Materials*, 120(3), 325-330.
- Kusic, H., Koprivanac, N., & Selanec, I. (2006). Fe-exchanged zeolite as the effective heterogeneous Fenton-type catalyst for the organic pollutant minimization: UV irradiation assistance. *Chemosphere*, 65(1), 65-73.
- Laik, B., Durandetti, M., & Perichon, J. (2007). Formation and electrochemical behavior characterizations of dibromo 2,2'-bipyridine manganese(II) systems in DMF solution. *Journal of Electroanalytical Chemistry*, 602(2), 275-279.
- Laik, B., Durandetti, M., & Périchon, J. (2007). Formation and electrochemical behavior characterizations of dibromo 2, 2'-bipyridine manganese (II) systems in DMF solution. *Journal of Electroanalytical Chemistry*, 602(2), 275-279.
- Li, B., Zhang, Y., Ma, D., Li, L., Li, G., Li, G., et al. (2012). A strategy toward constructing a bifunctionalized MOF catalyst: post-synthetic modification of MOFs on organic ligands and coordinatively unsaturated metal sites. *Chemical Communications*, 48(49), 6151-6153.
- Li, C.-P., & Du, M. (2011). Role of solvents in coordination supramolecular systems. *Chemical Communications*, 47(21), 5958-5972.

- Li, D.-S., Wu, Y.-P., Zhao, J., Zhang, J., & Lu, J. Y. (2014). Metal-organic frameworks based upon non-zeotype 4-connected topology. *Coordination Chemistry Reviews*, 261, 1-27.
- Li, S.-L., & Xu, Q. (2013a). Metal-organic frameworks as platforms for clean energy. *Energy & Environmental Science*, 6(6), 1656.
- Li, S. L., & Xu, Q. (2013b). Metal-organic frameworks as platforms for clean energy. *Energy & Environmental Science*, 6(6), 1656.
- Li, Y., & Zhang, A. (2014). Removal of steroid estrogens from waste activated sludge using Fenton oxidation: Influencing factors and degradation intermediates. *Chemosphere*, 105(0), 24-30.
- Liao, H.-C. (2004). A data envelopment analysis method for optimizing multi-response problem with censored data in the Taguchi method. *Computers & Industrial Engineering*, 46(4), 817-835.
- Lin, C.-Y., & Cheng, H.-H. (2012). Application of mesoporous catalysts over palm-oil biodiesel for adjusting fuel properties. *Energy Conversion and Management*, 53(1), 128-134.
- Liotta, L., Gruttadauria, M., Di Carlo, G., Perrini, G., & Librando, V. (2009). Heterogeneous catalytic degradation of phenolic substrates: catalysts activity. *Journal of Hazardous Materials*, 162(2), 588-606.
- Liu, H., Zhang, S., Liu, Y., Yang, Z., Feng, X., Lu, X., et al. (2015). Well-Dispersed and Size-Controlled Supported Metal Oxide Nanoparticles Derived from MOF Composites and Further Application in Catalysis. *Small*, 11(26), 3130-3134.
- Liu, W.-J., Qian, T.-T., & Jiang, H. (2014a). Bimetallic Fe nanoparticles: Recent advances in synthesis and application in catalytic elimination of environmental pollutants. *Chemical Engineering Journal*, 236, 448-463.

- Liu, W. J., Qian, T. T., & Jiang, H. (2014b). Bimetallic Fe nanoparticles: Recent advances in synthesis and application in catalytic elimination of environmental pollutants. *Chemical Engineering Journal*, 236, 448-463.
- Lucas, M. S., & Peres, J. A. (2006). Decolorization of the azo dye Reactive Black 5 by Fenton and photo-Fenton oxidation. *Dyes and Pigments*, 71(3), 236-244.
- Lucking, F., Koser, H., Jank, M., & Ritter, A. (1998). Iron powder, graphite and activated carbon as catalysts for the oxidation of 4-chlorophenol with hydrogen peroxide in aqueous solution. *Water Research*, 32(9), 2607-2614.
- Luo, M., Lv, L., Deng, G., Yao, W., Ruan, Y., Li, X., et al. (2014). The mechanism of bound hydroxyl radical formation and degradation pathway of Acid Orange II in Fenton-like  $\text{Co}^{2+}$ - $\text{HCO}_3^-$  system. *Applied Catalysis A: General*, 469, 198-205.
- Madrahimov, S. T., Atesin, T. A., Karagiari, O., Sarjeant, A. A., Farha, O. K., Hupp, J. T., et al. (2014). Metal–Organic Frameworks Containing (Alkynyl) Gold Functionalities: A Comparative Evaluation of Solvent-Assisted Linker Exchange, de Novo Synthesis, and Post-synthesis Modification. *Crystal Growth & Design*, 14(12), 6320-6324.
- Mahata, P., Madras, G., & Natarajan, S. (2006). Novel Photocatalysts for the Decomposition of Organic Dyes Based on Metal-Organic Framework Compounds. *The Journal of Physical Chemistry B*, 110(28), 13759-13768.
- Mansoor, M. A., Huang, N. M., McKee, V., Peiris, T. A. N., Wijayantha, K. G. U., Arifin, Z., et al. (2015). Single phased  $\text{MnZnO}_3$  solid solution thin films for solar energy harvesting applications. *Solar Energy Materials and Solar Cells*, 137, 258-264.
- Matta, R., Hanna, K., & Chiron, S. (2007). Fenton-like oxidation of 2,4,6-trinitrotoluene using different iron minerals. *Science of The Total Environment*, 385(1–3), 242-251.
- Maza, W. A., Ahrenholtz, S. R., Epley, C. C., Day, C. S., & Morris, A. J. (2014). Solvothermal Growth and Photophysical Characterization of a Ruthenium (II)

Tris (2, 2'-Bipyridine)-Doped Zirconium UiO-67 Metal Organic Framework Thin Film. *The Journal of Physical Chemistry C*, 118(26), 14200-14210.

Meric, S., Kaptan, D., & Tunay, O. (2003). Removal of Color and COD from a Mixture of Four Reactive Azo Dyes Using Fenton Oxidation Process. *Journal of Environmental Science and Health, Part A*, 38(10), 2241-2250.

Moezzi, A., McDonagh, A. M., & Cortie, M. B. (2012). Zinc oxide particles: Synthesis, properties and applications. *Chemical Engineering Journal*, 185-186, 1-22.

Montes, V., Boutonnet, M., Järås, S., Lualdi, M., Marinas, A., Marinas, J. M., et al. (2014). Preparation and characterization of Pt-modified Co-based catalysts through the microemulsion technique: Preliminary results on the Fischer–Tropsch synthesis. *Catalysis Today*, 223(0), 66-75.

Morozan, A., & Jaouen, F. (2012). Metal organic frameworks for electrochemical applications. *Energy & Environmental Science*, 5(11), 9269.

Navalon, S., Alvaro, M., & Garcia, H. (2010). Heterogeneous Fenton catalysts based on clays, silicas and zeolites. *Applied Catalysis B: Environmental*, 99(1–2), 1-26.

Navarro, J. A., Barea, E., Salas, J. M., Masciocchi, N., Galli, S., Sironi, A., et al. (2006). H<sub>2</sub>, N<sub>2</sub>, CO, and CO<sub>2</sub> sorption properties of a series of robust sodalite-type microporous coordination polymers. *Inorganic chemistry*, 45(6), 2397-2399.

Nayak, S. S., Wollgarten, M., Banhart, J., Pabi, S. K., & Murty, B. S. (2010). Nanocomposites and an extremely hard nanocrystalline intermetallic of Al-Fe alloys prepared by mechanical alloying. *Materials Science and Engineering A*, 527(9), 2370-2378.

Nazir, R., Ahmed, S., Mazhar, M., Akhtar, M. J., Siddique, M., Khan, N. A., et al. (2013). A chemical approach toward low temperature alloying of immiscible iron and molybdenum metals. *Materials Research Bulletin*, 48(11), 4661-4666.

- Nazir, R., Mazhar, M., Wakeel, T., Akhtar, M., Siddique, M., Nadeem, M., et al. (2012). Pyrolysis mechanism of trisbipyridineiron(II) chloride to iron nanoparticles. *Journal of Thermal Analysis and Calorimetry*, 110(2), 707-713.
- Nazir, R., Mazhar, M., Wakeel, T., Akhtar, M. J., Siddique, M., Nadeem, M., et al. (2011). Pyrolysis mechanism of trisbipyridineiron(II) chloride to iron nanoparticles. *Journal of Thermal Analysis and Calorimetry*, 110(2), 707-713.
- Neyens, E., & Baeyens, J. (2003). A review of classic Fenton's peroxidation as an advanced oxidation technique. *Journal of Hazardous Materials*, 98(1-3), 33-50.
- Ngo, T.-A., Kim, J., Kim, S. K., & Kim, S.-S. (2010). Pyrolysis of soybean oil with H-ZSM5 (Proton-exchange of Zeolite Socony Mobil #5) and MCM41 (Mobil Composition of Matter No. 41) catalysts in a fixed-bed reactor. *Energy*, 35(6), 2723-2728.
- Ni, Y., Sun, A., Wu, X., Hai, G., Hu, J., Li, T., et al. (2011). The preparation of nano-sized H[Zn, Al]ZSM-5 zeolite and its application in the aromatization of methanol. *Microporous and Mesoporous Materials*, 143(2-3), 435-442.
- Nidheesh, P. V. (2015). Heterogeneous Fenton catalysts for the abatement of organic pollutants from aqueous solution: a review. *RSC Advances*, 5(51), 40552-40577.
- NIST. Bipyridine Infrared Spectrum *Standard Reference Database 69*.
- Noro, S.-i., Kitagawa, S., Yamashita, M., & Wada, T. (2002). New microporous coordination polymer affording guest-coordination sites at channel walls. *Chemical Communications*(3), 222-223.
- Oliveira, L. C. A., Gonçalves, M., Guerreiro, M. C., Ramalho, T. C., Fabris, J. D., Pereira, M. C., et al. (2007). A new catalyst material based on niobia/iron oxide composite on the oxidation of organic contaminants in water via heterogeneous Fenton mechanisms. *Applied Catalysis A: General*, 316(1), 117-124.

- Ong, Y. K., & Bhatia, S. (2010). The current status and perspectives of biofuel production via catalytic cracking of edible and non-edible oils. *Energy*, 35(1), 111-119.
- Parveen, N., Nazir, R., & Mazhar, M. (2012). Thermal degradation pathways of nickel(II) bipyridine complexes to size-controlled nickel nanoparticles. *Journal of Thermal Analysis and Calorimetry*, 111(1), 93-99.
- Parveen, N., Nazir, R., & Mazhar, M. (2013). Thermal degradation pathways of nickel (II) bipyridine complexes to size-controlled nickel nanoparticles. *Journal of thermal analysis and calorimetry*, 111(1), 93-99.
- Patete, J. M., Peng, X., Koenigsmann, C., Xu, Y., Karn, B., & Wong, S. S. (2011a). Viable methodologies for the synthesis of high-quality nanostructures. *Green Chemistry*, 13(3), 482.
- Patete, J. M., Peng, X., Koenigsmann, C., Xu, Y., Karn, B., & Wong, S. S. (2011b). Viable methodologies for the synthesis of high quality nanostructures. *Green Chemistry*, 13(3), 482.
- Pirkanniemi, K., & Sillanpaa, M. (2002). Heterogeneous water phase catalysis as an environmental application: a review. *Chemosphere*, 48(10), 1047-1060.
- Prajapati, R., Mishra, L., Kimura, K., & Raghavaiah, P. (2009). Metal-organic frameworks (MOFs) constructed from ZnII/CdII-2,2'-bipyridines and polycarboxylic acids: Synthesis, characterization and microstructural studies. *Polyhedron*, 28(3), 600-608.
- Prihod'ko, R., Stolyarova, I., Gündüz, G., Taran, O., Yashnik, S., Parmon, V., et al. (2011). Fe-exchanged zeolites as materials for catalytic wet peroxide oxidation. Degradation of Rodamine G dye. *Applied Catalysis B: Environmental*, 104(1), 201-210.
- Qian, L., & Yang, X. (2008). Dendrimer films as matrices for electrochemical fabrication of novel gold/palladium bimetallic nanostructures. *Talanta*, 74(5), 1649-1653.

- Qin, X., Zhang, J., Zhang, X., & Yang, Y. (2014). Induction, purification and characterization of a novel manganese peroxidase from *Irpex lacteus* CD2 and its application in the decolorization of different types of dye. *PLoS One*, 9(11), e113282.
- Qiu, Z., He, Y., Liu, X., & Yu, S. (2005a). Catalytic oxidation of the dye wastewater with hydrogen peroxide. *Chemical Engineering and Processing*, 44(9), 1013-1017.
- Qiu, Z., He, Y., Liu, X., & Yu, S. (2005b). Catalytic oxidation of the dye wastewater with hydrogen peroxide. *Chemical Engineering and Processing: Process Intensification*, 44(9), 1013-1017.
- Queiros, S., Morais, V., Rodrigues, C. S. D., Maldonado-Hodar, F. J., & Madeira, L. M. (2015). Heterogeneous Fenton's oxidation using Fe/ZSM-5 as catalyst in a continuous stirred tank reactor. *Separation and Purification Technology*, 141(0), 235-245.
- Rahim Pouran, S., Abdul Aziz, A. R., Wan Daud, W. M. A., & Shafeeyan, M. S. (2015). Effects of niobium and molybdenum impregnation on adsorption capacity and Fenton catalytic activity of magnetite. *RSC Advances*, 5(106), 87535-87549.
- Ramya, G., Sudhakar, R., Joice, J. A. I., Ramakrishnan, R., & Sivakumar, T. (2012). Liquid hydrocarbon fuels from jatropha oil through catalytic cracking technology using AlMCM-41/ZSM-5 composite catalysts. *Applied Catalysis A: General*, 433-434, 170-178.
- Ren, P., Liu, M.-L., Zhang, J., Shi, W., Cheng, P., Liao, D.-Z., et al. (2008). 1D, 2D and 3D luminescent zinc (II) coordination polymers assembled from varying flexible thioether ligands. *Dalton Transactions*(35), 4711-4713.
- Roberts, D. A., Nys, R., & Paul, N. A. (2013). The effect of CO<sub>2</sub> on algal growth in industrial waste water for bioenergy and bioremediation applications. *PloS one*, 8(11), e81631.

- Rowsell, J. L. C., & Yaghi, O. M. (2004). Metal–organic frameworks: a new class of porous materials. *Microporous and Mesoporous Materials*, 73(1–2), 3-14.
- Salavati-Niasari, M., Davar, F., & Khansari, A. (2011). Nanosphericals and nanobundles of ZnO: Synthesis and characterization. *Journal of Alloys and Compounds*, 509(1), 61-65.
- Samaele, N., Amornpitoksuk, P., & Suwanboon, S. (2010). Effect of pH on the morphology and optical properties of modified ZnO particles by SDS via a precipitation method. *Powder Technology*, 203(2), 243-247.
- Sang, S., Chang, F., Liu, Z., He, C., He, Y., & Xu, L. (2004). Difference of ZSM-5 zeolites synthesized with various templates. *Catalysis today*, 93, 729-734.
- Sani, Y. M., Alaba, P. A., Raji-Yahya, A. O., Aziz, A. A., & Daud, W. M. A. W. (2015). Facile synthesis of sulfated mesoporous Zr/ZSM-5 with improved Brønsted acidity and superior activity over SZr/Ag, SZr/Ti, and SZr/W in transforming UFO into biodiesel. *Journal of the Taiwan Institute of Chemical Engineers*.
- Sankar, M., Dimitratos, N., Miedziak, P. J., Wells, P. P., Kiely, C. J., & Hutchings, G. J. (2012). Designing bimetallic catalysts for a green and sustainable future. *Chem Soc Rev*, 41(24), 8099-8139.
- Savin, I. I., & Butnaru, R. (2008). Wastewater characteristics in textile finishing mills. *Environmental Engineering and Management Journal*, 7(6), 859-864.
- Senkovska, I., & Kaskel, S. (2006). Solvent-Induced Pore-Size Adjustment in the Metal-Organic Framework [Mg<sub>3</sub>(ndc)<sub>3</sub>(dmf)<sub>4</sub>](ndc= naphthalenedicarboxylate). *European journal of inorganic chemistry*, 2006(22), 4564-4569.
- Shahbazi, A., Gonzalez Olmos, R., Kopinke, F. D., Zarabadi Poor, P., & Georgi, A. (2014). Natural and synthetic zeolites in adsorption/oxidation processes to remove surfactant molecules from water. *Separation and Purification Technology*, 127(0), 1-9.

- Shahrezaei, F., Mansouri, Y., Zinatizadeh, A. A. L., & Akhbari, A. (2012). Process modeling and kinetic evaluation of petroleum refinery wastewater treatment in a photocatalytic reactor using TiO<sub>2</sub> nanoparticles. *Powder Technology*, 221(0), 203-212.
- Shen, Y., Zhang, Z., & Xiao, K. (2015). Evaluation of cobalt oxide, copper oxide and their solid solutions as heterogeneous catalysts for Fenton-degradation of dye pollutants. *RSC Advances*, 5(111), 91846-91854.
- Shirzad-Siboni, M., Jafari, S. J., Giahi, O., Kim, I., Lee, S.-M., & Yang, J.-K. (2014). Removal of acid blue 113 and reactive black 5 dye from aqueous solutions by activated red mud. *Journal of Industrial and Engineering Chemistry*, 20(4), 1432-1437.
- Shu, H. Y., Chang, M. C., Chen, C. C., & Chen, P. E. (2010). Using resin supported nano zero-valent iron particles for decoloration of Acid Blue 113 azo dye solution. *Journal of Hazardous Materials*, 184(1), 499-505.
- Singh, P., Raizada, P., Kumari, S., Kumar, A., Pathania, D., & Thakur, P. (2014). Solar-Fenton removal of malachite green with novel Fe<sup>0</sup>-activated carbon nanocomposite. *Applied Catalysis A: General*, 476(0), 9-18.
- Soon, A. N., & Hameed, B. H. (2013). Degradation of Acid Blue 29 in visible light radiation using iron modified mesoporous silica as heterogeneous Photo-Fenton catalyst. *Applied Catalysis A: General*, 450(0), 96-105.
- Sreekanth, P. M., Pena, D. A., & Smirniotis, P. G. (2006). Titania Supported Bimetallic Transition Metal Oxides for Low-Temperature SCR of NO with NH<sub>3</sub>. *Industrial & Engineering Chemistry Research*, 45(19), 6444-6449.
- Sugikawa, K., Nagata, S., Furukawa, Y., Kokado, K., & Sada, K. (2013). Stable and functional gold nanorod composites with a metal-organic framework crystalline shell. *Chemistry of Materials*, 25(13), 2565-2570.

- Sultan, M., Tahir, A. A., Mazhar, M., Zeller, M., & Wijayantha, K. U. (2012). Hexanuclear copper–nickel and copper–cobalt complexes for thin film deposition of ceramic oxide composites. *New Journal of Chemistry*, 36(4), 911-917.
- Sun, F., Yin, Z., Wang, Q. Q., Sun, D., Zeng, M. H., & Kurmoo, M. (2013). Tandem postsynthetic modification of a metal–organic framework by thermal elimination and subsequent bromination: effects on absorption properties and photoluminescence. *Angewandte Chemie International Edition*, 52(17), 4538-4543.
- Sun, J.-H., Sun, S.-P., Wang, G.-L., & Qiao, L.-P. (2007). Degradation of azo dye Amido black 10B in aqueous solution by Fenton oxidation process. *Dyes and Pigments*, 74(3), 647-652.
- Suyanta, S., & Izul, F. I. (2012). Cracking of Palm Oil over H-AIMCM-41 Catalyst. *Journal of Chemistry and Chemical Engineering*, 6(6), 531-535.
- Szeto, K. C., Lillerud, K. P., Tilset, M., Bjørgen, M., Prestipino, C., Zecchina, A., et al. (2006). A thermally stable Pt/Y-based metal-organic framework: Exploring the accessibility of the metal Centers with spectroscopic methods using H<sub>2</sub>O, CH<sub>3</sub>OH, and CH<sub>3</sub>CN as probes. *The Journal of Physical Chemistry B*, 110(43), 21509-21520.
- Szeto, K. C., Prestipino, C., Lamberti, C., Zecchina, A., Bordiga, S., Bjørgen, M., et al. (2007). Characterization of a new porous Pt-containing metal-organic framework containing potentially catalytically active sites: Local electronic structure at the metal centers. *Chemistry of materials*, 19(2), 211-220.
- Szostak, R., Nair, V., & Thomas, T. L. (1987). Incorporation and stability of iron in molecular-sieve structures. Ferrisilicate analogues of zeolite ZSM-5. *Journal of the Chemical Society, Faraday Transactions 1: Physical Chemistry in Condensed Phases*, 83(2), 487-494.
- Tabares, L. C., Navarro, J. A., & Salas, J. M. (2001). Cooperative guest inclusion by a zeolite analogue coordination polymer. Sorption behavior with gases and amine and group 1 metal salts. *Journal of the American Chemical Society*, 123(3), 383-387.

- Tang, J., Salunkhe, R. R., Liu, J., Torad, N. L., Imura, M., Furukawa, S., et al. (2015). Thermal Conversion of Core–Shell Metal–Organic Frameworks: A New Method for Selectively Functionalized Nanoporous Hybrid Carbon. *Journal of the American Chemical Society*, 137(4), 1572-1580.
- Tantak, N. P., & Chaudhari, S. (2006). Degradation of azo dyes by sequential Fenton's oxidation and aerobic biological treatment. *Journal of Hazardous Materials*, 136(3), 698-705.
- Taufiqurrahmi, N., & Bhatia, S. (2011). Catalytic cracking of edible and non-edible oils for the production of biofuels. *Energy & Environmental Science*, 4(4), 1087-1112.
- Tekbaş, M., Yatmaz, H. C., & Bektaş, N. (2008). Heterogeneous photo-Fenton oxidation of reactive azo dye solutions using iron exchanged zeolite as a catalyst. *Microporous and Mesoporous Materials*, 115(3), 594-602.
- Tekin, H., Bilkay, O., Ataberk, S. S., Balta, T. H., Ceribasi, I. H., Sanin, F. D., et al. (2006). Use of Fenton oxidation to improve the biodegradability of a pharmaceutical wastewater. *Journal of Hazardous Materials*, 136(2), 258-265.
- Thomas, J. M., Raja, R., Johnson, B. F. G., Hermans, S., Jones, M. D., & Khimyak, T. (2003). Bimetallic Catalysts and Their Relevance to the Hydrogen Economy. *Industrial & Engineering Chemistry Research*, 42(8), 1563-1570.
- Thomas, J. M., & Thomas, W. J. (2014). *Principles and practice of heterogeneous catalysis*: John Wiley & Sons.
- Tian, Y. Q., Zhao, Y. M., Chen, Z. X., Zhang, G. N., Weng, L. H., & Zhao, D. Y. (2007). Design and generation of extended zeolitic metal–organic frameworks (ZMOFs): synthesis and crystal structures of zinc (II) imidazolate polymers with zeolitic topologies. *Chemistry–A European Journal*, 13(15), 4146-4154.

- Turhan, K., Durukan, I., Ozturkcan, S. A., & Turgut, Z. (2012). Decolorization of textile basic dye in aqueous solution by ozone. *Dyes and Pigments*, 92(3), 897-901.
- Twaiq, F. A., Mohamad, A., & Bhatia, S. (2004a). Performance of composite catalysts in palm oil cracking for the production of liquid fuels and chemicals. *Fuel Processing Technology*, 85(11), 1283-1300.
- Twaiq, F. A., Mohamed, A. R., & Bhatia, S. (2003a). Liquid hydrocarbon fuels from palm oil by catalytic cracking over aluminosilicate mesoporous catalysts with various Si/Al ratios. *Microporous and Mesoporous Materials*, 64(1-3), 95-107.
- Twaiq, F. A., Zabidi, N. A. M., Mohamed, A. R., & Bhatia, S. (2003b). Catalytic conversion of palm oil over mesoporous aluminosilicate MCM-41 for the production of liquid hydrocarbon fuels. *Fuel Processing Technology*, 84(1-3), 105-120.
- Twaiq, F. A. A., Mohamad, A. R., & Bhatia, S. (2004b). Performance of composite catalysts in palm oil cracking for the production of liquid fuels and chemicals. *Fuel Processing Technology*, 85(11), 1283-1300.
- Uemura, T., Kitagawa, K., Horike, S., Kawamura, T., Kitagawa, S., Mizuno, M., et al. (2005). Radical polymerisation of styrene in porous coordination polymers. *Chem. Commun.*(48), 5968-5970.
- Uemura, T., Kitaura, R., Ohta, Y., Nagaoka, M., & Kitagawa, S. (2006). Nanochannel-Promoted Polymerization of Substituted Acetylenes in Porous Coordination Polymers. *Angewandte Chemie*, 118(25), 4218-4222.
- Ulson, S. M. d. A. G., Bonilla, K. A. S., & de Souza, A. A. U. (2010). Removal of COD and color from hydrolyzed textile azo dye by combined ozonation and biological treatment. *Journal of Hazardous Materials*, 179(1), 35-42.
- Unnu, B. A., Gundüz, G., & Dukkancı, M. (2015). Heterogeneous Fenton-like oxidation of crystal violet using an iron loaded ZSM-5 zeolite. *Desalination and Water Treatment*(ahead-of-print), 1-15.

- Uslu, M. O., & Balcioglu, I. A. (2009). Comparison of the ozonation and Fenton process performances for the treatment of antibiotic containing manure. *Science of The Total Environment*, 407(11), 3450-3458.
- Venderbosch, R. H., & Prins, W. (2010). Fast pyrolysis technology development. *Biofuels, Bioproducts and Biorefining*, 4(2), 178-208.
- Vinod, C. P., Wilson, K., & Lee, A. F. (2011). Recent advances in the heterogeneously catalysed aerobic selective oxidation of alcohols. *Journal of Chemical Technology and Biotechnology*, 86(2), 161-171.
- Vinodgopal, K., & Peller, J. (2003). Hydroxyl radical-mediated advanced oxidation processes for textile dyes: a comparison of the radiolytic and sonolytic degradation of the monoazo dye Acid Orange 7. *Research on Chemical Intermediates*, 29(3), 307-316.
- Vitillo, J. G., Regli, L., Chavan, S., Ricchiardi, G., Spoto, G., Dietzel, P. D., et al. (2008). Role of exposed metal sites in hydrogen storage in MOFs. *Journal of the American Chemical Society*, 130(26), 8386-8396.
- Vu, H. X., Schneider, M., Bentrup, U., Dang, T. T., Phan, B. M., Nguyen, D. A., et al. (2015a). Hierarchical ZSM-5 materials for an enhanced formation of gasoline-range hydrocarbons and light olefins in catalytic cracking of triglyceride-rich biomass. *Industrial & Engineering Chemistry Research*, 54(6), 1773-1782.
- Vu, X. H., Nguyen, S., Dang, T. T., Phan, B. M. Q., Nguyen, D. A., Armbruster, U., et al. (2015b). Catalytic Cracking of Triglyceride-Rich Biomass toward Lower Olefins over a Nano-ZSM-5/SBA-15 Analog Composite. *Catalysts*, 5(4), 1692-1703.
- Wang, B., Sun, W., Zhu, J., Ran, W., & Chen, S. (2012a). Pd-Pb/SDB Bimetallic Catalysts for The Direct Oxidative Esterification of Methacrolein to Methyl Methacrylate. *Ind. Eng. Chem. Res.*, 51(46), 15004-15010.

Wang, H.-Y., Jiao, T.-T., Li, Z.-X., Li, C.-S., Zhang, S.-J., & Zhang, J.-L. (2015a). Study on palm oil hydrogenation for clean fuel over Ni–Mo–W/ $\gamma$ -Al<sub>2</sub>O<sub>3</sub>–ZSM-5 catalyst. *Fuel Processing Technology*, 139, 91-99.

Wang, N., Feng, Y.-C., Shi, W., Zhao, B., Cheng, P., Liao, D.-Z., et al. (2012b). Synthesis, structure, fluorescent and magnetic properties of a series of coordination polymers based on a long and flexible bis-triazole ligand. *CrystEngComm*, 14(8), 2769-2778.

Wang, S., Cai, Q., Chen, J., Zhang, L., Zhu, L., & Luo, Z. (2015b). Co-cracking of bio-oil model compound mixtures and ethanol over different metal oxide-modified HZSM-5 catalysts. *Fuel*, 160, 534-543.

Wang, X., Zhong, W., & Li, Y. (2015c). Nanoscale Co-based catalysts for low-temperature CO oxidation. *Catalysis Science & Technology*, 5(2), 1014-1020.

Wang, Z., & Cohen, S. M. (2007). Postsynthetic covalent modification of a neutral metal-organic framework. *Journal of the American Chemical Society*, 129(41), 12368-12369.

Wijngaarden, R. I., Westerterp, K. R., Kronberg, A., & Bos, A. (2008). *Industrial catalysis: optimizing catalysts and processes*: John Wiley & Sons.

Wu, C.-D., Hu, A., Zhang, L., & Lin, W. (2005a). A homochiral porous metal-organic framework for highly enantioselective heterogeneous asymmetric catalysis. *Journal of the American Chemical Society*, 127(25), 8940-8941.

Wu, C.-D., Hu, A., Zhang, L., & Lin, W. (2005b). A Homochiral Porous Metal–Organic Framework for Highly Enantioselective Heterogeneous Asymmetric Catalysis. *Journal of the American Chemical Society*, 127(25), 8940-8941.

Xamena, F. X. L., Abad, A., Corma, A., & Garcia, H. (2007). MOFs as catalysts: activity, reusability and shape-selectivity of a Pd-containing MOF. *Journal of Catalysis*, 250(2), 294-298.

- Xie, J., Li, Y., Zhao, W., Bian, L., & Wei, Y. (2011). Simple fabrication and photocatalytic activity of ZnO particles with different morphologies. *Powder Technology*, 207(1), 140-144.
- Xu, P., Zeng, G. M., Huang, D. L., Feng, C. L., Hu, S., Zhao, M. H., et al. (2012a). Use of iron oxide nanomaterials in wastewater treatment: A review. *Science of The Total Environment*, 424(0), 1-10.
- Xu, X., Cao, R., Jeong, S., & Cho, J. (2012b). Spindle-like mesoporous  $\alpha$ -Fe<sub>2</sub>O<sub>3</sub> anode material prepared from MOF template for high-rate lithium batteries. *Nano letters*, 12(9), 4988-4991.
- Yaman, C., & Gunduz, G. (2015). A parametric study on the decolorization and mineralization of CI Reactive Red 141 in water by heterogeneous Fenton-like oxidation over FeZSM-5 zeolite. *Journal of Environmental Health Science and Engineering*, 13(1), 1-12.
- Yan, Y., Jiang, S., & Zhang, H. (2014). Efficient catalytic wet peroxide oxidation of phenol over Fe-ZSM-5 catalyst in a fixed bed reactor. *Separation and Purification Technology*, 133, 365-374.
- Yan, Y., Jiang, S., & Zhang, H. (2016). Catalytic wet oxidation of phenol with Fe-ZSM-5 catalysts. *RSC Advances*, 6(5), 3850-3859.
- Yang, S. J., Im, J. H., Kim, T., Lee, K., & Park, C. R. (2011). MOF-derived ZnO and ZnO@ C composites with high photocatalytic activity and adsorption capacity. *Journal of Hazardous Materials*, 186(1), 376-382.
- Yang, W., & Xiaohong, P. (2014). RuRh Bimetallic Nanoparticles Stabilized by 15-membered Macrocycles-terminated Poly(propylene imine) Dendrimer: Preparation and Catalytic Hydrogenation of Nitrile-Butadiene Rubber. *Nano-Micro Letters*, 6(1), 55-62.

- Yigezu, Z. D., & Muthukumar, K. (2014). Catalytic cracking of vegetable oil with metal oxides for biofuel production. *Energy Conversion and Management*, 84, 326-333.
- Yin, Z., Zhou, W., Gao, Y., Ma, D., Kiely, C. J., & Bao, X. (2012). Supported Pd-Cu bimetallic nanoparticles that have high activity for the electrochemical oxidation of methanol. *Chemistry*, 18(16), 4887-4893.
- Yoon, M., Srirambalaji, R., & Kim, K. (2011). Homochiral metal-organic frameworks for asymmetric heterogeneous catalysis. *Chemical reviews*, 112(2), 1196-1231.
- Yu, L., Yang, X., Ye, Y., & Wang, D. (2015). Efficient removal of atrazine in water with a Fe<sub>3</sub>O<sub>4</sub>/MWCNTs nanocomposite as a heterogeneous Fenton-like catalyst. *RSC Advances*, 5(57), 46059-46066.
- Zayani, G., Bousselmi, L., Pichat, P., Mhenni, F., & Ghrabi, A. (2008). Photocatalytic degradation of the Acid Blue 113 textile azo dye in aqueous suspensions of four commercialized TiO<sub>2</sub> samples. *Journal of Environmental Science and Health Part A*, 43(2), 202-209.
- Zhang, G., Hou, S., Zhang, H., Zeng, W., Yan, F., Li, C. C., et al. (2015). High-Performance and Ultra-Stable Lithium-Ion Batteries Based on MOF-Derived ZnO@ ZnO Quantum Dots/C Core-Shell Nanorod Arrays on a Carbon Cloth Anode. *Advanced Materials*, 27(14), 2400-2405.
- Zhang, M., Gao, B., Yao, Y., Xue, Y., & Inyang, M. (2012). Synthesis of porous MgO-biochar nanocomposites for removal of phosphate and nitrate from aqueous solutions. *Chemical Engineering Journal*, 210(0), 26-32.
- Zhao, X., Wei, L., Cheng, S., Yu, Y., & Julson, J. (2015). *Catalytic cracking of carinata oil for hydrocarbon biofuel over Zn/Na-ZSM-5*. Paper presented at the 2015 ASABE Annual International Meeting.